Dissertation zur Erlangung des Doktorgrades
der Fakultät für Chemie und Pharmazie
der Ludwig-Maximilians-Universität München

Exploring 5-substituted nipecotic acid derivatives in the search for novel GABA uptake inhibitors by means of MS based screening of pseudostatic combinatorial hydrazone libraries

Tobias Josef Hauke

aus

Augsburg, Deutschland

2018

Erklärung

Diese Dissertation wurde im Sinne von § 7 der Promotionsordnung vom 28. November 2011 von Herrn Prof. Dr. Klaus T. Wanner betreut.

Eidesstattliche Versicherung

Diese Dissertation wurde eigenständig und ohne unerlaubte Hilfe erarbeitet.

München, den 22.11.2018

Tobias Hauke

Dissertation eingereicht am	22.11.2018
1. Gutachter	Prof. Dr. Klaus T. Wanner
2. Gutachter	Prof. Dr. Franz F. Paintner
Mündliche Prüfung am	19.12.2018

Die vorliegende Arbeit entstand in der Zeit von Oktober 2013 bis November 2018
am Department Pharmazie – Zentrum für Pharmaforschung – der
Ludwig-Maximilians-Universität München auf Anregung und unter Leitung von

Herrn Prof. Dr. Klaus T. Wanner

Für die hervorragende und sehr engagierte Betreuung und Förderung
meiner Arbeit sowie die ausgezeichneten Forschungsbedingungen danke ich
Herrn Prof. Dr. Klaus T. Wanner sehr herzlich.

Herrn Prof. Dr. Franz F. Paintner danke ich herzlich
für die Übernahme des Korreferats.

Danksagung

Für die gute Zusammenarbeit und die schöne gemeinsame Zeit möchte ich mich bei allen aktuellen und ehemaligen Mitarbeiterinnen und Mitarbeitern des Arbeitskreises recht herzlich bedanken.

Besonderer Dank gilt meinen beiden ehemaligen Laborkollegen Dr. Ludwig Angermeier und Dr. Toni Lutz sowie meinen aktuellen Laborkollegen Maren Schaarschmidt und Annerose Kärtner für die angenehme Atmosphäre im C.1051.

Dr. Ludwig Angermeier, Dr. Toni Lutz und Dr. Tim Hellenbrand danke ich weiterhin für die gute Zeit auch außerhalb des Labors – etwa bei Fussballspielen, Schafkopfrunden oder dem ein oder anderen Feierabendbier. Dr. Thejavathi Renukappa-Gutke danke ich für die stets freundlichen und motivierenden Worte.

Dr. Lars Allmendinger, Simone Huber, Mark Währa, Dr. Patrick Neiens sowie den Kollegen vom AK Bracher, insbesondere Dr. Benedikt Melzer, Alexandra Kamlah, Eva Plesch und Dr. Christoph Müller, danke ich für gemeinsame „kulinarische“ Erlebnisse, sei es bei Mittagessen, bei Weihnachtsfeiern des „2. Stocks“ etc.

Dr. Georg Höfner, Dr. Thomas Wein, Dr. Lars Allmendinger und Dr. Jörg Pabel gilt besonderer Dank für Hilfestellungen und technische Ratschläge beim Verfassen der Manuskripte. Dr. Miriam Sindelar möchte ich für die Einarbeitung in die Anwendung der MS-Bindungsassays danken. Simone Huber und Dr. Karuna Bhokare danke ich für die Zusammenarbeit beim Zusammenstellen der Aldehyd-Bibliotheken. Auch Miriam Schulz, Hans Brabec, Janine Piecek und Ronan McShane, die im Rahmen studentischer Forschungspraktika bzw. einer Bachelorarbeit einen Beitrag zu dieser Arbeit geleistet haben, gilt besonderer Dank für die stets engagierte Unterstützung.

Dr. Georg Höfner, Silke Duensing-Kropp, Miriam Sandner und Tanja Franz danke ich für die biologische Testung der von mir synthetisierten Substanzen, und v.a. für die aufwendigen Sättigungsexperimente.

Dem ganzen Team der analytischen Abteilung, insbesondere Dr. Lars Allmendinger und Claudia Glas, danke ich für die Aufnahme zahlreicher NMR-Spektren und Kinetik-Messungen.

Katharina Heimberger und Annerose Kärtner danke ich für die Unterstützung bei diversen organisatorischen Aufgaben und der Versorgung mit Büro- und Labormaterialien.

Für die gute Organisation aller von mir betreuten Studentenpraktika möchte ich den Oberassistenten, Dr. Jörg Pabel, Dr. Georg Höfner und Dr. Lars Allmendinger, herzlich danken.

Besonderer Dank gilt auch all meinen Freunden und ehemaligen Kommilitonen, die mich während dieser Promotionszeit begleitet haben, für die gemeinsamen Erlebnisse.

Größter Dank gebührt meiner Familie, besonders meiner Frau Corina, meinen Eltern, meinen Großeltern und meiner Schwester Martina, für die bindungslose Unterstützung und den permanenten Rückhalt. Ihr habt diese Doktorarbeit erst ermöglicht und euch sei diese Arbeit schließlich gewidmet – vielen Dank!

This cumulative thesis is based on the following original publications and manuscripts:

Reprinted with permission,

Tobias J. Hauke, Thomas Wein, Georg Höfner and Klaus T. Wanner; *Journal of Medicinal Chemistry* **2018**, *61*, 10310–10332.

“Novel allosteric ligands of γ-aminobutyric acid transporter 1 (GAT1) by MS based screening of pseudostatic hydrazone libraries”

Tobias J. Hauke, Georg Höfner and Klaus T. Wanner; manuscript submitted to *ChemMedChem.*

“MS based screening of 5-substituted nipecotic acid derived hydrazone libraries as ligands of the GABA transporter 1”

Tobias J. Hauke, Georg Höfner and Klaus T. Wanner; *Bioorganic & Medicinal Chemistry* **2019**, *27*, 144–152.

“Generation and screening of pseudostatic hydrazone libraries derived from 5-substituted nipecotic acid derivatives at the GABA transporter mGAT4”

Table of contents

1 Introduction

1.1 GABA transporters as pharmacological targets

GABA transporters of the SLC6 gene family

The solute carrier (SLC) group comprises more than 400 membrane-bound proteins that exhibit a pivotal role by carrying soluble molecules such as ions, nutrients and signaling molecules across lipid cell membranes in a secondary active transport (that is by utilizing an electrochemical gradient of a co-substrate).[1] Members of the solute carrier 6 (SLC6) gene family are amongst the most important neurotransmitter transporters widely expressed in the mammalian brain. These SLC6 transporters translocate several substrates including γ-aminobutyric acid (GABA; **1**; Figure 1), dopamine, glycine, norepinephrine, and serotonin by utilizing a sodium- and chloride-dependent cotransport trough cell membranes. By removing such neurotransmitters from the synaptic cleft, SLC6 transporters can effectively terminate downstream neurotransmitter signaling and thus are important regulators of homeostatic processes.

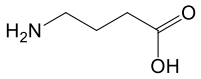

GABA (**1**)

Figure 1: Structure of the neurotransmitter γ-aminobutyric acid (GABA; **1**)

The SLC6 gene family can be divided phylogenetically into four subfamilies, i.e. in monoamine, GABA, amino acid and amino acid/orphan transporters.[2] GABA is the most important inhibitory neurotransmitter in the mammalian central nervous system (CNS) and amongst the GABA transporters (GATs) from the SCL6 gene family, four different subtypes of membrane-bound proteins have been cloned. The GABA transporter subtypes are designated as GAT1, BGT1, GAT2 and GAT3 according to the Human Genome Organisation (HUGO). However, there is a notable degree of inconsistency in the nomenclature in dependence on the species from which the transporters are cloned;[i] for instance, the four subtypes are termed mGAT1 (≙ GAT1), mGAT2 (≙ BGT1), mGAT3 (≙ GAT2) and mGAT4 (≙ GAT3), when expressed in mice

[i] Throughout this thesis the HUGO nomenclature is generally applied for the different GABA transporter subtypes except when a GAT subtype from a particular species should be emphasized, e.g. for detailing experimental conditions.

(see Table 1).[3,4] GATs consist of 599–632 amino acids[2,5] and, based on sequence identity, GAT1 diverges most from other subtypes, while BGT1 and GAT2 are phylogenetically most closely related to each other.[4]

Table 1: Nomenclature of GABA transporters across species with the gene and HUGO nomenclature being highlighted

	Gene name:	**SLC6A1**	**SLC6A12**	**SLC6A13**	**SLC6A11**
	HUGO:	**GAT1**	**BGT1**	**GAT2**	**GAT3**
species	Human:	hGAT1	hBGT1	hGAT2	hGAT3
	Mouse:	mGAT1	mGAT2	mGAT3	mGAT4
	Rat:	rGAT1	rBGT1	rGAT2	rGAT3

Affinities of GABA and localizations of the transporters differ distinctly amongst the individual GAT subtypes. GAT1, GAT2 and GAT3 bind GABA specifically and with high affinity, whereas BGT1 is characterized by a lower affinity and transports also betaine as substrate.[5] Regarding localization, GAT1 and GAT3 are predominately found in the mammalian brain usually in vicinity to GABAergic synapses,[2,6,7] where GAT1 is mainly located on presynaptic neurons and GAT3 on astrocytes. Hence, GAT1 mediates neuronal GABA uptake, while GAT3 is responsible for GABA uptake into glial cells.[8–10] Conversely, BGT1 and GAT2 are only weakly expressed in most parts of the mammalian brain and are currently assumed to have greater physiological importance in peripheral organs such as kidney and liver.[11] So far, GAT1 is the best studied GABA transporter, while the elucidation of the physiological role of other GAT subtypes is retarded due to a lack of highly potent and selective inhibitors (see section 1.2).

GABAergic neurotransmission and pathophysiology

It is estimated that about 30–40% of all neurons in the mammalian CNS utilize GABA as their primary neurotransmitter[12] and at least 40% of inhibitory processing at synapses in the brain is mediated by GABA.[13] These numbers doubtlessly demonstrate the physiological importance of GABA as inhibitory neurotransmitter.

In the adult mammalian brain, GABA is principally synthesized from glutamate in a single step catalyzed by glutamate decarboxylase (GAD)[14] and loaded into synaptic vesicles by means of a vesicular neurotransmitter transporters (VGAT) for storage.[15]

After liberation from presynaptic neurons by a calcium-dependent exocytosis into the synaptic cleft, GABA can address its corresponding pre- and postsynaptic receptors, which can be differentiated into two main types. Ionotropic $GABA_A$ receptors, mostly located on postsynaptic neurons, represent ligand-gated chloride channels; upon activation by GABA they allow an influx of chloride ions, which leads to hyperpolarisation and finally deactivation of the postsynaptic neuron. Metabotropic $GABA_B$ receptors, located on both pre- and postsynaptic neurons, represent G-protein coupled receptors (GPCRs) acting in two different mechanisms. Activated presynaptic $GABA_B$ receptors reduce the calcium current and subsequently decrease neurotransmitter exocytosis; thereby these receptors serve as a negative feedback mechanism for GABA release. In contrast, activated $GABA_B$ receptors with postsynaptic localization stimulate potassium outward currents and thus again hyperpolarize and deactivate the corresponding neuron.[15] The extracellular GABA concentration is regulated by the aforementioned GABA transporters (GATs) and accordingly GABAergic neurotransmission is terminated by the neurotransmitter reuptake into neurons and surrounding glial cells. Finally, GABA can be recycled or metabolized by enzymatic degradation catalyzed by GABA transaminase (GABA-T).[15] In principal, this described GABAergic neurotransmission is illustrated in Figure 2.

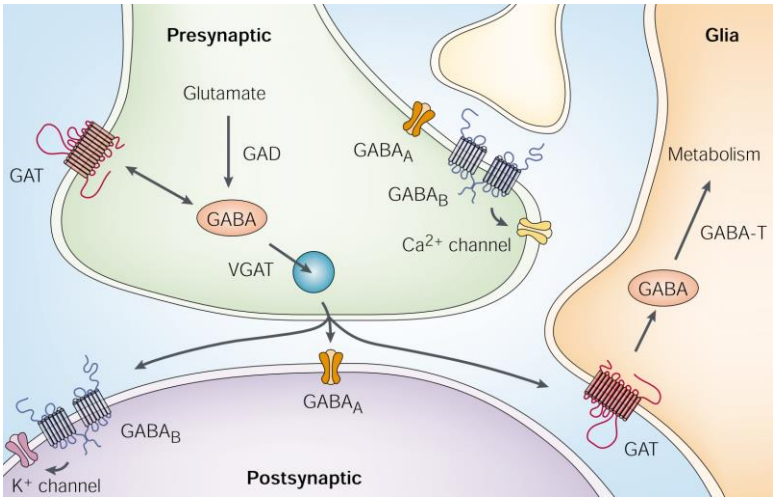

Figure 2: GABAergic neurotransmission according to Owens and Kriegstein.[15] GABA is synthesized from glutamate (via GAD), loaded into vesicles (via VGAT) and released to the synaptic cleft by exocytosis, where it can bind to pre- and postsynaptic $GABA_A$ and $GABA_B$ receptors. Neurotransmission is terminated by neuronal or glial reuptake (via GATs) and recycling or metabolizing (via GABA-T) of GABA

Given the physiological importance of GABA, it is not surprising that pathologically impaired GABAergic neurotransmission is associated with a number of neuronal and psychiatric diseases such as epilepsy,[16-18] Parkinson's disease,[18,19] Huntington's disease,[18,20] Alzheimer's disease,[21] depression[22,23] and neuropathic pain.[24,25] For treatment, reduced GABAergic neurotransmission can be adjusted by two basic principles, i.e. by directly stimulating GABA receptor activity or by enhancing GABA concentration. Currently approved drugs address several major targets: For instance, benzodiazepines such as diazepam (**2**; Figure 3) and barbiturates such as phenobarbital (**3**) are positive allosteric modulators of ionotropic $GABA_A$ receptors, while metabotropic $GABA_B$ receptors are activated by baclofen (**4**). Vigabatrin (**5**) prevents the enzymatic degradation of GABA as a suicide inhibitor of GABA-T and tiagabine (**6**) increases the GABA concentration in the synaptic cleft by a selective inhibition of GAT1. Novel targets associated with GABAergic neurotransmission and diversely more experimental compounds are continuously explored in order to find potentially new drugs as recently reviewed by Kowalczyk and Kulig.[26]

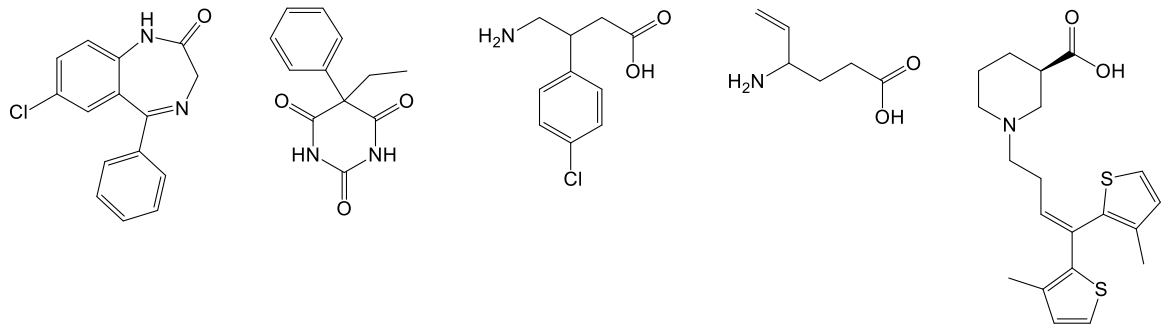

Figure 3: Structures of approved drugs targeting the GABAergic system

GAT1-selective tiagabine (**6**) is the only GAT inhibitor in clinical use. It was approved as an anticonvulsant medication for the add-on treatment of partial-onset seizures;[27,28] however, the use of tiagabine (**6**) is accompanied by a number of side effects including dizziness, asthenia, nervousness, tremor, diarrhea, and depression that limit its applicability.[29,30] By the application of potent and selective inhibitors such as tiagabine (**6**) GAT1 emerged as a well-known target mediating anticonvulsants effects. Conversely, the pharmacological potential of non-GAT1 GABA transporter subtypes is still less well understood but more recently published evidence implies that particularly

BGT1 and GAT3 could be promising new targets for the treatment of epilepsy and other neurological disorders such as anxiety and pain.[2,3,7] According to the World Health Organization (WHO), epilepsy affects about 50 million people worldwide, making this disease one of the most prevalent neurological disorders globally.[31] Although there were more than 15 antiepileptic drugs introduced in the last decades, about one-third of patients continue to have seizures despite receiving medication and, generally, antiepileptic treatment is often associated with several complex psychiatric side effects.[32] Hence, there is an ongoing need of developing new antiepileptic drugs and evaluating novel molecular targets.

1.2 GABA uptake inhibitors

Development of GABA uptake inhibitors

Since the discovery of an active transport system for GABA in the late 1960s, there have been extensive efforts by medicinal chemists to synthesize and establish selective GABA transporter inhibitors.[33] In the early development the *Amanita muscaria* mushroom constituent muscimol (**7**; Figure 4), which can be considered a 3-isoxazolol bioisostere of GABA (**1**), was found to inhibit GATs, but it also targets $GABA_A$ receptors and GABA-T. Due to these multiple effects the use of **7** as a tool compound is limited; however, it served as a lead structure for structural variations.[4] Inspired by the structure of muscimol (**7**), the compounds 4,5,6,7-tetrahydroisoxazolo[4,5-*c*]pyridin-3-ol (THPO; **8**), and later nipecotic acid (**9**) and guvacine (**10**) were evaluated as more selective GAT inhibitors and found to exhibit moderate potency at defined GAT subtypes without targeting $GABA_A$ receptors.[4,33] The (*R*)-enantiomere of nipecotic acid [(*R*)-**9**], in particular, still represents one of the most potent small, substrate-related GAT inhibitors known up to date[33] and it is commonly utilized as a starting point for the development of more potent, larger GAT inhibitors. Nipecotic acid (**9**) displays inhibitory potencies in a similar order of magnitude at all GAT subtypes except BGT1, at which it is distinctly less active. However, due to their hydrophilicity nipecotic acid (**9**) and related small, cyclic amino acids are not capable of crossing the blood-brain barrier and thus are nearly inactive *in vivo* upon peripheral administration.[34]

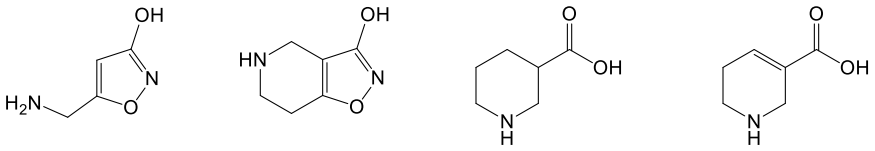

Muscimol (**7**) THPO (**8**) Nipecotic acid (**9**) Guvacine (**10**)

Figure 4: Structures of small substrate-related GAT inhibitors **7**–**10**

The attachment of a bulky, lipophilic 4,4-diphenyl-3-butenyl residue to the cyclic amino acid moiety led to the discovery of a new generation of GAT inhibitors, with the nipecotic acid derivative SK&F-89976A (**11**; Figure 5) being one of the first representatives of this kind of compounds.[35] This new generation of GAT inhibitors is characterized by a general amphiphilic structure, that is a lipophilic, aromatic moiety attached to a hydrophilic amino acid "head". The increased lipophilicity allowed these compounds to penetrate the blood-brain barrier. Further representatives of this generation of GAT inhibitors are the aforementioned tiagabine (**6**), which is the only GAT inhibitor in clinical use (see section 1.1), and the guvacine derivative NO711 (**12**). The lipophilic attachments in these compounds **6**, **11** and **12** further enhanced potencies at and selectivities for GAT1 over other GABA transporter subtypes compared to their unsubstituted parent compounds nipecotic acid (**9**) and guvacine (**10**). Hence, compounds **6**, **11** and **12** represent orally active, selective and potent GAT1 inhibitors with inhibitory potencies at this GABA transporter subtype in the upper- to mid-nanomolar range.[36,37] More recently, guvacine derivative DDPM-2571 (**13**), a new GAT1-selective compound, was synthesized in our group; it was found to exceed the inhibitory potency of tiagabine (**6**) at GAT1 by more than one log unit and mediated anticonvulsant, anxiolytic, antidepressant and antinociceptive effects in mouse models.[38] 3-Hydroxy-4-amino-4,5,6,7-tetrahydro-1,2-benzisoxazols (*exo*-THPO) derivative **14** represents an example of a selective GAT1 inhibitor with micromolar potency structurally more diverse from aforementioned compounds **6** and **11**–**13**.[39] Conversely, another, closely related *exo*-THPO derivative, EF1502 (**15**), is inhibiting the two transporter subtypes GAT1 and BGT1 with similar potency[40] and this compound was found to mediate anticonvulsant effects *in vivo* with a mechanistic profile distinctly different from tiagabine (**6**).[41]

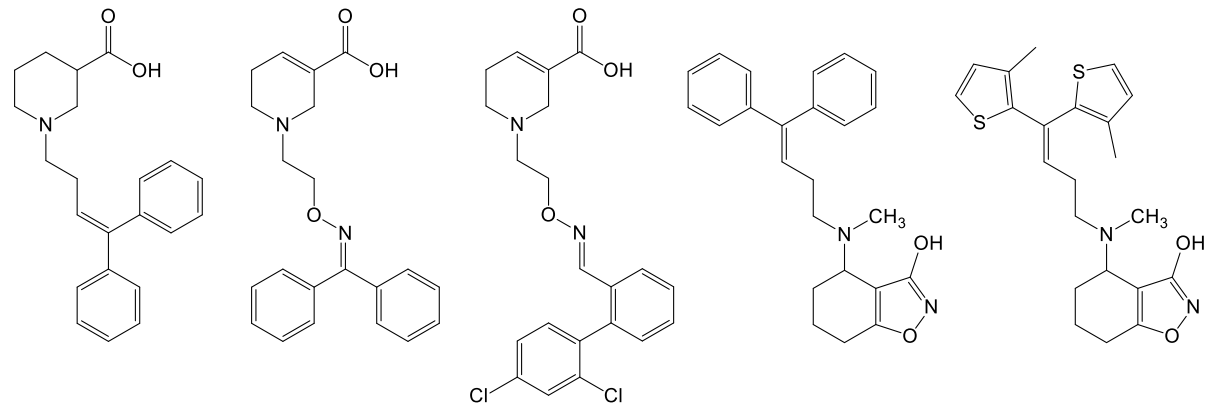

Figure 5: Structures of GAT1 inhibitors **11**–**15**

Apart from these GAT1-selective and mixed inhibitors several synthetic approaches also led to the discovery of compounds with selectivities towards non-GAT1 GABA transporters. The nipecotic acid derivative (*S*)-SNAP-5114 (**16**; Figure 6) represents the first prototypic inhibitor with moderate potency at and selectivity for GAT3.[42] Later, chemically more stable carba analogs of this trityloxy derivative **16** could be synthesized by our group, of which DDPM-1457 (**17**) displays a similar potency at GAT3.[43] These compounds **16** and **17**, which possess a 4,4',4''-trimethoxytrityl residue as lipophilic moiety, demonstrate that the choice of the aromatic domain can influence the selectivity for the GABA transporter subtypes. Besides such nipecotic acid derived compounds, a series of isatin derivatives including compound **18** was more recently reported representing a new class of GAT3 inhibitors.[44] Furthermore, bicyclo[3.1.0]hexane derivative **19** was proposed being the first highly selective BGT1 inhibitor[45] and compound **20** represents a lately published example of a selective BGT1 inhibitor with micromolar potency.[46]

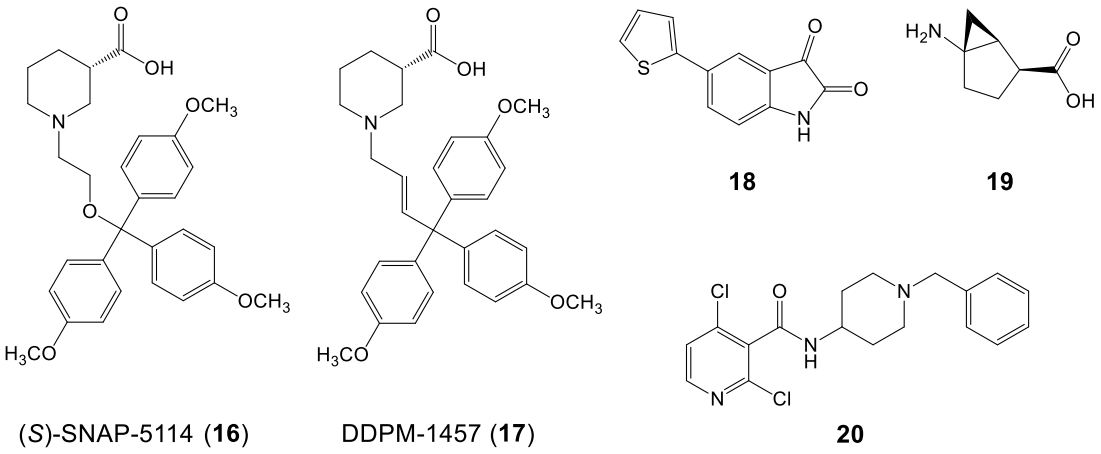

Figure 6: Structures of non-GAT1-selective inhibitors **16**–**20**

Inhibitory potencies of selected GAT inhibitors, which were already tested in our group at the different GABA transporter subtypes, are displayed in Table 2. It is remarkable that the inhibitory potencies of best GAT1-selective inhibitors are clearly higher than those of GABA transporter inhibitors with selectivities towards other transporter subtypes. There is still a lack of highly potent, non-GAT1-selective inhibitors that could be employed as pharmacological tools for elucidating the therapeutic potential of these GAT subtypes.

Classical GAT inhibitors with selectivities for either GAT1 or GAT3, which are derived from small cyclic amino acids such as nipecotic acid (**9**) and guvacine (**10**), typically exhibit amphiphilic structures: These compounds possess a hydrophilic amino acid “head” and a lipophilic aromatic moiety. The lipophilic residue is connected to the hydrophilic domain via a spacer attached to the nitrogen atom of the amino group. Hence, nipecotic acid and guvacine derived GAT inhibitors are usually substituted at the 1-position of the cyclic amino acid.

Table 2: Functional inhibitory potencies of selected GAT inhibitors tested in our group at the different GABA transporter subtypes cloned from mice

Compound	Inhibitory potencies (pIC_{50}±SEM)[a]			
	mGAT1	**mGAT2**	**mGAT3**	**mGAT4**
Tiagabine (**6**)	6.88±0.12	50%[b]	64%[b]	73%[b]
(*RS*)-Nipecotic acid (**9**)	4.88±0.07	3.10±0.09	4.64±0.07	4.70±0.07
(*R*)-Nipecotic acid [(*R*)-**9**]	5.19±0.03	3.39±0.05	4.76±0.05	4.95±0.05
(*S*)-Nipecotic acid [(*S*)-**9**]	4.24±0.05	3.13±0.14	3.83±0.04	3.63±0.06
Guvacine (**10**)	4.87±0.06	3.31±0.03	4.59±0.05	4.59±0.05
SK&F-89976A (**11**)	6.16±0.05	3.43±0.07	3.71±0.04	3.56±0.06
NO711 (**12**)	6.83±0.06	3.20±0.09	3.62±0.04	3.07±0.05
DDPM-2571 (**13**)	7.90±0.09	4.31[c]	4.35[c]	4.07[c]
(*S*)-SNAP-5114 (**16**)	4.07±0.09	63%[b]	5.29±0.04	5.65±0.02
DDPM-1457 (**17**)	4.40±0.05	4.42±0.11	5.47±0.02	5.87±0.08
18	4.53[c]	52%[b]	44%[b]	4.61[c]
rac-**24**	4.58±0.10	108%[b]	68%[b]	76%[b]

[a] For sake of comparability all listed inhibitory potencies derive from the biological tests of our research group based on [^{3}H]GABA uptake assays with HEK293 cells stably expressing the different GAT subtypes mGAT1–mGAT4. Values are usually given as means±SEM from at least three independently performed experiments.

[b] In case of low inhibitory potencies percentages are given that represent the remaining [^{3}H]GABA uptake in presence of 100 µM test compound.

[c] Obtained from less than three experiments and accordingly no SEM value is stated.

Moreover, in the last years several attempts have been made to synthesize analogous compounds substituted in different positions of the cyclic amino acid moiety that were tested for their potential to inhibit GABA uptake. For instance, 5-substituted arecoline derivatives as well as the *N*-methyl guvacine derivative **21** (Figure 7) were synthesized by Müller-Uri et al.[47] N'Goka et al.[48–50] synthesized 6-substituted nipecotic acid and guvacine derivatives of which compound **22** showed an *in vitro* inhibitory potency of the GABA uptake at GAT1 comparable to that of compound **11**. In our group, an asymmetric route was explored that led to the synthesis of 6-substituted nipecotic acid derivatives such as compound **23**[51] and, more recently, nipecotic acid and *N*-methyl nipecotic acid derivatives substituted in the 4-position (e.g. compound *rac*-**24**) were synthesized.[52] However, in none of these approaches GABA uptake inhibitors as effective as N-substituted derivatives could be achieved. Only compound **22** showed a biological activity comparable to those of known GAT1-selective inhibitors **6**, **11** and

12 in *in vitro* assays, but was nearly inactive *in vivo*, possibly due to an insufficient blood/brain concentration ratio.[48]

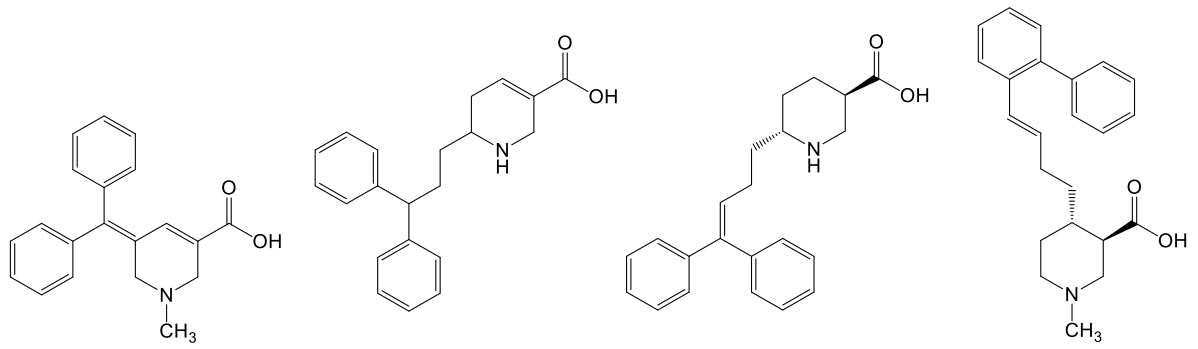

21 ($pK_i = 4.9$)[a] **22** ($pIC_{50} = 7.0$)[b] **23** (90%/100 µM)[c] ***rac*-24** ($pIC_{50} = 4.6$)[d]

Figure 7: Structures of GAT inhibitor derivatives with different substitution pattern and their inhibitory potencies as reported in literature [a) inhibitory effect on [^{3}H]GABA uptake at synaptosomes according to reference[47]; b) inhibitory effect on [^{3}H]GABA uptake at synaptosomes according to reference[48]; c) remaining percentage of [^{3}H]GABA uptake in presence of 100 µM test compound at bovine GAT1 according to reference[51]; d) inhibitory effect on [^{3}H]GABA uptake at mGAT1 according to reference[52]]

Structure of GATs and binding mode of GABA uptake inhibitors

The elucidation of the binding mode of GABA uptake inhibitors at the corresponding transporters requires an understanding of the structure of GAT proteins. As a first example of a neurotransmitter-sodium symporter, GAT1, isolated from rat brain, was initially sequenced and cloned by Guastella et al.[53] Since then, several homologous proteins were examined and it became evident that these amino acid and monoamine transporters, respectively, are consisting of twelve transmembrane helices (TMs), which are connected via both extracellular and intracellular loops.[54] Finally, the successful crystallization of a bacterial leucine transporter LeuT in presence of its substrate leucine and two sodium ions, which was accomplished by Yamashita et al.,[55] revealed the actual three-dimensional structure. Despite having only 20–25% total sequence identity, the prokaryotic LeuT is generally considered a good model for eukaryotic SLC6 transporters,[56] particularly since the sequences in the proximity of the substrate binding sites are substantially more highly conserved.[57] The structure of this bacterial LeuT is illustrated in Figure 8.

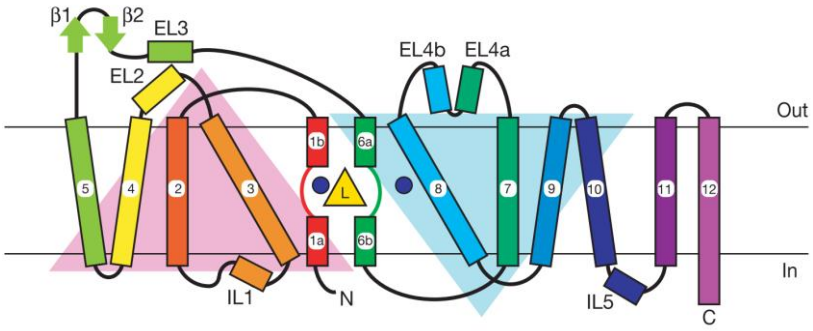

Figure 8: Structure of LeuT from the bacterium *Aquifex aeolicus* according to Yamashita et al.[55]

Amongst the 12 TMs, the first 10 TMs form the essential core of neurotransmitter-sodium symporters and the region around the helical segments TM1 and TM6, which are arranged in an antiparallel orientation, comprises the binding site for the substrate and sodium ions.[55] Based on these structural insights, Yamashita et al.[55] furthermore proposed a general transport mechanism following a model of “alternate access”: The neurotransmitter-sodium symporters basically possess two “gates”, which can alternately allow access to the binding site from either the extracellular or intracellular side of the membrane bilayer. The gate towards the extracellular side is primarily defined by the amino acid side chains of Tyr108, Phe253, Arg30 and Asp404, of which particularly the latter two that can form a charged pair are highly conserved amongst neurotransmitter-sodium symporters. Conversely, the gate towards the intracellular side is composed of a larger region of the protein in the vicinity of the helical segments TM1a, TM6b and TM8. The transporter has to pass several conformations during transport and at least three major states can be defined: I) An “outward facing” state, at which the extracellular gate is open and the substrate can access the binding site, II) a “substrate occluded” state, at which both gates are closed and the substrate is trapped at the binding site, and III) an “inward facing” state, at which the intracellular gate is open and the substrate can leave the binding site towards the cytoplasm. This postulated transport mechanism is illustrated in Figure 9. In the original work of Yamashita et al.[55] the “substrate occluded” state was crystallized. Meanwhile it was achieved to crystallize different states of LeuT basically supporting the proposed transport mechanism.[58] Furthermore, the general structural resemblance of the prokaryotic LeuT with eukaryotic SLC6 transporters has been confirmed recently by achieving crystal structures of the dopamine transporter from *Drosophila melanogaster*[59] and the human serotonin transporter.[60]

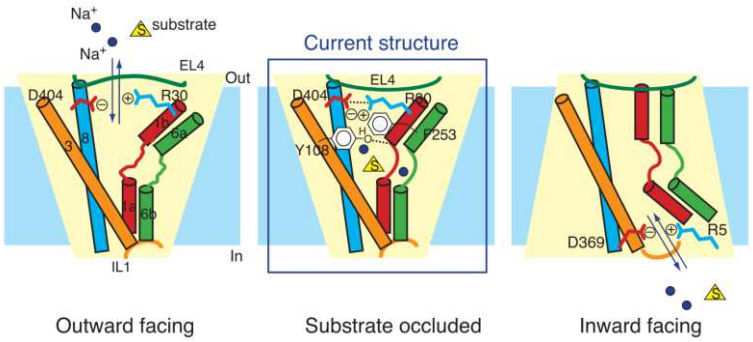

Figure 9: Postulated transport mechanism of LeuT according to Yamashita et al.[55]

Since its crystallographic elucidation in the year 2005, the structure of LeuT was used as the base for homology modeling in several studies in order to create a three-dimensional model of the human GAT1 (hGAT1). In this context, two investigations analyzed the binding of GABA (**1**) and small inhibitors such as nipecotic acid (**9**) towards hGAT1.[61,62] Accordingly, the carboxylic acid function of GABA (**1**) is bound to one sodium atom and additionally fixed in a set of hydrogen bonds mostly mediated by the side chain OH group of Tyr140 and the backbone NH of Leu64 and Gly65. Furthermore, the GABA (**1**) amino function is encompassed in a different network of hydrogen bonds which includes side chain OH groups of Thr400, Ser396 and Tyr60 as well as backbone carbonyl functions of Tyr60 and Ser396. The different substrate specificity of hGAT1 as compared to LeuT can mostly be explained by three amino acid mutations that result in slightly modified interactions, i.e. Ser256 to Gly297 at helical segment TM6a, Asn21 to Tyr60 at TM1a and Ile359 to Thr400 at TM8 (LeuT to hGAT1).[62] Successive studies examined the binding of the larger inhibitor tiagabine (**6**) using homology modeling, docking and molecular dynamics simulations[63] and compared the binding modes of small and large inhibitors.[64] Nipecotic acid (**9**), as an example of a small inhibitor, addresses exactly the same binding site as GABA (**1**), which is termed S1 site, and also adapts a similar pose, in which the amino nitrogen is facing towards the intracellular side of the protein interacting again with Tyr60 in particular (Figure 10a). Conversely, the bindings of tiagabine (**6**) and related larger inhibitors differ remarkably from the aforementioned due to the presence of the bulky lipophilic side chain (Figure 10b): While the orientation of the carboxylic acid function is largely retained allowing strong interactions with Tyr140, the pose of the piperidine ring of the nipecotic acid moiety is switched with the amino nitrogen and the lipophilic residue facing towards the extracellular side of the protein. In this position the amino

function only forms hydrogen bonding interactions with the backbone carbonyl function of Phe294. The lipophilic aromatic residue, which is linked to the amino group via a spacer, is too large to fit in the S1 pocket and accordingly binds to an extracellular vestibule that is occasionally designated as S2 site. Hence, the binding of tiagabine (**6**) premises the gate towards the extracellular side to be opened and consequently GAT1 is constrained in the "outward facing" conformation.[63,64]

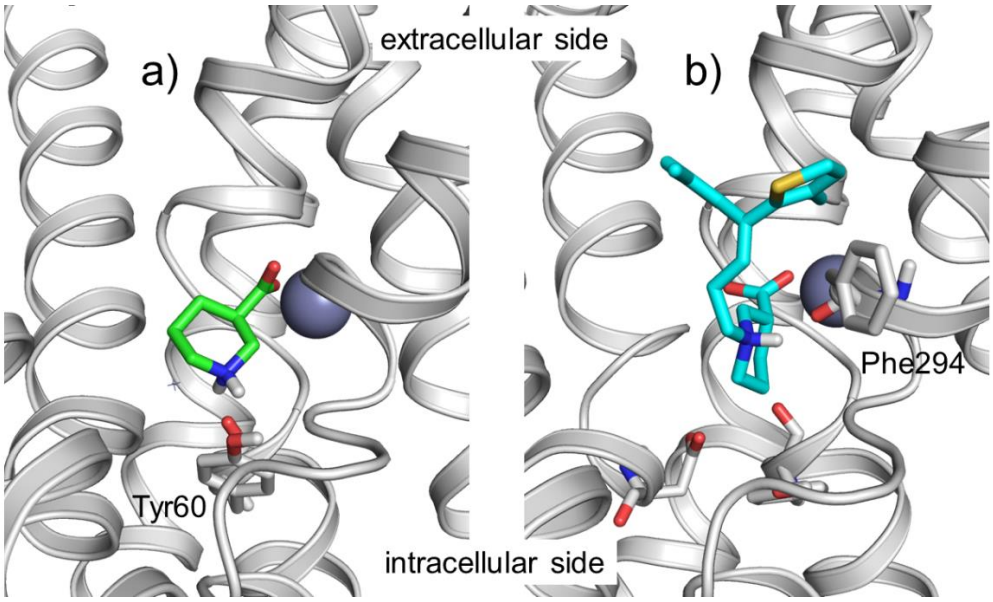

Figure 10: Binding of a) nipecotic acid (**9**; green) and b) tiagabine (**6**; cyan) towards hGAT1. The amino group of nipecotic acid (**9**) is interacting particularly with the backbone carbonyl function as well as the side chain of Tyr60, while the amino group of tiagabine (**6**) is interacting with the backbone carbonyl function of Phe294. The figure was prepared and kindly provided by Dr. Thomas Wein using our in-house hGAT1 homology model refined by molecular dynamics calculations (see also references[62,64])

Based on these insights, a majority of GABA uptake inhibitors can be considered to inhibit GABA binding at GAT proteins in a competitive manner. Conversely, more recently described GAT inhibitors including compounds **14**, **15**, **18** and **20** (see above) have been proposed to exhibit a noncompetitive interaction mode at the corresponding GAT subtypes. For the sake of clarity, the term "noncompetitive" is commonly applied phenomenologically based on observed behaviours in functional assays throughout the literature without specifying the underlying mechanism. There are different mechanisms that can result in such noncompetitive behaviours, including an allosteric modulation as well as an inhibition by an irreversible or slow dissociating orthosteric

ligand.[65] However, at least for some of these noncompetitive GAT inhibitors an allosteric modulation could be supported as underlying mechanism.

For instance, a hypothetical allosteric binding site located between helical segments TM10 and TM11 at hGAT3 was revealed by molecular modeling studies for compound **18**, which was proposed as a noncompetitive GAT3 inhibitor.[44] Besides, a potential allosteric binding site at TM10 of hBGT1 was evaluated for compound **20** by experimental studies using chimeric constructs of transporters with different pharmacological properties and computational studies based on a homology model of hBGT1.[46] Still, the physiological role and the pharmacological importance of possible allosteric binding sites at the different GAT subtypes have yet to be established in future studies, for which noncompetitive GAT inhibitors might emerge as promising tool compounds.

1.3 Developments of biological test systems for GAT inhibitors

General test systems for GAT inhibitors

The aforementioned, ongoing development of new GAT inhibitors is permanently accompanied by advancements of test systems enabling to elucidate the bioactivities of synthesized compounds. In this context, computational methodologies increasingly gain in importance for structure-activity studies and the rational design of novel bioactive compounds in general.[66] And as outlined in section 1.2, *in silico* techniques such as homology modeling, docking and molecular dynamics simulations, have already been applied, in particular, to facilitate our understanding of GAT inhibitors and their interaction modes at the corresponding molecular targets. However, these computer-aided approaches are reliant on the input of concrete experimental data from appropriate bioassays in order to be able to generate precise predictions.

Since the 1960s the functional activities of potential GAT inhibitors could be determined in uptake assays utilizing tritium-labelled GABA ([^{3}H]GABA) and measuring radioactivity by liquid scintillation counting as read-out. In those early [^{3}H]GABA uptake assays slices of rat cerebral cortex[67] and later synaptosomal preparations were used as target materials.[68] Though, such preparations were gradually replaced as target materials when cell lines transfected with the different GAT subtypes became available in the 1990s.[69–71] In our group, a [^{3}H]GABA uptake

assay was established and described in detail by Kragler et al.[72] in 2005 that was based on the murine proteins mGAT1–mGAT4 transiently expressed in COS-7 and HEK293 cells, respectively. Later, this assay was transferred to a 96-well plate format in order to increase throughput and it was furthermore modified by using HEK293 cells that are stably expressing the murine GAT proteins.[73] This latter assay is still routinely used in our group in order to evaluate functional activities and subtype selectivities of test compounds. In principle, intact cells expressing the corresponding transporter subtype are incubated with [^{3}H]GABA in this kind of assay. If no inhibitor is present, GABA can be transported into the cytoplasm of the cells unaffectedly. The uptake is terminated by a filtration step and after removing the incubation medium the cells are lyzed to liberate the included [^{3}H]GABA. Finally, the radioactivity of this transported [^{3}H]GABA is quantified by means of liquid scintillation counting. Conversely, in case of an inhibitor being present the amount of transported [^{3}H]GABA and consequently also the quantifiable radioactivity is reduced compared to the sample without inhibitor. By increasing the inhibitor concentrations, concentration-inhibition curves can be obtained from which the inhibitory potencies are calculable as IC_{50} values. As a more recent improvement, this principle concept of measuring GABA transport was transferred to a new kind of assay using mass spectrometry (MS) for quantification instead of the radiometric read-out in order to be devoid of all the drawbacks that result from using radioactive material. These so called MS Transport Assays were originally developed for all GAT subtypes in our group and described in detail by Schmitt et al.[74,75] In contrast to the [^{3}H]GABA uptake assays established in our group, these MS Transport Assays utilize the human equivalents of the four GABA transporters hGAT1–hGAT3 and hBGT1, respectively, stably expressed in COS-7 cells. As native GABA is endogenously present in those COS-7 cells employed as the GAT expression system, deuterated ($^2H_6$)GABA is used as substrate to differentiate transported from endogenous GABA.

In addition to the aforementioned functional assays, affinity-based assays are basically applicable to study target-ligand interactions. Due to their suitability to be used in high-throughput screenings (HTS) they have become important tools in earlier stages of the drug discovery process.[76,77] MS has emerged as a widely used read-out technique for affinity-based assays and several different MS based concepts have been evolved for this purpose including affinity selection-mass spectrometry (AS-MS) approaches that have a widespread application in drug screening.[78] Besides the AS-MS techniques,

MS Binding Assays represent another example of affinity-based assays utilizing MS as read-out. MS Binding Assays may be considered as an improvement of the commonly used radioligand binding assays, as they can be employed analogously but without the requirement of a radio-labelled ligand, which is usually associated with an expensive production and relatively high safety standards.[79] Instead of the radioligand, the binding of a native marker (MS marker) is quantified with high sensitivity by LC-ESI-MS/MS (as a replacement for the scintillation counting). The marker is typically a well-known ligand with high affinity and selectivity towards the particular target. Like radioligand binding assays, MS Binding Assays are generally applicable for saturation, competition and kinetic experiments. The basic workflow of a competitive MS Binding Assay is outlined in Figure 11. In short, the test compound is incubated together with the target and the MS marker. Incubation is terminated by filtration (or alternatively centrifugation) in order to isolate the target-ligand complexes from unbound ligands. Then the isolated target-ligand complexes are denatured and eluted with methanol for liberation of the bound ligands. Finally, the MS marker formerly bound to the target, which among other compounds is present in the eluate, is quantified by LC-ESI-MS/MS, serving as an indirect measure for the test compounds' binding affinity towards the target (i.e. competitive replacement of the marker from the target by the test compound and accordingly a decreased amount of bound marker indicates high activity of the test compound and vice versa). Meanwhile, MS Binding Assays have been established by our group for several targets such as dopamine receptors[80,81] as well as SLC6 transporters for serotonin,[82–84] dopamine,[83,84] norepinephrine,[83,84] and GABA (i.e. mGAT1), the latter of which uses NO711 (**12**) as MS marker and membrane preparation of HEK293 cells stably expressing mGAT1.[85,86]

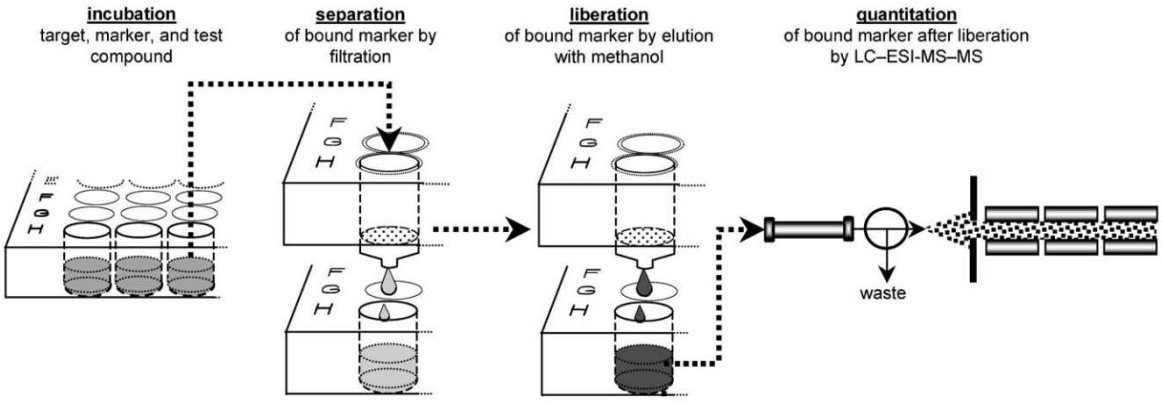

Figure 11: Basic workflow of a competitive MS Binding Assay according to Zepperitz et al.[85]

Generation and MS based screening of pseudostatic hydrazone libraries

More recently, a new kind of approach has been established in our group and described in detail by Sindelar and Wanner[87] in 2012 that combines the generation of libraries by means of dynamic combinatorial chemistry (DCC) with the read-out of their binding affinities towards mGAT1 in competitive MS Binding Assays.

Basically, dynamic combinatorial libraries (DCLs) are generated by a reversible combination of molecular building blocks of suitable reactivity to afford potential ligands for the corresponding target. Per definition, all DCL components are in a thermodynamic equilibrium, which requires the interconversion of library members into one another. Typically, simple and efficient chemical reactions are primarily applied for DCL generation, including acylhydrazone, disulfide, hydrazone, imine, or oxime formations.[88,89] In the initial approach established in our group, hydrazone formation was utilized as DCC reaction of choice. The building blocks were designed to allow the generation of libraries composed of compounds structurally related to known GAT1 inhibitors such as compounds **6** or **11** (see section 1.2). Accordingly, a nipecotic acid moiety was chosen as parent structure and substituted at the 1-postion with a spacer containing a terminal hydrazine function (affording compound **25**). Reaction of this hydrazine building block **25** with diverse, mostly aromatic aldehydes **26** as corresponding, more lipophilic building blocks yielded the desired hydrazone libraries with general structures **27** (Figure 12). For library generation, the single hydrazine **25**, which was converted with four individual aldehydes **26** per library, was applied in large excess compared to the total aldehyde concentration in order to obtain all library constituents in similar amounts (without the need of guaranteeing all components to be isoenergetic). In this manner an almost constant hydrazone library composition was achieved despite the dynamic nature, i.e. hydrazone libraries were rendered pseudostatic.

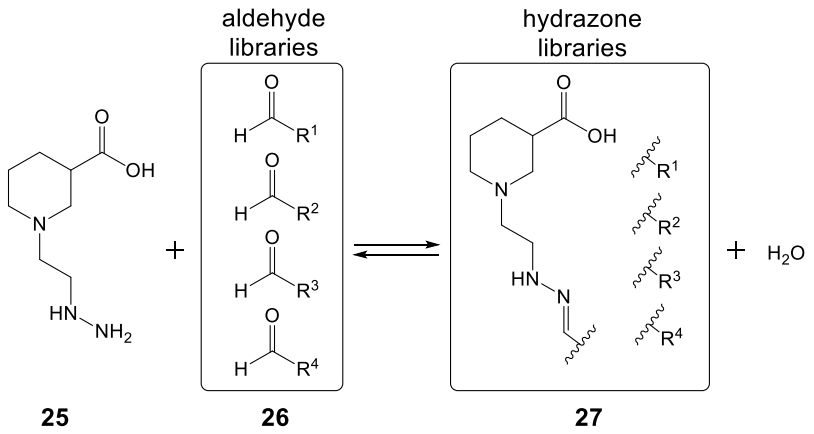

Figure 12: Condensation of hydrazine building block **25** (in excess) with diverse aldehydes **26** yielding hydrazones with general structure **27** as described by Sindelar and Wanner[87]

Libraries were generated in the presence of the target mGAT1 to improve assay performance. After incubating the mixture of library building blocks and the target proteins for a time period sufficient to allow quantitative hydrazone formation, binding affinities of libraries were determined in an MS based screening (Figure 13). The screening was adapted from the competitive MS Binding Assays originally developed by Zepperitz et al.[85,86] for the target mGAT1; however, instead of a single test compound hydrazone libraries containing several constituents were analyzed. For analysis, MS marker NO711 (**12**) was added to the incubation mixture and, after additional equilibration, the samples were further processed as described above to finally quantify the MS marker **12** by LC-ESI-MS/MS. The affinity of a particular library towards mGAT1 could be expressed accordingly as percentage of remaining NO711 (**12**) binding with low values indicating highly active libraries and vice versa. If a library fulfilled the set “activity-criteria”, its most active components were identified by deconvolution, i.e. screening experiments were performed with single hydrazones instead of libraries containing several hydrazones. Finally, hits from the screening experiments were resynthesized in pure form and evaluated in full-scale binding experiments to establish their binding affinities as pK_i values towards mGAT1.

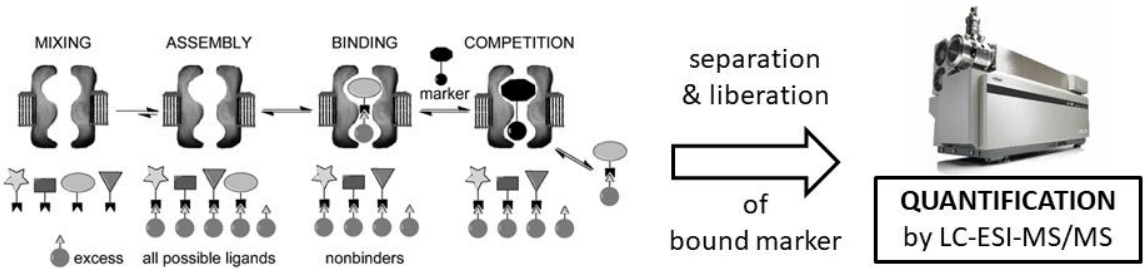

Figure 13: Basic concept of the approach combining the generation of pseudostatic hydrazone libraries and analysis of binding affinities by competitive MS Binding Assays, modified from Sindelar and Wanner[87]

In a first application serving as proof of concept study, nine libraries were applied each constituted with four individual aldehydes. This study yielded compounds with submicromolar affinity towards mGAT1 resembling yet known GAT inhibitors devoid of a hydrazone function in the spacer.[87] Subsequently, a second application based on the same hydrophilic building block **25** converted with focussed aldehyde libraries derived from biphenyl-carbaldehydes revealed new compounds with even higher potencies.[90] Later, the concept of an MS based screening of libraries generated by DCC reactions was transferred to the application of oxime formation as means of linking building blocks.[91] Oximes basically display a higher hydrolytic stability than hydrazones;[92] however, their formation requires a longer reaction time. Due to this lower reactivity, oxime formation was decoupled from the MS based screening and oxime libraries were generated in the absence of the target proteins by preincubating the corresponding building blocks for a sufficient time period. Notably, this approach, in which a guvacine instead of a nipecotic acid moiety was used as parent structure, revealed compound **13** that is still one of the most potent GAT1 inhibitors known up to date (see section 1.2).[91]

Hence, the MS based screening of libraries generated by DCC reaction has already been proven to represent a powerful tool for structure-activity relationship studies with the capability of revealing new, highly potent GAT inhibitors. It enables to screen for the binding affinities of a diverse set of compounds without the need of synthesizing, isolating and purifying all individual components, thus saving expenditure of time and costs. Notably, the amount of individual components per libraries is not restricted to a certain number, although in those aforementioned, initial applications only four compounds per library were tested. In order to increase throughput, the library size

could easily be increased, particularly if it should be exclusively screened for highly potent compounds and thus the concentration of individual components is kept low.

2 Aims and scope

In the research group of Prof. Klaus T. Wanner it is continuously aimed to closely connect the molecular modeling of ligand-target interactions, the organic synthesis of novel compounds and the biological testing of newly synthesized molecules as a medicinal chemical approach of developing advanced bioactive compounds. In an iterative manner, molecular modeling is used to interpret the structure-activity relationship of synthesized and biologically tested compounds in order to be able to design novel compounds with optimized potencies, which can then again be synthesized and evaluated for their biological activities.

For an *in silico* screening, which was conducted previously by Dr. Thomas Wein using our in-house hGAT1 homology model, a virtual library derived from 4- and 5-substituted nipecotic acid derivatives was built. The hypothetical molecules were equipped with a biphenyl or diphenyl residue as lipophilic domain attached to the nipecotic acid moiety in the 4- or 5-position of the piperidine ring via a spacer with 3, 4, 5, or 6 carbon atoms and bearing a double bond in conjugation with the aromatic moiety. The results of this virtual screening at hGAT1 revealed that the substitution of nipecotic acid (**9**) particularly in the 5-position and with a five atom spacer (as in molecule **28**; Figure 14) represents a possible means of obtaining GAT1 ligands with promising docking scores.

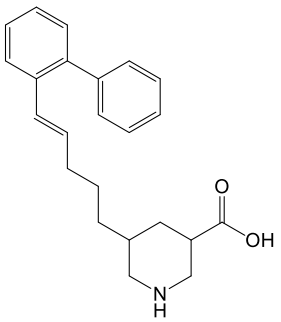

28

Figure 14: Structure of hypothetical molecule **28**

Furthermore, docking calculations showed that in this hypothetical molecule **28** and related 5-substituted nipecotic acid derivatives the piperidine amino group was able to point towards the intracellular side of the binding site and could thus interact with two different hydrogen bond acceptors in this position, while the lipophilic residue would

point to the extracellular side of the pocket (Figure 15). So the binding pose of the piperidine moiety of 5-substituted derivatives would be more similar compared to that of the unsubstituted nipecotic acid (**9**) and opposing to that of tiagabine (**6**), of which the amino group and the attached arylalkyl moiety are facing towards the extracellular side (see section 1.2 and Figure 10).

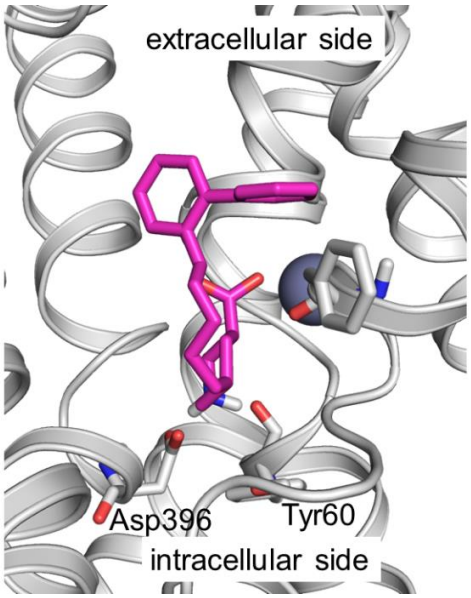

Figure 15: Binding of hypothetical molecule **28** towards hGAT1. The amino group of compound **28** is interacting particularly with the side chain of Asp396 as well as the backbone carbonyl function of Tyr60. The figure was prepared and kindly provided by Dr. Thomas Wein using our in-house hGAT1 homology model refined by molecular dynamics calculations

Based on these *in silico* studies nipecotic acid derivatives substituted in the 5- instead of the common 1-position of the core structure were chosen as target structures of this thesis. These target compounds possessing a lipophilic residue attached to the 5-position of the nipecotic acid moiety via a spacer should be evaluated as potential GABA uptake inhibitors. In order to be able to achieve a vast and easy to perform variety of lipophilic residues it was decided to analyze compound libraries generated by DCC following the approach by Sindelar and Wanner[87] with mGAT1 as target (see section 1.3). Therefore, nipecotic acid derivatives were required as building blocks that were equipped with a hydrazine function (i.e. compounds with general structures **29**–**31**). These hydrazines **29**–**31** should then be converted with diverse aldehydes **26** to afford the corresponding hydrazones with general structures **32**–**34** (Figure 16).

Inspired by the results of the molecular modeling, particularly hydrazones **34** with a total spacer length of five atoms were desired as target structures, which required the nipecotic acid derived building block to possess a two carbon spacer (C2), at the end of which a hydrazine function is attached (i.e. hydrazines **31**). However, also the shorter chained analogs with a total of four (i.e. **33**) and three atoms (i.e. **32**), respectively, which could be obtained from hydrazine building blocks with C1 (i.e. **30**) and C0 spacers (i.e. **29**), should be included in this thesis in order to allow a more comprehensive analysis of the structure-activity relationship of 5-substituted nipecotic acid derivatives. Notably, of all those nipecotic acid derived hydrazines **29**–**31** and hydrazones **32**–**34**, respectively, the attached residue in 5-position can be *cis*- and *trans*-oriented relative to the carboxylic acid function in 3-position of the piperidine moiety. If synthetically accessible, the two diastereomeres of each hydrazone should be examined.

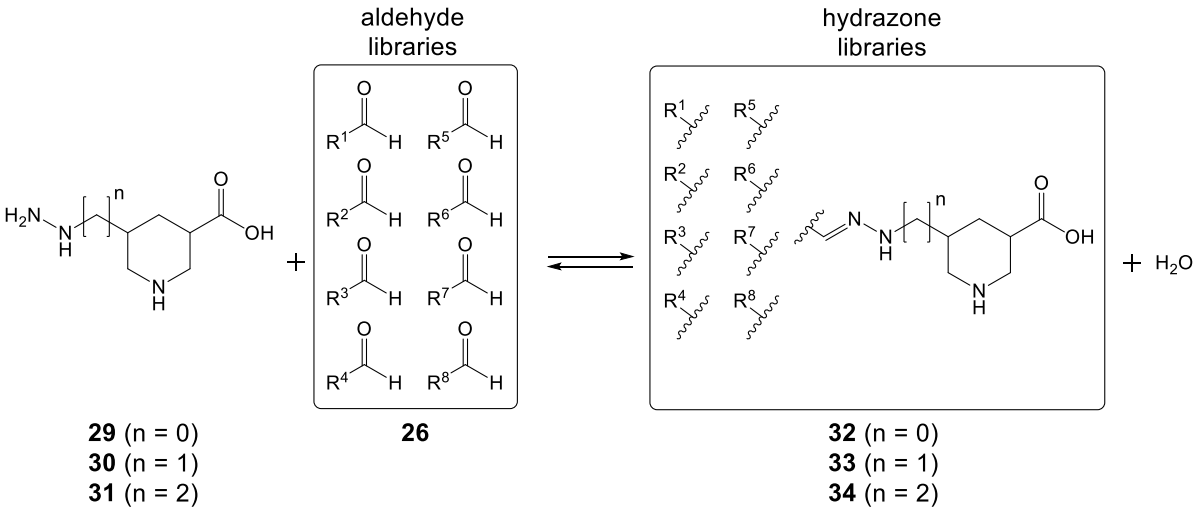

Figure 16: Condensation of hydrazine building blocks **29–31** (in excess) with diverse aldehydes **26** affording target compounds with general structures **32–34**

Besides the syntheses of the hydrazine building blocks **29**–**31**, also new appropriate aldehydes **26** should be gathered in order to be able to screen for a greater structural diversity of potential GAT1 inhibitors. Thus, the total number of aldehydes **26** accessible for the screening experiments should be increased as well as the number of individual aldehydes **26** per library compared to four aldehydes per library employed

in previous approaches using N-substituted nipecotic acid and guvacine derivatives, respectively.

Accordingly, the aims of this thesis were to develop a synthetic concept yielding the hydrazine building blocks **29**–**31**, to compile appropriate aldehyde libraries **26**, and to generate hydrazone libraries **32**–**34** from the aforementioned building blocks, **26** and **29**–**31**, which were then intended to be screened for their binding affinities towards mGAT1 by means of MS Binding Assays. In case hydrazone libraries **32**–**34** were found to be “active” at mGAT1, the whole procedure would furthermore comprise the identification of the most active library components by deconvolution experiments as well as the verification of potential hits by resynthesis of individual hydrazones **32**–**34** and the evaluation of their binding affinities towards mGAT1 in full-scale competitive MS Binding Assays.

Besides this approach allowing to screen for potential GAT1 inhibitors, it was also intended to utilize those hydrazone libraries **32**–**34** generated by DCC in a new kind a screening at mGAT4 (≙ GAT3) by means of functional [^{3}H]GABA uptake assays at this GABA transporter subtype. Considering that the nipecotic acid moiety is also present as parent structure in prototypic mGAT4/GAT3 inhibitors such as (*S*)-SNAP-5114 (**16**) and that the hydrazone libraries **32**–**34** should comprise a vast diversity of different compounds, their screening at mGAT4 was hoped to reveal new insights into the structure-activity relationship and to yield potentially new mGAT4/GAT3 inhibitors.

Despite several antiepileptic drugs have been developed in the past, not all epilepsy patients show a sufficient resolution of symptoms by current medical treatment (see section 1.1). In this context, these two screening approaches of 5-substituted nipecotic acid derivatives at mGAT1 and mGAT4, whereupon those GABA transporters are considered as antiepileptic drug targets, were generally aimed to reveal new structural scaffolds of GABA uptake inhibitors, which could then be utilized as starting points to increase our understanding of the structure-activity relationship and to develop new GABA uptake inhibitors with a different pharmacological profile than previously known compounds.

3 Summary of manuscripts and published results

3.1 Novel allosteric ligands of γ-aminobutyric acid transporter 1 (GAT1) by MS based screening of pseudostatic hydrazone libraries

Molecular modeling studies conducted in our group indicated that substituting the nipecotic acid moiety with lipophilic arylalkyl residues in the 5-position instead, as common, in the 1-position of the core structure could represent an interesting means of obtaining novel GAT1 inhibitors. For proving this *in silico* based hypothesis, it was aimed in this study to develop 5-substituted nipecotic acid derivatives and evaluate their binding affinities towards the murine GABA transporter mGAT1. In order to allow a vast and easy to perform variation of the lipophilic residues attached to the 5-position of the nipecotic acid moiety via a spacer, an approach was chosen that combines the generation of dynamic combinatorial hydrazone libraries with the screening of their binding affinities towards mGAT1 in competitive MS Binding Assays analogously as initially developed by Sindelar and Wanner.[87] As hydrophilic building blocks nipecotic acid derivatives with a one (C1) and two carbon atom (C2) spacer at the 5-position bearing a terminal hydrazine function were synthesized, each in both diastereomeric forms, i.e. the spacer in 5-position being either *cis*- or *trans*-oriented with respect to the carboxylic acid function in 3-position of the piperidine ring. Besides, 224 mostly aromatic aldehydes were compiled representing the lipophilic building blocks. These aldehydes were grouped in 28 libraries, each containing eight individual compounds. For hydrazone library generation, each of the four hydrazine derived building blocks was separately incubated with all aldehyde libraries in presence of the target mGAT1 to yield the hydrazones with a total spacer length of four (derived from C1 hydrazines) and five atoms (from C2 hydrazines). Hence, four sets of hydrazone libraries, termed as *cis*-C1, *trans*-C1, *cis*-C2 and *trans*-C2, respectively, to indicate their relative configurations and different spacer lengths, were generated comprising a total of nearly 900 compounds, which were then screened for their binding affinities towards mGAT1 in MS Binding Assays. Libraries found to be “active” were further examined in deconvolution experiments using only single hydrazones in order to identify their most active components. For hit verification, the most active compounds from the screening and deconvolution experiments were resynthesized in pure form and evaluated in full-scale competitive MS Binding Assays in order to establish their pK_i values. Ten

exclusively *cis*-configured hydrazones were found to be potent mGAT1 ligands exhibiting pK_i values > 6, of which the compound bearing a 5-(1-naphthyl)furan-2-yl residue and a four atom spacer showed the highest binding affinity (pK_i = 6.67±0.03). Surprisingly, the inhibitory potencies (pIC_{50} values) for these hydrazones at mGAT1 established in functional [^{3}H]GABA uptake assays were clearly lower than the pK_i values determined in the MS Binding Assays. This discrepancy of functional activities and binding affinities prompted us to perform further experiments in order to examine the hydrazones' interaction mode at mGAT1. MS based saturation experiments at mGAT1 with NO711 as reporter ligand in the absence and presence of selected hydrazones revealed a noncompetitive inhibition of NO711 binding and further experiments indicated an allosteric mode of action. Accordingly, the evaluated 5-substituted nipecotic acid derived hydrazones display a pharmacological profile distinctly different to that of bench mark mGAT1/GAT1 inhibitors such as tiagabine and could thus represent interesting novel tool compounds for investigations of mGAT1/GAT1 mediated GABA transport.

The original publication is included in the appendix (chapter 8) at the end of this thesis.

Declaration of contributions:

The previous *in silico* studies, which gave the basic idea for this research, were conducted by Dr. Thomas Wein. New aldehydes were gathered and aldehyde libraries were compiled by Simone Huber and me, supported by Dr. Karuna Bhokare, Hans Brabec and Janine Piecek in different post-doc's and undergraduate students' projects, respectively. The syntheses of the nipecotic acid derived building blocks containing a hydrazine function, the generation of the hydrazone libraries and the screening experiments, the generation of single hydrazones and the deconvolutions experiments as well as the syntheses of "active" hydrazones in pure form for hit verification and the determination of their binding affinities (pK_i values) towards mGAT1 were done by me. Further biological studies comprising the [^{3}H]GABA uptake assays, MS Transport Assays as well as the saturation experiments for elucidating the test compounds' interaction modes were accomplished by technical assistants of our group under the supervision of Dr. Georg Höfner. I wrote the manuscript and prepared the figures, schemes and tables, assisted by Dr. Thomas Wein and Dr. Georg Höfner. Prof. Klaus T. Wanner corrected the manuscript.

3.2 MS based screening of 5-substituted nipecotic acid derived hydrazone libraries as ligands of the GABA transporter 1

In the previous study (see section 3.1) 5-substituted nipecotic acid derivatives with novel structures were revealed as new ligands for mGAT1 with interesting pharmacological characteristics. To this end, dynamic combinatorial hydrazone libraries containing nipecotic acid derivatives with a four and five atom spacer between the 5-position of the piperidine ring and the lipophilic moiety, with the spacer being attached in both *cis*- and *trans*-orientation with respect to the carboxylic acid function, were examined. Ten hits were found to be potent mGAT1 ligands exhibiting pK_i values > 6, which exclusively derived from *cis*-configured hydrazones, and amongst these, most were bearing the shorter chained, i.e. including four atoms, spacer.

In order to complement the aforementioned study, 5-substituted nipecotic acid derived hydrazones with a three atom spacer in *cis*-orientation were intended to be screened at mGAT1 by means of MS Binding Assays. As hydrophilic building block, the nipecotic acid derivative bearing a hydrazine function directly attached to the 5-position of the piperidine ring without any additional carbon spacer (C0) and *cis*-oriented with respect to the carboxylic acid function in 3-position was synthesized. This hydrazine was again reacted with the 28 aldehyde libraries, each containing eight individual aldehydes, which were already employed in the previous study, to form the corresponding hydrazone libraries in the presence of the target mGAT1. Amongst the 28 hydrazone libraries, one was found to be “active” by the MS based screening experiments. Deconvolution experiments, performed for identifying the most active components of this “active” library, revealed one hydrazone with promising binding affinity towards mGAT1, which was considered to be the hit of this screening campaign. For hit verification, this hydrazone, bearing a 5-(2-phenylethynyl)thiophen-2-yl residue as lipophilic domain, was resynthesized in pure form and a submicromolar binding affinity (pK_i = 6.62±0.04) was established in full-scale competitive MS Binding Assays. Again, the functional activity, as determined in [^{3}H]GABA uptake assays, was clearly lower and additional MS based saturation experiments revealed a noncompetitive inhibition mode. Thus, the novel hydrazone bearing a three-atom spacer attached to the nipecotic acid moiety likely follows the same mechanistic rationale as the 5-substituted nipecotic acid derived ligands of mGAT1 with longer spacers that had been revealed in the previous screening campaign. Thereby, the herein described hydrazone adds

new insights into the structure-activity relationship of this novel class of ligands for the GABA transporter mGAT1 and could accordingly represent another interesting tool compound for future studies.

The original manuscript is included in the appendix (chapter 8) at the end of this thesis.

Declaration of contributions:

The synthesis of the nipecotic acid derived building block containing a hydrazine function, the generation of the hydrazone libraries and the screening experiments, the generation of single hydrazones and the deconvolutions experiments as well as the synthesis of the "active" hydrazone in pure form for hit verification and the determination of its binding affinity (pK_i value) towards mGAT1 were done by me. Further biological studies comprising the [^{3}H]GABA uptake assays and the saturation experiments for elucidating the test compound's interaction mode were accomplished by technical assistants of our group under the supervision of Dr. Georg Höfner. I wrote the manuscript and prepared the figures, schemes and tables, assisted by Dr. Georg Höfner. Prof. Klaus T. Wanner corrected the manuscript.

3.3 Generation and screening of pseudostatic hydrazone libraries derived from 5-substituted nipecotic acid derivatives at the GABA transporter mGAT4

The GABA transporter mGAT4 (≙ GAT3) is considered a promising drug target for mediating antiepileptic effects. However, due to a lack of highly potent inhibitors for this GAT subtype the elucidation of its full pharmacological potential as a drug target is still retarded (see section 1.2). In order to screen for a vast diversity of compounds aiming to reveal potentially new mGAT4/GAT3 inhibitors, the same pseudostatic hydrazone libraries initially generated as described in the previous two studies (see sections 3.1 and 3.2) and screened at mGAT1 were intended to be utilized in a new kind of screening at mGAT4.

This study describes the generation and screening of these dynamic combinatorial hydrazone libraries at mGAT4. The hydrazone libraries, which included more than 1,100 compounds, are derived from a nipecotic acid moiety as parent structure that was – in contrast to yet known mGAT4 inhibitors – substituted at the 5-position instead of the common 1-position of the core structure. After generating the libraries by preincubating the hydrazine and aldehyde building blocks, respectively, the libraries were screened for their inhibitory potencies in a [^{3}H]GABA uptake assay at mGAT4. Accordingly, two notable adjustments for the library screening at mGAT4 in comparison with the yet established screening at mGAT1 had to be made, while the principle procedure (comprising the steps library generation, library screening, deconvolutions experiments and hit verification) remained the same: I) For screening a functional assay (i.e. [^{3}H]GABA uptake assay) was utilized instead of an MS Binding Assay since due to a lack of a highly potent and selective mGAT4 inhibitors, which could be employed as MS marker, an MS Binding Assay for the target mGAT4 is not yet available. II) The library generation had to be decoupled from the screening experiments since the [^{3}H]GABA uptake assay is based on intact cells expressing the corresponding target proteins (instead of membrane fragments employed in the MS Binding Assay), which would be impaired by the conditions required for *in situ* library generation.

By the screening and subsequent, for identifying most active library components, deconvolution experiments, two new compounds could be identified with promising inhibitory potencies at mGAT4. These two hydrazones were resynthesized in pure form

and evaluated for their inhibitory potencies at mGAT4 and additionally at the other murine GABA transporter subtypes (mGAT1–mGAT3) using a standardized [^{3}H]GABA uptake assay based on HEK cells. Besides, inhibitory potencies at the human equivalent of the target GABA transporter mGAT4, i.e. hGAT3, were established in an MS Transport Assay more recently developed by our group that uses COS cells. The results show that the potencies of the newly synthesized compounds at mGAT4/hGAT3 are in the low micromolar range and close to that of bench mark mGAT4/hGAT3 inhibitor (*S*)-SNAP-5114. Notably, the hydrazones comprise novel structural scaffolds for inhibitors of this target with respect to both the substitution pattern of the nipecotic acid moiety (i.e. in 5-position) and the aromatic residue (i.e. a biphenyl residue). Hence, these compounds add new insights into the structure-activity of mGAT4/hGAT3 inhibitors and could make interesting candidates for further investigation.

The original publication is included in the appendix (chapter 8) at the end of this thesis.

Declaration of contributions:

The syntheses of the nipecotic acid derived building blocks containing a hydrazine function (as described in the previous two studies), the generation of the hydrazone libraries for the screening experiments, the generation of single hydrazones for the deconvolutions experiments and the syntheses of “active” hydrazones in pure form for hit verification were done by me. Conversely, the biological studies comprising the screening experiments, the deconvolution experiments and the full-scale [^{3}H]GABA uptake assays as well as MS Transport Assays were accomplished by technical assistants of our group under the supervision of Dr. Georg Höfner. I wrote the manuscript and prepared the figures, schemes and tables, assisted by Dr. Georg Höfner. Prof. Klaus T. Wanner corrected the manuscript.

4 Further experiments

Besides the research covered in the previous listed publications and manuscripts, which addressed the main aims of this thesis, some additional experiments were performed. Basically, intermediate compounds that were required for the syntheses of hydrazines **29**–**31**, the syntheses of which are described in the first publication (see section 3.1), served as starting points to synthesize nipecotic acid derivatives bearing small substituents in the 5-position, which were intended to be biologically tested on their capability to inhibit GAT mediated GABA uptake. These experiments are described in the following.

4.1 Synthesis of the (*S*)-SNAP-5114 derivative *rac*-**35**

Compound *rac*-**35**, which can be considered a 5-hydroxy nipecotic acid derivative of bench mark GAT3 inhibitor (*S*)-SNAP-5114 (**16**), was intended to be synthesized as target structure in order to examine which influence a hydrophilic substituent in the 5-position of the nipecotic acid moiety would have on the inhibitory potency at GAT3.
The synthesis of *rac*-**35** is outlined in Figure 17. In short, the *tert*-butyloxycarbonyl (Boc) protected, 5-hydroxy nipecotic acid derivative *rac*-**36** (from the first publication, see section 3.1) was, after cleaving the Boc group and without isolating the intermediate, reacted with the tosylate **37**, the latter of which was obtained by the reaction of trityl derivative **38**[93] with 4-toluenesulfonyl chloride and triethylamine (NEt_3). This yielded the methyl ester derivative of *rac*-**35**, *rac*-**39**, in a yield of 70%. By hydrolyzing the ester function of *rac*-**39** with aqueous sodium hydroxide the target compound *rac*-**35** was obtained in a yield of 87%.

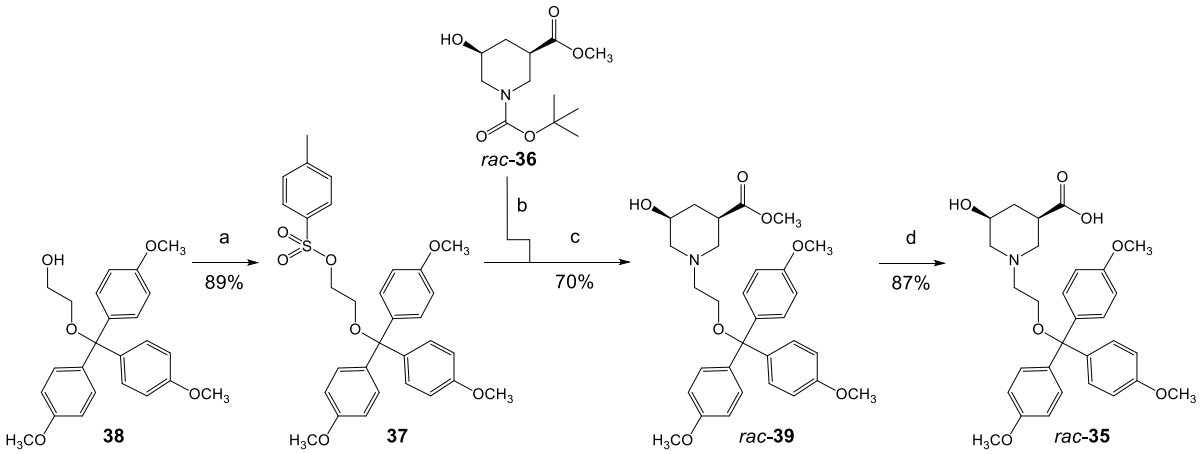

Figure 17: Synthesis of (*S*)-SNAP-5114 derivative *rac*-**35**. Reagents and conditions: a) 4-toluenesulfonyl chloride, NEt_3, DCM, 0 °C→rt, 16 h; b) 2 M etheric HCl, MeOH, rt, 17 h; c) Na_2CO_3, acetone/*iso*-hexane, reflux, 2 d; d) 2 M aqueous NaOH, MeOH, 0 °C→rt, 5 h

4.2 Syntheses of fluorinated nipecotic acid derivatives

The experiments described in this section 4.2 were performed under my supervision by "ERASMUS" student Ronan McShane as well as "Pharmazie-Staatsexamen" students Miriam Schulz and Janine Piecek in course of their research internships in the research group of Prof. Klaus T. Wanner.

Small nipecotic acid derivatives bearing one or two fluorine atoms in the 5-position of the piperidine moiety were intended to be synthesized and biologically tested for their capability to inhibit the different GAT subtypes. To this end, appropriate, 5-substituted nipecotic acid derivatives were employed in deoxofluorination reactions using the reagents diethylaminosulfur trifluoride (DAST; **40**, see Figure 18) or diethylaminodifluorosulfinium tetrafluoroborate (XtalFluor-E; **41**), the latter of which was applied in combination with triethylamine trihydrofluoride ($NEt_3 \cdot 3$ HF) or 1,8-diazabicyclo(5.4.0)undec-7-ene (DBU), analogously as described for different reactions in literature.[94–96]

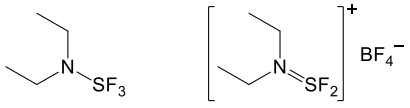

Figure 18: Reagents employed for deoxofluorination reactions

The deoxofluorination reactions were initially employed to alcohol *rac*-**36** and yielded *rac*-**42** as well as the elimination byproduct **43** (see Figure 19). Notably, the stereochemistry of the substituent in 5-position was retained, i.e. the fluoro substituent of *rac*-**42** was still *cis*-oriented after the fluorination reaction with respect to the carboxylic acid function in 3-position.

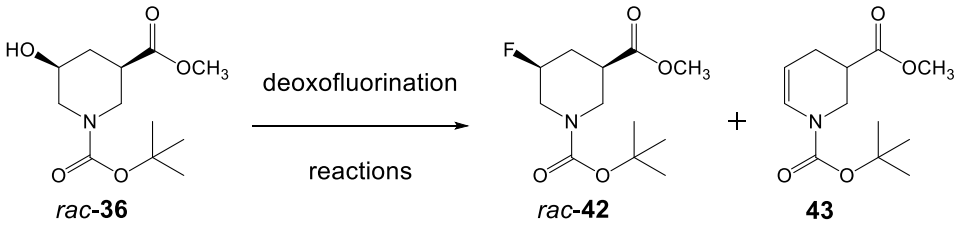

rac-**36** *rac*-**42** **43**

Figure 19: Synthesis of fluorination product *rac*-**42** and elimination byproduct **43** from alcohol *rac*-**36** (reagents and conditions see Table 3)

Based on this synthesis, it was furthermore examined which influence the applied reagent (compound **40** and **41**, respectively) and other varying reaction conditions would have on the yield of *rac*-**42** as well as on the ratio of fluorination (i.e. compound *rac*-**42**) versus elimination product (i.e. **43**). The reagents and conditions as well as the results of these experiments are shown in Table 4. In summary, by utilizing DAST (**40**) as fluorination reagent the yields of the desired product *rac*-**42** were in a similar order of magnitude as those of the elimination byproduct **43** (Table 3, entries 1–3), while by using XtalFluor-E (**41**) the selectivity towards the formation of *rac*-**42** appeared to be increased in most of the attempts (Table 3, entries 4–10, with a notable exception from the tendency of an increased selectivity being entry 6, at which additional amounts of base, NEt_3, were added). However, despite the higher selectivity, the total yield of the desired product *rac*-**42** could apparently not be increased by using XtalFluor-E (**41**). Interestingly, the highest nominal yields of both *rac*-**42** (34%) and **43** (32%) were obtained by using DAST (**40**; Table 3, entry 3).

Table 3: Different reagents and conditions employed for the synthesis of fluorination product *rac*-**42** and elimination byproduct **43** from alcohol *rac*-**36** according to Figure 19

entry	reagents (equivalents)	solvent	temp.	atmos-phere	time	products' ratio[a]	yield[b] *rac*-**42**	yield[b] **43**
1	DAST (1.6 eq.)	DCM	0 °C	air	18 h	1:1	22%	27%
2	DAST (1.7 eq.)	DCM	-78 °C	air	16 h	2:3	14%	24%
3	DAST (1.7 eq.)	DCM	0 °C→rt	air	16 h	1:1	34%	32%
4	XtalFluor-E (1.5 eq.), $NEt_3 \cdot 3$ HF (2.1 eq.)	DCM	0 °C	N_2	72 h	>10:1[c]	21%	2%
5	XtalFluor-E (1.7 eq.), DBU (1.6 eq.)	DCM	0 °C	N_2	16 h	5:2[d]	1%[d]	3%[d]
6	XtalFluor-E (1.5 eq.), $NEt_3 \cdot 3$ HF (2.0 eq.), NEt_3 (1.0 eq.)	DCM	0 °C→rt	Ar	2.5 h	1:1	31%	32%
7	XtalFluor-E (2.3 eq.), $NEt_3 \cdot 3$ HF (3.0 eq.)	DCM	0 °C→rt	Ar	17.5 h	4:1	33%	9%
8	XtalFluor-E (1.5 eq.), $NEt_3 \cdot 3$ HF (1.0 eq.)	DCE	85 °C	Ar	3.5 h	9:1	17%	5%
9	XtalFluor-E (1.3 eq.), $NEt_3 \cdot 3$ HF (3.0 eq.)	DCM	0 °C→rt	Ar	3 h	n.d.[e]	23%	16%
10	XtalFluor-E (2.3 eq.), $NEt_3 \cdot 3$ HF (1.5 eq.)	DCM	0 °C→rt	Ar	3 h	n.d.[e]	18%	1%

[a] The crude ratio of products *rac*-**42**/**43** was determined by ^{1}H NMR.

[b] The isolated yields were determined after purification by flash column chromatography.

[c] Negligible elimination and thus an exact ratio could not be determined.

[d] The observed conversion was very low and accordingly the stated numbers are imprecise.

[e] Not determined.

Simultaneous removal of the protecting groups of compound *rac*-**42** with hydrochloric acid, i.e. cleavage of the Boc group and hydrolysis of the ester function, yielded the free amino acid *rac*-**44**[97] (see Figure 20).

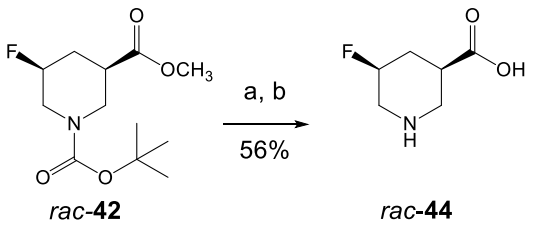

rac-**42** *rac*-**44**

Figure 20: Synthesis of compound *rac*-**44** from *rac*-**42**. Reagents and conditions: a) 1 M aqueous HCl, THF, reflux, 2 h; b) strongly acidic cation exchange chromatography

Besides compound *rac*-**42**, the *trans*-oriented analog of *rac*-**42**, that is *rac*-**45**, and the 5,5-difluoro substituted compound **46** were synthesized in analogous reactions from alcohol *rac*-**47** and ketone **48**, respectively (the syntheses of both starting materials are described in the first publication, see section 3.1). While the difluorinated compound **46** was obtained in moderate to good yield (66%), the yield of *rac*-**45** was rather poor (18%); notably, minor amounts of *rac*-**42** and **43** were observed in the ^{1}H NMR of crude *rac*-**45**, whereas none of these byproducts, *rac*-**42** and **43**, were observed during the formation of compound **46**. Subsequent deprotection reactions again yielded the desired free amino acids *rac*-**49** and **50**, respectively (see Figure 21).

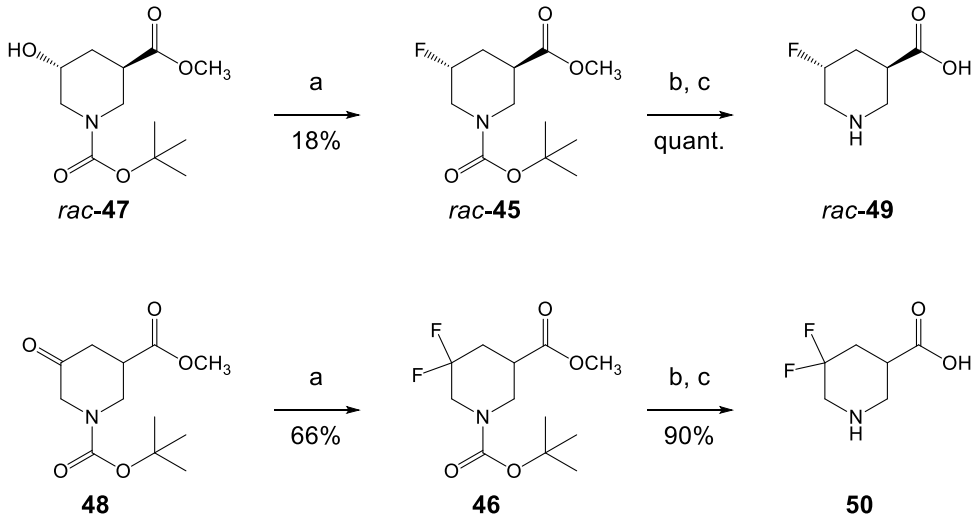

rac-**47** *rac*-**45** *rac*-**49**

48 **46** **50**

Figure 21: Syntheses of compounds *rac*-**49** and **50**, respectively. Reagents and conditions: a) XtalFluor-E, $NEt_3 \cdot 3$ HF, DCM, 0 °C, Ar, 2.3 h (for *rac*-**45**) or 3.7 h (for **46**); b) 1 M aqueous HCl, THF, reflux, 3 h; c) strongly acidic cation exchange chromatography

In addition to the aforementioned amino acids *rac*-**44**, *rac*-**49** and **50**, respectively, the *N*-butyl derivative of *rac*-**44**, i.e. *rac*-**51**, was synthesized. Therefore, compound *rac*-**42**, after cleaving the Boc group, was successively converted with potassium iodide, potassium carbonate and 1-bromobutane to the *N*-butyl derivative *rac*-**52**; finally, by hydrolyzing the ester function the desired compound *rac*-**51** was obtained (see Figure 22).

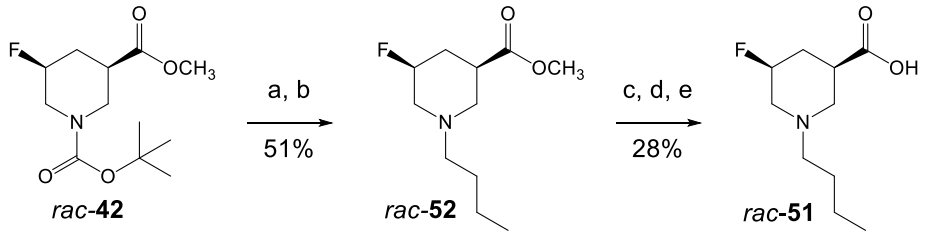

rac-**42** *rac*-**52** *rac*-**51**

Figure 22: Synthesis of compound *rac*-**51** from *rac*-**42**. Reagents and conditions: a) 2 M etheric HCl, MeOH, 6.5 h, rt; b) KI, K_2CO_3, 1-bromobutane, acetone, reflux, 5 d; c) 1 M aqueous HCl, THF, reflux, 1 h; d) 2 M aqueous NaOH, rt, 23 h; e) strongly acidic cation exchange chromatography [note that after step c) minor amounts of starting material remained; so for completing ester hydrolysis, step d) was additionally performed]

4.3 Results of the biological testing

The free amino acids synthesized as described in sections 4.1 and 4.2, i.e. *rac*-**35**, *rac*-**44**, *rac*-**49**, **50** as well as *rac*-**51**, were tested for their inhibitory potencies at the different GAT subtypes in functional assays. To this end, the [^{3}H]GABA uptake assays routinely used in our group (see section 1.3 and literature reference[73]) were employed, which were accomplished by technical assistants of our group under the supervision of Dr. Georg Höfner; the results obtained thereby are summarized in Table 4.

The structure of compound *rac*-**35** was inspired by bench mark GAT3/mGAT4 inhibitor (*S*)-SNAP-5114 (**16**); with *rac*-**35** it should be examined what effect a small, polar substituent, i.e. a hydroxy group, in the 5-position of the nipecotic acid moiety would have on the capability of inhibiting mGAT4. However, the functional activity of *rac*-**35** at this transporter subtype, mGAT4, is clearly lower than that of (*S*)-SNAP-5114 (**16**; see section 1.2, Table 2). Although taking into account that *rac*-**35** is racemic and thus the eutomer could be slightly more potent, it may be concluded that a hydroxy function

in the 5-position of nipecotic acid derived GAT3/mGAT4 inhibitors is not well tolerated and reduces the inhibitory potency at this GAT subtype.

Table 4: Functional activities of compounds *rac*-**35**, *rac*-**44**, *rac*-**49**, **50** and *rac*-**51** at the different GAT subtypes mGAT1–mGAT4

Compound	Inhibitory potencies (pIC_{50})[a]			
	mGAT1	mGAT2	mGAT3	mGAT4
rac-**35**	59%[b]	85%[b]	4.09[c]	4.07[c]
rac-**44**	4.71[c]	82%[b]	73%[b]	87%[b]
rac-**49**	4.89±0.12[d]	67%[b]	4.07±0.06[d]	4.15±0.13[d]
50	3.48[c]	87%[b]	95%[b]	94%[b]
rac-**51**	3.16[c]	108%[b]	101%[b]	113%[b]

[a] The inhibitory potencies derive from the biological tests of our research group based on [^{3}H]GABA uptake assays with HEK293 cells stably expressing the different GAT subtypes mGAT1–mGAT4.

[b] In case of low inhibitory potencies percentages are given that represent the remaining [^{3}H]GABA uptake in presence of 100 µM test compound.

[c] Obtained from less than three experiments and accordingly no SEM value is stated.

[d] Values are given as means±SEM from at least three independently performed experiments.

In addition, a series of 5-fluoro substituted nipecotic acid derivatives, *rac*-**44**, *rac*-**49**, **50** and *rac*-**51**, was synthesized in order to examine what effects one or two fluorine atoms would have on the functional activities at the different GAT subtypes. All these compounds, *rac*-**44**, *rac*-**49**, **50** and *rac*-**51**, show their highest inhibitory potencies at mGAT1, while they appear generally less active at the other GAT subtypes, mGAT2–mGAT4. Remarkably, compounds *rac*-**44** and *rac*-**49** show approximately the same potency at mGAT1 as the unsubstituted, racemic nipecotic acid (**9**; see section 1.2, Table 2), while at the same time the subtype selectivity of the fluorinated compounds *rac*-**44** and *rac*-**49** for mGAT1 appears to be increased. The *trans*-oriented *rac*-**49** appears nominally more potent at all GAT subtypes than the *cis*-oriented *rac*-**44**, although the differences are minor. Conversely, the disubstituted derivative **50** is clearly less potent at mGAT1. Thus it may be concluded that one fluorine atom is well tolerated in the 5-position of the nipecotic acid moiety, retaining potency at and increasing subtype selectivity for mGAT1, while two fluorine atoms in the 5-position reduce the inhibitory potency distinctly. Possibly, the latter observation might be due to the fact that the fluoro substituents decrease the basicity of the amino group; two

fluorine atoms may reduce the basicity to such an extent that the amino group is not sufficiently protonated anymore under physiological conditions, thus leading to impaired ligand-protein interactions.

As described by Wein et al.[64] not pure but N-butylated amino acids might allow a better estimate of the activity at GAT1/mGAT1 when larger arylalkyl residues such as those in tiagabine (**6**) or SK&F-89976A (**11**) are added. Accordingly, the fluorinated, *N*-butyl derivative *rac*-**51** was synthesized and evaluated for its inhibitory potency at mGAT1. The established pIC_{50} value of *rac*-**51** at mGAT1 (i.e. pIC_{50} = 3.16) is in a similar order of magnitude as that of *N*-butyl nipecotic acid without fluoro substituent [reference values for the *R*-enantiomer (pIC_{50} = 3.72) and the *S*-enantiomer (pIC_{50} = 3.12) from literature reference[64]], also taking into account that *rac*-**51** is racemic and thus the eutomer could be slightly more potent. Hence, nipecotic acid derivatives bearing one fluoro substituent in the 5-position of the piperidine ring could be considered as interesting starting points for the development of larger, highly potent GAT1/mGAT1 inhibitors.

4.4 Experimental details and compound characterization data

General methodologies for the syntheses of compounds listed in sections 4.1–4.2: Solvents for synthesis, extraction and flash chromatography were distilled before use. Anhydrous THF was prepared by drying over benzophenone/Na. Other commercially available reagents (by ABCR, Acros, Alfa Aesar, Fisher Scientific, Maybridge, Merck, Sigma-Aldrich, TCI and VWR) were used without further purification. Thin-layer chromatography was carried out on precoated silica gel F_{254} glass plates (Merck) and detected under UV light (λ = 254 and 366 nm) or by staining with a ninhydrin solution (0.3 g ninhydrin and 3 mL acetic acid dissolved in 100 mL 1-butanol).[98] Flash column chromatography was performed on silica gel 60 (grading 0.035–0.070 mm, purchased from Merck and Acros). Strongly acidic cation exchange chromatography was performed on Amberlite® IRA-120 (H^+ form; Merck) with a 25 % aqueous NH_3 solution as solvent. NMR spectroscopy was performed on Avance III HD Bruker BioSpin (Bruker; ^{1}H NMR: 400 or 500 MHz; ^{13}C NMR: 101 or 126 MHz; ^{19}F NMR: 376 MHz) or JNMR-GX (JEOL; ^{1}H NMR: 400 or 500 MHz; ^{13}C NMR: 101 or 126 MHz) spectrometers. The spectra were processed with the NMR software MestReNova, versions 8.1, 10.0 and 12.0 (Mestrelab Research S.L.). Chemical shifts

were internally referenced to TMS or MeOH (for samples dissolved in D_2O). IR spectroscopy was performed on a FT-IR Paragon 1000 (Perkin-Elmer) spectrometer and analyzed with the software Spectrum v2.00 (Perkin-Elmer). Samples were either pressed in KBr pellets or prepared as films between NaCl plates. Mass spectra were measured with a mass spectrometer 59827A with 59980 particle beam LC/MS interface (Hewlett Packard) and high-resolution mass spectrometry was performed with Jeol MStation sector field mass spectrometer (Jeol), Thermo Finnigan MAT 95 (ThermoFischer Scientific) (both EI) or Thermo Finnigan LTQ FT Ultra mass spectrometer (ThermoFischer Scientific) (ESI). Melting points were determined in open capillaries on a BÜCHI 510 melting point apparatus and are uncorrected.

2-[Tris(4-methoxyphenyl)methoxy]ethyl 4-methylbenzene-1-sulfonate (37):

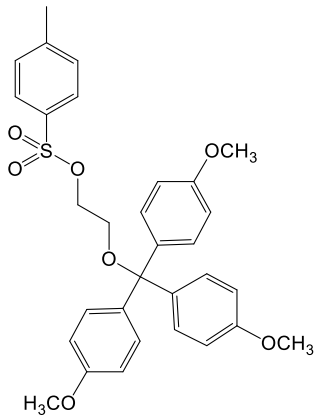

2-[Tris(4-methoxyphenyl)methoxy]ethan-1-ol[93] (**38**; 300 mg; 0.761 mmol) was dissolved in DCM (0.8 mL). Under cooling in an ice bath it was successively added triethylamine (0.16 mL; 1.1 mmol) and 4-toluenesulfonyl chloride (176 mg; 0.921 mmol). The mixture was stirred over night (16 h) while it was allowed to reach rt (0 °C→rt). The reaction was quenched by the addition of H_2O (25 mL). It was extracted with DCM (4 x 25 mL), the combined organic phases were dried over Na_2SO_4 and concentrated under reduced pressure. The crude product was purified by column chromatography (silica gel; ethyl acetate/*iso*-hexane = 1:4) to yield **37** as white solid (371 mg; 89%). mp: 135 °C. R_f = 0.24 (ethyl acetate/*iso*-hexane = 1:4). IR (KBr): $\tilde{\nu}$ = 2953, 2929, 2840, 1736, 1608, 1579, 1509, 1458 cm^{-1}. ^1H NMR (500 MHz, $CDCl_3$, 25 °C, TMS): δ = 2.46 (s, 3 H, CCH_3), 3.24–3.29 (m, 2 H, SOCH$_2$CH_2O), 3.77 (s, 9 H, OCH_3), 4.11–4.15 (m, 2 H, SOCH_2CH$_2$O), 6.76–6.80 (m, 6 H, CCHCHCOCH$_3$), 7.21–7.26 (m, 6 H, CCHCHCOCH$_3$), 7.33 (d, J = 8.0 Hz, 2 H, SCCHCHC), 7.82 (d, J = 8.3

Hz, 2 H, SCC*H*CHC) ppm. ^{13}C NMR (125 MHz, $CDCl_3$, 25 °C, TMS): δ = 14.19 (C*C*H$_3$), 55.18 (O*C*H$_3$), 61.26 (SOCH$_2$*C*H$_2$O), 69.67 (SO*C*H$_2$CH$_2$O), 85.85 (CH$_2$O*C*), 113.06 (CCH*C*HCOCH$_3$), 127.97 (SC*C*HCHC), 129.65 (C*C*HCHCOCH$_3$), 129.82 (SCCH*C*HC), 133.06 (S*C*CHCHC), 136.12 (*C*CHCHCOCH$_3$), 144.67 (SCCHCH*C*), 158.36 (CCHCH*C*OCH$_3$) ppm. MS (ESI): *m/z* = 571.2 (40%, [M+Na]$^+$). HRMS (ESI): [M+Na]$^+$ calcd. for $C_{31}H_{32}O_7SNa$: 571.1766; found 571.1764.

rac-(3*R*,5*S*)-(Methyl 5-hydroxy-1-{2-[tris(4-methoxyphenyl)methoxy]ethyl}piperidine-3-carboxylate) (_rac_-39):

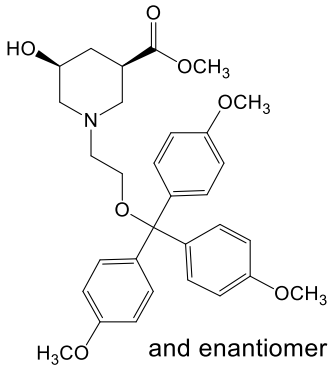

Compound *rac*-**36** (163 mg; 0.629 mmol) was dissolved in MeOH (3.0 mL) and a 2 M etheric HCl (3.0 mL; 6.0 mmol) was added. The mixture was stirred at rt over night (17 h). Then the reaction was quenched by the addition of a saturated aqueous $NaHCO_3$ solution (10 mL) and diluted with H_2O (20 mL). The aqueous phase was washed with ethyl acetate (1 x 20 mL) and freeze dried. To the residue Na_2CO_3 (320 mg; 3.02 mmol) and subsequently **37** (164 mg; 0.299 mmol), dissolved in acetone (2.0 mL) and *iso*-hexane (0.5 mL), were added. Further acetone (3.0 mL) was added and the mixture was stirred at room temperature for 5 h and then refluxed for 2 d. The reaction was quenched with H_2O (30 mL) and extracted with DCM (4 x 25 mL). The combined organic phases were dried over Na_2SO_4 and concentrated under reduced pressure. After purification by column chromatography (silica gel; ethyl acetate) *rac*-**39** was obtained as white amorphous solid (113 mg; 70%). R_f = 0.30 (ethyl acetate). IR (KBr): $\tilde{\nu}$ = 3429, 2950, 2933, 2835, 1734, 1607, 1508, 1463, 1440 cm^{-1}. ^{1}H NMR (400 MHz, $CDCl_3$, 25 °C, TMS): δ = 2.03–2.20 (m, 1 H, NCH$_2$CHC*H*$_{ax}$H$_{eq}$), 2.08 (t, *J* = 9.7 Hz, 1 H, NC*H*$_{ax}$H$_{eq}$CH$_{ax}$OH), 2.15 (d, *J* = 12.9 Hz, 1 H, NCH$_2$CHCH$_{ax}$*H*$_{eq}$), 2.33 (t, *J* = 10.5 Hz, 1 H, NC*H*$_{ax}$H$_{eq}$CH$_{ax}$C=O), 2.57–2.69 (m, 1 H, NCH$_{ax}$H$_{eq}$C*H*$_{ax}$C=O), 2.68 (t, *J* = 5.9 Hz, 2 H, NC*H*$_2$CH$_2$O), 2.86 (d, *J* = 8.8 Hz, 1 H, NCH$_{ax}$*H*$_{eq}$CH$_{ax}$OH), 2.92 (d, *J* = 11.2

Hz, 1 H, $NCH_{ax}H_{eq}CH_{ax}C{=}O$), 3.19 (t, J = 5.9 Hz, 2 H, NCH_2CH_2O), 3.66 (s, 3 H, $COOCH_3$), 3.72–3.77 (m, 1 H, $NCH_{ax}H_{eq}CH_{ax}OH$), 3.78 (s, 9 H, $CCHCHCOCH_3$), 6.79–6.84 (m, 6 H, $CCHCHCOCH_3$), 7.29–7.35 (m, 6 H, $CCHCHCOCH_3$) ppm. ^{13}C NMR (125 MHz, $CDCl_3$, 25 °C, TMS): δ = 34.85 (NCH_2CHCH_2), 40.18 ($NCH_2CHC{=}O$), 51.93 ($COOCH_3$), 55.04 ($NCH_2CHC{=}O$), 55.19 ($CCHCHCOCH_3$), 57.83 (NCH_2CH_2O), 60.94 (NCH_2CHOH), 61.27 (NCH_2CH_2O), 66.45 (NCH_2CHOH), 85.79 (CH_2OC), 113.03 ($CCHCHCOCH_3$), 129.73 ($CCHCHCOCH_3$), 136.79 ($CCHCHCOCH_3$), 158.26 ($CCHCHCOCH_3$), 174.27 ($NCH_2CHC{=}O$) ppm. MS (ESI): *m/z* = 536.3 (20%, $[M+H]^+$). HRMS (ESI): $[M+H]^+$ calcd. for $C_{31}H_{38}O_7N^+$: 536.2648; found 536.2643.

rac-(3*R*,5*S*)-(5-Hydroxy-1-{2-[tris(4-methoxyphenyl)methoxy]ethyl}piperidine-3-carboxylic acid) (_rac_-35):

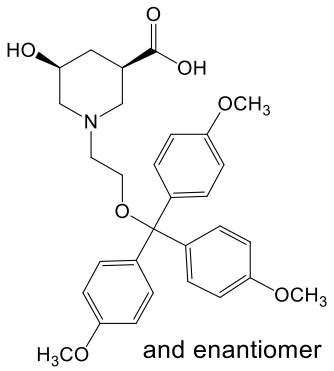

and enantiomer

Compound *rac*-**39** (102 mg; 0.190 mmol) was dissolved in MeOH (1.5 mL) and a 2 M aqueous NaOH solution (0.25 mL; 0.50 mmol) was added at 0 °C. The mixture was stirred at 0 °C for 2 h and at rt for further 3 h, before it was quenched with H_2O (25 mL). The mixture was neutralized with 2 M HCl, and after adding phosphate buffer (pH 7; 1.0 mL) the aqueous phase was extracted with DCM (5 x 25 mL). The combined organic phases were dried over Na_2SO_4 and concentrated under reduced pressure. The residue was redissolved in DCM and *iso*-hexane was added to the solution until the product precipitated. The solid was filtered off and dried under high vacuum to yield *rac*-**35** as white amorphous solid (91 mg; 87%). R_f = 0.15 (DCM + 7.5% MeOH). IR (Film): $\tilde{\nu}$ = 3301, 2928, 1606, 1507, 1462 cm^{-1}. ^1H NMR (500 MHz, DMSO-d_6, 25 °C, TMS): δ = 1.08 (q, *J* = 12.2 Hz, 1 H, $NCH_2CHCH_{ax}H_{eq}$), 1.67 (t, *J* = 10.2 Hz, 1 H, $NCH_{ax}H_{eq}CH_{ax}OH$), 1.85 (t, *J* = 11.2 Hz, 1 H, $NCH_{ax}H_{eq}CH_{ax}C{=}O$), 2.07 (d, *J* = 12.3 Hz, 1 H, $NCH_2CHCH_{ax}H_{eq}$), 2.35–2.47 (m, 1 H, $NCH_{ax}H_{eq}CH_{ax}C{=}O$), 2.55 (t, *J* = 5.8 Hz, 2 H, NCH_2CH_2O), 2.85 (dd, *J* = 10.6/4.3 Hz, 1 H, $NCH_{ax}H_{eq}CH_{ax}OH$), 2.96 (dd, *J* =

11.0/3.7 Hz, 1 H, $NCH_{ax}H_{eq}CH_{ax}C=O$), 2.98–3.05 (m, 2 H, NCH_2CH_2O), 3.47 (ddd, *J* = 14.8/9.4/4.2 Hz, 1 H, $NCH_{ax}H_{eq}CH_{ax}OH$), 3.73 (s, 9 H, $CCHCHCOCH_3$), 6.83–6.90 (m, 6 H, $CCHCHCOCH_3$), 7.22–7.29 (m, 6 H, $CCHCHCOCH_3$) ppm. ^{13}C NMR (126 MHz, DMSO-d_6, 25 °C, TMS): δ = 36.09 (NCH_2CHCH_2), 40.18 ($NCH_2CHC=O$), 54.89 ($CCHCHCOCH_3$), 55.11 ($NCH_2CHC=O$), 57.11 (NCH_2CH_2O), 61.16 (NCH_2CH_2O/NCH_2CHOH), 61.26 (NCH_2CH_2O/NCH_2CHOH), 65.43 (NCH_2CHOH), 85.01 (CH_2OC), 112.97 ($CCHCHCOCH_3$), 129.23 ($CCHCHCOCH_3$), 136.36 ($CCHCHCOCH_3$), 157.75 ($CCHCHCOCH_3$), 174.43 ($NCH_2CHC=O$) ppm. MS (ESI): *m/z* = 520.2 (100%, $[M-H]^-$). HRMS (ESI): $[M-H]^-$ calcd. for $C_{30}H_{34}O_7N^-$: 520.2341; found 520.2340.

rac-(3*R*,5*S*)-[1-(*tert*-Butyl) 3-methyl 5-fluoropiperidine-1,3-dicarboxylate] (_rac_-42):

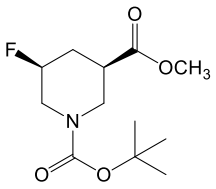

and enantiomer

Compound *rac*-**36** (955 mg; 3.68 mmol) was dissolved in DCM (15 mL) and cooled to 0 °C. DAST (**40**; 0.85 mL; 6.2 mmol) was added and it was stirred over night while the mixture was allowed to reach rt (0 °C→rt). The reaction was quenched with a 10 % Na_2CO_3 solution in ice water and stirred for further 15 min. Then the mixture was extracted with DCM (4 x 30 mL). The combined organic phases were dried over $MgSO_4$ and concentrated under reduced pressure. After purification by column chromatography (silica gel; ethyl acetate/*iso*-hexane = 1:5) *rac*-**42** was obtained as white amorphous solid (327 mg; 34%). R_f = 0.34 (ethyl acetate/*iso*-hexane = 1:5). IR (KBr): $\tilde{\nu}$ = 3008, 2977, 2955, 2873, 1737, 1695, 1475, 1451, 1421 cm^{-1}. ^1H NMR (400 MHz, $C_2Cl_4D_2$, 80 °C, TMS): δ = 1.45 (s, 9 H, $OC(CH_3)_3$), 1.78 (pseudo-quin, *J* ~ 11 Hz, 1 H, $NCH_2CHCH_{ax}H_{eq}$), 2.34–2.47 (m, 1 H, $NCH_2CHCH_{ax}H_{eq}$), 2.45–2.58 (m, 1 H, $NCH_{ax}H_{eq}CH_{ax}C=O$), 2.81 (ddd, *J* = 12.8/9.5/5.5 Hz, 1 H, $NCH_{ax}H_{eq}CH_{ax}F$), 2.88 (dd, *J* = 13.1/10.4 Hz, 1 H, $NCH_{ax}H_{eq}CH_{ax}C=O$), 3.69 (s, 3 H, OCH_3), 4.05–4.23 (m, 2 H, $NCH_{ax}H_{eq}CH_{ax}C=O$, $NCH_{ax}H_{eq}CH_{ax}F$), 3.65 (dtt, *J* = 47.6/9.8/4.6 Hz, 1 H, $NCH_{ax}H_{eq}CH_{ax}F$) ppm. ^{13}C NMR (101 MHz, $C_2Cl_4D_2$, 80 °C, TMS): δ = 28.37

(OC(CH$_3$)$_3$), 33.29 (d, J_{CF} = 20.9 Hz, NCH$_2$CHCH$_2$), 39.65 (d, J_{CF} = 8.9 Hz, NCH$_2$$C$HC=O), 44.86 (N$CH_2$CHC=O), 47.73 (d, J_{CF} = 28.5 Hz, NCH$_2$CHF), 51.90 (OCH$_3$), 80.45 (OC(CH$_3$)$_3$), 85.86 (d, J_{CF} = 176.5 Hz NCH$_2$$C$HF), 154.31 (N$C$=O), 171.90 (NCH$_2CHC$=O) ppm. ^{19}F {^{1}H} NMR (376 MHz, $C_2Cl_4D_2$, 80 °C): δ = 180.92 ppm. MS (EI, 70 eV): *m/z* = 261.1 (3%, [M]$^{+\bullet}$), 205.1 (25%), 188.1 (55%), 174.1 (40%), 160.1 (40%), 141.2 (100%). HRMS (EI, 70 eV): [M]$^{+\bullet}$ calcd. for $C_{12}H_{20}O_4NF$: 261.1376; found 261.1380.

***rac*-(3*R*)-[1-(*tert*-Butyl) 3-methyl 3,4-dihydropyridine-1,3(2*H*)-dicarboxylate] (43):**

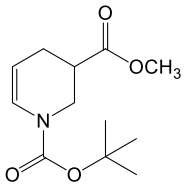

Compound **43** was obtained as byproduct in the synthesis of *rac*-**42** as colorless oil (280 mg; 32%). R_f = 0.47 (ethyl acetate/*iso*-hexane = 1:5). IR (Film): $\tilde{\nu}$ = 2977, 2954, 2934, 1739, 1706, 1654, 1476, 1457 cm^{-1}. ^{1}H NMR (400 MHz, $C_2Cl_4D_2$, 80 °C, TMS): δ = 1.47 (s, 9 H, OC(CH_3)$_3$), 2.23–2.32 (m, 2 H, NCH$_2$CHCH_{ax}H$_{eq}$, NCH$_2$CHCH$_{ax}$$H_{eq}$), 2.67–2.82 (m, 1 H, NCH$_{ax}$H$_{eq}$CH_{ax}C=O), 3.35 (dd, J = 12.8/9.7 Hz, 1 H, NCH_{ax}H$_{eq}$CH$_{ax}$C=O), 3.69 (s, 3 H, OCH_3), 4.03 (d, J = 12.2 Hz, 1 H, NCH$_{ax}$$H_{eq}CH_{ax}$C=O), 4.74–4.91 (m, 1 H, NCHCHCH$_2$), 6.77 (d, J = 8.5 Hz, 1 H, NCHCHCH$_2$) ppm. ^{13}C NMR (101 MHz, $C_2Cl_4D_2$, 80 °C, TMS): δ = 24.66 (NCH$_2$CHCH$_2$), 28.35 (OC(CH$_3$)$_3$), 38.32 (NCH$_2$$C$HC=O), 43.10 (N$CH_2$CHC=O), 51.79 (O$CH_3$), 80.94 (O$C$(CH$_3$)$_3$), 103.45 (NCH$CHCH_2$), 125.73 (N$C$HCHCH$_2$), 152.14 (N$C$=O), 173.35 (NCH$_2CHC$=O) ppm. MS (EI, 70 eV): *m/z* = 241.1 (20%, [M]$^{+\bullet}$), 185.1 (20%), 168.0 (15%), 141.0 (100%). HRMS (EI, 70 eV): [M]$^{+\bullet}$ calcd. for $C_{12}H_{19}O_4N$: 241.1314; found 241.1319.

***rac*-(3*R*,5*S*)-[5-Fluoropiperidine-3-carboxylic acid][97] (*rac*-44):**

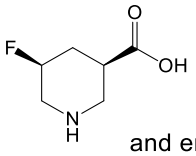

and enantiomer

Compound *rac*-**42** (112 mg; 0.429 mmol) was dissolved in THF (1.0 mL) and 1 M HCl (4.0 mL; 4.0 mmol) was added. The solution was refluxed for 2 h before the reaction was quenched with H_2O (20 mL). Then the aqueous phase was washed with DCM (3 x 15 mL) and freeze dried. The residue was purified by strongly acidic cation exchange chromatography with a 25 % aqueous NH_3 solution as solvent to yield *rac*-**44** as white lyophilisate (35 mg; 56%). IR (KBr): $\tilde{\nu}$ = 3434, 3176, 3011, 2965, 2923, 2852, 2679, 2518, 2377,2346, 2306, 1588, 1565, 1467, 1454 cm^{-1}. ^1H NMR (400 MHz, 1 M NaOD in D_2O, 25 °C, MeOH): δ = 1.79 (quin, J = 10.8 Hz, 1 H, $NCH_2CHCH_{ax}H_{eq}$), 2.27–2.49 (m, 2 H, $NCH_2CHCH_{ax}H_{eq}$, $NCH_{ax}H_{eq}CH_{ax}C{=}O$), 2.49–2.68 (m, 2 H, $NCH_{ax}H_{eq}CH_{ax}C{=}O$, $NCH_{ax}H_{eq}CH_{ax}F$), 3.01 (d, J = 12.3 Hz, 1 H, $NCH_{ax}H_{eq}CH_{ax}C{=}O$), 3.17 (t, J = 10.5 Hz, 1 H, $NCH_{ax}H_{eq}CH_{ax}F$), 4.67 (dm, J_{HF} = 47.7 Hz, 1 H, $NCH_{ax}H_{eq}CH_{ax}F$) ppm. ^{13}C NMR (101 MHz, 1 M NaOD in D_2O, 25 °C, MeOH): δ = 34.85 (d, J_{CF} = 18.8 Hz, NCH_2CHCH_2), 44.64 (d, J_{CF} = 7.6 Hz, $NCH_2CHC{=}O$), 47.81 ($NCH_2CHC{=}O$), 49.52 (d, J_{CF} = 25.2 Hz, NCH_2CHF), 90.20 (d, J_{CF} = 170.1 Hz NCH_2CHF), 182.60 ($NCH_2CHC{=}O$) ppm. ^{19}F {^1H} NMR (376 MHz, 1 M NaOD in D_2O, 25 °C): δ = 178.78 ppm. MS (ESI): m/z = 148.1 (100%, $[M+H]^+$). HRMS (ESI): $[M+H]^+$ calcd. for $C_6H_{11}O_2N$: 148.0768; found 148.0768.

No analytical data is described for compound *rac*-**44** in reference.[97]

***rac*-(3*R*,5*R*)-[1-(*tert*-Butyl) 3-methyl 5-fluoropiperidine-1,3-dicarboxylate] (*rac*-45):**

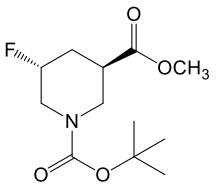

and enantiomer

Compound *rac*-**47** (137 mg; 0.528 mmol) was dissolved in DCM (2.0 mL) and cooled to 0 °C under argon atmosphere. Triethylamine trihydrofluoride (256 mg; 1.59 mmol)

and XtalFluor-E (**41**; 288 mg; 1.23 mmol), dissolved in DCM (1.7 mL), were successively added and the mixture was stirred at 0 °C for 140 min. The reaction was quenched with a 5 % aqueous Na_2CO_3 solution (10 mL), stirred at rt for further 15 min and then it was extracted with DCM (5 x 15 mL). The combined organic phases were dried over Na_2SO_4 and concentrated under reduced pressure. After purification by column chromatography (silica gel; ethyl acetate/*iso*-hexane = 1:5) *rac*-**45** was obtained as white amorphous solid (25 mg; 18%). R_f = 0.20 (ethyl acetate/*iso*-hexane = 1:5). IR (film): $\tilde{\nu}$ = 2976, 2956, 2935, 2868, 1737, 1698, 1478, 1456 cm^{-1}. ^1H NMR (400 MHz, $C_2Cl_4D_2$, 80 °C, TMS): δ = 1.44 (s, 9 H, OC(CH_3)$_3$), 1.81 (dddd, J = 38.2/14.1/11.1/2.6 Hz, 1 H, $NCH_2CHCH_{ax}H_{eq}$), 2.22–2.32 (m, 1 H, $NCH_2CHCH_{ax}H_{eq}$), 2.85 (tt, J = 10.6/3.9 Hz, 1 H, $NCH_{ax}H_{eq}CH_{ax}C$=O), 2.90–3.10 (m, 2 H, $NCH_{ax}H_{eq}CH_{ax}C$=O, $NCH_{ax}H_{eq}CH_{eq}F$), 3.68 (s, 3 H, OCH_3), 4.06–4.15 (m, 1 H, $NCH_{ax}H_{eq}CH_{eq}F$), 4.18 (d, J = 12.5 Hz, 1 H, $NCH_{ax}H_{eq}CH_{ax}C$=O), 4.75 (dtt, J = 46.6/4.4/2.3 Hz, 1 H, $NCH_{ax}H_{eq}CH_{eq}F$). ^{13}C NMR (101 MHz, $C_2Cl_4D_2$, 80 °C, TMS): δ = 28.38 (OC(CH_3)$_3$), 31.83 (d, J_{CF} = 21.5 Hz, NCH_2CHCH_2), 36.73 (d, J_{CF} = 1.9 Hz, NCH_2CHC=O), 45.21 (NCH_2CHC=O), 47.48 (d, J_{CF} = 22.7 Hz, NCH_2CHF), 51.79 (OCH_3), 80.18 (OC(CH_3)$_3$), 85.14 (d, J_{CF} = 174.6 Hz NCH_2CHF), 154.80 (NC=O), 173.04 (NCH_2CHC=O) ppm. ^{19}F {^1H} NMR (376 MHz, $C_2Cl_4D_2$, 80 °C): δ = 185.42 ppm. MS (EI, 70 eV): *m/z* = 261.1 (1%, $[M]^{+\bullet}$), 206.1 (9%), 205.1 (12%), 204.1 (14%), 202.1 (12%), 188.1 (32%), 174.1 (20%), 160.1 (29%), 141.1 (43%), 102.1 (15%), 82.1 (33%), 57.1 (100%). HRMS (EI, 70 eV): $[M]^{+\bullet}$ calcd. for $C_{12}H_{20}O_4NF$: 261.1376; found 261.1383.

rac-(3*R*)-[1-(*tert*-Butyl) 3-methyl 5,5-difluoropiperidine-1,3-dicarboxylate] (46):

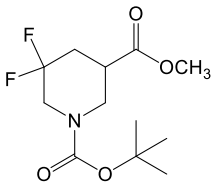

XtalFluor-E (**41**; 617 mg; 2.64 mmol) was dissolved in DCM (2.0 mL) and cooled to 0 °C under argon atmosphere. Triethylamine trihydrofluoride (545 mg; 3.38 mmol) and compound **48** (275 mg; 1.07 mmol), dissolved in DCM (1.7 mL) were successively added and the mixture was stirred at 0 °C for 220 min. The reaction was quenched with a 5 % aqueous Na_2CO_3 solution (10 mL), stirred at rt for further 15 min and then

it was extracted with DCM (5 x 15 mL). The combined organic phases were dried over Na_2SO_4 and concentrated under reduced pressure. After purification by column chromatography (silica gel; ethyl acetate/*iso*-hexane = 1:5) **46** was obtained as white amorphous solid (197 mg; 66%). R_f = 0.32 (ethyl acetate/*iso*-hexane = 1:5). IR (KBr): $\tilde{\nu}$ = 3028, 3009, 2986, 2972, 1737, 1701, 1465 cm^{-1}. ^1H NMR (400 MHz, $C_2Cl_4D_2$, 80 °C, TMS): δ = 1.45 (s, 9 H, OC(CH_3)$_3$), 1.99 (dddd, J = 31.1/13.8/11.8/5.3 Hz, 1 H, $NCH_2CHCH_{ax}H_{eq}$), 2.38–2.50 (m, 1 H, $NCH_2CHCH_{ax}H_{eq}$), 2.72–2.90 (m, 2 H, $NCH_{ax}H_{eq}CH_{ax}C{=}O$, $NCH_{ax}H_{eq}CH_{ax}C{=}O$), 2.99 (dddd, J = 29.1/13.8/1.7 Hz, 1 H, $NCH_{ax}H_{eq}CF_2$), 3.70 (s, 3 H, OCH_3), 4.17–4.28 (m, 1 H, $NCH_{ax}H_{eq}CF_2$), 4.31 (d, J = 11.6 Hz, 1 H, $NCH_{ax}H_{eq}CH_{ax}C{=}O$) ppm. ^{13}C NMR (101 MHz, $C_2Cl_4D_2$, 80 °C, TMS): δ = 28.30 (OC(CH_3)$_3$), 35.09 (t, J_{CF} = 25.0 Hz, NCH_2CHCH_2), 38.93 (d, J_{CF} = 8.7 Hz, $NCH_2CHC{=}O$), 44.72 ($NCH_2CHC{=}O$), 49.34 (dd, J_{CF} = 35.8/28.2 Hz, NCH_2CF_2), 52.07 (OCH_3), 80.94 ($OC(CH_3)_3$), 118.80 (t, J_{CF} = 244.3 Hz NCH_2CF_2), 154.24 ($NC{=}O$), 171.41 ($NCH_2CHC{=}O$) ppm. ^{19}F {^1H} NMR (376 MHz, $C_2Cl_4D_2$, 80 °C): δ = 101.24 (d, J_{FF} = 243.4 Hz), 104.28 (d, J_{FF} = 243.2 Hz) ppm. MS (EI, 70 eV): *m/z* = 279.1 (2%, $[M]^{+\bullet}$), 206.1 (11%), 159.1 (28%), 97.1 (11%), 83.1 (14%), 81.1 (11%), 71.1 (17%), 69.1 (19%), 57.1 (100%). HRMS (EI, 70 eV): $[M]^{+\bullet}$ calcd. for $C_{12}H_{19}O_4NF_2$: 279.1282; found 279.1263.

***rac*-(3*R*,5*R*)-(5-Fluoropiperidine-3-carboxylic acid) (*rac*-49):**

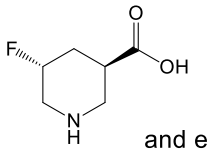

and enantiomer

Compound *rac*-**45** (53 mg; 0.20 mmol) was dissolved in THF (2.2 mL) and 1 M HCl (2.2 mL; 2.2 mmol) was added. The solution was refluxed for 3 h before the reaction was quenched with H_2O (20 mL). The aqueous phase was washed with DCM (3 x 15 mL) and freeze dried. The residue was purified by strongly acidic cation exchange chromatography with a 25 % aq. NH_3 solution as solvent to yield *rac*-**49** as white lyophilisate (30 mg; quant.). IR (KBr): $\tilde{\nu}$ = 3431, 3008, 2960, 2931, 2822, 2785, 2723, 2629, 2583, 2529, 2464, 2373, 2134, 1636, 1579, 1464, 1453 cm^{-1}. ^1H NMR (400 MHz, 1 M NaOD in D_2O, 25 °C, MeOH): δ = 1.76 (dddd, J = 45.6/14.5/12.6/2.3 Hz, 1 H, $NCH_{ax}H_{eq}CH(COOH)CH_{ax}H_{eq}$), 2.18–2.31 (m, 1 H, $NCH_{ax}H_{eq}CH(COOH)CH_{ax}H_{eq}$), 2.54 (dd, J = 12.6/11.2 Hz, 1 H, $NCH_{ax}H_{eq}CHCOOH$),

2.57–2.67 (m, 1 H, $NCH_{ax}H_{eq}CHCOOH$), 2.68 (dd, J = 41.3/14.8 Hz, 1 H, $NCH_{ax}H_{eq}CHF$), 3.04–3.15 (m, 2 H, $NCH_{ax}HCHCOOH$, $NCH_{ax}HCHF$), 4.79–4.91 (m, 1 H, $NCH_{ax}H_{eq}CHF$) ppm. ^{13}C NMR (101 MHz, 1 M NaOD in D_2O, 25 °C, MeOH): δ = 32.15 (d, J_{CF} = 22.1 Hz, $NCH_2CH(COOH)CH_2$), 40.64 ($NCH_2CHCOOH$), 47.30 ($NCH_2CHCOOH$), 47.78 (d, J_{CF} = 21.2 Hz, NCH_2CHF), 88.16 (d, J_{CF} = 163.8 Hz NCH_2CHF), 183.06 ($COOH$) ppm. ^{19}F {^1H} NMR (376 MHz, 1 M NaOD in D_2O, 25 °C): δ = 185.59 ppm. MS (EI, 70 eV): *m/z* = 147.1 (26%, $[M]^{+\bullet}$), 127.1 (100%), 101.0 (49%). HRMS (EI, 70 eV): $[M]^{+\bullet}$ calcd. for $C_6H_{10}O_2NF$: 147.0696; found 147.0688.

***rac*-(3*R*)-(5,5-difluoropiperidine-3-carboxylic acid) (50):**

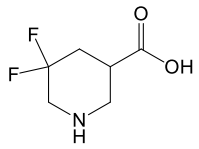

Compound **46** (128 mg; 0.458 mmol) was dissolved in THF (5.0 mL) and 1 M HCl (5.0 mL; 5.0 mmol) was added to the solution. The mixture was stirred at rt for 30 min and refluxed for 3 h, before the reaction was quenched with H_2O (25 mL). The aqueous phase was washed with DCM (3 x 20 mL) and freeze dried. The residue was purified by strongly acidic cation exchange chromatography with a 25 % aq. NH_3 solution as solvent to yield **50** as white lyophilisate (68 mg; 90%). IR (KBr): $\tilde{\nu}$ = 3430, 3022, 2979, 2807, 2671, 2528, 1595, 1460 cm^{-1}. ^1H NMR (400 MHz, 1 M NaOD in D_2O, 25 °C, MeOH): δ = 1.93–2.12 (m, 1 H, $NCH_2CHCH_{ax}H_{eq}$), 2.34–2.46 (m, 1 H, $NCH_2CHCH_{ax}H_{eq}$), 2.53–2.68 (m, 2 H, $NCH_{ax}H_{eq}CH_{ax}C{=}O$, $NCH_{ax}H_{eq}CH_{ax}C{=}O$), 2.83 (ddd, J = 30.4/13.9/1.8 Hz, 1 H, $NCH_{ax}H_{eq}CF_2$), 3.08–3.19 (m, 2 H, $NCH_{ax}HCH_{ax}C{=}O$, $NCH_{ax}HCF_2$) ppm. ^{13}C NMR (101 MHz, 1 M NaOD in D_2O, 25 °C, MeOH): δ = 36.21 (dd, J_{CF} = 24.3/22.2 Hz, NCH_2CHCH_2), 44.75 (d, J_{CF} = 7.3 Hz, $NCH_2CHC{=}O$), 47.47 ($NCH_2CHC{=}O$), 50.48 (dd, J_{CF} = 29.4/26.6 Hz, NCH_2CF_2), 121.95 (dd, J_{CF} = 243.5/240.9 Hz, NCH_2CF_2), 181.53 ($NCH_2CHC{=}O$) ppm. ^{19}F {^1H} NMR (376 MHz, 1 M NaOD in D_2O, 25 °C): δ = 99.42 (d, J_{FF} = 239.1 Hz), 103.53 (d, J_{FF} = 239.1 Hz) ppm. MS (EI, 70 eV): *m/z* = 165.1 (9%, $[M]^{+\bullet}$), 146.1 (9%), 145.1 (100%), 120.1 (29%), 119.1 (24%), 101.0 (18%), 100.1 (39%). HRMS (EI, 70 eV): $[M]^{+\bullet}$ calcd. for $C_6H_9O_2NF_2$: 165.0601; found 165.0592.

***rac*-(3*R*,5*S*)-(1-Butyl 3-methyl 5-fluoropiperidine-3-carboxylate) (*rac*-52):**

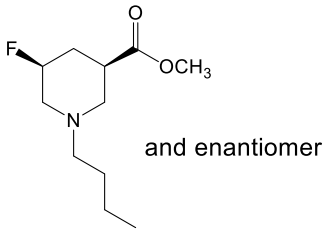

Compound *rac*-**42** (155 mg; 0.593 mmol) was dissolved in MeOH (3.0 mL) and 2 M etheric HCl (3.0 mL; 6.0 mmol) was added. The mixture was stirred at rt for 6.5 h, before it was quenched with K_2CO_3 (830 mg; 6.01 mmol), dissolved in H_2O (25 mL). It was extracted with DCM (5 x 20 mL) and the combined organic phases were concentrated under reduced pressure. The residue was dissolved in acetone (3.0 mL) and KI (39.9 mg; 0.240 mmol), K_2CO_3 (165 mg; 1.19 mmol) and 1-bromobutane (0.057 mL; 0.53 mmol) were successively added. The mixture was stirred at rt for 6 h and furthermore refluxed for 5 d. Then the reaction was quenched with H_2O (25 mL), extracted with DCM (5 x 20 mL) and the combined organic phases were concentrated under reduced pressure. After purification by column chromatography (silica gel; ethyl acetate/*iso*-hexane = 1:1 + 2% triethylamine) *rac*-**52** was obtained as colorless oil (51 mg; 51%). R_f = 0.27 (ethyl acetate/*iso*-hexane = 1:1 + 2% triethylamine). IR (film): $\tilde{\nu}$ = 2957, 2934, 2873, 2812, 2778, 1739, 1470, 1457 cm^{-1}. ^1H NMR (400 MHz, CCl_2D_2, 25 °C, TMS): δ = 0.90 (t, J = 7.3 Hz, 3 H, $NCH_2CH_2CH_2CH_3$), 1.23–1.37 (m, 2 H, $NCH_2CH_2CH_2CH_3$), 1.39–1.61 (m, 3 H, $NCH_2CH_2CH_2CH_3$, $NCH_2CHCH_{ax}H_{eq}$), 1.95 (td, J = 10.0/5.3 Hz, 1 H, $NCH_{ax}H_{eq}CH_{ax}F$), 2.00 (t, J = 11.1 Hz, 1 H, $NCH_{ax}H_{eq}CH_{ax}C{=}O$), 2.30–2.48 (m, 3 H, $NCH_2CHCH_{ax}H_{eq}$, $NCH_2CH_2CH_2CH_3$), 2.59 (ddtd, J = 12.6/10.8/4.0/1.8 Hz, 1 H, $NCH_{ax}H_{eq}CH_{ax}C{=}O$), 2.99 (dddt, J = 11.3/4.2/2.9/1.5 Hz, 1 H, $NCH_{ax}H_{eq}CH_{ax}C{=}O$), 3.06–3.17 (m, 1 H, $NCH_{ax}H_{eq}CH_{ax}F$), 3.66 (s, 3 H, OCH_3), 4.56 (dddt, J = 48.4/10.7/9.6/4.7, 1 H, $NCH_{ax}H_{eq}CH_{ax}F$) ppm. ^{13}C NMR (101 MHz, CCl_2D_2, 25 °C, TMS): δ = 14.16 ($NCH_2CH_2CH_2CH_3$), 20.89 ($NCH_2CH_2CH_2CH_3$), 29.34 ($NCH_2CH_2CH_2CH_3$), 33.75 (d, J_{CF} = 20.4 Hz, NCH_2CHCH_2), 40.34 (d, J_{CF} = 11.6 Hz, $NCH_2CHC{=}O$), 52.08 (OCH_3), 54.83 (d, J_{CF} = 1.6 Hz, $NCH_2CHC{=}O$), 57.81 (d, J_{CF} = 25.0 Hz, NCH_2CHF), 58.08 ($NCH_2CH_2CH_2CH_3$), 88.27 (d, J_{CF} = 171.3 Hz, NCH_2CHF), 173.35 (d, J_{CF} = 2.61 Hz, $NCH_2CHC{=}O$) ppm. ^{19}F {^1H} NMR (376 MHz, CCl_2D_2, 25 °C): δ = 181.64 ppm. MS (EI, 70 eV): *m/z* = 217.1 (2%, $[M]^{+\bullet}$), 174.1 (100%), 57.1 (13%). HRMS (EI, 70 eV): $[M]^{+\bullet}$ calcd. for $C_{11}H_{20}O_2NF$: 217.1478; found 217.1473.

***rac*-(3*R*,5*S*)-(1-Butyl-5-fluoropiperidine-3-carboxylic acid) (*rac*-51):**

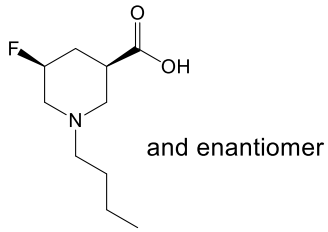

Compound *rac*-**52** (42 mg; 0.19 mmol) was dissolved in THF (2.0 mL) and 1 M HCl (2.0 mL; 2.0 mmol) was added to the solution. The mixture was stirred at rt for 50 min and refluxed for 1 h, before the reaction was quenched with H_2O (25 mL). The aqueous phase was washed with DCM (3 x 20 mL) and freeze dried. The residue was dissolved in 2 M NaOH (2.0 mL; 4.0 mmol) and stirred at rt for 23 h, before the reaction was quenched with H_2O (20 mL). The aqueous phase was washed with DCM (1 x 40 mL and 1 x 20 mL), acidified with 2 M HCl (5.0 mL; 10.0 mmol), again washed with DCM (2 x 20 mL) and freeze dried. The residue was purified by strongly acidic cation exchange chromatography with a 25 % aq. NH_3 solution as solvent to yield *rac*-**51** as white lyophilisate (11 mg; 28%). IR (KBr): $\tilde{\nu}$ = 3429, 2960, 2928, 2872, 1604, 1458 cm^{-1}. ^1H NMR (400 MHz, 1 M NaOD in D_2O, 25 °C, MeOH): δ = 0.94 (t, J = 7.3 Hz, 3 H, $NCH_2CH_2CH_2CH_3$), 1.34 (sext, J = 7.3 Hz, 2 H, $NCH_2CH_2CH_2CH_3$), 1.45–1.61 (m, 3 H, $NCH_2CH_2CH_2CH_3$, $NCH_2CHCH_{ax}H_{eq}$), 1.98–2.09 (m, 2 H, $NCH_{ax}H_{eq}CH_{ax}C{=}O$, $NCH_{ax}H_{eq}CH_{ax}F$), 2.37–2.56 (m, 4 H, $NCH_{ax}H_{eq}CH_{ax}C{=}O$, $NCH_2CHCH_{ax}H_{eq}$, $NCH_2CH_2CH_2CH_3$), 3.07 (d, J = 11.5 Hz, 1 H, $NCH_{ax}H_{eq}CH_{ax}C{=}O$), 3.22–3.30 (m, 1 H, $NCH_{ax}H_{eq}CH_{ax}F$), 4.72 (dm, J = 48.0, 1 H, $NCH_{ax}H_{eq}CH_{ax}F$) ppm. ^{13}C NMR (101 MHz, 1 M NaOD in D_2O, 25 °C, MeOH): δ = 14.33 ($NCH_2CH_2CH_2CH_3$), 21.27 ($NCH_2CH_2CH_2CH_3$), 28.72 ($NCH_2CH_2CH_2CH_3$), 35.17 (d, J_{CF} = 18.8 Hz, NCH_2CHCH_2), 43.25 (d, J_{CF} = 10.6 Hz, $NCH_2CHC{=}O$), 55.87 ($NCH_2CHC{=}O$), 57.16 (d, J_{CF} = 25.9 Hz, NCH_2CHF), 58.41 ($NCH_2CH_2CH_2CH_3$), 89.65 (d, J_{CF} = 168.1 Hz, NCH_2CHF), 182.04 ($NCH_2CHC{=}O$) ppm. ^{19}F {^1H} NMR (376 MHz, D_2O, 25 °C): δ = 181.93 ppm. MS (EI, 70 eV): *m/z* = 203.1 (13%, $[M]^{+\bullet}$), 161.1 (67%), 160.1 (100%), 140.1 (33%). HRMS (EI, 70 eV): $[M]^{+\bullet}$ calcd. for $C_{10}H_{18}O_2NF$: 203.1322; found 203.1316.

Biological testing: [^{3}H]GABA uptake assays were performed as previously described[73] by technical assistants of our group under the supervision of Dr. Georg Höfner.

5 Summary of the thesis

Epilepsy and several other CNS diseases are associated with an impaired GABAergic neurotransmission. By the inhibition of membrane-bound GABA transporters (GATs), the GABA (**1**) concentration available in the synaptic cleft for downstream receptors can be enhanced, thus adjusting the reduced inhibitory neurotransmission. Particularly the GABA transporter subtype GAT1 (≙ mGAT1) emerged as a well-known drug target mediating anticonvulsant effects, while other GAT subtypes including GAT3 (≙ mGAT4) are still evaluated for their pharmacological potential as drug targets. Prototypic GAT inhibitors such as the GAT1-selective, highly potent tiagabine (**6**), which is the first GAT inhibitor in clinical use, and the GAT3-selective (*S*)-SNAP-5114 (**16**) are typically derivatives of small cyclic amino acids such as nipecotic acid (**9**), of which the 1-position of the piperidine moiety is substituted with a lipophilicity-enhancing residue.

The aim of this thesis was to synthesize nipecotic acid derivatives substituted in the 5-position of the core structure with a lipophilic residue attached to it via a spacer in order to explore this uncommon substitution pattern as possible means of obtaining novel GABA uptake inhibitors. The idea for this project was based on previous *in silico* studies in our group, in which hypothetical, 5-substituted nipecotic acid derivatives were indicated to exhibit an interesting binding pose at the target GAT1. To be able to explore a vast and easy to perform variation of lipophilic residues of the target compounds, the aims of this thesis should be addressed in an approach that combines the generation of dynamic combinatorial hydrazone libraries and the screening of their binding affinities towards mGAT1 by means of MS Binding Assays as initially employed to N-substituted nipecotic acid derivatives and described by Sindelar and Wanner.[87]

The first two studies of this cumulative thesis comprise the syntheses of appropriate hydrazine building blocks **29**–**31**, the compilation of aldehyde libraries **26**, the generation of hydrazone libraries **32**–**34**, the screening and deconvolution experiments of these hydrazone libraries **32**–**34** at mGAT1 as well as the hit verification and examinations on the interaction mode. To this end, a synthetic route had first to be developed that yielded the building blocks equipped with different spacer lengths containing zero, one or two carbon atoms between the nipecotic acid moiety and the hydrazine function as well as with different relative orientations (i.e. *cis*- or *trans*-oriented) of the residue in 5-position with respect the carboxylic acid function in 3-

position of the piperidine ring; that are *cis*-C0, *cis*-C1, *trans*-C1, *cis*-C2 and *trans*-C2 nipecotic acid derived hydrazines **29**–**31**. Each of the five individual hydrazines **29**–**31** was separately reacted with all 28 aldehyde libraries **26** in order to allow the formation of the hydrazone libraries **32**–**34**. The generation of the hydrazone libraries **32**–**34** was performed in the presence of the target mGAT1 and competitive MS Binding Assays served as read-out for their binding affinities towards this target. Libraries found to be active were furthermore examined in deconvolution experiments in order to identify their most active components. In total, 17 exclusively *cis*-oriented hydrazones **32**–**34** with promising binding affinities towards mGAT1 were revealed by the screening and deconvolution experiments; for hit verification, these 17 compounds were resynthesized in pure form and their binding affinities (pK_i values) were established in full-scale MS binding experiments. Thereby, eleven hydrazones **32**–**34** were found to be potent ligands of mGAT1 with pK_i values in the submicromolar range. With respect to both the substitution in the 5-position and the lipophilic residues these new hydrazones **32**–**34** comprise structural scaffolds so far unprecedented for GAT1/mGAT1 inhibitors. Although exhibiting clearly lower inhibitory potencies (pIC_{50}) at mGAT1 (as established by functional [^{3}H]GABA uptake assays and compared to their good pK_i values determined in MS Binding Assays), these novel hydrazones (represented by one C0-derived hydrazone **32** and two C1-derived hydrazones **33** in further experiments) are particularly interesting since they were found to exhibit a noncompetitive interaction mode at mGAT1 by MS based saturation experiments; likely, they address a so far uncharacterized, allosteric binding site at GAT1/mGAT1. Thus, the herein introduced 5-substituted nipecotic acid derivatives exhibit a different pharmacological profile as bench mark GAT1 inhibitors and could represent interesting tool compounds for exploring GAT1 mediating GABA transport.

In the third study of this cumulative thesis, all the libraries comprising the same hydrazones **32**–**34** as utilized in the previous studies were intended to be examined in a new kind of screening at mGAT4. Therefore, hydrazone libraries **32**–**34** were generated by preincubating the hydrazine building blocks **29**–**31** with the aldehyde libraries **26** in the absence of the target mGAT4. The thus generated hydrazone libraries **32**–**34** were successively diluted and examined for their inhibitory potencies at mGAT4 in functional [^{3}H]GABA uptake assays. The screening and subsequent deconvolution experiments revealed two hydrazones **32** with promising inhibitory potencies at mGAT4. For hit verification, both compounds were resynthesized in pure

form and their inhibitory potencies (pIC_{50} values) were established in full-scale [^{3}H]GABA uptake assays. These two compounds, which both possess a three-atom spacer in *cis*-orientation with respect to the carboxylic acid function and a lipophilic moiety derived from a biphenyl residue, exhibit inhibitory potencies at mGAT4 close to that of bench mark GAT3/mGAT4 inhibitor (*S*)-SNAP-5114 (**16**). Accordingly, the herein introduced compounds comprise new structural scaffolds so far unprecedented for GAT3/mGAT4 inhibitors and the substitution in the 5-position of the nipecotic acid moiety was again found to represent an interesting means of obtaining potentially novel GABA uptake inhibitors.

Besides the aforementioned approaches addressing the main aims and goals of this thesis, some additional nipecotic acid derivatives bearing a hydroxy group or one or two fluorine atoms in the 5-position of the piperidine ring were synthesized and tested for their functional activities at the different GAT subtypes as structural analogs of known GAT inhibitors. Most notably, one fluoro substituent in 5-position of the nipecotic acid moiety apparently retains the potency at but increases the subtype selectivity for mGAT1, making 5-fluoro substituted nipecotic acid derivatives *rac*-**44** and *rac*-**49** interesting starting points for the development of potentially new highly potent GAT1/mGAT1 inhibitors.

6 List of abbreviations

AS-MS	affinity selection-mass spectrometry
BGT	betaine/γ-aminobutyric acid transporter 1
Boc	*tert*-butyloxycarbonyl
CNS	central nervous system
DAST	diethylaminosulfur trifluoride
DBU	1,8-diazabicyclo(5.4.0)undec-7-ene
DCC	dynamic combinatorial chemistry
DCE	1,2-dichloroethane
DCL	dynamic combinatorial library
DCM	dichloromethane
eq.	equivalent
ESI	electrospray ionization
GABA	γ-aminobutyric acid
GABA-T	GABA transaminase
GAD	glutamate decarboxylase
GAT	membrane-bound GABA transporters
GPCR	G-protein coupled receptors
HTS	high-throughput screening
HUGO	Human Genome Organisation
LC	liquid chromatography
MeOH	methanol
MS	mass spectrometry
NEt_3	triethylamine

rt	room temperature
SEM	standard error of the mean
SLC	solute carrier
temp.	temperature
THF	tetrahydrofuran
TM	transmembrane helix
VGAT	vesicular neurotransmitter transporters
WHO	World Health Organization

7 References

[1] Perland, E.; Fredriksson, R. Classification systems of secondary active transporters. *Trends Pharmacol. Sci*. **2017**, *38*, 305–315.

[2] Kristensen, A. S.; Andersen, J.; Jørgensen, T. N.; Sørensen, L.; Eriksen, J.; Loland, C. J.; Strømgaard, K.; Gether, U. SLC6 neurotransmitter transporters: structure, function, and regulation. *Pharmacol. Rev.* **2011**, *63*, 585–640.

[3] Madsen, K. K.; Clausen, R. P.; Larsson, O. M.; Krogsgaard-Larsen, P.; Schousboe, A.; White, H. S. Synaptic and extrasynaptic GABA transporters as targets for anti-epileptic drugs. *J. Neurochem*. **2009**, *109*, 139–144.

[4] Wellendorph, P.; Jacobsen, J.; Skovgaard-Petersen, J.; Jurik, A.; Vogensen, S. B.; Ecker, G.; Schousboe, A.; Krogsgaard-Larsen, P.; Clausen, R. P. γ-Aminobutyric Acid and Glycine Neurotransmitter Transporters. In *Transporters as Drug Targets*, 1st ed.; Ecker, G. F., Clausen, R. P., Sitte, H. H., Eds.; Wiley-VCH: Weinheim, 2017; pp 69–106.

[5] Palacín, M.; Estévez, R.; Bertran, J.; Zorzano, A. Molecular biology of mammalian plasma membrane amino acid transporters. *Physiol. Rev*. **1998**, *78*, 969–677.

[6] Borden, L. A. GABA transporter heterogeneity: pharmacology and cellular localization. *Neurochem. Int*. **1996**, *29*, 335–356.

[7] Madsen, K. K.; White, H. S.; Schousboe, A. Neuronal and non-neuronal GABA transporters as targets for antiepileptic drugs. *Pharmacol. Ther*. **2010**, *125*, 394–401.

[8] Minelli, A.; DeBiasi, S.; Brecha, N. C.; Zuccarello, L. V.; Conti, F. GAT-3, a high-affinity GABA plasma membrane transporter, is localized to astrocytic processes, and it is not confined to the vicinity of GABAergic synapses in the cerebral cortex. *J. Neurosci*. **1996**, *16*, 6255–6264.

[9] Jin, X. T.; Galvan, A.; Wichmann, T.; Smith, Y. Localization and function of GABA transporters GAT-1 and GAT-3 in the basal ganglia. *Front. Syst. Neurosci*. **2011**, *5*, 63.

[10] Zhou, Y.; Danbolt, N. C. GABA and glutamate transporters in brain. *Front. Endocrinol.* **2013**, *4*, 165.

[11] Zhou, Y.; Holmseth, S.; Hua, R.; Lehre, A. C.; Olofsson, A. M.; Poblete-Naredo, I.; Kempson, S. A.; Danbolt, N. C. The betaine-GABA transporter (BGT1, slc6a12) is predominantly expressed in the liver and at lower levels in the kidneys and at the brain surface. *Am. J. Physiol. Renal. Physiol*. **2012**, *302*, F316–F328.

[12] Belboni, R. O.; Carolino, R. O. G.; Pizzo, A. B.; Castellan-Baldan, L.; Coutinho-Netto, J.; dos Santos, W. F.; Coimbra, N. C. Pharmacological and biochemical aspects of GABAergic neurotransmission: pathological and neuropsychobiological relationships. *Cell. Mol. Neurobiol*. **2004**, *24*, 707–728.

[13] Bowery, N. G.; Smart, T. G. GABA and glycine as neurotransmitters: a brief history. *Br. J. Pharmacol*. **2006**, *147*, S109–S119.

[14] Martin, D. L.; Rimvall, K. Regulation of y-aminobutyric acid synthesis in the brain. *J. Neurochem*. **1993**, *60*, 395–407.

[15] Owens, D. F.; Kriegstein, A. R. Is there more to GABA than synaptic inhibition? *Nat. Rev. Neurosci*. **2002**, *3*, 715–727.

[16] Bradford, H. F. Glutamate, GABA and epilepsy. *Prog. Neurobiol*. **1995**, *47*, 477–511.

[17] Treiman, D. M. GABAergic mechanisms in epilepsy. *Epilepsia* **2001**, *42*, 8–12.

[18] Kleppner, S. R.; Tobin, A. J. GABA signalling: therapeutic targets for epilepsy, Parkinson's disease and Huntington's disease. *Expert Opin. Ther. Targets* **2001**, *5*, 219–239.

[19] Ishiwari, K.; Mingote, S.; Correa, M.; Trevitt, J. T.; Carlson, B. B.; Salamone, J. D. The GABA uptake inhibitor β-alanine reduces pilocarpine-induced tremor and increases extracellular GABA in substantia nigra pars reticulata as measured by microdialysis. *J. Neurosci. Methods* **2004**, *140*, 39–46.

[20] Zádori, D.; Geisz, A.; Vámos, E.; Vécsei, L.; Klivényi, P. Valproate ameliorates the survival and the motor performance in a transgenic mouse model of Huntington's disease. *Pharmacol. Biochem. Behav*. **2009**, *94*, 148–153.

[21] Aoyagi, T.; Wada, T.; Nagai, M.; Kojima, F.; Harada, S.; Takeuchi, T.; Takahashi, H.; Hirokawa, K.; Tsumita, T. Increased γ-aminobutyrate aminotransferase activity in brain of patients with Alzheimer's disease. *Chem. Pharm. Bull*. **1990**, *38*, 1748–1749.

[22] Kalueff, A. V.; Nutt, D. J. Role of GABA in anxiety and depression. *Depress. Anxiety* **2007**, *24*, 495–517.

[23] Krystal, J. H.; Sanacora, G.; Blumberg, H.; Anand, A.; Charney, D. S.; Marek, G.; Epperson, C. N.; Goddard, A.; Mason, G. F. Glutamate and GABA systems as targets for novel antidepressant and mood-stabilizing treatments. *Mol. Psychiatry* **2002**, *7*, S71–S80.

[24] Todorov, A. A.; Kolchev, C. B.; Todorov, A. B. Tiagabine and gabapentin for the management of chronic pain. *Clin. J. Pain* **2005**, *21*, 358–361.

[25] Daemen, M. A.; Hoogland, G.; Cijntje, J. M.; Spincemaille, G. H. Upregulation of the GABA-transporter GAT-1 in the spinal cord contributes to pain behaviour in experimental neuropathy. *Neurosci. Lett*. **2008**, *444*, 112–115.

[26] Kowalczyk, P.; Kulig, K. GABA system as target for new drugs. *Curr. Med. Chem*. **2014**, *21*, 3294–3309.

[27] Genton, P.; Guerrini, R.; Perucca, E. Tiagabine in clinical practice. *Epilepsia* **2001**, *42*, 42–45.

[28] LaRoche, S. M.; Helmers, S. L. The new antiepileptic drugs: scientific review. *JAMA* **2004**, *291*, 605–614.

[29] Leppik, I. E. Tiagabine: the safety landscape. *Epilepsia* **1995**, *36*, S10–S13.

[30] Leach, J. P.; Brodie, M. J. Tiagabine. *Lancet* **1998**, *351*, 203–207.

[31] World Health Organization (WHO). Fact sheet "Epilepsy"; online at: http://www.who.int/news-room/fact-sheets/detail/epilepsy; accessed 23 July 2018.

[32] Brodie, M. J.; Besag, F.; Ettinger, A. B.; Mula, M.; Gobbi, G.; Comai, S.; Aldenkamp, A. P.; Steinhoff, B. J. Epilepsy, antiepileptic drugs, and aggression: an evidence-based review. *Pharmacol. Rev*. **2016**, *68*, 563–602.

[33] Høg, S.; Greenwood, J. R.; Madsen, K. B.; Larsson, O. M.; Frølund, B.; Schousboe, A.; Krogsgaard-Larsen, P.; Clausen, R. P. Structure-activity relationships of selective GABA uptake inhibitors. *Curr. Top. Med. Chem*. **2006**, *6*, 1861–1882.

[34] Frey, H.-H.; Popp, C.; Löscher, W. Influence of the inhibitors of high affinity GABA uptake on seizure threshold in mice. *Neuropharmacology* **1979**, *18*, 581–590.

[35] Ali, F. E.; Bondinell, W. E.; Dandridge, P. A.; Frazee, J. S.; Garvey, E.; Girard, G. R.; Kaiser, C.; Ku, T. W.; Lafferty, J. J.; Moonsammy, G. I.; Oh, H.-J.; Rush, J. A.; Setler, P. E.; Stringer, O. D.; Venslavsky, J. W.; Volpe, B. W.; Yunger, L. M.; Zirkle, C. L. Orally active and potent inhibitors of γ-aminobutyric acid uptake. *J. Med. Chem.* **1985**, *28*, 653–660.

[36] Dalby, N. O. GABA-level increasing and anticonvulsant effects of three different GABA uptake inhibitors. *Neuropharmacology* **2000**, *39*, 2399–2407.

[37] Borden, L. A.; Dhar, T. G. M.; Smith, K. E.; Weinshank, R. L.; Branchek, T. A.; Gluchowski, C. Tiagabine, SK&F 89976-A, CI-966, and NNC-711 are selective for the cloned GABA transporter GAT-1. *Eur. J. Pharmacol*. **1994**, *269*, 219–224.

[38] Salat, K.; Podkowa, A.; Malikowska, N.; Kern, F.; Pabel, J.; Wojcieszak, E.; Kulig, K.; Wanner, K. T.; Strach, B.; Wyska, E. Novel, highly potent and *in vivo* active inhibitor of GABA transporter subtype 1 with anticonvulsant, anxiolytic, antidepressant and antinociceptive properties. *Neuropharmacology* **2017**, *113*, 331–342.

[39] Sarup, A.; Larsson, O. M.; Bolvig, T.; Frølund, B.; Krogsgaard-Larsen, P.; Schousboe, A. Effects of 3-hydroxy-4-amino-4,5,6,7-tetrahydro-1,2-benzisoxazol (*exo*-THPO) and its N-substituted analogs on GABA transport in cultured neurons and astrocytes and by the four cloned mouse GABA transporters. *Neurochem. Int*. **2003**, *43*, 445–451.

[40] White, H. S.; Watson, W. P.; Hansen, S. L.; Slough, S.; Perregaard, J.; Sarup, A.; Bolvig, T.; Petersen, G.; Larsson, O. M.; Clausen, R. P.; Frølund, B.; Falch, E.; Krogsgaard-Larsen, P.; Schousboe, A. First demonstration of a functional role for central nervous system betaine/γ-aminobutyric acid transporter (mGAT2) based on synergistic anticonvulsant action among inhibitors of mGAT1 and mGAT2. *J. Pharm. Exp. Ther.* **2005**, *312*, 866–874.

[41] Madsen, K. K.; Ebert, B.; Clausen, R. P.; Krogsgaard-Larsen, P.; Schousboe, A.; White, H. S. Selective GABA transporter inhibitors tiagabine and EF1502 exhibit mechanistic differences in their ability to modulate the ataxia and anticonvulsant action of the extrasynaptic $GABA_A$ receptor agonist gaboxadol. *J. Pharm. Exp. Ther.* **2011**, *338*, 214–219.

[42] Dhar, T. G. M.; Borden, L. A.; Tyagarajan, S.; Smith, K. E.; Branchek, T. A.; Weinshank, R. L.; Gluchowskit, C. Design, synthesis and evaluation of substituted triarylnipecotic acid derivatives as GABA uptake inhibitors: identification of a ligand with moderate affinity and selectivity for the cloned human GABA transporter GAT-3. *J. Med. Chem*. **1994**, *37*, 2334–2342.

[43] Pabel, J.; Faust, M.; Prehn, C.; Wörlein, B.; Allmendinger, L.; Höfner, G.; Wanner, K. T. Development of an (*S*)-1-{2-[tris(4-methoxyphenyl) methoxy]ethyl}piperidine-3-carboxylic acid [(*S*)-SNAP-5114] carba analogue inhibitor for murine gamma-aminobutyric acid transporter type 4. *ChemMedChem* **2012**, *7*, 1245–1255.

[44] Damgaard, M.; Al-Khawaja, A.; Vogensen, S. B.; Jurik, A.; Sijm, M.; Lie, M. E. K.; Bæk, M. I.; Rosenthal, E.; Jensen, A. A.; Ecker, G. F.; Frølund, B.; Wellendorph, P.; Clausen, R. P. Identification of the first highly subtype-selective inhibitor of human GABA transporter GAT3. *ACS Chem. Neurosci*. **2015**, *6*, 1591–1599.

[45] Kobayashi, T.; Suemasa, A.; Igawa, A.; Ide, S.; Fukuda, H.; Abe, H.; Arisawa, M.; Minami, M.; Shuto, S. Conformationally restricted GABA with bicyclo[3.1.0]hexane backbone as the first highly selective BGT-1 inhibitor. *ACS Med. Chem. Lett*. **2014**, *5*, 889–893.

[46] Jørgensen, L.; Al-Khawaja, A.; Kickinger, S.; Vogensen, S. B.; Skovgaard-Petersen, J.; Rosenthal, E.; Borkar, N.; Löffler, R.; Madsen, K. K.; Brauner-Osborne, H.; Schousboe, A.; Ecker, G. F.; Wellendorph, P.; Clausen, R. P. Structure−activity relationship, pharmacological characterization, and molecular modeling of noncompetitive inhibitors of the betaine/γ-aminobutyric acid transporter 1 (BGT1). *J. Med. Chem*. **2017**, *60*, 8834–8846.

[47] Müller-Uri, C.; Singer, E. A.; Fleischhacker, W. Synthesis of alkyl-substituted arecoline derivatives as γ-aminobutyric acid uptake inhibitors. *J. Med. Chem*. **1986**, *29*, 125–132.

[48] N'Goka, V.; Schlewer, G.; Linget, J.-M.; Chambon, J.-P.; Wermuth, C. G. GABA-uptake inhibitors: construction of a general pharmacophore model and successful prediction of a new representative. *J. Med. Chem*. **1991**, *34*, 2547–2557.

[49] N'Goka, V.; Bissantz, C.; Bisel, P.; Stenbøl, T. B.; Krogsgaard-Larsen, P.; Schlewer, G. Syntheses and GABA uptake properties of 6-ether- and 6-enol ether-substituted nipecotic acids. *Eur. J. Med. Chem*. **2004**, *39*, 633–638.

[50] N'Goka, V.; Stenbøl, T. B.; Krogsgaard-Larsen, P.; Schlewer, G. Synthesis and GABA uptake inhibitory properties of 6-aryl iminoxymethyl substituted nipecotic acids. *Eur. J. Med. Chem*. **2004**, *39*, 889–895.

[51] Hoesl, C. E.; Höfner, G.; Wanner, K. T. First asymmetric syntheses of 6-substituted nipecotic acid derivatives. *Tetrahedron* **2004**, *60*, 307–318.

[52] Hellenbrand, T.; Höfner, G.; Wein, T.; Wanner, K. T. Synthesis of 4-substituted nipecotic acid derivatives and their evaluation as potential GABA uptake inhibitors. *Bioorg. Med. Chem*. **2016**, *24*, 2072–2096.

[53] Guastella, J.; Nelson, N.; Nelson, H.; Czyzyk, L.; Keynan, S.; Miedel, M. C.; Davidson, N.; Lester, H. A.; Kanner, B. I. Cloning and expression of a rat brain GABA transporter. *Science* **1990**, *249*, 1303–1306.

[54] Chen, J.-G.; Liu-Chen, S.; Rudnick, G. Determination of external loop topology in the serotonin transporter by site-directed chemical labeling. *J. Biol. Chem*. **1998**, *273*, 12675–12681.

[55] Yamashita, A.; Singh, S. K.; Kawate, T.; Jin, Y.; Gouaux, E. Crystal structure of a bacterial homologue of Na^+/Cl^--dependent neurotransmitter transporters. *Nature* **2005**, *437*, 215–223.

[56] Penmatsa, A.; Gouaux, E. How LeuT shapes our understanding of the mechanisms of sodium-coupled neurotransmitter transporters. *J. Physiol*. **2014**, *592*, 863–869.

[57] Beuming, T.; Shi, L.; Javitch, J. A.; Weinstein, H. A comprehensive structure-based alignment of prokaryotic and eukaryotic neurotransmitter/Na^+ symporters (NSS) aids in the use of the LeuT structure to probe NSS structure and function. *Mol. Pharmacol.* **2006**, *70*, 1630–1642.

[58] Krishnamurthy, H.; Gouaux, E. X-ray structures of LeuT in substrate-free outward-open and apo inward-open states. *Nature* **2012**, *481*, 469–474.

[59] Penmatsa, A.; Wang, K. H.; Gouaux, E. X-ray structure of the dopamine transporter in complex with tricyclic antidepressant. *Nature* **2013**, *503*, 85–90.

[60] Coleman, J. A.; Green, E. M.; Gouaux, E. X-ray structures and mechanism of the human serotonin transporter. *Nature* **2016**, *532*, 334–339.

[61] Palló, A.; Bencsura, Á.; Héja, L.; Beke, T.; Perczel, A.; Kardos, J.; Simon, Á. Major human γ-aminobutyrate transporter: *in silico* prediction of substrate efficacy. *Biochem. Biophys. Res. Commun*. **2007**, *364*, 952–958.

[62] Wein, T.; Wanner, K. T. Generation of a 3D model for human GABA transporter hGAT-1 using molecular modeling and investigation of the binding of GABA. *J. Mol. Model*. **2010**, *16*, 155–161.

[63] Skovstrup, S.; Taboureau, O.; Bräuner-Osborne, H.; Jørgensen, F. S. Homology modelling of the GABA transporter and analysis of tiagabine binding. *ChemMedChem* **2010**, *5*, 986–1000.

[64] Wein, T.; Petrera, M.; Allmendinger, L.; Höfner, G.; Pabel, J.; Wanner, K. T. Different binding modes of small and large binders of GAT1. *ChemMedChem* **2016**, *11*, 509–518.

[65] Christopoulos, A.; Changeux, J.-P.; Catterall, W. A.; Fabbro, D.; Burris, T. P.; Cidlowski, J. A.; Olsen, R. W.; Peters, J. A.; Neubig, R. R.; Pin, J.-P.; Sexton, P. M.; Kenakin, T. P.; Ehlert, F. J.; Spedding, M.; Langmead, C. J. International Union of Basic and Clinical Pharmacology. XC. Multisite pharmacology: recommendations for the nomenclature of receptor allosterism and allosteric ligands. *Pharmacol. Rev*. **2014**, *66*, 918–947.

[66] Klebe, G. *Wirkstoffdesign*; Spektrum Akademischer Verlag: Heidelberg, **2009**.

[67] Iversen, L. L.; Neal, M. J. The uptake of [^{3}H]GABA by slices of rat cerebral cortex. *J. Neurochem*. **1968**, *15*, 1141–1149.

[68] Raiteri, M.; Federico, R.; Coletti, A.; Levi, G. Release and exchange relating to the synaptosomal uptake of GABA. *J. Neurochem*. **1975**, *24*, 1243–1250.

[69] Nelson, H.; Mandiyan, S.; Nelson N. Cloning of the human brain GABA transporter. *FEBS Lett*. **1990**, *269*, 181–184.

[70] Borden, L. A.; Smith, K. E.; Hartig, P. R.; Branchek, T. A.; Weinshank, R. L. Molecular heterogeneity of the γ-aminobutyric acid (GABA) transport system. *J. Biol. Chem*. **1992**, *267*, 21098–21104.

[71] Thomsen, C.; Sørensen, P. O.; Egebjerg, J. 1-(3-(9H-Carbazol-9-yl)-1-propyl)-4-(2-methoxyphenyl)-4-piperidinol, a novel subtype selective inhibitor of the mouse type II GABA-transporter. *Br. J. Pharmacol*. **1997**, *120*, 983–985.

[72] Kragler, A.; Höfner, G.; Wanner, K. T. Novel parent structures for inhibitors of the murine GABA transporters mGAT3 and mGAT4. *Eur. J. Pharmacol*. **2005**, *519*, 43–47.

[73] Kragler, A.; Höfner, G.; Wanner, K. T. Synthesis and biological evaluation of aminomethylphenol derivatives as inhibitors of the murine GABA transporters mGAT1–GAT4. *Eur. J. Med. Chem*. **2008**, *43*, 2404–2411.

[74] Schmitt, S.; Höfner, G.; Wanner, K. T. MS Transport Assays for γ-aminobutyric acid transporters – an efficient alternative for radiometric assays. *Anal. Chem*. **2014**, *86*, 7575–7583.

[75] Schmitt, S.; Höfner, G.; Wanner, K. T. Application of MS Transport Assays to the four human γ-aminobutyric acid transporters. *ChemMedChem* **2015**, *10*, 1498–1510.

[76] Makara, G. M.; Athanasopoulos, J. Improving success rates for lead generation using affinity binding technologies. *Curr. Op. Biotech*. **2005**, *16*, 666–673.

[77] Zhu, Z.; Cuozzo, J. High-throughput affinity-based technologies for small-molecule drug discovery. *J. Biomol. Screen*. **2009**, *14*, 1157–1164.

[78] Annis, D. A.; Nickbarg, E.; Yang, X.; Ziebell, M. R.; Whitehurst, C. E. Affinity selection-mass spectrometry screening techniques for small molecule drug discovery. *Curr. Opin. Chem. Biol*. **2007**, *11*, 518–526.

[79] Höfner, G.; Zepperitz, C.; Wanner, K. T. MS Binding Assays – An Alternative to Radioligand Binding. In *Mass Spectrometry in Medicinal Chemistry: Applications in*

Drug Discovery, 1st ed.; Höfner, G., Wanner, K. T., Eds.; Wiley-VCH: Weinheim, 2007; pp 247–283.

[80] Höfner, G.; Wanner, K. T. Competitive binding assays made easy with a native marker and mass spectrometric quantification. *Angew. Chem. Int. Ed*. **2003**, *42*, 5235–5237.

[81] Niessen, K. V.; Höfner, G.; Wanner, K. T. Competitive MS Binding Assays for dopamine D_2 receptors employing spiperone as a native marker. *ChemBioChem* **2005**, *6*, 1769–1775.

[82] Hess, M.; Höfner, G. Wanner, K. T. (*S*)- and (*R*)-fluoxetine as native markers in mass spectrometry (MS) binding assays addressing the serotonin transporter. *ChemMedChem* **2011**, *6*, 1900–1908.

[83] Grimm, S. H.; Höfner, G.; Wanner, K. T. MS Binding Assays for the three monoamine transporters using the triple reuptake inhibitor (1*R*,3*S*)-indatraline as native marker. *ChemMedChem* **2015**, *10*, 1027–1039.

[84] Neiens, P.; De Simone, A.; Höfner, G.; Wanner, K. T. Simultaneous multiple MS Binding Assays for the dopamine, norepinephrine, and serotonin transporters. *ChemMedChem* **2018**, *13*, 453–463.

[85] Zepperitz, C.; Höfner, G.; Wanner, K. T. MS-Binding Assays: kinetic, saturation and competitive experiments based on quantitation of bound marker – exemplified by the GABA transporter mGAT1. *ChemMedChem* **2006**, *1*, 208–217.

[86] Zepperitz, C.; Höfner, G.; Wanner, K. T. Expanding the scope of MS Binding Assays to low-affinity markers as exemplified for mGAT1. *Anal. Bioanal. Chem*. **2008**, *391*, 309–316.

[87] Sindelar, M.; Wanner, K. T. Library screening by means of MS Binding Assays – exemplarily demonstrated for a pseudo-static library addressing GAT1. *ChemMedChem* **2012**, *7*, 1678–1690.

[88] Corbett, P. T.; Leclaire, J.; Vial, L.; West, K. R.; Wietor, J.-L.; Sanders, J. K. M.; Otto, S. Dynamic combinatorial chemistry. *Chem. Rev*. **2006**, *106*, 3652–3711.

[89] Mondal, M.; Hirsch, A. K. H. Dynamic combinatorial chemistry: a tool to facilitate the identification of inhibitors for protein targets. *Chem. Soc. Rev*. **2015**, *44*, 2455–2488.

[90] Sindelar, M.; Lutz, T. A.; Petrera, M.; Wanner, K. T. Focused pseudostatic hydrazone libraries screened by mass spectrometry binding assay: optimizing affinities toward γ-aminobutyric acid transporter 1. *J. Med. Chem*. **2013**, *56*, 1323–1340.

[91] Kern, F. T.; Wanner, K. T. Generation and screening of oxime libraries addressing the neuronal GABA transporter GAT1. *ChemMedChem* **2015**, *10*, 396–410.

[92] Kalia, J.; Raines, R. T. Hydrolytic stability of hydrazones and oximes. *Angew. Chem. Int. Ed.* **2008**, *47*, 7523–7526.

[93] Sitka, I.; Allmendinger, L.; Fülep, G.; Höfner, G.; Wanner, K. T. Synthesis of *N*-substituted acyclic β-amino acids and their investigation as GABA uptake inhibitors. *Eur. J. Med. Chem*. **2013**, *65*, 487–499.

[94] Beaulieu, F.; Beauregard, L.-P.; Courchesne, G.; Couturier, M.; LaFlamme, F.; L'Heureux, A. Aminodifluorosulfinium tetrafluoroborate salts as stable and crystalline deoxofluorinating reagents. *Org. Lett*. **2009**, *11*, 5050–5053.

[95] L'Heureux, A.; Beaulieu, F.; Bennett, C.; Bill, D. R.; Clayton, S.; LaFlamme, F.; Mirmehrabi, M.; Tadayon, S.; Tovell, D.; Couturier, M. Aminodifluorosulfinium salts: selective fluorination reagents with enhanced thermal stability and ease of handling. *J. Org. Chem*. **2010**, *75*, 3401–3411.

[96] Mahé, O.; L'Heureux, A.; Couturier, M.; Bennett, C.; Clayton, S.; Tovell, D.; Beaulieu, F.; Paquin, J.-F. Deoxofluorination reactions using *N,N*-disubstituted aminodifluorosulfinium tetrafluoroborate salts. *J. Fluorine Chem*. **2013**, *153*, 57–60.

[97] An alternative synthetic route (excluding analytical data) for compound *rac*-**44** was described in: Lankin, D. C.; Chandrakumar, N. S.; Rao, S. N.; Spangler, D. P.; Snyder, J. P. Protonated 3-fluoropiperidines: an unusual fluoro directing effect and a test for quantitative theories of solvation. *J. Am. Chem. Soc*. **1993**, *115*, 3356-3357.

[98] Merck, E. *Anfärbereagenzien für Dünnschicht- und Papier-Chromatographie*; MERCK: Darmstadt, 1970.

8 Appendix: Publications and manuscripts

1. *Novel allosteric ligands of γ-aminobutyric acid transporter 1 (GAT1) by MS based screening of pseudostatic hydrazone libraries*
   (including Supporting Information)

2. *MS based screening of 5-substituted nipecotic acid derived hydrazone libraries as ligands of the GABA transporter 1*
   (including Supporting Information)

3. *Generation and screening of pseudostatic hydrazone libraries derived from 5-substituted nipecotic acid derivatives at the GABA transporter mGAT4*

Journal of Medicinal Chemistry

Article

Cite This: J. Med. Chem. 2018, 61, 10310−10332

pubs.acs.org/jmc

Novel Allosteric Ligands of γ-Aminobutyric Acid Transporter 1 (GAT1) by MS Based Screening of Pseudostatic Hydrazone Libraries

Tobias J. Hauke, Thomas Wein, Georg Höfner, and Klaus T. Wanner*

Department of Pharmacy—Center of Drug Research, Ludwig-Maximilians-Universität München, Butenandtstrasse 5-13, 81377 Munich, Germany

Supporting Information

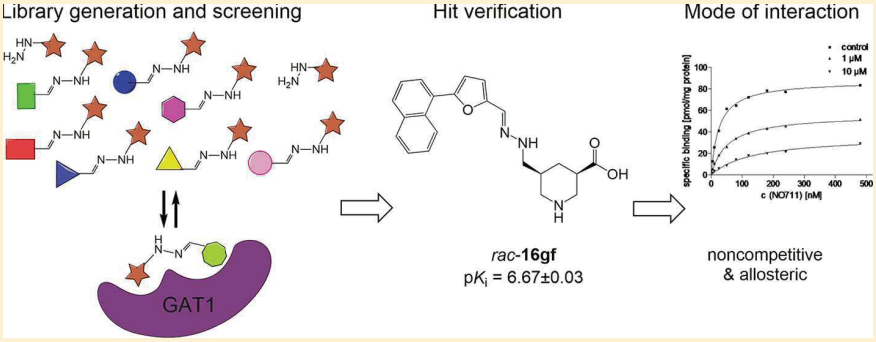

ABSTRACT: This study describes the screening of dynamic combinatorial libraries based on nipecotic acid as core structure with substituents attached to the 5- instead of the common 1-position for the search of novel inhibitors of the GABA transporter GAT1. The generated pseudostatic hydrazone libraries included a total of nearly 900 compounds and were screened for their binding affinities toward GAT1 in competitive mass spectrometry (MS) based Binding Assays. Characterization of the hydrazones with the highest affinities (with *cis*-configured *rac*-**16gf** bearing a 5-(1-naphthyl)furan-2-yl residue and a four atom spacer being the most potent) in binding and uptake experiments revealed an allosteric interaction at GAT1, which was not reported for any other nipecotic acid derivative up to now. Therefore, the herein introduced 5-substituted nipecotic acid derivatives could serve as valuable tools for investigations of allosterically modulated GABA transport mediated by GAT1 and furthermore as starting point for a new class of GAT1 inhibitors.

INTRODUCTION

γ-Aminobutyric acid (GABA; **1**; Chart 1) is the most important inhibitory neurotransmitter in the mammalian central nervous system (CNS), and pathological abnormalities of the GABAergic neurotransmission are associated with a number of neuronal diseases such as epilepsy,[1−3] Parkinson's disease,[3,4] depression,[4,5] and neuropathic pain.[6,7] For the treatment of such diseases, GABAergic neurotransmission can be enhanced by agonists of GABA receptors, by targeting metabolic enzymes, or by inhibiting GABA transport proteins (GATs).[8] With exception of one vesicular GABA transporter, GATs are membrane bound proteins encoded by the solute carrier 6 gene family (SLC6) that remove GABA from the synaptic cleft by utilizing a cotransport of sodium and chloride through cell membranes.[9] Among the four different subtypes of membrane bound transporters designated as GAT1, BGT1, GAT2, and GAT3 (as suggested by HUGO and corresponding to mGAT1, mGAT2, mGAT3, and mGAT4 when expressed in mice),[10,11] GAT1 is mainly responsible for the neuronal reuptake of GABA in the CNS and emerged as a drug target, while the pharmacological role and therapeutic potential of other GAT subtypes is still less well understood.[10−13] Many of the known GAT inhibitors are derivatives of small cyclic amino acids such as nipecotic acid (**2**) and guvacine (**3**), which already show in vitro activity as GABA uptake inhibitors by their own.[14,15] By introducing a lipophilic side chain to the cyclic amino acids a new generation of inhibitors, represented by SK&F-89976A (**4**), tiagabine (**5**), or NO711 (**6**), was established that has an increased potency and selectivity toward GAT1 compared to unsubstituted amino acids.[16−19] Furthermore, the increased lipophilicity of those molecules (**4**−**6**) enabled them to cross the blood−brain barrier in contrast to the more hydrophilic, unsubstituted amino acids (**2**,**3**).[20] Tiagabine (**5**) is well characterized with respect to its anticonvulsant activity, and it is the only selective GAT1 inhibitor in clinical use.[21] Recently, DDPM-2571 (**7**), a new GAT1 selective compound, was found to exceed the inhibitory potency of tiagabine (**5**) at GAT1 by more than one log unit, and it was demonstrated to mediate anticonvulsant, anxiolytic, antidepressant, and antinociceptive effects in mouse models.[22] All these selective and potent GAT1 inhibitors possess a hydrophilic amino acid "head" and a lipophilic aromatic moiety that is connected to the amino acid via a spacer originating from the amino nitrogen of the amino

Received: October 15, 2018
Published: October 30, 2018

DOI: 10.1021/acs.jmedchem.8b01602
J. Med. Chem. 2018, 61, 10310−10332

Chart 1. Structures of GABA (1), GAT1 Inhibitors (2–9), and Hypothetical Molecule 10

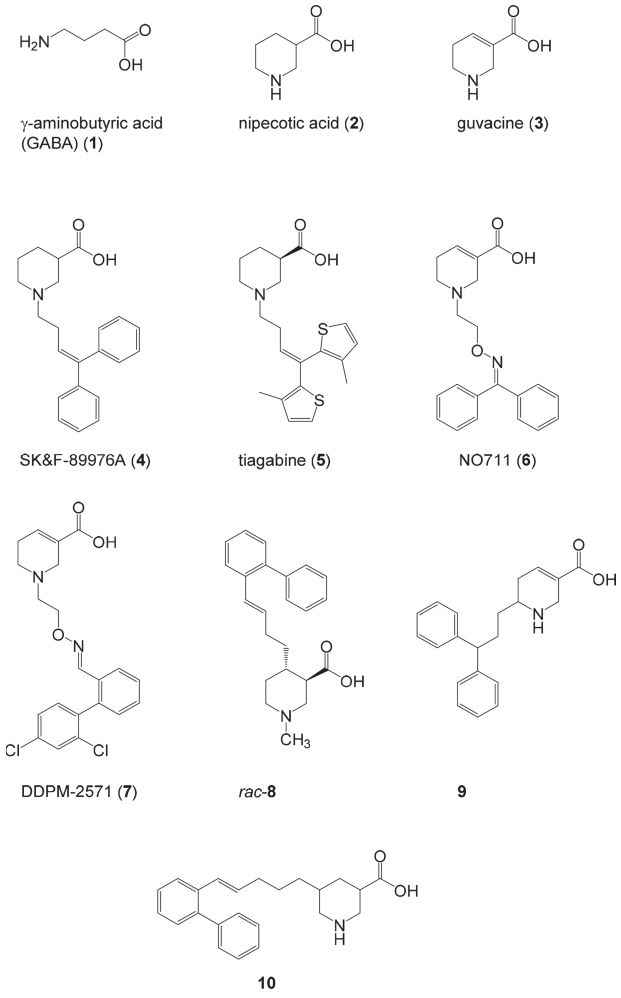

acid. There have been extensive efforts[23−29] to develop analogous GAT1 inhibitors with a different substitution pattern of the cyclic amino acid. For example, 4-substituted nipecotic acid derivatives including compound *rac*-**8**[29] and 6-substituted guvacine derivatives including compound **9**[24] were synthesized and tested for their inhibitory potencies of the GABA transport. However, among these only compound **9** showed in vitro activity comparable to N-substituted derivatives but was inactive in anticonvulsant models in vivo, likely due to an insufficient blood/brain concentration ratio.[24]

In 2005, the first crystal structure of a bacterial leucine transporter (LeuT) was reported,[30] which represents a homologue of the SLC6 GABA transporters. Since then, two investigations used this structure as a base for homology modeling and analysis of the binding of small inhibitors toward GAT1.[31,32] Later, the binding of tiagabine (**5**) and related compounds was evaluated using homology modeling, docking, and molecular dynamics simulations,[33] and different binding modes of small and large inhibitors were proposed.[34] We have used our in-house hGAT1 homology model refined by molecular dynamics calculations and described in detail in Wein et al.[34] to investigate the possibility of attaching the lipophilic arylalkyl residue to the 4- or 5-position of nipecotic acid (**2**). For an in silico screening, we built a virtual library of 4- and 5-substituted nipecotic acid derivatives, of which the lipophilic residues were chosen to be biphenyl or diphenyl residues. For the linker, carbon chains with 3, 4, 5, or 6 atoms and bearing a double bond in conjugation with the aromatic moiety were examined (example see hypothetical molecule **10**). The substitution of nipecotic acid (**2**), particularly in the 5-position and with a five carbon spacer (as in molecule **10**), was found to achieve the highest docking scores among the hypothetical compounds. Docking calculations showed for nipecotic acid derivative **10** and related 5-substituted derivatives that the nitrogen atom was able to point toward the intracellular side of the binding cavity and could potentially interact with two different hydrogen bond acceptors in this position. Thereby, the lipophilic residue would point to the extracellular side of the pocket (Figure 1c). So the binding pose of the piperidine ring of 5-substituted derivatives would be more similar compared to that of the unsubstituted nipecotic acid (**2**; Figure 1a) and opposing to that of tiagabine (**5**), of which the piperidine nitrogen and the attached arylalkyl moiety are facing toward the extracellular side (Figure 1b).[34]

On the basis of these results obtained from in silico studies, we concluded that nipecotic derivatives bearing a lipophilic moiety attached to the 5-position via a spacer might possibly represent a new class of potent GABA uptake inhibitors. For a vast and most of all easy to perform variation of the structure of the lipophilic residues attached to the 5-position of the nipecotic acid moiety, we decided to analyze compound libraries generated by dynamic combinatorial chemistry (DCC). Hence, we followed an approach that is based on pseudostatic hydrazone libraries and uses a competitive mass spectrometry (MS) based Binding Assay for their analysis as reported from our group, recently.[35] MS Binding Assays have the advantage to enable the label-free determination of binding affinities[36] and can be employed analogous to radioligand Binding Assays but are devoid of the drawbacks that result from using radioactive material.[37] The MS Binding Assay for the target murine GAT1 (mGAT1) that is required for this study and that uses NO711 (**6**) as a native marker had already been established by us and employed in related screening campaigns.[38]

For the present study, we intended to synthesize nipecotic acid derivatives substituted at the 5-position with a C1 (*rac*-**11** and *rac*-**12**) and a C2 spacer (*rac*-**13** and *rac*-**14**) and with a hydrazine function at the end of the spacer. By reaction with appropriate aldehydes **15**, these nipecotic acid derived hydrazines should allow generation of libraries with a hydrazone function containing a total spacer length of four atoms (*rac*-**16** and *rac*-**17**, resulting from the conversion of hydrazines *rac*-**11** and *rac*-**12**) and five atoms (*rac*-**18** and *rac*-**19**, resulting from hydrazines *rac*-**13** and *rac*-**14**) (Scheme 1), which should be screened for their affinities toward mGAT1 and evaluated as potential GABA uptake inhibitors. Hence, compounds with a five atom spacer, as suggested by molecular modeling, as well as with a four atom spacer, which appeared beneficial in some previously reported cases when potentially new N-substituted GAT1 inhibitors were synthesized,[39,40] should be examined in this study.

In addition to the generation and screening of the hydrazone libraries in competitive Binding Assays the whole screening process would further comprise deconvolution of the most potent libraries (testing only single hydrazones) and hit verification by resynthesis and determination of pK_i values. Finally, the best binders should be tested in [^{3}H]GABA uptake assays for their functional activity (IC_{50}) and subtype selectivity.

DOI: 10.1021/acs.jmedchem.8b01602
J. Med. Chem. 2018, 61, 10310−10332

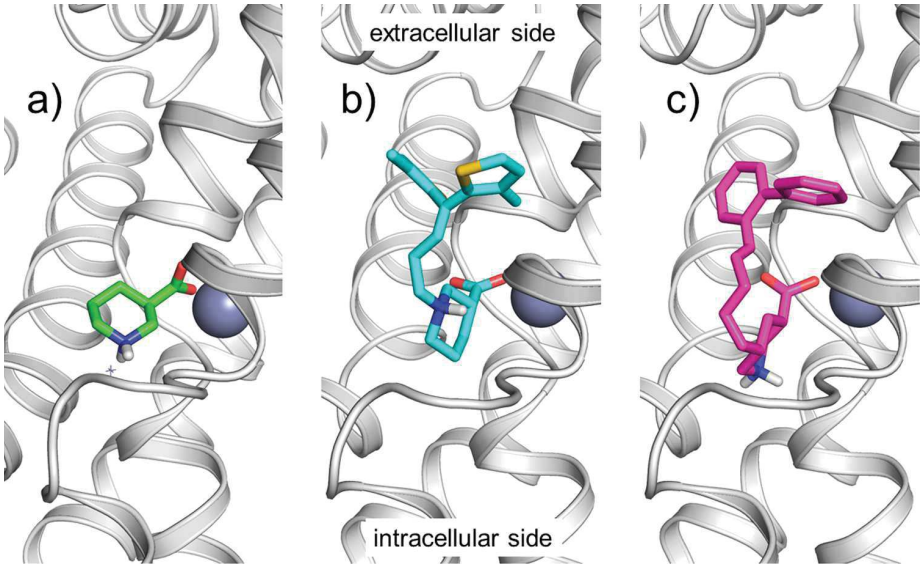

Figure 1. Side view of the hGAT1 model along the membrane plane showing the active site of the transporter. The extracellular side is on the top and the intracellular side is at the bottom of the picture. Docking poses of (a) nipecotic acid (**2**; green), (b) tiagabine (**5**; cyan), and (c) hypothetical molecule **10** (magenta) in the molecular dynamics refined homology model of hGAT1 are shown. The transmembrane helices TM10, TM11, and TM12 are not displayed for clarity.

Scheme 1. Condensation of Nipecotic Acid Derived Hydrazines *rac*-11–*rac*-14 with Diverse Aldehydes 15 to Afford Hydrazones with General Structures *rac*-16–*rac*-19

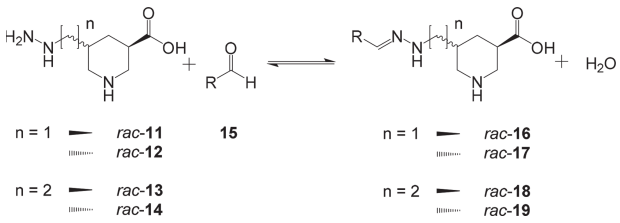

RESULTS AND DISCUSSION

Chemistry. *Synthesis of Hydrazines.* For the synthesis of the desired hydrazines *rac*-**11**–*rac*-**14**, a carbon side chain had to be introduced in the 5-position of nipecotic acid (or derivatives thereof) exhibiting a terminal function suitable for further derivatization, i.e., the introduction of a hydrazine moiety. As common precursors required for all hydrazine derivatives, the aldehydes *rac*-**20** and *rac*-**21** were chosen. These aldehydes were synthesized from commercially available nicotinate **22** as shown in Scheme 2. Compounds *rac*-**23** and *rac*-**24** were obtained by a hydrogenation of nicotinate **22** and a subsequent protection of the amino function with a *tert*-butyloxycarbonyl (Boc) group. To this end, conditions as described in a patent[41] were applied initially. However, under these conditions, the hydrogenation reaction did not lead to a conversion of the starting material (**22**). Accordingly, the procedure was modified by adding sulfuric acid to the reaction mixture in the hydrogenation step. With this modified protocol, the two diastereomeres *rac*-**23** and *rac*-**24** (in 3:1 ratio) were obtained in yields of 55% (*rac*-**23**) and 19% (*rac*-**24**) after separation by flash chromatography. The major diastereomere *rac*-**23** was oxidized with Dess–Martin periodinane analogous to a patent,[42] yielding the ketone **25** (74%; the oxidation of the two diastereomeres *rac*-**23** and *rac*-**24** as a mixture afforded **25** in approximately the same yield).

To introduce the side chain in the 5-position of **25**, we performed a Wittig reaction (analogously as it was described in literature for different compounds)[43] with the ylide generated from methoxymethyl triphenylphosphonium chloride by means of potassium *tert*-butoxide, which yielded the enol ether **26** (57%; 1:1 mixture of *E*- and *Z*-isomer; isomers not separated). The hydrolysis of the enol ether group was accomplished by a modified protocol for an analogous reaction from literature[43] using 2 M HCl (instead of 4 and 6 M) and a higher proportion of the solvent THF (6:1 instead of 1:1 of THF/acid). That way the undesired additional hydrolysis of the ester function could be reduced and diastereomeric aldehydes *rac*-**20**[44] and *rac*-**21** could be obtained in a yield of 78% as a 1:1 mixture, the separation of which appeared to be laborious due to their nearly identical chromatographic retention.

For the synthesis of the nipecotic acid derived hydrazine derivatives with a C1 spacer, *rac*-**11** and *rac*-**12**, at first a direct reductive hydrazine formation was attempted by converting the mixture of aldehydes *rac*-**20** and *rac*-**21** with *tert*-butyl carbazate applying different reducing agents (e.g., sodium cyanoborohydride or sodium borohydride). This, however, did not lead to the desired Boc-protected hydrazine derivatives. As an alternative, the introduction of the required hydrazine function should be accomplished by a Mitsunobu reaction following a protocol of Brosse et al.[45−47] Alcohols *rac*-**27**[44] and *rac*-**28**[48] required for this purpose were prepared by reduction of aldehydes *rac*-**20** and *rac*-**21** (in 1:1 mixture) with sodium borohydride (*rac*-**27** and *rac*-**28**; 1:1 mixture; 76%). The thus obtained 1:1 mixture of *rac*-**27** and *rac*-**28** (yield 76%) was treated with hydrazine derivative **29**,[47] triphenylphosphine, and diisopropyl azodicarboxylate (DIAD) in a Mitsunobu reaction. The formed product was subsequently freed from the phthalimide protecting group with methylhydrazine, yielding the hydrazine precursors *rac*-**30** and *rac*-**31** in good yields (38% and 43%, respectively) after separation with flash chromatography. Target compound *rac*-**12** as hydrochloride[49] was finally obtained in good yield (87%) by simultaneous hydrolysis of the ester function and cleavage of

DOI: 10.1021/acs.jmedchem.8b01602
J. Med. Chem. 2018, 61, 10310−10332

Scheme 2. Synthesis of Nipecotic Acid Derived Hydrazines with C1 Spacer (*rac*-11 and *rac*-12) and C2 Spacer (*rac*-13 and *rac*-14)[a]

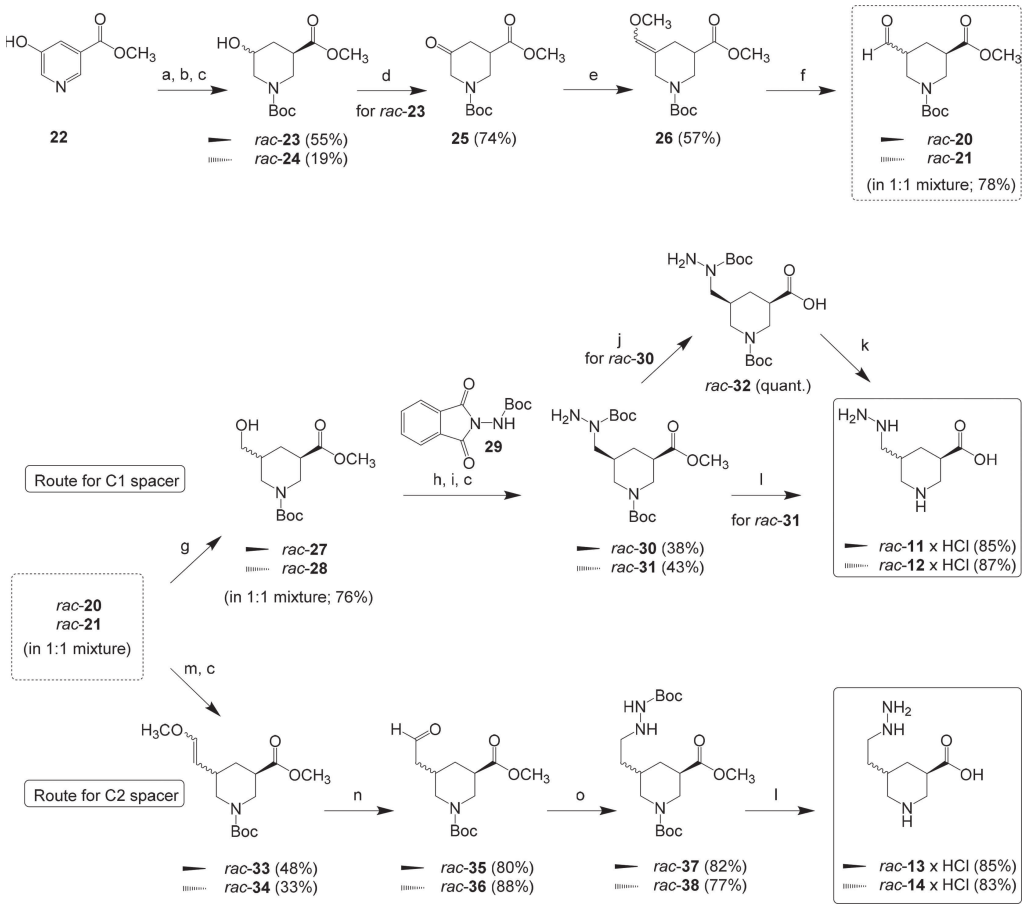

[a]Reagents and conditions: (a) H_2 (10 bar), Rh/Al_2O_3, H_2SO_4, MeOH, 80 °C, 16 h; (b) Boc_2O, NEt_3, dioxane, rt, 3 h; (c) separation of diastereomeres by flash chromatography; (d) Dess−Martin periodinane, DCM, rt, 2.5 h; (e) $Ph_3PCH_2OCH_3Cl$, *t*-BuOK, THF, −78 °C → rt, 2 h; (f) aq HCl (2 M), THF, 0 °C → rt, 2 d; (g) $NaBH_4$, EtOH, 0 °C, 1 h; (h) PPh_3, DIAD, **29**,[47] THF, 0 °C, 105 min; (i) CH_3NHNH_2, THF, 0 °C, 2 h; (j) aq NaOH (1 M), MeOH, 0 °C → rt, 15 h; (k) HCl in Et_2O (2 M), rt, 3 d; (l) aq HCl (1 M), H_2O, 60 °C (sealed high-pressure tube), 3 h; (m) $Ph_3PCH_2OCH_3Cl$, *t*-BuOK, THF, 0 °C → rt, 1.5 h; (n) aq HCl (2 M), THF, 0 °C → rt, 7−9 h; (o) Boc-$NHNH_2$, NaH_3BCN, AcOH, MeOH, 0 °C → rt, 2.5−3.5 h.

the Boc group of *rac*-**31** by heating to 60 °C in aqueous HCl and in a sealed high-pressure tube. The same procedure applied to *rac*-**30**, however, did not lead to the pure product *rac*-**11**. Instead, a mixture of *rac*-**11** with a side product was obtained, which presumably resulted from an intramolecular cyclization reaction of the hydrazine moiety with the carboxylic acid ester function. Hence, the procedure was modified. To avoid the undesired cyclization reaction, the deprotection of the functional groups was performed in two steps. First, the ester was hydrolyzed with NaOH to give the free acid *rac*-**32**, and then the Boc groups were cleaved in etheric HCl, giving the desired *rac*-**11** as hydrochloride[49] in good yield (85% over two steps).

For the preparation of nipecotic acid derivatives with the hydrazine function attached to a C2 spacer, we performed the Wittig reaction with aldehydes *rac*-**20** and *rac*-**21** analogous as for the synthesis of the enol ether **26**. The two diastereomeric enol ethers, *rac*-**33** and *rac*-**34**, could be isolated by flash chromatography in pure form (*rac*-**33**, 48%; *rac*-**34**, 33%). The enol ether hydrolysis of the individual diastereomeres proceeded more smoothly than with the analogues with shorter side chains, giving aldehydes *rac*-**35** and *rac*-**36** in yields of 80% and 88%. When reacted with *tert*-butyl carbazate in the presence of sodium cyanoborohydride and acetic acid following an analogous literature method,[50] the Boc-protected hydrazines *rac*-**37** and *rac*-**38** were obtained in good yields (85% and 83%, respectively). The protective groups in *rac*-**37** and *rac*-**38** (Boc and ester function) could finally be removed in one step by heating the compounds in hydrochloric acid to 60 °C in a sealed high-pressure tube. The hydrochlorides of the desired nipecotic acid derived hydrazines with C2 spacer, *rac*-**13** and *rac*-**14**,[49] were thus obtained in yields of 85% and 83%, respectively.

Aldehydes. Aldehydes **15a−15hp** (Chart 2), required for library generation, were mostly purchased from commercial suppliers and some synthesized by literature methods.[51,52] Aldehydes **15fd**, **15ff**, **15fh**, **15fi**, **15fn**, **15fp**, **15fs**, and **15gr** were synthesized in a Suzuki−Miyaura reaction[51,53] (see Supporting Information). Following previous approaches,[35,51,52] preferentially lipophilic, aromatic aldehydes were included in the libraries taking into account known structure−activity relationships for benchmark GAT inhibitors typically possessing a polar core structure (mostly an amino acid), a spacer of variable

DOI: 10.1021/acs.jmedchem.8b01602
J. Med. Chem. 2018, 61, 10310−10332

Chart 2. Libraries Consisting of Aldehydes 15a−15hp

length, and aromatic moieties (see compounds **4**–**9**). New aldehydes were added in the order of their availability.

Synthesis of Hydrazones. For the hit verification individual hydrazones, *rac*-**16** or *rac*-**18** were separately synthesized by combining 1.0 equiv of hydrazine, *rac*-**11**·HCl or *rac*-**13**·HCl, with 1.0 equiv of aldehyde **15** as shown in Scheme 1. Additionally, stoichiometric amounts of NaOD were added to neutralize HCl, introduced with the hydrazines.[49] For practical reasons, the reactions were performed in deuterated solvents

DOI: 10.1021/acs.jmedchem.8b01602
J. Med. Chem. 2018, 61, 10310−10332

Scheme 3. Example for the Conversion of Aldehyde Library 1 with Hydrazine *rac*-11 into *cis*-C1 Hydrazone Library 1

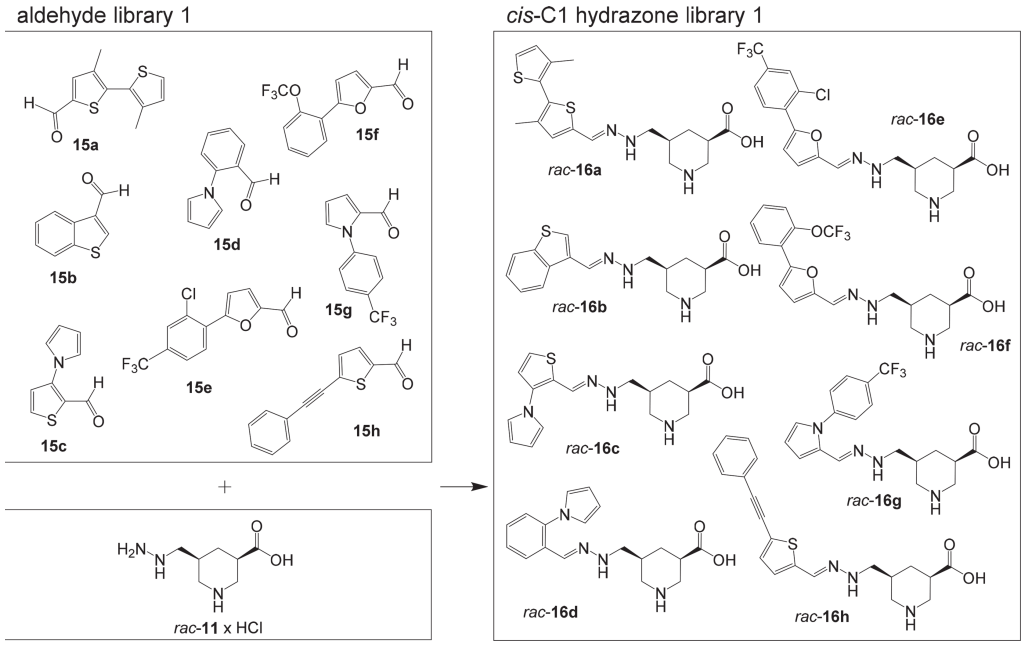

(DMSO-d_6/D_2O = 9:1) to be able to monitor reaction progress by NMR.[54]

General Aspects of Library Generation. The generation and screening of the hydrazone libraries delineated from hydrazine derivatives *rac*-**11**−*rac*-**14**, the synthesis of which was described above, should be accomplished analogous to a method recently published by us.[35]

In that case, a nipecotic acid derivative provided with a hydrazine function attached to the N-atom via a linker was incubated with aldehyde libraries, each library containing four constituents. For the sake of simplicity, hydrazone library formation was performed in the presence of the target, mGAT1. The incubation time was set to four hours, which was found sufficient for a complete conversion, and the pH adjusted to 7.1 being compatible with the presence of the proteins. The hydrazine was applied in excess (100 μM) compared to the aldehydes (four different aldehydes, concentration of each 10 μM) in order to render composition of the libraries constant, pseudostatic, although they are still dynamic. To determine the activity of the libraries, the incubation mixtures were directly used for competitive MS binding experiments. To this end, the MS marker NO711 (**6**) was directly added to the incubation mixture. After additional 40 min of incubation, the amount of specifically bound MS marker **6**, which is serving as a measure of the activity of the library (after liberation from the target), was quantified by LC-ESI-MS/MS.

Basically, for the present study, the experimental conditions were analogous to those in the initial approach as well as in a second subsequent application.[35,51] Hence, libraries were generated in the presence of the target mGAT1 and their activities were then analyzed by competitive MS Binding Assays as described above. However, the following changes were made: The library size was increased from four to eight (aldehydes per library), and the concentration of individual aldehydes was set to 1.0 μM. Finally, a library containing eight constituents in a concentration of 1 μM should be considered "active", if it reduced the amount of bound MS marker to <50%. Provided the activity of a library (i.e., the reduction of MS marker binding to <50%) was due to a single component, the affinity of this binder (IC_{50} value) should be at least 1 μM or lower. Besides, the concentration of the hydrazine derivatives *rac*-**11**−*rac*-**14** was raised to 200 μM as hydrazine concentrations of 100 μM (as in previous approaches)[35,51] did not lead to a complete hydrazone formation within the given incubation period (see Supporting Information). Hence, the 25-fold amount of hydrazines (*rac*-**11**−*rac*-**14**) as compared to total aldehyde concentration was applied for hydrazone library generation in the present study.

Screening and Deconvolution of Hydrazone Libraries. In the present study, a total of 224 aldehydes grouped in 28 libraries, each containing eight individual aldehydes in a concentration of 1.0 μM, were used (Chart 2). Each of the 28 aldehyde libraries was converted with all four hydrazines (*rac*-**11**−*rac*-**14**, applied as hydrochlorides,[49] 200 μM) in separate experiments into the corresponding libraries of hydrazones (Scheme 3). In the following, hydrazone libraries are termed "*cis*-C1", "*trans*-C1", "*cis*-C2", and "*trans*-C2" for hydrazones derived from *rac*-**16**, *rac*-**17**, *rac*-**18**, and *rac*-**19**, respectively, thus indicating their relative configurations and different spacer lengths.

The results of the screening experiments for the hydrazone libraries are shown in Figure 2. Control experiments with the aldehyde libraries 1−28 (aldehydes **15a**−**15hp**) and hydrazines *rac*-**11**−*rac*-**14** alone were performed to ensure that in the applied concentrations none of the building blocks affected the marker binding to a remarkable extent (see Supporting Information).

Nine *cis*-C1 hydrazone libraries (*rac*-**16**; libraries 1, 3, 6, 10, 23, 24, 25, 27, and 28; Figure 2a) and four *cis*-C2 hydrazone libraries (*rac*-**18**; libraries 1, 19, 23 and 24; Figure 2c) were found to reduce the remaining MS marker binding below 50% (by mean values of four replicates) and thus were considered active. Interestingly, all active libraries derived from *cis*-configured nipecotic acid derivatives, while the *trans*-C1 (*rac*-**17**, Figure 2b) and *trans*-C2 hydrazone libraries (*rac*-**19**, Figure

DOI: 10.1021/acs.jmedchem.8b01602
J. Med. Chem. 2018, 61, 10310−10332

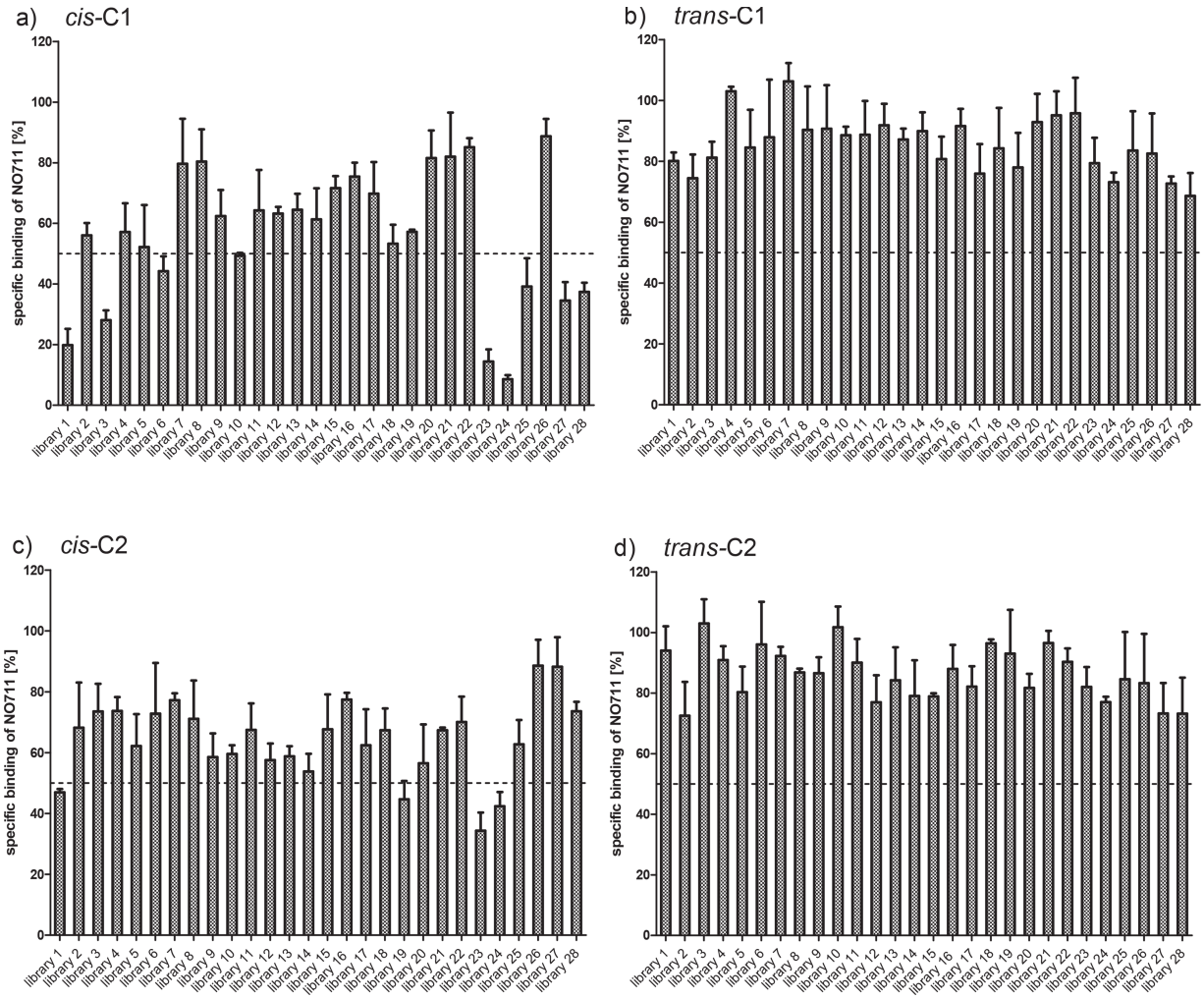

Figure 2. Screening of (a) *cis*-C1 (*rac*-**16**), (b) *trans*-C1 (*rac*-**17**), (c) *cis*-C2 (*rac*-**18**), and (d) *trans*-C2 hydrazone libraries (*rac*-**19**). The bars indicate the percentage of remaining specific binding of NO711 (**6**) after an incubation time of 4 h for library generation and 40 min for marker binding to mGAT1; data represent means ± SD of four replicates. The limit for further analysis of a library was defined as 50% remaining marker binding (indicated by the dashed line).

2d) did not show any striking activity toward mGAT1. All of the 13 hydrazone libraries considered active were further examined in deconvolution experiments in order to identify their most active components. For these experiments, single hydrazones were studied in the same way as the libraries except that only single aldehydes were employed in the test procedure (incubation of aldehydes in a concentration of 1.0 μM with hydrazine *rac*-**11** and *rac*-**13**, respectively, in a concentration of 200 μM). As summarized in Table 1, 16 hydrazones reduced MS marker binding below the set limit of 50%, while none of the corresponding aldehydes alone showed remarkable activity. Fourteen of the active compounds were represented by the shorter chained hydrazones *rac*-**16**, showing remaining MS marker binding of 16−49% (*rac*-**16e**, *rac*-**16r**, *rac*-**16fv**, *rac*-**16fw**, *rac*-**16fy**, *rac*-**16fz**, *rac*-**16ga**, *rac*-**16gb**, *rac*-**16gc**, *rac*-**16ge**, *rac*-**16gf**, *rac*-**16gg**, *rac*-**16gk**, and *rac*-**16ho**; Table 1, entries 5, 10, 42−43, 45−49, 51−53, 57, and 79). Among the longer chained derivatives, only hydrazones *rac*-**18e** and *rac*-**18fy** fulfilled the criterion for further analysis by reducing MS marker binding to 47% and 41%, respectively (Table 1, entries 5 and 45). As mentioned above, with a reduction of the marker binding to 50% or lower when applied in a concentration of 1 μM, "active" test compounds should correspond to a maximum IC_{50} of ~1 μM. Thus, we considered it worthwhile to subject all these 16 hydrazones to further analysis.

Hit Verification. For hit verification the 16 hydrazones found most active in deconvolution experiments were synthesized in pure form, and their binding affinities (pK_i values) were established in full-scale competitive MS binding experiments.

The pK_i values found for the hydrazones are in a range from 5.64 to 6.67 (Table 2). The binding affinities of the best 5-substituted nipecotic acid derived hydrazones (e.g., *rac*-**16gf**, Table 2, entry 11, or *rac*-**16gg**, Table 2, entry 12) are almost as good as those of yet established potent GAT1 inhibitors such as tiagabine (**5**, pK_i = 7.56) with the difference in the nominal pK_i values being only about one log unit.

Among the best binders from this study, one possesses a 3-phenoxyphen-1-yl (*rac*-**16r**, pK_i = 6.02, Table 2, entry 2), another a 2-(2-naphthyl)pyrimidin-5-yl (*rac*-**16ho**, pK_i = 6.03, Table 2, entry 14) residue. All other compounds are characterized by the presence of a 5-arylfuran-2-yl residue.

DOI: 10.1021/acs.jmedchem.8b01602
J. Med. Chem. 2018, 61, 10310−10332

Table 1. Results of the Deconvolution Experiments for "Active" Hydrazone Libraries

entry	library	compd 15/*rac*-16/*rac*-18	specific binding of NO711 [%][a] aldehyde 15	*cis*-C1 (*rac*-16)	*cis*-C2 (*rac*-18)	entry	library	compd 15/*rac*-16/*rac*-18	specific binding of NO711 [%][a] aldehyde 15	*cis*-C1 (*rac*-16)	*cis*-C2 (*rac*-18)
	library						library				
1	1	**-a**	106±6	74±8	79±6	41	23	**-fu**	82±16	68±6	61±9
2		**-b**	77±18	82±4	75±10	42		**-fv**	99±14	48±4	52±11
3		**-c**	82±17	86±9	72±6	43		**-fw**	103±9	46±6	69±14
4		**-d**	92±11	91±5	82±2	44		**-fx**	75±12	56±2	62±11
5		**-e**	98±4	40±2	47±4	45		**-fy**	97±8	40±7	41±5
6		**-f**	88±25	66±10	59±13	46		**-fz**	90±12	49±9	60±6
7		**-g**	87±21	75±5	74±14	47		**-ga**	88±13	38±4	54±4
8		**-h**	90±16	51±6	71±10	48		**-gb**	72±4	37±3	60±6
	library						library				
9	3	**-q**	100±14	74±15	-	49	24	**-gc**	70±5	38±2	70±4
10		**-r**	109±11	46±10	-	50		**-gd**	93±10	81±11	72±8
11		**-s**	114±6	81±1	-	51		**-ge**	99±3	36±2	72±7
12		**-t**	98±23	85±3	-	52		**-gf**	92±12	16±1	58±13
13		**-u**	107±10	87±3	-	53		**-gg**	103±18	32±1	76±4
14		**-v**	108±12	85±6	-	54		**-gh**	97±9	67±9	64±14
15		**-w**	113±12	83±14	-	55		**-gi**	86±15	84±11	73±4
16		**-x**	119±6	93±6	-	56		**-gj**	97±6	59±2	65±9
	library						library				
17	6	**-ao**	97±3	66±15	-	57	25	**-gk**	129±3	36±6	-
18		**-ap**	98±11	73±11	-	58		**-gl**	127±5	55±13	-
19		**-aq**	107±7	58±3	-	59		**-gm**	126±4	53±13	-
20		**-ar**	112±10	90±11	-	60		**-gn**	115±10	69±6	-
21		**-as**	108±13	72±11	-	61		**-go**	118±3	67±8	-
22		**-at**	101±11	80±9	-	62		**-gp**	112±15	55±3	-
23		**-au**	111±11	52±2	-	63		**-gq**	107±10	89±4	-
24		**-av**	112±2	70±15	-	64		**-gr**	121±5	93±4	-
	library						library				
25	10	**-bu**	113±7	85±2	-	65	27	**-ha**	98±7	85±7	-
26		**-bv**	118±5	80±13	-	66		**-hb**	108±17	52±10	-
27		**-bw**	116±9	81±16	-	67		**-hc**	107±18	75±6	-
28		**-bx**	121±7	84±8	-	68		**-hd**	104±26	61±7	-
29		**-by**	124±17	80±7	-	69		**-he**	101±5	87±16	-
30		**-bz**	129±6	88±3	-	70		**-hf**	122±10	50±7	-
31		**-ca**	121±15	84±6	-	71		**-hg**	118±8	64±12	-
32		**-cb**	113±8	80±13	-	72		**-hh**	113±19	55±7	-
	library						library				
33	19	**-eo**	107±15	-	60±7	73	28	**-hi**	103±15	60±15	-
34		**-ep**	103±1	-	62±5	74		**-hj**	116±9	68±11	-
35		**-eq**	99±10	-	62±20	75		**-hk**	118±7	73±12	-
36		**-er**	106±9	-	83±5	76		**-hl**	116±15	53±5	-
37		**-es**	105±12	-	61±15	77		**-hm**	118±2	60±3	-
38		**-et**	93±17	-	64±14	78		**-hn**	108±21	69±11	-
39		**-eu**	109±3	-	83±10	79		**-ho**	110±11	27±4	-
40		**-ev**	106±2	-	80±4	80		**-hp**	124±3	61±13	-

[a]Percentage of remaining specific binding of NO711 (**6**) in the presence of either pure aldehyde **15** or *cis*-C1 (*rac*-**16**) or *cis*-C2 hydrazones (*rac*-**18**) after an incubation time of 4 h for hydrazone formation and 40 min for marker binding to mGAT1; data represent means ± SD of four replicates. The limit for further analysis of a hydrazone was defined as 50% remaining marker binding (hydrazones considered active are highlighted in yellow).

Thereby, the furanyl moiety is linked to differently substituted phenyl residues or to a naphthyl residue. The hydrazone *rac*-**16gf** (pK_i = 6.67, Table 2, entry 11) bearing a 5-(1-naphthyl)furan-2-yl residue showed the highest binding affinity toward mGAT1 among all hydrazones in this study. For compounds with a 5-phenylfuran-2-yl residue monosubstituted at the phenyl ring, a chlorine atom in *ortho*-position gives rise to a binding affinity (*rac*-**16fv**, pK_i = 5.91, Table 2, entry 3) nominally slightly superior to that with a chlorine atom in *meta*-position (*rac*-**16fw**, pK_i = 5.73, Table 2, entry 4), while a trifluoromethyl substituent gives rise to a higher affinity in *meta*-(*rac*-**16gc**, pK_i = 6.15, Table 2, entry 9) than in *ortho*-position (*rac*-**16fz**, pK_i = 5.64, Table 2, entry 6). Compound *rac*-**16gk** (pK_i = 5.84, Table 2, entry 13) with a bromine atom in *ortho*-position of the phenyl ring showed a similar binding affinity as its chloro analogue *rac*-**16fv** (pK_i = 5.91, Table 2, entry 3). Except for compounds *rac*-**16gb** with an *ortho*-nitro and a *para*-chloro substituted phenyl ring (pK_i = 5.83, Table 2, entry 8) and *rac*-**16ge** with a *meta*-trifluoromethyl and a *para*-fluoro substitution (pK_i = 5.90, Table 2, entry 10), a second substituent (i.e., chloro or trifluoromethyl) at the phenyl ring was generally favorable, leading to pK_i values in a range of 6.19−6.61 (for *rac*-**16e**, *rac*-**16fy**, *rac*-**16ga**, *rac*-**16gg**, *rac*-**18e**, and *rac*-**18fy**). The hydrazone *rac*-**16gg** (pK_i = 6.61, Table 2, entry 12) bearing a 3,5-di(trifluoromethyl)phen-1-ylfuran-2-yl residue was found to be the best binder among all disubstituted phenyl moieties and in total second best after naphthylfuranyl derivative *rac*-**16gf** among all hydrazones. The shorter spacer length as in hydrazones *rac*-**16** (4 atoms) appears to be more favorable than the longer one in *rac*-**18** (5 atoms), as among *cis*-C1 hydrazones (*rac*-**16**) as compared to *cis*-C2 hydrazones (*rac*-**18**), more compounds fulfilling the activity criteria were found with higher affinities (pK_i = 6.67 for *rac*-**16gf** versus pK_i = 6.32 for *rac*-**18fy**). Still, with pK_i values of 6.21 (*rac*-**18e**, Table 2, entry 15) and 6.32 (*rac*-**18fy**, Table 2, entry 16), certain *cis*-C2 hydrazones (*rac*-**18**) also showed good binding affinities toward mGAT1 and their pK_i values are similar to the ones of their direct (i.e., possessing the same lipophilic moieties) shorter-spaced analogues *rac*-**16e** (pK_i = 6.35, Table 2, entry 1) and *rac*-**16fy** (pK_i = 6.19, Table 2, entry 5).

DOI: 10.1021/acs.jmedchem.8b01602
J. Med. Chem. 2018, 61, 10310−10332

Table 2. Binding Affinities (pK_i) Determined in Competitive Binding Assays at mGAT1 of Hydrazones Synthesized in Pure Form

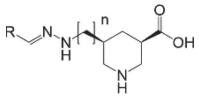

entry	compd[a]	n	R	pK_i[b,c]	entry	compd[a]	n	R	pK_i[b,c]
1	*rac*-**16e**	1	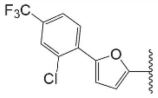	6.35±0.02	9	*rac*-**16gc**	1	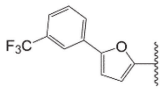	6.15±0.01
2	*rac*-**16r**	1	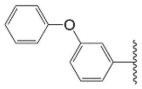	6.02±0.11	10	*rac*-**16ge**	1	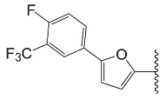	5.90±0.04
3	*rac*-**16fv**	1	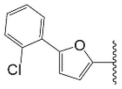	5.91±0.08	11	*rac*-**16gf**	1	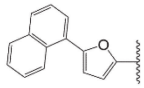	6.67±0.03
4	*rac*-**16fw**	1	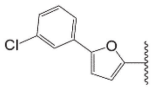	5.73±0.10	12	*rac*-**16gg**	1	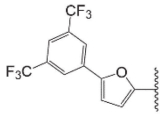	6.61±0.00
5	*rac*-**16fy**	1	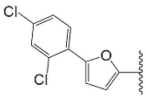	6.19±0.05	13	*rac*-**16gk**	1	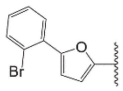	5.84±0.09
6	*rac*-**16fz**	1	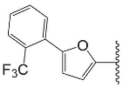	5.64±0.14	14	*rac*-**16ho**	1	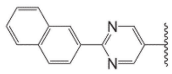	6.03±0.06
7	*rac*-**16ga**	1	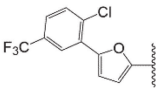	6.33±0.11	15	*rac*-**18e**	2	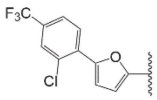	6.21±0.08
8	*rac*-**16gb**	1	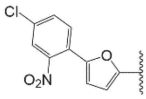	5.83±0.09	16	*rac*-**18fy**	2	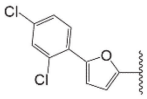	6.32±0.05

[a]Individually synthesized from appropriate aldehydes and hydrazines, see also ref 54. [b]pK_i values are given as means ± SEM of three independent experiments. [c]Tiagabine (**5**) was used as reference in all experiments, and a pK_i of 7.56 ± 0.06 (n = 8) was found for this compound.

Table 3. Comparison of Inhibitory Potencies (pIC_{50}) of Best Binders at mGAT1-mGAT4 from [^{3}H]GABA Uptake Experiments

		pIC_{50}[a]			
entry	compd	mGAT1	mGAT2	mGAT3	mGAT4
1	*rac*-**16e**	4.38 ± 0.15	65%	59%	53%
2	*rac*-**16ga**	4.09 ± 0.07	91%	57%	57%
3	*rac*-**16gf**	4.64 ± 0.10	64%	4.48 ± 0.09	4.12 ± 0.08
4	*rac*-**16gg**	50%	84%	65%	79%
5	*rac*-**18e**	4.35 ± 0.10	4.27 ± 0.09	4.23 ± 0.09	4.38 ± 0.03
6	*rac*-**18fy**	4.45 ± 0.10	4.27 ± 0.03	4.59 ± 0.09	4.82 ± 0.012

[a]Results of [^{3}H]GABA uptake assays performed with HEK cells stably expressing mGAT1-mGAT4; pIC_{50} values are given as means ± SEM of three independent experiments. In the case of low inhibitory potencies, percentages are given that represent remaining [^{3}H]GABA uptake in the presence of 100 μM test compound.

Interestingly, none of the evaluated hydrazones possesses an *ortho*-biphenyl residue as a lipophilic domain which was found to play a dominant role among the best binders from our previous library screening approaches focusing on nipecotic acid derivatives with the lipophilic arylalkyl domain being attached to the amino funcion.[35,51,52] Instead, the described screening of pseudostatic DCC libraries of 5-substituted nipecotic acid derivatives revealed mGAT1 ligands with good binding affinities exhibiting lipophilic aromatic moieties so far unprecedented for this type of bioactive compounds: The 3-phenoxyphenyl, 2-(2-naphthyl)pyrimidin-5-yl, 5-(1-naphthyl)furan-2-yl, and 5-phenylfuran-2-yl residue. Notably, the latter showed its highest binding affinities when the phenyl moiety was substituted with chloro or trifluoromethyl substituents. In case of the other three moieties, no corresponding substituted aldehydes were available that could have been included in the screening process.

After characterization of the binding affinities (pK_i values), we examined the functional activities, i.e., the inhibitory potencies (pIC_{50} values), at the four GABA transporter subtypes for the six best binders, *rac*-**16e**, *rac*-**16ga**, *rac*-**16gf**, *rac*-**16gg**, *rac*-**18e**, and *rac*-**18fy**. The results obtained in [^{3}H]GABA uptake assays with HEK cells stably expressing mGAT1-mGAT4[55] are summarized

DOI: 10.1021/acs.jmedchem.8b01602
J. Med. Chem. 2018, 61, 10310−10332

in Table 3. The pIC_{50} values at mGAT1 are in a range from 4.09 to 4.64 except for compound *rac*-**16gg**, which did not show an inhibitory potency high enough for reliable determination of a pIC_{50} value in concentrations up to 100 μM (Table 3, entry 4). Compound *rac*-**16gf**, which showed the highest affinity in the Binding Assays (pK_i = 6.67; Table 2, entry 11), also displayed the highest inhibitory potency of this series of hydrazones in the uptake assays at mGAT1 (pIC_{50} = 4.64; Table 3, entry 3). The observed subtype selectivities for the investigated compounds toward mGAT1 are considerably low and *rac*-**18fy** even showed its highest potency toward mGAT4 (pIC_{50} = 4.82, Table 3, entry 6).

The pIC_{50} values at mGAT1 from the uptake experiments are surprisingly low compared to the pK_i values from the binding experiments and the nominal differences of the values (pIC_{50} and pK_i) obtained in the two different test systems amounts to almost two log units. For comparison, for tiagabine (**5**) a pIC_{50} of 6.88 ± 0.12 was established in [^{3}H]GABA uptake assays at mGAT1,[55] which is less than about 0.7 log units lower than its nominal pK_i value from the MS binding experiments. To verify this unexpected outcome, i.e., the large difference between the binding affinities (pK_i) and the inhibitory potencies (pIC_{50}) at mGAT1, we characterized GAT1 mediated GABA uptake also at hGAT1 (i.e., the human equivalent of this GABA transporter subtype). The results obtained from these experiments (see Supporting Information) were, however, essentially the same as those obtained in the [^{3}H]GABA uptake assays for mGAT1.

So far, several hundreds of derivatives of nipecotic acid (**2**), guvacine (**3**), and related heterocyclic amino acids functionalized at the nitrogen atom with lipophilic arylalkyl residues have been characterized in our group in binding and uptake assays.[34,39,40,51,52,56] For all these compounds, pK_i values (from Binding Assays) were observed that are typically higher than the pIC_{50} values (from uptake experiments) but no more than about one log unit. Possibly, this discrepancy is due to differences in experimental parameters of the two test systems such as the target material (i.e., whole cells versus membrane fragments), the buffer constituents or the incubation protocol. Furthermore, it is worth mentioning that this phenomenon was reported by others also for monoamine transporter inhibitors characterized in binding and uptake assays (e.g., at the serotonin transporter).[57]

Hence, the disappointingly low inhibitory potencies of the synthesized hydrazones determined in mGAT1 uptake assays (pIC_{50}) as compared to the binding affinities (pK_i) were rather surprising. Even taking into account that there is a certain degree of uncertainty in the stated values, it could be concluded that this extent of discrepancy between affinity and inhibitory potency was remarkably higher than that observed by us for other GAT1 inhibitors so far. A possible instability of the hydrazones in the "Krebs" incubation buffer of the uptake experiments (containing glucose and Tris)[55] as explanation of this phenomenon could be ruled out by control experiments (see Supporting Information). Thus, the question arose if the synthesized hydrazones address the predicted binding site of known bench mark GAT1 inhibitors such as tiagabine (**5**) and NO711 (**6**).

Mode of Interaction. To shed light on the mode of interaction of the herein introduced hydrazones, *rac*-**16gf** (chosen as the most potent compound of the described series of hydrazones) and *rac*-**16gg** (chosen as the compound showing the highest difference between affinity in Binding Assays and inhibitory potency in uptake assays) were exemplarily examined, whether they inhibit the binding of NO711 (**6**) at mGAT1 in a competitive or noncompetitive manner. For this purpose, saturation experiments with NO711 (**6**) at mGAT1 in the presence of fixed concentrations of *rac*-**16gf**, *rac*-**16gg**, and tiagabine (**5**) were performed. The latter was applied as a GAT1 ligand generally assumed to inhibit NO711 (**6**) binding in a competitive way. Finally, the resulting saturation isotherms were compared with those obtained in the absence of these compounds (for experimental details, see Experimental Section).

In the presence of 100 nM and 1 μM tiagabine (**5**; the applied concentrations are about 0.6 and 1.6 log units higher than its corresponding pK_i value), the obtained saturation isotherms showed that the density of binding sites (B_{max}) for NO711 (**6**) remained unchanged, whereas the "apparent" equilibrium dissociation constants (K_{d_app}) of **6** were significantly enhanced (see Figure 3 and Table 4). Both results are completely in line with a competitive inhibition of NO711 (**6**) binding by tiagabine (**5**). According to Hulme and Trevethick,[58] a competitive binding interaction in this kind of saturation experiment can also be proven with a Schild-like plot. In a Schild-like plot, the logarithm of the term $\left(\frac{K_{d\_app}}{K_d} - 1\right)$, whereby K_{d_app} is the "apparent" K_d (in the presence of the test compound) and K_d is the "true" K_d (in the absence of test compounds), is displayed as a function of the concentration of the test compound. In the present case, a slope (here for the sake of simplicity referred to as Schild-like coefficient, see Table 4) of 1.05 ± 0.05 was found which further demonstrates the competitive character of the interaction between tiagabine (**5**) and NO711 (**6**) at mGAT1.

The saturation isotherms obtained in the presence of *rac*-**16gf** and *rac*-**16gg** in concentrations of 1 and 10 μM (i.e., concentrations about 0.6 and 1.7 log units higher than their corresponding pK_i values) were distinctly different as compared to those obtained in the presence of tiagabine (**5**). Both compounds, *rac*-**16gf** and *rac*-**16gg**, led to a significant decrease of B_{max}, indicating a noncompetitive interaction with respect to binding of NO711 (**6**) and the investigated hydrazones at mGAT1. The "apparent" K_d values in the presence of *rac*-**16gf** and *rac*-**16gg** are increased as well, but in this case in contrast to tiagabine (**5**), the calculated Schild-like coefficients amounted to only 0.49 ± 0.10 and 0.57 ± 0.12 for *rac*-**16gf** and *rac*-**16gg**, respectively (Table 4), arguing for a negative cooperativity according to Hulme and Trevethick.[58] Taken together, these results indicate that inhibition of NO711 (**6**) binding at mGAT1 by the investigated hydrazones *rac*-**16gf** and *rac*-**16gg** is noncompetitive and possibly not due to binding at the same site addressed by the reporter ligand **6** as well as by tiagabine (**5**).

For the sake of clarity, it should be pointed out that the term "noncompetitive" is used only phenomenologically, both in literature[59−62] and herein, to indicate that interactions of ligands with GAT1 give rise to altered saturation isotherms (with respect to GABA uptake and NO711 (**6**) binding experiments, respectively). Hence and as commonly accepted, the term "noncompetitive" does not specify the underlying mechanism by which a ligand interacts with its target, in the present case mGAT1. For instance, noncompetitive inhibition modes can be the result of an allosteric modulation or be caused by an irreversible binding or very slow dissociating orthosteric ligand.[63] To our knowledge, no studies have been published so far that experimentally verified the localization of an allosteric binding site at GAT1 (e.g., by site-directed mutagenesis experiments). To rule out the aforementioned kinetic phenomena (i.e., inhibition by irreversibly binding or very

DOI: 10.1021/acs.jmedchem.8b01602
J. Med. Chem. 2018, 61, 10310−10332

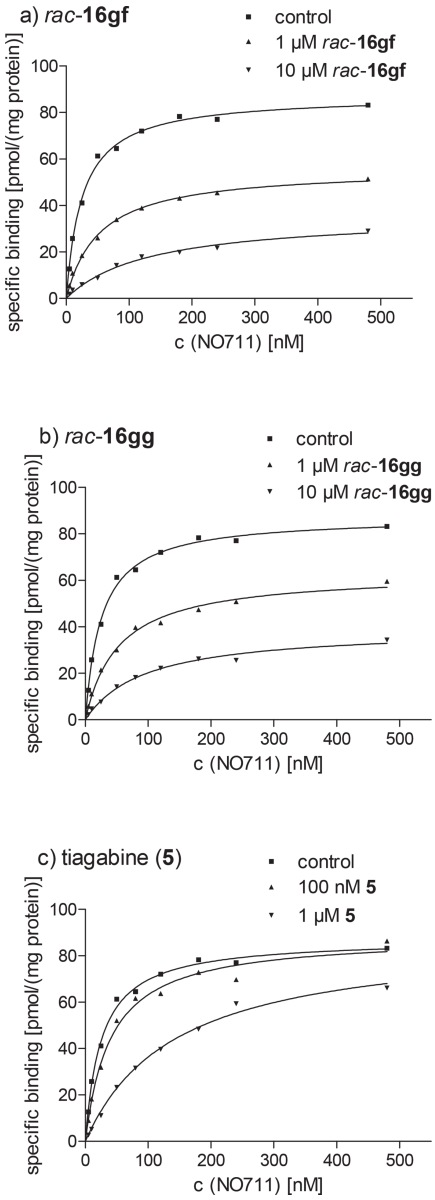

Figure 3. Saturation isotherms for NO711 (**6**) as reporter ligand addressing mGAT1. Data points represent specific binding (means from triplicates) obtained in the presence of (a) *rac*-**16gf**, (b) *rac*-**16gg**, and (c) tiagabine (**5**) (in different fixed concentrations as indicated) and for control also in the absence of any additional test compound.

slow dissociating orthosteric ligands) as cause for the noncompetitive inhibition mode of the hydrazones under discussion, the inhibitory potencies (pIC_{50}) of these compounds were determined in additional GABA uptake experiments using different time periods for preincubation, i.e., in one set of experiments 0 min instead of the commonly applied 25 min. The experimental details as well as the results obtained thereby are included in the Supporting Information. In short, the inhibitory potencies of the six hydrazones, *rac*-**16e**, *rac*-**16ga**, *rac*-**16gf**, *rac*-**16gg**, *rac*-**18e**, and *rac*-**18fy**, obtained when the preincubation time amounted to 0 min, are in a similar order of magnitude (i.e., pIC_{50} values in a range from 3.77 to 4.57) as those recorded for the previous experiments (i.e., with the preincubation time amounting to 25 min, pIC_{50} values in a range from 3.87 to 4.51 were obtained) with the nominal differences obtained for the two different incubation periods being minor and insignificant (nominal differences between 0 and 25 min preincubation amounting to only 0.1−0.4 log units). According to these results, a kinetic phenomenon as explanation for the observed noncompetitive behavior appears highly unlikely, thus supporting an allosteric mode of action at GAT1.

To gain insights in the functional consequences (i.e., regarding the inhibition of the GABA transport) associated with the noncompetitive interaction of the hydrazones *rac*-**16gf** and *rac*-**16gg** with GAT1, further GABA uptake experiments were performed in which either no inhibitor was applied, or hydrazones *rac*-**16gf** and *rac*-**16gg**, or finally tiagabine (**5**) as an example for a competitively acting compound. These experiments were carried out in form of MS based GABA uptake saturation experiments with ($^2H_6$)GABA as substrate using COS cells stably expressing hGAT1 as previously reported.[64,65] The saturation curves obtained from the saturation experiments in presence of the hydrazones *rac*-**16gf** and *rac*-**16gg** as well as tiagabine (**5**), which were applied in concentrations of about or below their pIC_{50} values, together with those from the control experiments (i.e., saturation curves obtained in the absence of GAT inhibitors) are exemplarily depicted in Figure 4. The K_m and K_{m_app} ("apparent" Michaelis−Menten constants in the presence of GAT inhibitors) as well as V_{max} values calculated from the data of these saturation experiments are shown in Table 5. As can be seen from these data, in the presence of tiagabine (**5**), the maximum velocities for ($^2H_6$)GABA transport at hGAT1 (i.e., V_{max}) are slightly decreased while the "apparent" Michaelis−Menten constants (K_{m_app}) are distinctly increased (see Table 5). The higher K_{m_app} values effected by tiagabine (**5**) are in line with a competitive inhibition mode, whereas the reduced V_{max} values are atypical for a competitive inhibitor, which is a result, however, that has already been reported before in literature for this compound (referred to as mixed competitive/noncompetitive inhibition mode).[66] Given that tiagabine (**5**) is commonly considered to competitively address the substrate binding site at GAT1,[33,34] we assume that the slightly decreased V_{max} values are at least partly due to the experimental conditions of the uptake experiment (with a 25 min preincubation period for preequilibration of the test compound with the target). Conversely, the observed behavior of the hydrazones *rac*-**16gf** and *rac*-**16gg** appeared to be completely different: both the V_{max} values and the K_{m_app} values are substantially decreased (see Table 5), again indicating a noncompetitive behavior of the hydrazones *rac*-**16gf** and *rac*-**16gg**, this time affecting the inhibition of the GABA transport at hGAT1 (while in the initial experiments described above a noncompetitive inhibition of the NO711 (**6**) binding at mGAT1 was observed).

Most notably, the herein introduced hydrazones lead to an increase of the affinity for the substrate GABA (**1**) toward its particular transporter, given the fact that the "apparent" Michaelis−Menten constants (K_{m_app}, see Table 5) for the GABA uptake at GAT1 are distinctly reduced in the presence of *rac*-**16gf** and *rac*-**16gg**. This observation, as well as the aforementioned results of the experiments using different incubation periods, clearly indicate an allosteric mode of action as explanation for the noncompetitive interaction between the aforementioned hydrazones and GAT1.

As noted above molecular modeling had indicated that nipecotic acid derivatives with lipophilic residues attached to the 5-position via an appropriate spacer might represent a new class

DOI: 10.1021/acs.jmedchem.8b01602
J. Med. Chem. 2018, 61, 10310−10332

Table 4. Characterization of the Mode of Interaction between the Reporter Ligand (6) and Compounds *rac*-16gf, *rac*-16gg, and 5[a]

		inhibitor[b]					
compd	parameters	100 nM	1 μM	10 μM	absent	coefficient[c]	conclusion
rac-**16gf**	B_{max} [pmol/mg]		48.4 ± 3.9**	28.3 ± 4.1**		0.49 ± 0.10	noncompetitive
	K_{d_app} [nM]		56.0 ± 7.1	111.9 ± 11.9*			
rac-**16gg**	B_{max} [pmol/mg]		57.1 ± 3.6*	38.9 ± 1.9**		0.57 ± 0.12	noncompetitive
	K_{d_app} [nM]		57.7 ± 3.8**	154.2 ± 45.9			
5	B_{max} [pmol/mg]	79.9 ± 4.3	81.0 ± 7.2			1.05 ± 0.05	competitive
	K_{d_app} [nM]	40.5 ± 1.0**	146.8 ± 7.7**				
control	B_{max} [pmol/mg]				79.5 ± 5.0		
	K_d [nM]				28.3 ± 1.5		

[a]Determined in saturation experiments using NO711 (**6**) as reporter ligand for mGAT1. [b]Saturation experiments were performed in the presence and absence (control) of *rac*-**16gf**, *rac*-**16gg**, and **5** (in different fixed concentrations as indicated). [c]Schild-like coefficients calculated according to Hulme and Trevethick.[58] All results are presented as means ± SEM from three independently performed experiments. Statistically significant differences from control values are indicated by asterisks (*P < 0.025, **P < 0.01 according to two-tailed Student's t-tests).

of GAT1 inhibitors. Being designed for the binding region representing the putative binding site of competitive GAT1 inhibitors such as tiagabine (**5**), these compounds had to be expected to show the same mode of action, in other words, to be competitive GAT1 inhibitors as well. Hence, it can be considered as a matter of serendipity that though the design aimed at competitive inhibitors, allosteric inhibitors most likely addressing a different binding site have been identified.

The distinct numerical differences observed between the pK_i values from the binding experiments and the pIC_{50} values from uptake experiments can hardly be explained by the allosteric mode of action of the hydrazone inhibitors alone. A conceivable explanation could be that binding of ligands or just different experimental conditions (including target material and buffer composition as already mentioned in the previous section) cause differences in the GAT1 conformation and the structure of the allosteric and the substrate binding site, which influence affinity and potency of investigated test compounds in the way observed in this study. Although such phenomena are well-known for neurotransmitter receptors such as the nicotinic acetylcholine receptor,[67] they have not yet been reported for GABA transporters so far. Hence, further investigations are required to elucidate this issue and also to improve the understanding of GAT1 mediated GABA transport in general.

The identified hydrazine inhibitors will be valuable tool compounds for mechanistic and pharmacological studies, although their pK_i and pIC_{50} values are lower than those for common competitive GAT1 inhibitors such as tiagabine (**5**), to which, however, they cannot be compared, as they address a different, namely, an allosteric instead of the competitive binding site (though it is generally desirable to have benchmark inhibitors as reference compounds in the assays used to characterize biological activities in a medicinal chemistry study—as we did with tiagabine herein).

Potential of the Identified Hydrazone Hits Allosterically Interacting with GAT1. Up to now, only few examples of noncompetitive inhibitors of GAT1 are known, for most of which the mechanistic rationale (e.g., allosteric modulation or irreversible binding) for their noncompetitive behaviors has still to be elucidated. Sarup et al.[59] described different N-substituted 3-hydroxy-4-amino-4,5,6,7-tetrahydro-1,2-benzisoxazols of which some, such as compound **39** (see Chart 3, pIC_{50} ~5.7 for inhibition of GABA uptake at mGAT1), were revealed as GAT1 inhibitors with noncompetitive mode of inhibition (based on reduced V_{max} values in GABA uptake saturation experiments). A structurally related compound of **39**, referred to as EF1502 (**40**), was shown to inhibit both mGAT1 and mGAT2 (≙ BGT1 according to HUGO) noncompetitively (pIC_{50} ~5.4 at mGAT1 and pIC_{50} ~4.7 at mGAT2, data refer to the more potent (*R*)-enantiomer of **40**).[60,61] Timple et al.[62] described the lignan derivative **41** as a noncompetitive inhibitor of several neurotransmitter transporters of the SLC6 family including the dopamine and the norepinephrine transporters as well as GAT1 (pIC_{50} ~4.7 at hGAT1). For the latter target, an allosteric modulation of the GABA (**1**) transport was proposed (based on reduced V_{max} and K_{m_app} values in GABA uptake saturation experiments). Remarkably, none of the aforementioned noncompetitive inhibitors, **39**–**41**, contains a free amino acid moiety let alone a nipecotic acid (**2**) subunit. Only compounds **39** and **40** can be considered to display a subunit analogous to an amino acid by accounting the 3-hydroxyisoxazol moiety as a bioisosteric replacement for a carboxylic acid.[68,69] Still, the hydrazones described herein represent a new class of allosteric GAT1 inhibitors differing substantially from the noncompetitive inhibitors known so far.

Interestingly, the (*R*)-enantiomer of EF1502 (**40**), despite being clearly less potent than tiagabine (**5**) at GAT1 in vitro, has already been shown to exhibit potent anticonvulsant effects in different in vivo models and, furthermore, to interact synergistically with tiagabine (**5**), while potential adverse effects were only additive.[61] Although the pharmacological profile of the hydrazones *rac*-**16gf** and *rac*-**16gg** is not sufficiently evaluated so far, it can be assumed that these compounds could also mediate promising pharmacological effects, as these compounds share several common features with EF1502 (**40**), i.e., they interact noncompetitively at GAT1, address other GAT subtypes apart from GAT1, and have inhibitory potencies in a similar range. However, the herein introduced hydrazones also display noteworthy differences in the biological activities as compared to EF1502 (**40**), making hydrazones *rac*-**16gf** and *rac*-**16gg** highly interesting complementary compounds. For instance, they exhibit a different profile of subtype selectivities: While EF1502 (**40**) inhibits both mGAT1 and mGAT2 (≙ BGT1) with similar potencies, hydrazones *rac*-**16gf** and *rac*-**16gg** are less potent at mGAT2 but show potencies at mGAT3 and mGAT4, respectively, almost as high as at mGAT1 (see

DOI: 10.1021/acs.jmedchem.8b01602
J. Med. Chem. 2018, 61, 10310−10332

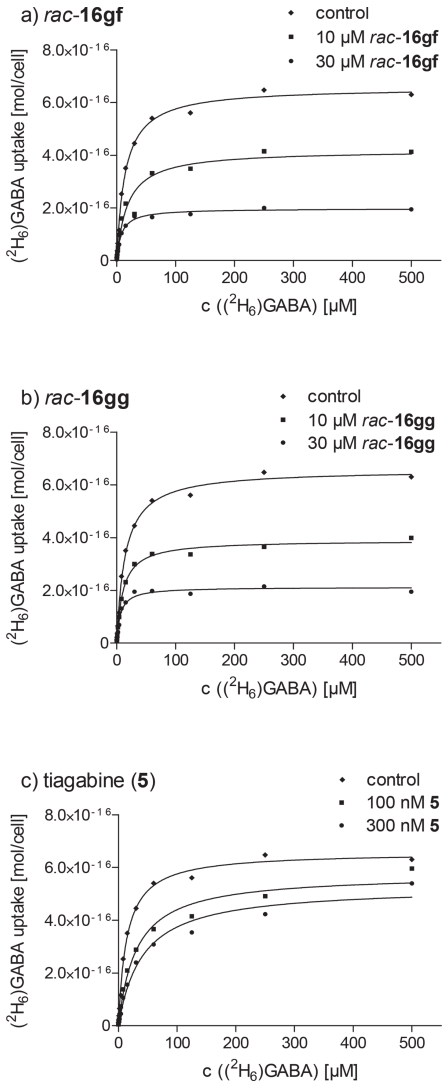

Figure 4. Saturation isotherms for the ($^2H_6$)GABA uptake at hGAT1. Data points represent specific uptake (means from triplicates) obtained in the presence of (a) *rac*-**16gf**, (b) *rac*-**16gg**, and (c) tiagabine (**5**) (in different fixed concentrations as indicated) and for control (i.e., in the absence of any GAT inhibitor).

Chart 3. Compounds Proposed As Noncompetitive GAT1 Inhibitors (39−41) in Literature

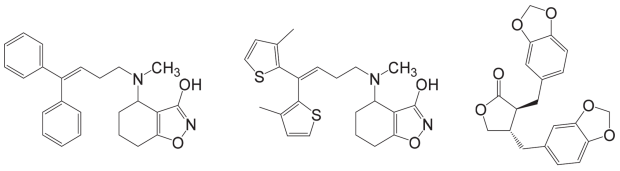

39 EF1502 (**40**) **41**

Table 3). Furthermore, and possibly even more important, the capability of compounds *rac*-**16gf** and *rac*-**16gg** to increase the affinity for the substrate at GAT1 (i.e., reducing the "apparent" Michaelis−Menten constants, K_{m_app}) and at the same time to reduce the maximum velocity (V_{max}) of GABA transport provides a pharmacological potential that has not been explored up to date. To our knowledge, only the lignan derivative **41** has so far been reported to reduce the "apparent" Michaelis−Menten constants (K_{m_app}) for the substrate at GAT1 similarly as it is shown here for the hydrazones *rac*-**16gf** and *rac*-**16gg**. Conversely, this compound, **41**, was more active at dopamine and norepinephrine transporters than at GAT1 and was thus published in the context of a potential drug therapy for the attention deficit hyperactivity disorder.[62] Hydrazone *rac*-**16gf** is about equally potent at GAT1 as lignan derivative **41** (with respect to the nominal pIC_{50} values), and in this context it is worth mentioning that the hydrazones are, in contrast to compound **41**, still racemic, therefore providing the possibility that the corresponding eutomers could be even slightly more potent.

Hence, the herein introduced 5-substituted nipecotic acid derivatives represent valuable new tools for investigation of allosteric modulation of GAT1 mediated GABA uptake in vitro. These compounds may also exert a promising new pharmacological profile by their specific mode of GAT inhibition and be a helpful starting point for the development of distinctly more affine and potent GAT1 inhibitors addressing the allosteric binding site under discussion. Finally, on the basis of experiences with analogous compounds,[51] it appears reasonable to assume that the hydrazone function within the spacer of this class of synthesized compounds can be replaced by a corresponding propenyl group, leading to stable carba analogues without

Table 5. Characterization of the Mode of GABA Uptake Inhibition at GAT1 by Compounds *rac*-16gf, *rac*-16gg, and 5[a]

			inhibitor[c]					
compd	pIC_{50}[b] (hGAT1)	parameters	100 nM	300 nM	10 µM	30 µM	absent	conclusion
rac-**16gf**	4.37 ± 0.06	V_{max}[d]			332 ± 56**	165 ± 27**		noncompetitive
		K_{m_app}[d]			10.1 ± 4.0	5.7 ± 1.1**		
rac-**16gg**	3.87 ± 0.03	V_{max}[d]			341 ± 26**	183 ± 26**		noncompetitive
		K_{m_app}[d]			8.2 ± 1.2*	5.1 ± 0.6**		
5	6.81 ± 0.15[e]	V_{max}[d]	491 ± 61*	419 ± 59**				mixed[f]
		K_{m_app}[d]	19.7 ± 5.5	29.4 ± 5.8*				
control		V_{max}[d]					570 ± 53	
		K_m[d]					12.0 ± 1.2	

[a]Determined in saturation experiments based on MS Transport Assays at hGAT1. [b]The inhibitory potencies (pIC_{50}) at hGAT1 were determined in competition experiments based on MS Transport Assays. [c]Saturation experiments were performed in the presence and absence (control) of *rac*-**16gf**, *rac*-**16gg**, and **5** (in different fixed concentrations as indicated). All results are presented as means ± SEM from three independently performed experiments. [d]V_{max} values are given in [amol/cell·min], K_m values in [µM]. Statistically significant differences from control values are indicated by asterisks (*P < 0.05, **P < 0.01 according to paired, one-tailed Student's t-tests). [e]Value from ref 64. [f]Mixed competitive/noncompetitive, see discussions in the text.

DOI: 10.1021/acs.jmedchem.8b01602
J. Med. Chem. 2018, 61, 10310−10332

remarkable loss of functional activity that should be well suitable for future in vivo experiments.

CONCLUSION

In summary, nipecotic acid derivatives with a novel substitution pattern were explored with the aim of finding new GABA uptake inhibitors. Therefore, the 5-substituted nipecotic acid derivatives *rac*-**11**−*rac*-**14** possessing a hydrazine function were synthesized and applied as building blocks in DCC reactions with appropriate aldehydes for the generation of pseudostatic hydrazone libraries, which were screened for their affinities toward mGAT1 by means of MS Binding Assays.[35,51] This approach, i.e., the combined generation and screening of pseudostatic hydrazone libraries by means of MS Binding Assays, was again found to represent a powerful tool for structure−activity relationship studies of ligands for mGAT1, and it finally revealed new lipophilic moieties for 5-substituted nipecotic acid derivatives as GAT1 ligands. A total of nearly 900 hydrazones could be screened toward mGAT1, of which the 16 most active were selected for further evaluation of their binding affinities. The six best binders, *rac*-**16e**, *rac*-**16ga**, *rac*-**16gf**, *rac*-**16gg**, *rac*-**18e**, and *rac*-**18fy**, with pK_i values of 6.21−6.67, are *cis*-configured with respect to the substituents of the piperidine ring and are characterized by 5-arylfuran-2-yl residues as lipophilic domains, a moiety that is not known so far in GABA uptake inhibitors. With a pK_i value of 6.67 compound *rac*-**16gf** bearing a 5-(1-naphthyl)furan-2-yl residue and a four atom spacer showed the highest binding affinity within the series of hydrazones described in this study. Furthermore, the six best binders were subjected to functional characterization at the different GABA transporter subtypes, at which, however, they displayed rather low to moderate inhibitory potencies (pIC_{50} values up to 4.64 at mGAT1) and low subtype selectivities. In MS binding experiments with NO711 (**6**) as a reporter ligand addressing mGAT1 and compound *rac*-**16gf** as well as *rac*-**16gg**, a noncompetitive mode of interaction between the binding of the evaluated hydrazones and the reporter ligand could be demonstrated. Additional uptake experiments furthermore suggested an allosteric mode of action of the GABA (**1**) transport at GAT1.

Hence, it can be concluded that substitution of the 5-position of nipecotic acid represents an interesting structural variation leading to new GAT1 inhibitors with an interaction mode that differs distinctly from that of well-known GAT1 inhibitors such as tiagabine (**5**). And, more notably, those hydrazones, which represent the first allosteric modulators of GAT1 derived from nipecotic acid (**2**), might emerge as valuable tools for investigations with the aim to gain more insights in the physiological relevance of allosteric modulation of GAT1.

EXPERIMENTAL SECTION

Chemistry. Solvents for synthesis, extraction, and flash chromatography were distilled before use. Anhydrous THF was prepared by drying over benzophenone/Na. Other commercially available reagents (by ABCR, Acros, Alfa Aesar, Fisher Scientific, Maybridge, Merck, Sigma-Aldrich, TCI, and VWR) were used without further purification. TLC was carried out on precoated silica gel F_{254} glass plates (Merck) and detected under UV light (λ = 254 and 366 nm) or by staining with a ninhydrin solution (0.3 g of ninhydrin and 3 mL of acetic acid dissolved in 100 mL 1-butanol).[70] Flash column chromatography was performed on silica gel 60 (grading 0.035−0.070 mm, purchased from Merck and Acros). NMR spectroscopy was performed on Avance III HD Bruker BioSpin (Bruker: ^{1}H NMR, 400 or 500 MHz; ^{13}C NMR, 101 or 126 MHz; ^{19}F NMR, 376 MHz) or JNMR-GX (JEOL: ^{1}H NMR, 400 or 500 MHz; ^{13}C NMR, 101 or 126 MHz) spectrometers. The spectra were processed with the NMR software MestReNova, versions 8.1, 10.0, and 12.0 (Mestrelab Research SL). Chemical shifts were internally referenced to TMS or MeOH (for samples dissolved in D_2O), except for hydrazones, which were referenced to DMSO solvent signals (^{1}H NMR, 2.53 ppm; ^{13}C NMR, 39.13 ppm). IR spectroscopy was performed on a FT-IR Paragon 1000 (PerkinElmer) spectrometer and analyzed with the software Spectrum v2.00 (PerkinElmer). Samples were either pressed in KBr pellets or prepared as films between NaCl plates. High-resolution mass spectrometry was performed with Jeol MStation sector field mass spectrometer (Jeol), Thermo Finnigan MAT 95 (ThermoFischer Scientific) (both EI), or Thermo Finnigan LTQ FT Ultra mass spectrometer (ThermoFischer Scientific) (ESI). Elemental analysis for hydrazines *rac*-**11**−*rac*-**14** was performed with a Vario Micro Cube or Vario EL Cube (Elementar) and an 888 Titrando (Metrohm) in order to determine the corresponding amounts of hydrogen chloride and water of hydration.[49] Melting points were determined in open capillaries on a Büchi 510 melting point apparatus and are uncorrected. For purity testing, quantitative NMR spectroscopy (qNMR) was performed in accordance to the journal protocol[71,72] on a Avance III HD Bruker BioSpin (Bruker: ^{1}H NMR, 400 MHz) spectrometer. As internal calibrants (IC) dimethyl sulfone (TraceCERT certified reference compound, lot no. BCBH9813V, purity: 99.73%) or maleic acid (TraceCERT certified reference compound, lot no. BCBM8127V, purity: 99.94%) purchased from Sigma-Aldrich were used. The purity was calculated with the NMR software MestReNova, versions 10.0 and 12.0 (Mestrelab Research SL). The newly synthesized aldehydes and hydrazines were ≥95% pure. The metastable hydrazones[54] were used without purity determination but were synthesized from ≥95% pure building blocks in a 1:1 mixture, and completeness of the reaction was monitored by NMR. All individually synthesized hydrazones were checked for PAINS[73] with ZINC (http://zinc15.docking.org/patterns/home/);[74] no potential PAINS liabilities were identified with this in silico tool.

General Procedure for the Simultaneous Hydrolysis of Ester and Cleavage of Boc Protecting Groups (GP1). The corresponding hydrazine precursor (1.0 equiv) was suspended in a 1 M aqueous HCl (30 equiv, 30 mL/mmol), and the mixture was heated to 60 °C in a sealed high-pressure tube for 3 h. Then the reaction was cooled to rt, diluted with H_2O (15 mL), and washed with DCM (3 × 15 mL). The aqueous solution was freeze-dried.

General Procedure for the Hydrolysis of Enol Ethers (GP2). The corresponding enol ether (1.0 equiv) was dissolved in THF (11 mL/mmol), cooled to 0 °C, and a 2 M aqueous HCl (3.7 equiv) was added. The reaction was stirred at 0 °C for 2 h and at rt for further 5−7 h. Then the reaction was quenched with $NaHCO_3$ (4.6 equiv) and dissolved in H_2O (20 mL). *iso*-Hexane (5 mL) was added, the phases were separated, and the aqueous phase was further extracted with DCM (4 × 25 mL). The combined organic phases were dried over Na_2SO_4 and concentrated under reduced pressure. The crude product was purified by flash chromatography on silica gel (EtOAc/*iso*-hexane = 1:3).

General Procedure for the Reductive Hydrazine Formation (GP3). The corresponding aldehyde (1.0 equiv) and *tert*-butyl carbazate (1.6 equiv) were dissolved in MeOH (33 mL/mmol) under Ar and stirred at rt for 1 h. Then the mixture was cooled to 0 °C, AcOH (2.5 equiv), and subsequently $NaBH_3CN$ (4.0 equiv, in portions) were added. It was stirred at 0 °C for 2 h and at rt for further 80 min. Then the mixture was concentrated under reduced pressure, quenched with an aqueous $NaHCO_3$ solution (20 mL), and extracted with DCM (5 × 20 mL). The combined organic phases were dried over Na_2SO_4 and concentrated under reduced pressure. The crude product was purified by flash chromatography on silica gel (EtOAc/*iso*-hexane = 1:1).

General Procedure for the Preparation of Hydrazones (GP4). The reactions were performed in sealed 1.5 mL tubes under Ar. To 850 μL of DMSO-d_6, a 200 mM stock solution of the corresponding hydrazine hydrochloride[49] in D_2O (50 μL, 1.0 equiv, 0.010 mmol), a 1 M solution of NaOD in D_2O (20 μL, 2.0 equiv, 0.020 mmol for *rac*-**11**·HCl and 30 μL, 3.0 equiv, 0.030 mmol for *rac*-**13**·HCl) and D_2O (30 or

DOI: 10.1021/acs.jmedchem.8b01602
J. Med. Chem. 2018, 61, 10310−10332

20 μL) were added to reach a total volume of 950 μL. The reaction was started by the addition of a 200 mM stock solution of the appropriate aldehyde in DMSO-d_6 (50 μL, 1.0 equiv, 0.010 mmol). The mixture was sonicated for 5−15 min and stored at rt overnight. All NMR and HRMS measurements as well as the MS Binding Assays and GABA uptake assays were performed using this 10 mM solution without further purification.[54] Analysis of the ^{1}H NMR spectra showed that the reaction equilibrium was ≥96% on the side of the products (determined by integration of the remaining signal of the aldehyde proton) and the hydrazones existed to ≥83% as *E*-isomers.

***rac*-(3*R*,5*S*)-[5-(Hydrazinylmethyl)piperidine-3-carboxylic Acid]−Hydrogen Chloride−Water (1/2/1) (*rac*-11·HCl).** *rac*-**32** (53 mg; 0.14 mmol) was dissolved in a 2 M etheric HCl (4.8 mL, 9.6 mmol). The solution was stirred under Ar at rt for 3 d. Then the mixture was concentrated under reduced pressure, diluted with H_2O (15 mL), and washed with DCM (3 × 15 mL). The aqueous solution was freeze-dried, and *rac*-**11**·HCl was obtained as white solid (36 mg, 85%); mp 130 °C (decomposition). ^{1}H NMR (500 MHz, 1 M NaOD in D_2O, 25 °C): δ 1.14 (q, *J* = 12.4 Hz, 1 H), 1.65−1.77 (m, 1 H), 2.02 (d, *J* = 12.8 Hz, 1 H), 2.14 (t, *J* = 11.9 Hz, 1 H), 2.32 (tt, *J* = 12.0/3.7 Hz, 1 H), 2.43 (t, *J* = 11.9 Hz, 1 H), 2.57 (dd, *J* = 11.9/6.8 Hz, 1 H), 2.60 (dd, *J* = 11.9/6.8 Hz, 1 H), 2.98 (dm, *J* = 12.0 Hz, 1 H), 3.11 (dm, *J* = 11.9 Hz, 1 H) ppm.[75] ^{13}C NMR (126 MHz, 1 M NaOD in D_2O, 25 °C): δ 32.9, 34.2, 45.9, 48.2, 49.1, 57.9, 183.7 ppm. IR (film): $\tilde{\nu}$ 3421, 2962, 2839, 2810, 1723, 1589 cm^{-1}. HRMS (ESI): [M + H]$^+$ calcd for $C_7H_{16}N_3O_2$ 174.1237, found 174.1236. Purity (qNMR: 1 M NaOD in D_2O, 25 °C, maleic acid, m_S = 6.951 mg, m_{IC} = 9.117 mg): 96%.

***rac*-(3*R*,5*R*)-[5-(Hydrazinylmethyl)piperidine-3-carboxylic Acid]−Hydrogen Chloride−Water (1/3/1) (*rac*-12·HCl).** According to GP1 with *rac*-**31** (85 mg, 0.22 mmol) and a 1 M aqueous HCl (6.6 mL, 6.6 mmol). *rac*-**12**·HCl was obtained as white solid (57 mg; 87%); mp 135 °C (decomposition). ^{1}H NMR (400 MHz, 1 M NaOD in D_2O, 25 °C): δ 1.56−1.65 (m, 1 H), 1.74−1.85 (m, 1 H), 1.87−1.96 (m, 1 H), 2.41 (tt, *J* = 7.7/4.3 Hz, 1 H), 2.48 (dd, *J* = 13.1/6.8 Hz, 1 H), 2.66 (dd, *J* = 12.0/6.7 Hz, 1 H), 2.70 (dd, *J* = 12.0/7.4 Hz, 1 H), 2.75−2.92 (m, 3 H) ppm.[75] ^{13}C NMR (101 MHz, 1 M NaOD in D_2O, 25 °C): δ 30.9, 31.2, 41.2, 47.5, 48.0, 56.3, 183.7 ppm. IR (film): $\tilde{\nu}$ 3428, 2958, 2851, 2366, 1719, 1618, 1595, 1560 cm^{-1}. HRMS (ESI): [M + H]$^+$ calcd for $C_7H_{16}N_3O_2$ 174.1237, found 174.1241. Purity (qNMR: 1 M NaOD in D_2O, 25 °C, maleic acid, m_S = 6.166 mg, m_{IC} = 5.709 mg): 98%.

***rac*-(3*R*,5*R*)-[5-(2-Hydrazinylethyl)piperidine-3-carboxylic acid]−Hydrogen Chloride−Water (1/3/1) (*rac*-13·HCl).** According to GP1 with *rac*-**37** (69 mg, 0.17 mmol) and 1 M aqueous HCl (5.3 mL, 5.3 mmol). *rac*-**13**·HCl was obtained as white solid (46 mg, 85%); mp 145 °C (decomposition). ^{1}H NMR (500 MHz, 1 M NaOD in D_2O, 25 °C): δ 1.11 (q, *J* = 12.3 Hz, 1 H), 1.29−1.43 (m, 2 H), 1.44−1.55 (m, 1 H), 2.02 (d, *J* = 12.8 Hz, 1 H), 2.11 (t, *J* = 11.8 Hz, 1 H), 2.30 (tt, *J* = 12.0/3.7 Hz, 1 H), 2.42 (t, *J* = 11.9 Hz, 1 H), 2.73 (dd, *J* = 12.3/7.0 Hz, 1 H), 2.76 (dd, *J* = 12.1/6.8 Hz, 1 H), 2.94 (dm, *J* = 12.2 Hz, 1 H), 3.09 (dm, *J* = 12.2 Hz, 1 H) ppm.[75] ^{13}C NMR (126 MHz, 1 M NaOD in D_2O, 25 °C): δ 31.5, 33.9, 34.8, 46.2, 48.2, 50.9, 51.1, 184.0 ppm. IR (film): $\tilde{\nu}$ 3409, 2955, 2802, 2562, 2347, 1723, 1560 cm^{-1}. HRMS (ESI): [M + H]$^+$ calcd for $C_8H_{18}N_3O_2$ 188.1394, found 188.1393. Purity (qNMR: 1 M NaOD in D_2O, 25 °C, maleic acid, m_S = 11.26 mg, m_{IC} = 8.962 mg): ≥99%.

***rac*-(3*R*,5*S*)-[5-(2-Hydrazinylethyl)piperidine-3-carboxylic Acid]−Hydrogen Chloride−Water (1/3/1) (*rac*-14·HCl).** According to GP1 with *rac*-**38** (154 mg; 0.384 mmol) and 1 M aqueous HCl (11.5 mL, 11.5 mmol). *rac*-**14**·HCl was obtained as white solid (101 mg, 83%); mp 143 °C (decomposition). ^{1}H NMR (400 MHz, 1 M NaOD in D_2O, 25 °C): δ 1.37−1.53 (m, 2 H), 1.53−1.66 (m, 2 H), 1.86−1.97 (m, 1 H), 2.34−2.51 (m, 2 H), 2.68−2.82 (m, 4 H), 2.85 (dd, *J* = 13.1/6.4 Hz, 1 H) ppm.[75] ^{13}C NMR (101 MHz, 1 M NaOD in D_2O, 25 °C): δ 29.6, 31.0, 32.7, 41.3, 47.5, 49.7, 51.5, 184.0 ppm. IR (film): $\tilde{\nu}$ 3415, 2955, 2850, 2569, 1719, 1571 cm^{-1}. HRMS (EI, 70 eV): M$^+$ calcd for $C_8H_{17}N_3O_2$ 187.1321, found 187.1332. Purity (qNMR: 1 M NaOD in D_2O, 25 °C, maleic acid, m_S = 5.076 mg, m_{IC} = 7.986 mg): ≥99%.

***rac*-(3*R*,5*S*)-(5-{[(*E*)-2-({5-[2-Chloro-4-(trifluoromethyl)-phenyl]furan-2-yl}methylidene)hydrazin-1-yl]methyl}-piperidine-3-carboxylic Acid)−Sodium Chloride (1/2) (*rac*-16e).**[54] According to GP4 with *rac*-**11**·HCl, 5-[2-chloro-4-(trifluoromethyl)phenyl]-2-furaldehyde (**15e**) and 1 M NaOD (20 μL) *rac*-**16e** was obtained quantitatively in solution. Besides the major *E*-isomer, the *Z*-isomer is present in 8%. ^{1}H NMR (500 MHz, DMSO-d_6/D_2O = 9:1, 25 °C): δ 1.22 (q, *J* = 12.5 Hz, 1 H), 1.99−2.10 (m, 1 H), 2.13 (d, *J* = 13.5 Hz, 1 H), 2.44−2.60 (m, 2 H), 2.73 (t, *J* = 12.5 Hz, 1 H), 3.09 (dd, *J* = 13.5/6.7 Hz, 1 H), 3.14 (dd, *J* = 13.7/6.2 Hz, 1 H), 3.28 (dd, *J* = 12.5/4.2 Hz, 1H), 3.35 (dd, *J* = 12.5/4.0 Hz, 1 H), 6.67 (d, *J* = 3.7 Hz, 1 H), 7.41 (d, *J* = 3.7 Hz, 1 H), 7.56 (s, 1 H), 7.80 (dd, *J* = 8.5/1.9 Hz, 1 H), 7.92 (s, 1 H), 8.07 (d, *J* = 8.4 Hz, 1 H) ppm.[75,76] ^{13}C NMR (126 MHz, DMSO-d_6/D_2O = 9:1, 25 °C): δ 30.4, 32.7, 39.8, 45.2, 46.0, 50.6, 109.3, 115.5, 123.3 (q, J_{CF} = 272.7 Hz), 123.8, 124.4 (q, J_{CF} = 4.4 Hz), 127.7 (q, J_{CF} = 4.1 Hz), 127.9, 128.1 (q, J_{CF} = 32.8 Hz), 128.9, 131.6, 146.7, 152.7, 173.9 ppm.[76] ^{19}F {^{1}H} NMR (376 MHz, DMSO-d_6/D_2O = 9:1, 25 °C): δ −61.1 ppm.[76] HRMS (ESI): [M + H]$^+$ calcd for $C_{19}H_{20}N_3O_3ClF_3$ 430.1140, found 430.1139.

***rac*-(3*R*,5*S*)-(5-{[(*E*)-2-[(3-Phenoxyphenyl)methylidene]-hydrazin-1-yl]methyl}piperidine-3-carboxylic Acid)−Sodium Chloride (1/2) (*rac*-16r).**[54] According to GP4 with *rac*-**11**·HCl, 3-phenoxybenzaldehyde (**15r**), and 1 M NaOD (20 μL), *rac*-**16r** was obtained quantitatively in solution. Besides the major *E*-isomer, the *Z*-isomer is present in 3%. ^{1}H NMR (500 MHz, DMSO-d_6/D_2O = 9:1, 25 °C): δ 1.19 (q, *J* = 12.3 Hz, 1 H), 1.97−2.06 (m, 1 H), 2.10 (d, *J* = 13.6 Hz, 1 H), 2.40−2.59 (m, 2 H), 2.71 (t, *J* = 12.5 Hz, 1 H), 3.02 (dd, *J* = 13.4/7.0 Hz, 1 H), 3.07 (dd, *J* = 13.5/6.2 Hz, 1 H), 3.25 (dd, *J* = 12.3/3.9 Hz, 1H), 3.33 (dd, *J* = 12.6/4.1 Hz, 1 H), 6.87 (ddd, *J* = 8.2/2.5/1.1 Hz, 1 H), 6.98−7.04 (m, 2 H), 7.09−7.13 (m, 1 H), 7.16 (tt, *J* = 7.6/1.1 Hz, 1 H), 7.24 (dd, *J* = 7.9/0.9 Hz, 1 H), 7.35 (t, *J* = 7.9 Hz, 1 H), 7.39−7.44 (m, 2 H), 7.57 (s, 1 H) ppm.[75,76] ^{13}C NMR (126 MHz, DMSO-d_6/D_2O = 9:1, 25 °C): δ 30.5, 32.8, 40.0, 45.2, 46.1, 50.9, 114.2, 117.6, 118.7, 120.7, 123.6, 130.2, 130.3, 133.6, 138.6, 156.6, 157.0, 174.0 ppm.[76] HRMS (ESI): [M + H]$^+$ calcd for $C_{20}H_{24}N_3O_3$ 354.1812, found 354.1811.

***rac*-(3*R*,5*S*)-(5-{[(*E*)-2-{[5-(2-Chlorophenyl)furan-2-yl]-methylidene}hydrazin-1-yl]methyl}piperidine-3-carboxylic Acid)−Sodium Chloride (1/2) (*rac*-16fv).**[54] According to GP4 with *rac*-**11**·HCl, 5-(2-chlorophenyl)-2-furaldehyde (**15fv**), and 1 M NaOD (20 μL), *rac*-**16fv** was obtained quantitatively in solution. Besides the major *E*-isomer, the *Z*-isomer is present in 9%. ^{1}H NMR (500 MHz, DMSO-d_6/D_2O = 9:1, 25 °C): δ 1.21 (q, *J* = 12.5 Hz, 1 H), 2.02−2.09 (m, 1 H), 2.13 (d, *J* = 13.7 Hz, 1 H), 2.42−2.61 (m, 2 H), 2.73 (t, *J* = 12.5 Hz, 1 H), 3.07 (dd, *J* = 13.4/6.9 Hz, 1 H), 3.12 (dd, *J* = 13.5/6.2 Hz, 1 H), 3.28 (dd, *J* = 12.6/4.0 Hz, 1H), 3.34 (dd, *J* = 12.6/4.0 Hz, 1 H), 6.62 (d, *J* = 3.6 Hz, 1 H), 7.19 (d, *J* = 3.6 Hz, 1 H), 7.33 (td, *J* = 7.7/1.7 Hz, 1 H), 7.45 (td, *J* = 7.6/1.3 Hz, 1 H), 7.55 (dd, *J* = 7.2/1.0 Hz, 1 H), 7.56 (s, 1 H), 7.86 (dd, *J* = 8.0/1.7 Hz, 1 H) ppm.[75,76] ^{13}C NMR (126 MHz, DMSO-d_6/D_2O = 9:1, 25 °C): δ 30.4, 32.7, 39.8, 45.1, 46.0, 50.8, 109.2, 113.2, 124.6, 127.5, 127.6, 128.1, 128.7, 128.7, 130.8, 148.1, 151.5, 173.9 ppm.[76] HRMS (ESI): [M + H]$^+$ calcd for $C_{18}H_{21}N_3O_3Cl$ 362.1266, found 362.1265.

***rac*-(3*R*,5*S*)-(5-{[(*E*)-2-{[5-(3-Chlorophenyl)furan-2-yl]-methylidene}hydrazin-1-yl]methyl}piperidine-3-carboxylic Acid)−Sodium Chloride (1/2) (*rac*-16fw).**[54] According to GP4 with *rac*-**11**·HCl, 5-(3-chlorophenyl)-2-furaldehyde (**15fw**), and 1 M NaOD (20 μL), *rac*-**16fw** was obtained quantitatively in solution. Besides the major *E*-isomer, the *Z*-isomer is present in 9%. ^{1}H NMR (500 MHz, DMSO-d_6/D_2O = 9:1, 25 °C): δ 1.22 (q, *J* = 12.5 Hz, 1 H), 1.99−2.09 (m, 1 H), 2.13 (d, *J* = 13.6 Hz, 1 H), 2.44−2.59 (m, 2 H), 2.74 (t, *J* = 12.5 Hz, 1 H), 3.07 (dd, *J* = 13.5/6.9 Hz, 1 H), 3.12 (dd, *J* = 13.6/6.4 Hz, 1 H), 3.28 (dd, *J* = 12.7/3.8 Hz, 1H), 3.35 (dd, *J* = 12.6/4.0 Hz, 1 H), 6.58 (d, *J* = 3.5 Hz, 1 H), 7.09 (d, *J* = 3.6 Hz, 1 H), 7.33 (dd, *J* = 8.1/2.1 Hz, 1 H), 7.45 (t, *J* = 7.9 Hz, 1 H), 7.55 (s, 1 H), 7.66 (dt, *J* = 8.0/1.2 Hz, 1 H), 7.74 (t, *J* = 1.9 Hz, 1 H) ppm.[75,76] ^{13}C NMR (126 MHz, DMSO-d_6/D_2O = 9:1, 25 °C): δ 30.4, 32.7, 39.8, 45.1, 46.0, 50.8, 109.4, 109.7, 121.8, 122.7, 124.9, 127.1, 131.0, 132.0, 133.8, 150.4, 151.9, 173.9 ppm.[76] HRMS (ESI): [M + H]$^+$ calcd for $C_{18}H_{21}N_3O_3Cl$ 362.1266, found 362.1265.

DOI: 10.1021/acs.jmedchem.8b01602
J. Med. Chem. 2018, 61, 10310−10332

***rac*-(3*R*,5*S*)-(5-{[(*E*)-2-{[5-(2,4-Dichlorophenyl)furan-2-yl]methylidene}hydrazin-1-yl]methyl}piperidine-3-carboxylic Acid)−Sodium Chloride (1/2) (*rac*-16fy).**[54] According to GP4 with *rac*-**11**·HCl, 5-(2,4-dichlorophenyl)-2-furaldehyde (**15fy**), and 1 M NaOD (20 μL), *rac*-**16fy** was obtained quantitatively in solution. Besides the major *E*-isomer, the *Z*-isomer is present in 9%. ^{1}H NMR (500 MHz, DMSO-d_6/D_2O = 9:1, 25 °C): δ 1.23 (q, J = 12.5 Hz, 1 H), 1.99−2.10 (m, 1 H), 2.14 (d, J = 13.3 Hz, 1 H), 2.45−2.61 (m, 2 H), 2.75 (t, J = 12.4 Hz, 1 H), 3.08 (dd, J = 13.5/6.7 Hz, 1 H), 3.12 (dd, J = 13.6/6.3 Hz, 1 H), 3.28 (dd, J = 12.4/3.9 Hz, 1H), 3.36 (dd, J = 12.6/4.0 Hz, 1 H), 6.63 (d, J = 3.6 Hz, 1 H), 7.23 (d, J = 3.6 Hz, 1 H), 7.53 (dd, J = 8.6/2.2 Hz, 1 H), 7.55 (s, 1 H), 7.70 (d, J = 2.2 Hz, 1 H), 7.87 (d, J = 8.6 Hz, 1 H) ppm.[75,76] ^{13}C NMR (126 MHz, DMSO-d_6/D_2O = 9:1, 25 °C): δ 30.3, 32.7, 39.8, 44.9, 46.0, 50.7, 109.3, 113.7, 124.3, 127.1, 127.9, 128.6, 129.5, 130.2, 132.1, 147.2, 151.8, 173.7 ppm.[76] HRMS (ESI): $[M + H]^+$ calcd for $C_{18}H_{20}N_3O_3Cl_2$ 396.0876, found 396.0875.

***rac*-(3*R*,5*S*)-(5-{[(*E*)-2-({5-[2-(Trifluoromethyl)phenyl]furan-2-yl}methylidene)hydrazin-1-yl]methyl}piperidine-3-carboxylic Acid)−Sodium Chloride (1/2) (*rac*-16fz).**[54] According to GP4 with *rac*-**11**·HCl, 5-[2-(trifluoromethyl)phenyl]-2-furaldehyde (**15fz**), and 1 M NaOD (20 μL), *rac*-**16fz** was obtained quantitatively in solution. Besides the major *E*-isomer the *Z*-isomer is present in 12%. ^{1}H NMR (500 MHz, DMSO-d_6/D_2O = 9:1, 25 °C): δ 1.21 (q, J = 12.5 Hz, 1 H), 1.97−2.08 (m, 1 H), 2.12 (d, J = 13.6 Hz, 1 H), 2.43−2.59 (m, 2 H), 2.73 (t, J = 12.5 Hz, 1 H), 3.05 (dd, J = 13.4/6.9 Hz, 1 H), 3.10 (dd, J = 13.5/6.1 Hz, 1 H), 3.27 (dd, J = 12.6/3.9 Hz, 1H), 3.34 (dd, J = 12.5/4.1 Hz, 1 H), 6.61 (d, J = 3.5 Hz, 1 H), 6.83 (d, J = 3.5 Hz, 1 H), 7.54 (s, 1 H), 7.58 (t, J = 7.7 Hz, 1 H), 7.75 (t, J = 7.7 Hz, 1 H), 7.82 (d, J = 7.8 Hz, 1 H), 7.85 (d, J = 7.9 Hz, 1 H) ppm.[75,76] ^{13}C NMR (126 MHz, DMSO-d_6/D_2O = 9:1, 25 °C): δ 30.4, 32.8, 39.8, 45.0, 46.0, 50.8, 108.8, 112.3, 124.0 (q, J_{CF} = 273.4 Hz), 124.6, 124.7 (q, J_{CF} = 30.6 Hz), 126.8 (q, J_{CF} = 5.9 Hz), 128.5, 128.6 (q, J_{CF} = 1.7 Hz), 129.8, 132.8, 158.6, 152.5, 173.8 ppm.[76] ^{19}F {^{1}H} NMR (376 MHz, DMSO-d_6/D_2O = 9:1, 25 °C): δ −58.4 ppm.[76] HRMS (ESI): $[M + H]^+$ calcd for $C_{19}H_{21}N_3O_3F_3$ 396.1530, found 396.1528.

***rac*-(3*R*,5*S*)-(5-{[(*E*)-2-({5-[2-Chloro-5-(trifluoromethyl)phenyl]furan-2-yl}methylidene)hydrazin-1-yl]methyl}piperidine-3-carboxylic Acid)−Sodium Chloride (1/2) (*rac*-16ga).**[54] According to GP4 with *rac*-**11**·HCl, 5-[2-chloro-5-(trifluoromethyl)phenyl]-2-furaldehyde (**15ga**), and 1 M NaOD (20 μL), *rac*-**16ga** was obtained quantitatively in solution. Besides the major *E*-isomer, the *Z*-isomer is present in 8%. ^{1}H NMR (500 MHz, DMSO-d_6/D_2O = 9:1, 25 °C): δ 1.17 (q, J = 12.5 Hz, 1 H), 1.95−2.08 (m, 1 H), 2.12 (d, J = 13.1 Hz, 1 H), 2.30−2.42 (m, 1 H), 2.45−2.59 (m, 1 H), 2.67 (t, J = 12.5 Hz, 1 H), 3.08 (dd, J = 12.4/5.9 Hz, 1 H), 3.12 (dd, J = 12.7/5.3 Hz, 1 H), 3.25 (dd, J = 12.1/2.5 Hz, 1H), 3.31 (dd, J = 12.7/4.0 Hz, 1 H), 6.66 (d, J = 3.6 Hz, 1 H), 7.36 (d, J = 3.6 Hz, 1 H), 7.55 (s, 1 H), 7.65 (dd, J = 8.4/2.3 Hz, 1 H), 7.80 (d, J = 8.4 Hz, 1 H), 8.13 (d, J = 2.3 Hz, 1 H) ppm.[75,76] ^{13}C NMR (126 MHz, DMSO-d_6/D_2O = 9:1, 25 °C): δ 31.0, 32.7, 40.9, 45.9, 46.2, 50.5, 109.1, 114.8, 123.5 (q, J_{CF} = 4.0 Hz), 123.5, 123.7 (q, J_{CF} = 272.5 Hz), 124.6 (q, J_{CF} = 3.9 Hz), 128.4 (q, J_{CF} = 32.5 Hz), 129.0, 132.2, 132.5, 146.4, 152.5, 173.4 ppm.[76] ^{19}F {^{1}H} NMR (376 MHz, DMSO-d_6/D_2O = 9:1, 25 °C): δ −61.3 ppm.[76] HRMS (ESI): $[M + H]^+$ calcd for $C_{19}H_{20}N_3O_3ClF_3$ 430.1140, found 430.1139.

***rac*-(3*R*,5*S*)-(5-{[(*E*)-2-{[5-(4-Chloro-2-nitrophenyl)furan-2-yl]methylidene}hydrazin-1-yl]methyl}piperidine-3-carboxylic Acid)−sodium Chloride (1/2) (*rac*-16gb).**[54] According to GP4 with *rac*-**11**·HCl, 5-(4-chloro-2-nitrophenyl)-2-furaldehyde (**15gb**), and 1 M NaOD (20 μL), *rac*-**16gb** was obtained quantitatively in solution. Besides the major *E*-isomer, the *Z*-isomer is present in 13%. ^{1}H NMR (500 MHz, DMSO-d_6/D_2O = 9:1, 25 °C): δ 1.20 (q, J = 12.6 Hz, 1 H), 1.98−2.07 (m, 1 H), 2.11 (d, J = 13.3 Hz, 1 H), 2.41−2.60 (m, 2 H), 2.71 (t, J = 12.4 Hz, 1 H), 3.04 (dd, J = 13.5/6.9 Hz, 1 H), 3.09 (dd, J = 13.5/6.1 Hz, 1 H), 3.26 (dd, J = 13.1/3.8 Hz, 1H), 3.33 (dd, J = 12.6/4.2 Hz, 1 H), 6.60 (d, J = 3.6 Hz, 1 H), 6.93 (d, J = 3.5 Hz, 1 H), 7.44 (s, 1 H), 7.78 (dd, J = 8.6/2.1 Hz, 1 H), 7.86 (d, J = 8.5 Hz, 1 H), 8.05 (d, J = 2.1 Hz, 1 H) ppm.[75,76] ^{13}C NMR (126 MHz, DMSO-d_6/D_2O = 9:1, 25 °C): δ 30.5, 32.7, 40.0, 45.3, 46.1, 50.6, 108.8, 112.7, 121.3, 123.5, 123.8, 129.7, 132.4, 132.5, 145.5, 146.6, 153.6, 174.0 ppm.[76] HRMS (ESI): $[M + H]^+$ calcd for $C_{18}H_{20}N_4O_5Cl$ 407.1117, found 407.1117.

***rac*-(3*R*,5*S*)-(5-{[(*E*)-2-({5-[3-(Trifluoromethyl)phenyl]furan-2-yl}methylidene)hydrazin-1-yl]methyl}piperidine-3-carboxylic Acid)−Sodium Chloride (1/2) (*rac*-16gc).**[54] According to GP4 with *rac*-**11**·HCl, 5-[3-(trifluoromethyl)phenyl]-2-furaldehyde (**15gc**), and 1 M NaOD (20 μL), *rac*-**16gc** was obtained quantitatively in solution. Besides the major *E*-isomer, the *Z*-isomer is present in 7%. ^{1}H NMR (500 MHz, DMSO-d_6/D_2O = 9:1, 25 °C): δ 1.21 (q, J = 12.5 Hz, 1 H), 2.00−2.09 (m, 1 H), 2.13 (d, J = 13.2 Hz, 1 H), 2.43−2.60 (m, 2 H), 2.73 (t, J = 12.5 Hz, 1 H), 3.08 (dd, J = 13.5/6.8 Hz, 1 H), 3.12 (dd, J = 13.6/6.4 Hz, 1 H), 3.28 (dd, J = 12.6/3.9 Hz, 1H), 3.35 (dd, J = 12.6/4.0 Hz, 1 H), 6.60 (d, J = 3.5 Hz, 1 H), 7.19 (d, J = 3.5 Hz, 1 H), 7.56 (s, 1 H), 7.62 (d, J = 7.9 Hz, 1 H), 7.67 (t, J = 8.0 Hz, 1 H), 7.99 (s, 1 H), 8.00 (d, J = 6.6 Hz, 1 H) ppm.[75,76] ^{13}C NMR (126 MHz, DMSO-d_6/D_2O = 9:1, 25 °C): δ 30.5, 32.7, 39.9, 45.2, 46.0, 50.7, 109.7, 109.7, 119.4 (q, J_{CF} = 3.8 Hz), 123.7 (q, J_{CF} = 4.0 Hz), 124.1 (q, J_{CF} = 273.5 Hz), 124.7, 127.0, 129.9 (q, J_{CF} = 32.0 Hz), 130.2, 131.0, 150.4, 152.1, 174.0 ppm.[76] ^{19}F {^{1}H} NMR (376 MHz, DMSO-d_6/D_2O = 9:1, 25 °C): δ −61.3 ppm.[76] HRMS (ESI): $[M + H]^+$ calcd for $C_{19}H_{21}N_3O_3F_3$ 396.1530, found 396.1528.

***rac*-(3*R*,5*S*)-(5-{[(*E*)-2-({5-[4-Fluoro-3-(trifluoromethyl)phenyl]furan-2-yl}methylidene)hydrazin-1-yl]methyl}piperidine-3-carboxylic Acid)−Sodium Chloride (1/2) (*rac*-16ge).**[54] According to GP4 with *rac*-**11**·HCl, 5-[4-fluoro-3-(trifluoromethyl)phenyl]-2-furaldehyde (**15ge**), and 1 M NaOD (20 μL), *rac*-**16ge** was obtained quantitatively in solution. Besides the major *E*-isomer, the *Z*-isomer is present in 9%. ^{1}H NMR (500 MHz, DMSO-d_6/D_2O = 9:1, 25 °C): δ 1.22 (q, J = 12.5 Hz, 1 H), 1.99−2.11 (m, 1 H), 2.13 (d, J = 13.6 Hz, 1 H), 2.44−2.60 (m, 2 H), 2.74 (t, J = 12.5 Hz, 1 H), 3.07 (dd, J = 13.5/6.9 Hz, 1 H), 3.12 (dd, J = 13.5/6.3 Hz, 1 H), 3.28 (dd, J = 12.4/2.8 Hz, 1H), 3.35 (dd, J = 12.6/4.0 Hz, 1 H), 6.59 (d, J = 3.5 Hz, 1 H), 7.14 (d, J = 3.5 Hz, 1 H), 7.52−7.58 (m, 2 H), 7.99−8.07 (m, 2 H) ppm.[75,76] ^{13}C NMR (126 MHz, DMSO-d_6/D_2O = 9:1, 25 °C): δ 30.4, 32.7, 39.8, 45.1, 46.0, 50.7, 109.5, 109.8, 117.4 (qd, J_{CF} = 32.1/13.3 Hz), 118.2 (d, J_{CF} = 21.8 Hz), 121.6 (q, J_{CF} = 4.4 Hz), 122.5 (q, J_{CF} = 274.3 Hz), 124.8, 127.3 (d, J_{CF} = 3.7 Hz), 129.7 (d, J_{CF} = 8.7 Hz), 149.7, 152.0, 157.8 (dq, J_{CF} = 253.9/1.6 Hz), 173.9 ppm.[76] ^{19}F {^{1}H} NMR (376 MHz, DMSO-d_6/D_2O = 9:1, 25 °C): δ −117.65 (q, J_{FF} = 12.5 Hz), −60.14 (d, J_{FF} = 12.4 Hz) ppm.[76] HRMS (ESI): $[M + H]^+$ calcd for $C_{19}H_{20}N_3O_3F_4$ 414.1435, found 414.1434.

***rac*-(3*R*,5*S*)-(5-{[(*E*)-2-{[5-(Naphthalen-1-yl)furan-2-yl]methylidene}hydrazin-1-yl]methyl}piperidine-3-carboxylic Acid)−Sodium Chloride (1/2) (*rac*-16gf).**[54] According to GP4 with *rac*-**11**·HCl, 5-(naphthalen-1-yl)-2-furaldehyde (**15gf**), and 1 M NaOD (20 μL), *rac*-**16gf** was obtained quantitatively in solution. Besides the major *E*-isomer, the *Z*-isomer is present in 12%. ^{1}H NMR (500 MHz, DMSO-d_6/D_2O = 9:1, 25 °C): δ 1.23 (q, J = 12.5 Hz, 1 H), 2.02−2.11 (m, 1 H), 2.14 (d, J = 13.4 Hz, 1 H), 2.46−2.61 (m, 2 H), 2.75 (t, J = 12.5 Hz, 1 H), 3.07 (dd, J = 13.4/6.8 Hz, 1 H), 3.12 (dd, J = 13.5/6.2 Hz, 1 H), 3.29 (dd, J = 12.7/3.5 Hz, 1H), 3.36 (dd, J = 12.4/4.0 Hz, 1 H), 6.69 (d, J = 3.5 Hz, 1 H), 6.98 (d, J = 3.5 Hz, 1 H), 7.56−7.65 (m, 4 H), 7.80 (dd, J = 7.3/1.3 Hz, 1 H), 7.95 (d, J = 8.2 Hz, 1 H), 8.01 (dd, J = 7.9/1.7 Hz, 1 H), 8.42 (dd, J = 8.6/1.3 Hz, 1 H) ppm.[75,76] ^{13}C NMR (126 MHz, DMSO-d_6/D_2O = 9:1, 25 °C): δ 30.4, 32.8, 39.8, 45.1, 46.0, 50.9, 109.4, 111.7, 124.9, 125.3, 125.7, 125.7, 126.3, 127.1, 127.4, 128.6, 128.7, 129.2, 133.7, 151.6, 151.7, 173.8 ppm.[76] HRMS (ESI): $[M + H]^+$ calcd for $C_{22}H_{24}N_3O_3$ 378.1812, found 378.1811.

***rac*-(3*R*,5*S*)-(5-{[(*E*)-2-({5-[3,5-Bis(trifluoromethyl)phenyl]furan-2-yl}methylidene)hydrazin-1-yl]methyl}piperidine-3-carboxylic Acid)−Sodium Chloride (1/2) (*rac*-16gg).**[54] According to GP4 with *rac*-**11**·HCl, 5-[3,5-bis(trifluoromethyl)phenyl]-2-furaldehyde (**15gg**), and 1 M NaOD (20 μL), *rac*-**16gg** was obtained quantitatively in solution. Besides the major *E*-isomer, the *Z*-isomer is present in 9%. ^{1}H NMR (500 MHz, DMSO-d_6/D_2O = 9:1, 25 °C): δ 1.22 (q, J = 12.6 Hz, 1 H), 2.02−2.10 (m, 1 H), 2.14 (d, J = 13.3 Hz, 1 H), 2.41−2.63 (m, 2 H), 2.73 (t, J = 12.5 Hz, 1 H), 3.10 (dd, J = 11.9/5.2 Hz, 1 H), 3.14 (dd, J = 11.9/4.8 Hz, 1 H), 3.28 (dd, J = 12.2/3.7 Hz, 1H), 3.35 (dd, J = 12.5/3.9 Hz, 1 H), 6.64 (d, J = 3.6 Hz, 1 H), 7.42 (d, J = 3.6 Hz, 1 H), 7.56 (s, 1 H), 7.94 (s, 1 H), 8.30 (s, 2 H) ppm.[75,76] ^{13}C NMR (126 MHz, DMSO-d_6/D_2O = 9:1, 25 °C): δ 30.3, 32.5, 39.8,

DOI: 10.1021/acs.jmedchem.8b01602
J. Med. Chem. 2018, 61, 10310−10332

45.1, 45.9, 50.5, 109.6, 111.7, 119.9 (q, J_{CF} = 3.8 Hz), 123.2 (q, J_{CF} = 3.5 Hz), 123.2 (q, J_{CF} = 273.1 Hz), 123.9, 131.1 (q, J_{CF} = 33.0 Hz), 132.3, 148.8, 153.0, 173.8 ppm.[76] ^{19}F {^{1}H} NMR (376 MHz, DMSO-d_6/D_2O = 9:1, 25 °C): δ −61.6 ppm.[76] HRMS (ESI): $[M + H]^+$ calcd for $C_{20}H_{20}N_3O_3F_6$ 464.1403, found 464.1403.

***rac*-(3*R*,5*S*)-(5-{[(*E*)-2-{[5-(2-Bromophenyl)furan-2-yl]-methylidene}hydrazin-1-yl]methyl}piperidine-3-carboxylic Acid)−Sodium Chloride (1/2) (*rac*-16gk).**[54] According to GP4 with *rac*-**11**·HCl, 5-(2-bromophenyl)-2-furaldehyde (**15gk**), and 1 M NaOD (20 μL), *rac*-**16gk** was obtained quantitatively in solution. Besides the major *E*-isomer, the *Z*-isomer is present in 9%. ^{1}H NMR (500 MHz, DMSO-d_6/D_2O = 9:1, 25 °C): δ 1.22 (q, J = 12.5 Hz, 1 H), 2.00−2.10 (m, 1 H), 2.13 (d, J = 13.4 Hz, 1 H), 2.41−2.60 (m, 2 H), 2.74 (t, J = 12.5 Hz, 1 H), 3.07 (dd, J = 13.4/6.8 Hz, 1 H), 3.11 (dd, J = 13.5/6.2 Hz, 1 H), 3.28 (dd, J = 12.6/3.9 Hz, 1H), 3.35 (dd, J = 12.5/4.1 Hz, 1 H), 6.62 (d, J = 3.6 Hz, 1 H), 7.22 (d, J = 3.5 Hz, 1 H), 7.26 (td, J = 7.7/1.7 Hz, 1 H), 7.49 (td, J = 7.6/1.4 Hz, 1 H), 7.56 (s, 1 H), 7.73 (dd, J = 8.1/1.3 Hz, 1 H), 7.80 (dd, J = 7.9/1.7 Hz, 1 H) ppm.[75,76] ^{13}C NMR (126 MHz, DMSO-d_6/D_2O = 9:1, 25 °C): δ 30.4, 32.8, 39.8, 45.1, 46.0, 50.8, 109.0, 112.8, 118.6, 124.7, 128.1, 128.5, 129.2, 130.2, 134.2, 149.3, 151.6, 173.9 ppm.[76] HRMS (ESI): $[M + H]^+$ calcd for $C_{18}H_{21}N_3O_3Br$ 406.0761, found 406.0761.

***rac*-(3*R*,5*S*)-(5-{[(*E*)-2-{[2-(Naphthalen-2-yl)pyrimidin-5-yl]-methylidene}hydrazin-1-yl]methyl}piperidine-3-carboxylic Acid)−Sodium Chloride (1/2) (*rac*-16ho).**[54] According to GP4 with *rac*-**11**·HCl, 2-(naphthalen-2-yl)pyrimidine-5-carboxaldehyde (**15ho**), and 1 M NaOD (20 μL), *rac*-**16ho** was obtained quantitatively in solution. Besides the major *E*-isomer, the *Z*-isomer is present in 9%. ^{1}H NMR (500 MHz, DMSO-d_6/D_2O = 9:1, 25 °C): δ 1.27 (q, J = 12.8 Hz, 1 H), 2.06−2.22 (m, 2 H), 2.43−2.64 (m, 2 H), 2.76 (t, J = 12.4 Hz, 1 H), 3.16 (dd, J = 13.5/6.8 Hz, 1 H), 3.20 (dd, J = 13.6/6.0 Hz, 1 H), 3.32 (dd, J = 12.5/4.2 Hz, 1H), 3.37 (dd, J = 12.5/4.0 Hz, 1 H), 7.56−7.65 (m, 3 H), 7.96−8.00 (m, 1 H), 8.05 (d, J = 8.7 Hz, 1 H), 8.07−8.12 (m, 1 H), 8.48 (dd, J = 8.7/1.7 Hz, 1 H), 8.95 (s, 1 H), 9.00 (s, 2 H) ppm.[75,76] ^{13}C NMR (126 MHz, DMSO-d_6/D_2O = 9:1, 25 °C): δ 30.3, 32.7, 39.8, 45.0, 46.0, 50.5, 124.5, 126.8, 127.0, 127.5, 127.5, 127.7, 128.4, 128.5, 129.0, 132.8, 134.0, 134.4, 153.4, 161.0, 173.7 ppm.[76] HRMS (ESI): $[M + H]^+$ calcd for $C_{22}H_{24}N_5O_2$ 390.1925, found 390.1923.

***rac*-(3*R*,5*R*)-(5-{2-[(*E*)-2-({5-[2-Chloro-4-(trifluoromethyl)-phenyl]furan-2-yl}methylidene)hydrazin-1-yl]ethyl}-piperidine-3-carboxylic Acid)−Sodium Chloride (1/3) (*rac*-18e).**[54] According to GP4 with *rac*-**13**·HCl, 5-[2-chloro-4-(trifluoromethyl)phenyl]-2-furaldehyde (**15e**), and 1 M NaOD (30 μL), *rac*-**18e** was obtained quantitatively in solution. Besides the major *E*-isomer, the *Z*-isomer is present in 17%. ^{1}H NMR (500 MHz, DMSO-d_6/D_2O = 9:1, 25 °C): δ 1.10 (q, J = 12.5 Hz, 1 H), 1.45−1.60 (m, 2 H), 1.73−1.85 (m, 1 H), 2.11 (d, J = 13.3 Hz, 1 H), 2.30 (tt, J = 12.6/3.8 Hz, 1 H), 2.43 (t, J = 12.2 Hz, 1 H), 2.65 (t, J = 12.4 Hz, 1 H), 3.14−3.20 (m, 3 H), 3.28 (dd, J = 12.2/3.6 Hz, 1 H), 6.65 (d, J = 3.6 Hz, 1 H), 7.40 (d, J = 3.6 Hz, 1 H), 7.50 (s, 1 H), 7.80 (d, J = 8.6 Hz, 1 H), 7.92 (s, 1 H), 8.07 (d, J = 8.4 Hz, 1 H) ppm.[75,76] ^{13}C NMR (126 MHz, DMSO-d_6/D_2O = 9:1, 25 °C): δ 31.2, 31.3, 33.0, 41.4, 44.3, 46.1, 47.7, 108.9, 115.5, 122.8, 123.3 (q, J_{CF} = 272.2 Hz), 124.4 (q, J_{CF} = 3.9 Hz), 127.7 (q, J_{CF} = 4.0 Hz), 127.7, 127.94 (q, J_{CF} = 33.14 Hz), 128.8, 131.7, 146.4, 153.1, 174.7 ppm.[76] ^{19}F{^{1}H} NMR (376 MHz, DMSO-d_6/D_2O = 9:1, 25 °C): δ −61.1 ppm.[76] HRMS (ESI): $[M + H]^+$ calcd for $C_{20}H_{22}N_3O_3ClF_3$ 444.1296, found 444.1296.

***rac*-(3*R*,5*R*)-(5-{2-[(*E*)-2-{[5-(2,4-Dichlorophenyl)furan-2-yl]-methylidene}hydrazin-1-yl]ethyl}piperidine-3-carboxylic Acid)−Sodium Chloride (1/3) (*rac*-18fy).**[54] According to GP4 with *rac*-**13**·HCl, 5-(2,4-dichlorophenyl)-2-furaldehyde (**15fy**), and 1 M NaOD (30 μL), *rac*-**18fy** was obtained quantitatively in solution. Besides the major *E*-isomer, the *Z*-isomer is present in 14%. ^{1}H NMR (500 MHz, DMSO-d_6/D_2O = 9:1, 25 °C): δ 1.09 (q, J = 12.5 Hz, 1 H), 1.43−1.58 (m, 2 H), 1.72−1.84 (m, 1 H), 2.11 (d, J = 13.3 Hz, 1 H), 2.30 (tt, J = 12.3/3.8 Hz, 1 H), 2.43 (t, J = 12.1 Hz, 1 H), 2.65 (t, J = 12.5 Hz, 1 H), 3.11−3.21 (m, 3 H), 3.28 (dd, J = 12.4/4.0 Hz, 1 H), 6.61 (d, J = 3.5 Hz, 1 H), 7.22 (d, J = 3.5 Hz, 1 H), 7.49 (s, 1 H), 7.52 (dd, J = 8.6/2.3 Hz, 1 H), 7.69 (d, J = 2.3 Hz, 1 H), 7.87 (d, J = 8.6 Hz, 1 H) ppm.[75,76] ^{13}C NMR (126 MHz, DMSO-d_6/D_2O = 9:1, 25 °C): δ 31.3, 31.3, 33.0, 41.4, 44.4, 46.1, 47.7, 108.9, 113.7, 123.3, 127.2, 127.9, 128.5, 129.3, 130.1, 132.0, 146.9, 152.2, 174.7 ppm.[76] HRMS (ESI): $[M + H]^+$ calcd for $C_{19}H_{22}N_3O_3Cl_2$ 410.1033, found 410.1032.

***rac*-(3*R*,5*S*)-[1-(*tert*-Butyl) 3-Methyl 5-Formylpiperidine-1,3-dicarboxylate] (*rac*-20)**[44] **and *rac*-(3*R*,5*R*)-[1-(*tert*-Butyl) 3-Methyl 5-Formylpiperidine-1,3-dicarboxylate] (*rac*-21).** **26** (1:1 *E*-/*Z*-mixture, 424 mg, 1.49 mmol) was dissolved in THF (15 mL). The solution was cooled to 0 °C, and a 2 M aqueous HCl (2.5 mL; 5.0 mmol) was added. The mixture was stirred for 2 d, while the reaction was allowed to reach rt (0 °C → rt). It was quenched with $NaHCO_3$ (429 mg; 5.11 mmol) and concentrated under reduced pressure. H_2O (20 mL) was added to the residue, and it was extracted with DCM (5 × 20 mL). The combined organic phases were dried over Na_2SO_4 and concentrated under reduced pressure. After purification by flash chromatography (*iso*-hexanes/EtOAc = 3:1), *rac*-**20** and *rac*-**21** were obtained in 1:1 mixture (according to ^{1}H NMR) as colorless oil (296 mg, 73%). ^{1}H NMR (400 MHz, $C_2Cl_4D_2$, 80 °C): δ 1.43 (s, 9 H, *a* or *b*), 1.45 (s, 9 H, *a* or *b*), 1.59 (dt, J = 13.4/11.9 Hz, 1 H, *a*), 1.94 (ddd, J = 13.9/9.2/4.6 Hz, 1 H, *b*), 2.14−2.22 (m, 1 H, *b*), 2.32−2.54 (m, 3 H, *a* and *b*), 2.59−2.80 (m, 4 H, *a* and *b*), 3.31 (dd, J = 13.4/8.5 Hz, 1 H, *a*), 3.44 (dd, J = 13.8/4.3 Hz, 1 H, *b*), 3.68 (s, 3 H, *a* or *b*), 3.69 (s, 3 H, *a* or *b*), 3.79 (dd, J = 13.5/4.3 Hz, 1 H, *a*), 3.93 (dd, J = 13.7/5.2 Hz, 1 H, *b*), 4.22−4.33 (m, 2 H, *a* and *b*), 9.63 (d, J = 1 Hz, 1 H, *a*), 9.68 (s, 1 H, *b*) ppm. ^{13}C NMR (101 MHz, $C_2Cl_4D_2$, 80 °C): δ 25.8 (*b*), 27.5 (*a*), 28.4 (*a* or *b*), 28.5 (*a* or *b*), 38.3 (*b*), 40.7 (*a*), 43.3 (*b*), 43.6 (*a*), 45.7 (*a* or *b*), 45.8 (*a* or *b*), 45.8 (*a* or *b*), 47.6 (b), 51.9 (*a* or *b*), 52.0 (*a* or *b*), 80.4 (*a* or *b*), 80.5 (*a* or *b*), 154.3 (*a* or *b*), 154.4 (*a* or *b*), 172.8 (*a* or *b*), 173.1 (*a* or *b*), 200.7 (*a*), 201.1 (*b*) ppm. IR (film): $\tilde{\nu}$ 2977, 2955, 2933, 2871, 1735, 1694 cm^{-1}. HRMS (ESI): $[M + H]^+$ calcd for $C_{13}H_{22}NO_5$ 272.1493, found 272.1498.

***rac*-(3*R*,5*S*)-[1-(*tert*-Butyl) 3-Methyl 5-Hydroxypiperidine-1,3-dicarboxylate]**[41] **(*rac*-23).** Methyl 5-hydroxynicotinate (**22**, 309 mg, 1.97 mmol), Rh on Al_2O_3 (94 mg, 0.046 mmol), and conc H_2SO_4 (200 mg, 2.03 mmol) were suspended in MeOH (10 mL) under Ar. The mixture was hydrogenated (10 bar H_2) at 80 °C for 26 h. After cooling to rt, the Rh on Al_2O_3 catalyst was filtered off and the solvent was concentrated in vacuum. The residue was dissolved in dioxane (10 mL) and NEt_3 (1.1 mL, 7.8 mmol) and di-*tert*-butyl dicarbonate (401 mg; 1.80 mmol) were added. The reaction mixture was stirred at rt for 3 h before removing the solvent under vacuum. After purification by flash chromatography (*iso*-hexanes/EtOAc = 1:1), *rac*-**23** was obtained as white, amorphous solid (278 mg; 55%). ^{1}H NMR (400 MHz, $C_2Cl_4D_2$, 80 °C): δ 1.44 (s, 9 H), 1.55−1.70 (m, 1 H), 2.22 (d, J = 13.4 Hz, 1 H), 2.54 (tt, J = 9.3/4.1 Hz, 1 H), 2.75−2.86 (m, 1 H), 3.05 (d, J = 11.4 Hz, 1 H), 3.65 (tt, J = 8.9/3.9 Hz, 1 H), 3.69 (s, 3 H), 3.89 (d, J = 13.1 Hz, 1 H), 3.96 (d, J = 14.2 Hz, 1 H) ppm.[75] ^{13}C NMR (101 MHz, $C_2Cl_4D_2$, 80 °C): δ 28.4, 35.2, 40.0, 45.2, 50.6, 52.0, 65.5, 80.1, 154.5, 173.4 ppm. IR (KBr): $\tilde{\nu}$ 3463, 2986, 2957, 2936, 2870, 1732, 1673 cm^{-1}. HRMS (ESI): $[M + Na]^+$ calcd for $C_{12}H_{21}NO_5Na$ 282.1312, found 282.1312.

***rac*-(3*R*,5*R*)-[1-(*tert*-Butyl) 3-Methyl 5-Hydroxypiperidine-1,3-dicarboxylate] (*rac*-24).** *rac*-**24** was obtained as a side product from the preparation of *rac*-**23** as a colorless resin (97 mg; 19%). ^{1}H NMR (400 MHz, $C_2Cl_4D_2$, 80 °C): δ 1.44 (s, 9 H), 1.67 (br s, 1 H), 1.80 (t, J = 11.9 Hz, 1 H), 2.00 (d, J = 13.3 Hz, 1 H), 2.87 (tt, J = 9.8/4.1 Hz, 1 H), 3.02−3.17 (m, 2 H), 3.67 (s, 3 H), 3.75 (dd, J = 13.7/2.8 Hz, 1 H), 3.94−4.07 (m, 2 H) ppm.[75] ^{13}C NMR (101 MHz, $C_2Cl_4D_2$, 80 °C): δ 28.4, 34.0, 36.9, 45.8, 49.9, 51.7, 64.2, 80.1, 155.4, 173.6 ppm. IR (film): $\tilde{\nu}$ 3445, 2976, 2930, 1735, 1693, 1672 cm^{-1}. HRMS (ESI): $[M + Na]^+$ calcd for $C_{12}H_{21}NO_5Na$ 282.1312, found 282.1313.

***rac*-(3*R*)-(1-*tert*-Butyl 3-Methyl 5-Oxopiperidine-1,3-dicarboxylate)**[42] **(25).** *rac*-**23** (110 mg; 0.424 mmol) was dissolved in DCM (5 mL) and Dess−Martin periodinane (232 mg; 0.546 mmol) was added in portions over 45 min. After 2 h of stirring at rt, another portion of Dess−Martin periodinane (131 mg, 0.309 mmol) was added and it was stirred for further 0.5 h. The mixture was concentrated in vacuum, and after purification by flash chromatography (*iso*-hexanes/EtOAc = 3:7) **25** was obtained as a colorless resin (81 mg; 74%). ^{1}H NMR (400 MHz, $C_2Cl_4D_2$, 80 °C): δ 1.44 (s, 9 H), 2.58 (dd, J = 16.9/6.0 Hz, 1 H), 2.70 (dd, J = 16.9/7.3 Hz, 1 H), 3.03 (quin, J = 6.28 Hz, 1 H), 3.71 (s, 3 H), 3.76 (dd, J = 13.6/6.9 Hz, 1 H), 3.82 (dd, J = 13.7/5.0

DOI: 10.1021/acs.jmedchem.8b01602
J. Med. Chem. 2018, 61, 10310−10332

Hz, 1 H), 3.94 (d, J = 18.9 Hz, 1 H), 3.99 (d, J = 18.9 Hz, 1 H) ppm. ^{13}C NMR (101 MHz, $C_2Cl_4D_2$, 80 °C): δ 28.3, 39.6, 40.1, 44.2, 52.3, 54.3, 80.9, 154.1, 172.4, 203.2 ppm. IR (film): $\tilde{\nu}$ 2978, 2956, 2934, 1737, 1698 cm^{-1}. HRMS (EI, 70 eV): M$^+$ calcd for $C_{12}H_{19}NO_5$ 257.1263, found 257.1268.

***rac*-(3*R*)-{1-(*tert*-Butyl) 3-Methyl 5-[(*E*)-Methoxymethylene]-piperidine-1,3-dicarboxylate} and *rac*-(3*R*)-1-{(*tert*-Butyl) 3-Methyl 5-[(*Z*)-Methoxymethylene]piperidine-1,3-dicarboxylate} (26).** (Methoxymethyl)triphenylphosphonium chloride (1.73 g; 4.95 mmol) and potassium *tert*-butoxide (524 mg; 4.58 mmol) were suspended in anhydrous THF (10 mL) under Ar. The mixture was stirred for 30 min at rt, cooled to −78 °C, and then **25** (681 mg, 2.65 mmol), dissolved in anhydrous THF (5 mL), was added and stirred for further 75 min at −78 °C and 55 min at rt. Then the reaction was quenched with ammonium chloride (525 mg, 3.71 mmol) and dissolved in H_2O (25 mL). The aqueous phase was extracted with DCM (5 × 20 mL). The combined organic phases were dried over Na_2SO_4 and concentrated under reduced pressure. After purification by flash chromatography (*iso*-hexanes/EtOAc = 5:1), **26** was obtained as colorless oil (432 mg; 57%) and as a 1:1 mixture of the *E*- and *Z*-isomers according to ^{1}H NMR. ^{1}H NMR (400 MHz, $C_2Cl_4D_2$, 80 °C): δ 1.43 (s, 9 H, *E* or *Z*), 1.43 (s, 9 H, *E* or *Z*), 2.10 (t, J = 12.5 Hz, 1 H, *E*), 2.22 (t, J = 12.2 Hz, 1 H, *Z*), 2.37 (dd, J = 14.1/4.3 Hz, 1 H, *Z*), 2.43−2.52 (m, 2 H, *E* and *Z*), 2.93 (dd, J = 14.1/4.4 Hz, 1 H, *E*), 3.01−3.10 (m, 2 H, *E* and *Z*), 3.31 (d, J = 14.7 Hz, 1 H, *Z*), 3.36 (d, J = 14.1 Hz, 1 H, *E*), 3.55 (s, 3 H, *E*), 3.56 (s, 3 H, *E* or *Z*), 3.66 (s, 3 H, *E* or *Z*), 3.66 (s, 3 H, *E* or *Z*), 4.04−4.12 (m, 3 H, *E* and *Z*), 4.63 (d, J = 14.8 Hz, 1 H, *Z*), 5.81 (s, 1 H, *Z*), 5.97 (s, 1 H, *E*) ppm. ^{13}C NMR (101 MHz, $C_2Cl_4D_2$, 80 °C): δ 26.3 (*E*), 28.5 (*E* or *Z*), 28.5 (*E* or *Z*), 30.5 (*Z*), 41.5 (*E*), 42.1 (*Z*), 42.3 (*Z*), 45.8 (*Z*), 46.2 (*E*), 46.7 (*E*), 51.6 (*E*), 51.6 (*Z*), 59.6 (*E*), 59.6 (*Z*), 79.6 (*E* or *Z*), 79.7 (*E* or *Z*), 109.6 (*E* or *Z*), 109.7 (*E* or *Z*), 141.9 (*Z*), 142.6 (*E*), 154.4 (*E* or *Z*), 154.7 (*E* or *Z*), 173.2 (*E* or *Z*), 173.2 (*E* or *Z*) ppm. IR (film): $\tilde{\nu}$ 2976, 2953, 2935, 2844, 1737, 1698 cm^{-1}. HRMS (EI, 70 eV): M$^+$ calcd for $C_{14}H_{23}NO_5$ 285.1576, found 285.1577.

***rac*-(3*R*,5*S*)-[1-(*tert*-Butyl) 3-Methyl 5-(Hydroxymethyl)-piperidine-1,3-dicarboxylate][44] (*rac*-27) and *rac*-(3*R*,5*R*)-[1-(*tert*-Butyl) 3-Methyl 5-(Hydroxymethyl)piperidine-1,3-dicarboxylate][48] (*rac*-28).** *rac*-**20** and *rac*-**21** (in 1:1 mixture, 191 mg, 0.703 mmol) were dissolved in ethanol (5 mL) and cooled to 0 °C. Sodium borohydride (80 mg; 2.1 mmol) was added to the solution, and it was stirred for 1 h. The reaction was quenched with ammonium chloride (202 mg, 3.78 mmol), dissolved in H_2O (25 mL), and it was extracted with DCM (5 × 20 mL). The combined organic phases were dried over Na_2SO_4 and concentrated under reduced pressure. After purification by flash chromatography (*iso*-hexanes/EtOAc = 2:1), *rac*-**27** and *rac*-**28** were obtained in a 1:1 mixture (according to ^{1}H NMR) as colorless oil (145 mg, 76%). ^{1}H NMR (400 MHz, $C_2Cl_4D_2$, 80 °C): δ 1.25−1.36 (m, 1 H, *a*), 1.44 (s, 9 H, *a* or *b*), 1.44 (s, 9 H, *a* or *b*), 1.62−1.76 (m, 2 H, *a* and *b*), 1.86−1.99 (m, 2 H, *b*), 2.11 (dtt, J = 13.1/3.6/1.7 Hz, 1 H, *a*), 2.35−2.51 (m, 2 H, *a*), 2.58 (tt, J = 8.4/4.4 Hz, 1 H, *b*), 2.72 (dd, J = 13.2/11.3 Hz, 1 H, *a*), 3.31 (dd, J = 13.5/3.7 Hz, 1 H, *b*), 3.38−3.51 (m, 6 H, *a* and *b*), 3.66 (s, 3 H, *a* or *b*), 3.67 (s, 3 H, *a* or *b*), 3.72 (dd, J = 13.5/4.4 Hz, 1 H, *b*), 4.09−4.16 (m, 1 H, *a*), 4.22−4.30 (m, 1 H, *a*) ppm.[75] ^{13}C NMR (101 MHz, $C_2Cl_4D_2$, 80 °C): δ 28.4 (*a* or *b*), 28.5 (*a* or *b*), 28.5 (*b*), 30.4 (*a*), 35.2 (*b*), 38.0 (*a* or *b*), 38.1 (*a* or *b*), 41.3 (*a*), 45.3 (*b*), 45.9 (*a* or *b*), 46.0 (*a* or *b*), 46.7 (*a*), 51.7 (*a*), 51.7 (*b*), 63.2 (*a*), 65.1 (*b*), 79.8 (*a* or *b*), 79.9 (*a* or *b*), 154.6 (*a* or *b*), 155.0 (*a* or *b*), 173.4 (*a* or *b*), 173.5 (*a* or *b*) ppm. IR (film): $\tilde{\nu}$ 3450, 2976, 2932, 2868, 1736, 1691, 1672 cm^{-1}. HRMS (EI, 70 eV): M$^+$ calcd for $C_{13}H_{23}NO_5$ 273.1576, found 273.1576.

***rac*-(3*R*,5*S*)-[1-(*tert*-Butyl) 3-Methyl 5-{[1-(*tert*-Butoxycarbonyl)hydrazinyl]methyl}piperidine-1,3-dicarboxylate] (*rac*-30).** *rac*-**27** and *rac*-**28** (in 1:1 mixture, 464 mg, 1.70 mmol), *N*-(*tert*-butoxycarbonyl)aminophthalimide[47] (**29**, 710 mg, 2.71 mmol), and triphenylphosphine (1.06 g, 3.94 mmol) were dissolved in anhydrous THF (20 mL) under Ar. The solution was cooled to 0 °C, and diisopropyl azodicarboxylate (1.0 mL, 4.8 mmol) was added dropwise over 30 min under stirring. After additional 75 min of stirring, the reaction mixture was concentrated under reduced pressure. The crude intermediate was purified by flash chromatography (*iso*-hexanes/EtOAc = 3:1), and the resulting residue was dissolved in THF (20 mL) and cooled to 0 °C. Methylhydrazine (0.50 mL, 9.6 mmol) was added, and after 110 min of stirring, another portion of methylhydrazine (0.10 mL, 1.9 mmol) was added. The reaction mixture was stirred for further 10 min at 0 °C and then concentrated under reduced pressure. After purification by flash chromatography (*iso*-hexanes/EtOAc = 1:1), *rac*-**30** was obtained as colorless oil (249 mg; 38%). ^{1}H NMR (400 MHz, $C_2Cl_4D_2$, 80 °C): δ 1.15−1.31 (m, 1 H), 1.44 (s, 9 H), 1.46 (s, 9 H), 1.82−1.95 (m, 1 H), 2.02−2.09 (m, 1 H), 2.31 (dd, J = 13.2/11.5 Hz, 1 H), 2.45 (tt, J = 11.8/4.0 Hz, 1 H), 2.65 (dd, J = 13.2/11.5 Hz, 1 H), 3.20 (dd, J = 14.0/6.1 Hz, 1 H), 3.27 (dd, J = 14.0/7.4 Hz, 1 H), 3.67 (s, 3 H), 3.91 (br s, 2 H), 4.06 (dt, J = 13.2/1.8 Hz, 1 H), 4.31 (dt, J = 13.2 Hz, 1 H) ppm.[75] ^{13}C NMR (101 MHz, $C_2Cl_4D_2$, 80 °C): δ 28.4, 28.5, 31.9, 34.9, 41.6, 45.9, 47.8, 51.6, 53.7, 79.8, 80.7, 154.4, 156.7, 173.3 ppm. IR (film): $\tilde{\nu}$ 3334, 2975, 2931, 1736, 1693, 1631 cm^{-1}. HRMS (EI, 70 eV): M$^+$ calcd for $C_{18}H_{33}N_3O_6$ 387.2369, found 387.2369.

***rac*-(3*R*,5*R*)-[1-(*tert*-Butyl) 3-Methyl 5-{[1-(*tert*-Butoxycarbonyl)hydrazinyl]methyl}piperidine-1,3-dicarboxylate] (*rac*-31).** *rac*-**31** was obtained as additional product in the synthesis of *rac*-**30** as colorless oil (282 mg; 43%). ^{1}H NMR (400 MHz, $C_2Cl_4D_2$, 80 °C): δ 1.43 (s, 9 H), 1.45 (s, 9 H), 1.53−1.64 (m, 1 H), 1.85 (ddd, J = 12.7/8.0/4.3 Hz, 1 H), 2.15−2.25 (m, 1 H), 2.69 (ddt, J = 11.3/8.1/4.6 Hz, 1 H), 3.13−3.22 (m, 2 H), 3.36−3.45 (m, 2 H), 3.50−3.69 (m, 5 H), 3.98 (br s, 2 H) ppm.[75] ^{13}C NMR (101 MHz, $C_2Cl_4D_2$, 80 °C): δ 28.4, 28.4, 29.0, 31.7, 38.1, 45.6, 46.8, 51.5, 52.1, 79.6, 80.6, 154.5, 156.7, 173.6 ppm. IR (film): $\tilde{\nu}$ 3334, 3224, 2976, 2932, 2868, 1736, 1694 cm^{-1}. HRMS (EI, 70 eV): M$^+$ calcd for $C_{18}H_{33}N_3O_6$ 387.2369, found 387.2379.

***rac*-(3*R*,5*S*)-{1-[(*tert*-Butoxy)carbonyl] 5-({1-[(*tert*-Butoxy)-carbonyl]hydrazinyl}methyl)piperidine-3-carboxylic Acid} (*rac*-32).** *rac*-**30** (316 mg, 0.816 mmol) was dissolved in MeOH (10 mL), cooled to 0 °C, and a 1 M aqueous NaOH (3.0 mL, 3.0 mmol) was added. The mixture was stirred for 15 h, while the reaction was allowed to reach rt (0 °C → rt). Then it was concentrated under reduced pressure, diluted with H_2O (30 mL), washed with DCM (3 × 20 mL), and acidified with phosphoric acid (85%, 0.25 mL, 3.7 mmol). The aqueous phase was extracted with DCM (5 × 20 mL). The combined organic phases were dried over Na_2SO_4 and concentrated under reduced pressure. *rac*-**32** was obtained as colorless resin (313 mg, quant). ^{1}H NMR (400 MHz, $C_2Cl_4D_2$, 80 °C): δ 1.34−1.42 (m, 1 H), 1.54 (s, 9 H), 1.56 (s, 9 H), 1.92−2.07 (m, 1 H), 2.20 (dm, J = 13.3 Hz, 1 H), 2.42 (dd, J = 13.2/11.5 Hz, 1 H), 2.59 (tt, J = 11.7/3.9 Hz, 1 H), 2.78 (dd, J = 13.2/11.5 Hz, 1 H), 3.31 (dd, J = 14.0/6.2 Hz, 1 H), 3.38 (dd, J = 14.0/7.2 Hz, 1 H), 4.18 (dm, J = 13.2 Hz, 1 H), 4.44 (dm, J = 13.1 Hz, 1 H) ppm.[75] ^{13}C NMR (101 MHz, $C_2Cl_4D_2$, 80 °C): δ 28.4, 28.5, 31.8, 34.9, 41.0, 45.7, 47.7, 53.7, 80.0, 80.9, 154.5, 156.8, 175.2 ppm. IR (film): $\tilde{\nu}$ 3434, 2979, 2934, 1729, 1697 cm^{-1}. HRMS (ESI): [M + H]$^+$ calcd for $C_{17}H_{32}N_3O_6$ 374.2286, found 374.2290.

***rac*-(3*R*,5*R*)-{1-(*tert*-Butyl) 3-Methyl 5-[(*E*)-2-Methoxyethenyl]piperidine-1,3-dicarboxylate} and *rac*-(3*R*,5*R*)-{1-(*tert*-Butyl) 3-Methyl 5-[(*Z*)-2-Methoxyethenyl]-piperidine-1,3-dicarboxylate} (*rac*-33).** (Methoxymethyl)-triphenylphosphonium chloride (2.85 g; 8.16 mmol) and potassium *tert*-butoxide (856 mg; 7.48 mmol) were suspended in anhydrous THF (23 mL) under Ar. The mixture was stirred at rt for 30 min, cooled to 0 °C, and then *rac*-**20** and *rac*-**21** (in 1:1 mixture, 1.15 g, 4.25 mmol), dissolved in anhydrous THF (10 mL), were added. It was stirred for further 80 min at 0 °C and 20 min at rt. Then the reaction was quenched with ammonium chloride (905 mg, 16.9 mmol), dissolved in H_2O (30 mL), *iso*-hexane (15 mL) was added, the phases were separated, and the aqueous phase was further extracted with DCM (4 × 25 mL). The combined organic phases were dried over Na_2SO_4 and concentrated under reduced pressure. After purification by flash chromatography on silica gel (EtOAc/*iso*-hexane = 1:5), *rac*-**33** was obtained as colorless oil (614 mg; 48%) and as 1:0.43 mixture of the *E*- and *Z*-isomer according to ^{1}H NMR. ^{1}H NMR (400 MHz, $C_2Cl_4D_2$, 80 °C): δ 1.25−1.39 (m, 1 H + 0.43 × 1 H, *E* and *Z*), 1.54 (s, 0.43 × 9 H, *Z*), 1.54 (s, 9 H, *E*), 2.00−2.15 (m, 2 H + 0.43 × 1 H, *E* and *Z*), 2.28−2.38 (m, 1 H + 0.43 × 1 H, *E* and *Z*), 2.40−2.58 (m, 1 H + 0.43 × 2 H, *E* and *Z*), 2.60−2.70 (m, 1 H + 0.43 × 1 H, *E* and *Z*), 3.48 (s, 3 H, *E*), 3.56 (s, 0.43 × 3 H, *Z*), 3.65 (s,

DOI: 10.1021/acs.jmedchem.8b01602
J. Med. Chem. 2018, 61, 10310−10332

0.43 × 3 H, *Z*), 3.66 (s, 3 H, *E*), 3.96−4.05 (m, 1 H + 0.43 × 1 H, *E* and *Z*), 4.07 (dd, *J* = 8.2/6.3 Hz, 0.43 × 1 H, *Z*), 4.21−4.32 (m, 1 H + 0.43 × 1 H, *E* and *Z*), 4.57 (dd, *J* = 12.7/7.5 Hz, 1 H, *E*), 5.88 (dd, *J* = 6.3/1.1 Hz, 0.43 × 1 H, *Z*), 6.32 (dd, *J* = 12.7/0.8 Hz, 1 H, *E*) ppm. ^{13}C NMR (101 MHz, $C_2Cl_4D_2$, 60 °C): δ 28.4 (*E*), 28.4 (*Z*), 31.7 (*Z*), 34.2 (*Z*), 34.7 (*E*), 35.0 (*E*), 41.4 (*Z*), 41.5 (*E*), 45.4 (*E*), 45.4 (*Z*), 50.0 (*E*), 50.0 (*Z*), 51.6 (*Z*), 51.7 (*E*), 56.1 (*E*), 59.7 (*Z*), 79.6 (*Z*), 79.7 (*E*), 104.2 (*E*), 106.8 (*Z*), 147.4 (*Z*), 148.1 (*E*), 154.4 (*E*), 154.5 (*Z*), 173.4 (*E*), 173.5 (*Z*) ppm. IR (film): $\tilde{\nu}$ 2976, 2952, 2935, 2861, 1737, 1694, 1655 cm^{-1}. HRMS (ESI): $[M + H]^+$ calcd for $C_{15}H_{26}NO_5$ 300.1806, found 300.1806.

***rac*-(3*R*,5*S*)-{1-(*tert*-Butyl) 3-Methyl 5-[(*E*)-2-Methoxyethenyl]piperidine-1,3-dicarboxylate} and *rac*-(3*R*,5*S*)-{1-(*tert*-Butyl) 3-Methyl 5-[(*Z*)-2-Methoxyethenyl]-piperidine-1,3-dicarboxylate} (*rac*-34).** *rac*-**34** was obtained as additional product in the synthesis of *rac*-**33** as colorless oil (417 mg, 33%) and as 1:0.27 mixture of the *E*- and *Z*-isomer according to ^{1}H NMR. ^{1}H NMR (400 MHz, $C_2Cl_4D_2$, 80 °C): δ 1.43 (s, 0.27 × 9 H, *Z*), 1.43 (s, 9 H, *E*), 1.59 (ddd, *J* = 13.1/8.0/4.5 Hz, 1 H, *E*), 1.74 (ddd, *J* = 12.9/6.7/4.4 Hz, 0.27 × 1 H, *Z*), 1.89 (ddd, *J* = 12.8/8.3/4.3 Hz, 0.27 × 1 H, *Z*), 1.99 (ddd, *J* = 13.2/7.0/4.2 Hz, 1 H, *E*), 2.42 (qt, *J* = 7.7/4.0 Hz, 1 H, *E*), 2.54−2.70 (m, 1 H + 0.27 × 2 H, *E* and *Z*), 2.79−2.90 (m, 0.27 × 1 H, *Z*), 3.06 (dd, *J* = 13.0/7.4 Hz, 1 H, *E*), 3.26−3.32 (m, 0.27 × 1 H, *Z*), 3.40−3.54 (m, 5 H + 0.27 × 2 H, *E* and *Z*), 3.57 (s, 0.27 × 3 H, *Z*), 3.59−3.76 (m, 4 H + 0.27 × 4 H, *E* and *Z*), 4.24 (dd, *J* = 8.0/6.3 Hz, 0.27 × 1 H, *Z*), 4.65 (dd, *J* = 12.7/7.6 Hz, 1 H, *E*), 5.87 (dd, *J* = 6.3/1.3 Hz, 0.27 × 1 H, *Z*), 6.34 (dd, *J* = 12.8/1.0 Hz, 1 H, *E*) ppm. ^{13}C NMR (101 MHz, $C_2Cl_4D_2$, 60 °C): δ 28.4 (*E*), 28.4 (*Z*), 28.9 (*Z*), 31.7 (*E*), 32.5 (*Z*), 33.4 (*E*), 38.3 (*E*), 38.3 (*Z*), 45.2 (*E*), 45.2 (*Z*), 49.3 (*E*), 49.3 (*Z*), 51.6 (*E*), 51.6 (*Z*), 56.1 (*E*), 59.7 (*Z*), 79.3 (*Z*), 79.4 (*E*), 104.0 (*E*), 106.5 (*Z*), 147.0 (*Z*), 148.1 (*E*), 154.4 (*E*), 154.7 (*Z*), 173.6 (*E*), 173.9 (*Z*) ppm. IR (film): $\tilde{\nu}$ 2975, 2951, 2933, 2860, 1736, 1694, 1654 cm^{-1}. HRMS (ESI): $[M + H]^+$ calcd for $C_{15}H_{26}NO_5$ 300.1806, found 300.1808.

***rac*-(3*R*,5*R*)-[1-(*tert*-Butyl) 3-Methyl 5-(2-Oxoethyl)-piperidine-1,3-dicarboxylate] (*rac*-35).** According to GP2 with *rac*-**33** (568 mg; 1.90 mmol) and 2 M aqueous HCl (3.5 mL, 7.0 mmol) and a reaction time of 7 h, *rac*-**35** was obtained as a colorless oil (435 mg, 80%). ^{1}H NMR (400 MHz, $C_2Cl_4D_2$, 80 °C): δ 1.28 (q, *J* = 12.4 Hz, 1 H), 1.45 (s, 9 H), 1.97−2.09 (m, 1 H), 2.15 (dtt, *J* = 13.1/3.7/1.8 Hz, 1 H), 2.22−2.38 (m, 3 H), 2.50 (tt, *J* = 11.7/4.0 Hz, 1 H), 2.69 (dd, *J* = 13.2/11.5 Hz, 1 H), 3.67 (s, 3 H), 4.07 (dm, *J* = 13.0 Hz, 1 H), 4.29 (dm, *J* = 13.4 Hz, 1 H), 9.74 (t, *J* = 1.8 Hz, 1 H) ppm. ^{13}C NMR (101 MHz, $C_2Cl_4D_2$, 80 °C): δ 28.5, 30.4, 33.8, 41.5, 45.7, 47.4, 49.0, 51.7, 80.1, 154.4, 173.0, 200.0 ppm. IR (film): $\tilde{\nu}$ 2977, 2953, 2933, 2863, 2724, 1733, 1693 cm^{-1}. HRMS (ESI): $[M + H]^+$ calcd for $C_{14}H_{24}NO_5$ 286.1649, found 286.1656.

***rac*-(3*R*,5*S*)-[1-(*tert*-Butyl) 3-Methyl 5-(2-Oxoethyl)-piperidine-1,3-dicarboxylate] (*rac*-36).** According to GP2 with *rac*-**34** (326 mg, 1.09 mmol) and 2 M aqueous HCl (2.0 mL, 4.0 mmol) and a reaction time of 8.5 h, *rac*-**36** was obtained as a colorless oil (272 mg, 88%). ^{1}H NMR (400 MHz, $C_2Cl_4D_2$, 120 °C): δ 1.43 (s, 9 H), 1.61 (ddd, *J* = 13.6/6.1/4.4 Hz, 1 H), 1.99 (ddd, *J* = 13.6/8.2/3.8 Hz, 1 H), 2.24−2.44 (m, 3 H), 2.58 (tt, *J* = 8.1/4.4 Hz, 1 H), 3.19 (dd, *J* = 13.4/5.9 Hz, 1 H), 3.43 (dd, *J* = 13.3/3.3 Hz, 1 H), 3.54 (dd, *J* = 13.5/7.1 Hz, 1 H), 3.60−3.67 (m, 4 H), 9.74 (t, *J* = 1.7 Hz, 1 H) ppm. ^{13}C NMR (101 MHz, $C_2Cl_4D_2$, 80 °C): δ 27.5, 28.4, 31.9, 38.2, 45.5, 45.9, 48.1, 51.7, 79.8, 154.5, 173.2, 200.4 ppm. IR (film): $\tilde{\nu}$ 2976, 2952, 2932, 2868, 2723, 1731, 1693 cm^{-1}. HRMS (ESI): $[M + H]^+$ calcd for $C_{14}H_{24}NO_5$ 286.1649, found 286.1655.

***rac*-(3*R*,5*R*)-{1-(*tert*-Butyl) 3-Methyl 5-[2-({[(*tert*-Butoxy)-carbonyl]amino}amino)ethyl]piperidine-1,3-dicarboxylate} (*rac*-37).** According to GP3 with *rac*-**35** (86 mg, 0.30 mmol), *tert*-butyl carbazate (66 mg, 0.49 mmol), AcOH (0.043 mL, 0.75 mmol) and $NaBH_3CN$ (81 mg, 1.2 mmol, added in three portions). *rac*-**37** was obtained as a colorless oil (90 mg; 74%). ^{1}H NMR (400 MHz, $C_2Cl_4D_2$, 80 °C): δ 1.18 (q, *J* = 12.3 Hz, 1 H), 1.26−1.38 (m, 2 H), 1.44 (s, 9 H), 1.44 (s, 9 H), 1.50−1.58 (m, 1 H), 2.12 (dtt, *J* = 12.6/3.4/1.8 Hz, 1 H), 2.24 (dd, *J* = 12.9/11.8 Hz, 1 H), 2.43 (tt, *J* = 11.8/4.0 Hz, 1 H), 2.66 (dd, *J* = 12.9/11.8 Hz, 1 H), 2.85 (dd, *J* = 12.7/6.9 Hz, 1 H), 2.89 (dd, *J* = 12.8/7.5 Hz, 1 H), 3.66 (s, 3 H), 4.06 (dm, *J* = 13.1 Hz, 1 H), 4.27 (dm, *J* = 13.1 Hz, 1 H) ppm.[75] ^{13}C NMR (101 MHz, $C_2Cl_4D_2$, 80 °C): δ 28.4, 28.5, 31.9, 33.5, 34.2, 41.7, 45.8, 49.3, 49.6, 51.6, 79.7, 80.4, 154.5, 156.6, 173.4 ppm. IR (film): $\tilde{\nu}$ 3329, 2976, 2930, 2868, 1736, 1696 cm^{-1}. HRMS (ESI): $[M + H]^+$ calcd for $C_{19}H_{36}N_3O_6$ 402.2599, found 402.2599.

***rac*-(3*R*,5*S*)-{1-(*tert*-Butyl) 3-Methyl 5-[2-({[(*tert*-Butoxy)-carbonyl]amino}amino)ethyl]piperidine-1,3-dicarboxylate} (*rac*-38).** According to GP3 with *rac*-**36** (115 mg, 0.403 mmol), *tert*-butyl carbazate (89 mg, 0.66 mmol), AcOH (0.057 mL, 1.0 mmol), and $NaBH_3CN$ (112 mg, 1.69 mmol, added in three portions), *rac*-**38** was obtained as a colorless oil (125 mg; 77%). ^{1}H NMR (400 MHz, $C_2Cl_4D_2$, 120 °C): δ 1.29−1.40 (m, 2 H), 1.43 (s, 9 H), 1.44 (s, 9 H), 1.51−1.61 (m, 1 H), 1.80−1.90 (m, 1 H), 1.95 (ddd, *J* = 12.6/7.7/4.2 Hz, 1 H), 2.52−2.63 (m, 1 H), 2.81−2.94 (m, 2 H), 3.14 (dd, *J* = 13.2/6.6 Hz, 1 H), 3.40 (dd, *J* = 13.2/3.7 Hz, 1 H), 3.55 (dd, *J* = 13.4/6.6 Hz, 1 H), 3.58 (dd, *J* = 13.5/5.1 Hz, 1 H), 3.65 (s, 3 H), 5.94 (br s, 1 H) ppm.[75] ^{13}C NMR (101 MHz, $C_2Cl_4D_2$, 80 °C): δ 28.4, 28.5, 30.1, 30.8, 32.4, 38.2, 45.6, 48.4, 49.9, 51.6, 79.5, 80.3, 154.6, 156.6, 173.6 ppm. IR (film): $\tilde{\nu}$ 3320, 2976, 2930, 2861, 1735, 1796 cm^{-1}. HRMS (ESI): $[M + H]^+$ calcd for $C_{19}H_{36}N_3O_6$ 402.2599, found 402.2603.

Aldehydes. Synthetic protocols and detailed analytical data for aldehydes are provided in the Supporting Information.

MS Binding Experiments: mGAT1 Membrane Preparation. Membrane preparations of HEK293 cells stably expressing mGAT1[55] were prepared and applied as previously described.[35,51,77]

Library Screening. Library screening experiments were basically performed as reported[35,51] except for varying hydrazine and aldehyde concentrations and buffer composition: Quadruplicate samples in a total volume of 250 μL in 1.2 mL polysterene 96-deep-well plates (Sarstedt) were employed. The incubation buffer contained 12.5 mM $Na_2HPO_4·2H_2O$, 12.5 mM $NaH_2PO_4·H_2O$, 1 M NaCl, and 200 μM sodium L-ascorbate, and the pH was adjusted to 7.1 with 2 M NaOH. Solutions were added as 10-fold concentrated stock solutions, and all samples contained 1% DMSO (final concentration). Aldehydes were applied in a final concentration of 1.0 μM per sample (with each aldehyde library representing a mixture of eight different aldehydes) and hydrazines (*rac*-**11**, *rac*-**12**, *rac*-**13**, or *rac*-**14**, applied as hydrochlorides)[49] were applied in 200 μM. Directly after combining the hydrazine and aldehydes, the mGAT1 membrane preparation was added, which started the first incubation period of 4 h at 37 °C in a shaking water bath (for library generation). Then MS marker **6** was added in a concentration of 20 nM (final concentration in the sample), starting the second incubation period of 40 min at 37 °C. Total binding was determined with analogously constituted samples lacking any inhibitor and nonspecific binding was determined in the presence of 100 mM GABA. All experiments additionally obtained matrix blanks, zero samples, and matrix standards. The incubation was terminated by vacuum filtration (96-well filter plate, Acroprep, glass fiber, 1.0 μm, 350 μL; Pall). After five washing steps with ice-cold aqueous 1 M NaCl, the filter plates were dried at 50 °C for 60 min and cooled to room temperature. The marker **6** was subsequently liberated by elution with MeOH, and the eluate was collected in a 96-deep-well plate. To each sample (except the matrix blanks) 200 μL of 1 nM $[^2H_{10}]$NO711 in MeOH was added as internal standard. For calibration, blank matrix was supplemented with 200 μL of methanolic calibration standards with 20 pM, 50 pM, 100 pM, 200 pM, 500 pM, 1.0 nM, 2.5 nM, and 5.0 nM NO711, respectively (these samples were employed for generating calibration curves for marker quantitation). All samples were dried to completeness at 50 °C for 16 h and subsequently reconstituted in 200 μL of 10 mM ammonium formate buffer (pH 7.0) containing 5% MeOH. Quantification was performed by LC-ESI-MS/MS. As a control, analogous samples were employed in the library screening experiments for characterizing specific binding of pure aldehyde libraries and pure hydrazines (*rac*-**11**, *rac*-**12**, *rac*-**13**, or *rac*-**14**, applied as hydrochlorides),[49] respectively.

Deconvolution Experiments. The deconvolution experiments were analogously performed as the library screening experiments (as described above), but instead of a mixture of eight aldehydes, single aldehydes (1.0 μM per sample) were applied.

DOI: 10.1021/acs.jmedchem.8b01602
J. Med. Chem. 2018, 61, 10310−10332

Competition Experiments for Establishing Binding Affinities of Hydrazones. Full-scale MS binding experiments were performed as previously described[38,77] by applying pure hydrazones[54] and the incubation buffer as described under "Library screening".

Saturation Experiments for Investigation of Test Compounds' Mode of Interaction. MS based saturation experiments with NO711 as reporter ligand (concentration range: 2.5−480 nM) addressing mGAT1 were performed as previously described.[38,77] Pure hydrazones[54] and tiagabine were added in the desired concentrations to the binding samples before incubation was started by addition of the mGAT1 membrane preparation. All other conditions (e.g., incubation buffer, filtration, and washing of binding samples, drying of eluates, and reconstitution of samples) were exactly the same as described under "Library screening".

LC-ESI-MS/MS. Quantification by LC-ESI-MS/MS was performed on an API 3200 or 3200 Q TRAP triple-quadrupole mass spectrometer (AB Sciex). The injection volume was always 30 μL, and the LC conditions were exactly as described previously.[38] Detailed instrument settings of the mass spectrometers are specified in the Supporting Information.

Data Analysis in mGAT1MS Binding Assays. Data analysis was performed as previously described.[35,38,51,77] Binding affinities for test compounds are expressed as pK_i values (with K_i values calculated according to Cheng and Prussoff,[78] taking into account that the investigated test compounds and NO711 may not address the same binding site, the K_i values could be considered as apparent K_i values). Affinities (K_d) for NO711 and densities of binding sites (B_{max}) in the absence or presence of test compounds were calculated from saturation isotherms. B_{max} values are given in [pmol/(mg protein)], K_d values in [nM]. All results represent means ± SEM, determined in at least three separate experiments. To distinguish between competitive and noncompetitive binding interactions between test compounds and the reporter ligand NO711, a Schild-like coefficient was calculated according to Hulme and Trevethick[58] with coefficient = [log $(K_{d\_NO711\_app}/K_{d\_NO711} - 1)_{higher\ concentrated\ test\ compound}$ − log $(K_{d\_NO711\_app}/K_{d\_NO711} - 1)_{lower\ concentrated\ test\ compound}$]/[log (higher concentration test compound) − log (lower concentration test compound)]

GABA Uptake Assays. [^{3}H]GABA uptake assays were performed as previously described,[55] except that 200 μM sodium L-ascorbate was added to all samples as antioxidant.

MS Transport Assays: Competitive MS Transport Assays. Competitive MS Transport Assays were performed as reported,[64,65] except that sodium L-ascorbate (200 μM) was added to all samples (including controls) as antioxidant.

Saturation Experiments for Investigation of Test Compound's Mode of Interaction by Means of MS Transport Assays. Saturation experiments by means of MS Transport Assays with COS cells stably expressing hGAT1 were performed as previously described,[64,65] except that sodium L-ascorbate (200 μM) was added to all samples as antioxidant. Pure hydrazones *rac*-**16gf** and *rac*-**16gg** and tiagabine (**5**), respectively, were added in the desired concentrations to the samples containing the COS-hGAT1 cells, and after preincubation for 25 min, the addition of ($^2H_6$)GABA started the uptake. V_{max} and K_m values in the absence or presence of test compound were calculated from saturation isotherms. V_{max} values are given in [amol/cell·min], K_m values in [μM]. All results represent means ± SEM, determined in three separate experiments.

■ ASSOCIATED CONTENT

Supporting Information

The Supporting Information is available free of charge on the ACS Publications website at DOI: 10.1021/acs.jmedchem.8b01602.

General procedure for the synthesis of new aldehydes (**15fd**, **15ff**, **15fh**, **15fi**, **15fn**, **15fp**, **15fs**, and **15gr** with detailed analytical data of aldehydes, information regarding the reaction progress of hydrazone formation, control experiments for library screening with individual building blocks, control experiments for hydrazone stability in incubation buffers, control experiments for investigation of test compound's mode of interaction, detailed instrument settings of the mass spectrometers, and NMR spectra of compounds (PDF)

Coordinates of the hGAT1 model (PDB)

Molecular formula strings (CSV)

■ AUTHOR INFORMATION

Corresponding Author

*Phone: +49 2180 77249. Fax +49 2180 77247. E-mail: Klaus.Wanner@cup.uni-muenchen.de.

ORCID

Klaus T. Wanner: 0000-0003-4399-1425

Notes

The authors declare no competing financial interest.

■ ACKNOWLEDGMENTS

We thank Simone Huber, Dr. Karuna Bhokare, Hans Brabec, and Janine Piecek for the help of compiling aldehyde libraries, Dr. Lars Allmendinger and Dr. Jörg Pabel for technical assistance, and Silke Duensing-Kropp, Tanja Franz, and Miriam Sandner for performing GABA uptake assays and MS Transport Assays.

■ ABBREVIATIONS USED

BGT, betaine/γ-aminobutyric acid transporter; DCC, dynamic combinatorial chemistry; DIAD, diisopropyl azodicarboxylate; dm, doublet of a multiplet (NMR); GAT, γ-aminobutyric acid transporter; GP, general procedure; HUGO, human genome organization; LeuT, leucine transporter; PAINS, pan assay interference compounds; SLC6, solute carrier 6 gene family.

■ REFERENCES

(1) Bradford, H. F. Glutamate, GABA and epilepsy. *Prog. Neurobiol.* **1995**, *47*, 477−511.

(2) Treiman, D. M. GABAergic mechanisms in epilepsy. *Epilepsia* **2001**, *42*, 8−12.

(3) Kleppner, S. R.; Tobin, A. J. GABA signalling: therapeutic targets for epilepsy, Parkinson's disease and Huntington's disease. *Emerging Ther. Targets* **2001**, *5*, 219−239.

(4) Ishiwari, K.; Mingote, S.; Correa, M.; Trevitt, J. T.; Carlson, B. B.; Salamone, J. D. The GABA uptake inhibitor β-alanine reduces pilocarpine-induced tremor and increases extracellular GABA in substantia nigra pars reticulata as measured by microdialysis. *J. Neurosci. Methods* **2004**, *140*, 39−46.

(5) Kalueff, A. V.; Nutt, D. J. Role of GABA in anxiety and depression. *Depression Anxiety* **2007**, *24*, 495−517.

(6) Todorov, A. A.; Kolchev, C. B.; Todorov, A. B. Tiagabine and gabapentin for the management of chronic pain. *Clin. J. Pain* **2005**, *21*, 358−361.

(7) Daemen, M. A.; Hoogland, G.; Cijntje, J. M.; Spincemaille, G. H. Upregulation of the GABA-transporter GAT-1 in the spinal cord contributes to pain behaviour in experimental neuropathy. *Neurosci. Lett.* **2008**, *444*, 112−115.

(8) Kowalczyk, P.; Kulig, K. GABA system as target for new drugs. *Curr. Med. Chem.* **2014**, *21*, 3294−3309.

(9) Kristensen, A. S.; Andersen, J.; Jørgensen, T. N.; Sørensen, L.; Eriksen, J.; Loland, C. J.; Strømgaard, K.; Gether, U. SLC6 neurotransmitter transporters: structure, function, and regulation. *Pharmacol. Rev.* **2011**, *63*, 585−640.

(10) Madsen, K. K.; Clausen, R. P.; Larsson, O. M.; Krogsgaard-Larsen, P.; Schousboe, A.; White, H. S. Synaptic and extrasynaptic

DOI: 10.1021/acs.jmedchem.8b01602
J. Med. Chem. 2018, 61, 10310−10332

GABA transporters as targets for anti-epileptic drugs. *J. Neurochem.* **2009**, *109*, 139−144.
(11) Wellendorph, P.; Jacobsen, J.; Skovgaard-Petersen, J.; Jurik, A.; Vogensen, S. B.; Ecker, G.; Schousboe, A.; Krogsgaard-Larsen, P.; Clausen, R. P. γ-Aminobutyric Acid and Glycine Neurotransmitter Transporters. In *Transporters as Drug Targets*, 1st ed.; Ecker, G. F., Clausen, R. P., Sitte, H. H., Eds.; Wiley-VCH: Weinheim, 2017; pp 69−106.
(12) Krogsgaard-Larsen, P.; Frølund, B.; Frydenvang, K. GABA uptake inhibitors. Design, molecular pharmacology and therapeutic aspects. *Curr. Pharm. Des.* **2000**, *6*, 1193−1209.
(13) Zhou, Y.; Danbolt, N. C. GABA and glutamate transporters in brain. *Front. Endocrinol.* **2013**, *4*, 165.
(14) Krogsgaard-Larsen, P.; Johnston, G. A. R. Inhibition of GABA uptake in rat brain slices by nipecotic acid, various isoxazoles and related compounds. *J. Neurochem.* **1975**, *25*, 797−802.
(15) Krogsgaard-Larsen, P.; Falch, E.; Larsson, O. M.; Schousboe, A. GABA uptake inhibitors: relevance to antiepileptic drug research. *Epilepsy Res.* **1987**, *1*, 77−93.
(16) Yunger, L. M.; Fowler, P. J.; Zarevics, P.; Setler, P. E. Novel inhibitors of gamma-aminobutyric acid (GABA) uptake: anticonvulsant actions in rats and mice. *J. Pharmacol. Exp. Ther.* **1984**, *228*, 109−115.
(17) Ali, F. E.; Bondinell, W. E.; Dandridge, P. A.; Frazee, J. S.; Garvey, E.; Girard, G. R.; Kaiser, C.; Ku, T. W.; Lafferty, J. J.; Moonsammy, G. I.; Oh, H.-J.; Rush, J. A.; Setler, P. E.; Stringer, O. D.; Venslavsky, J. W.; Volpe, B. W.; Yunger, L. M.; Zirkle, C. L. Orally active and potent inhibitors of γ-aminobutyric acid uptake. *J. Med. Chem.* **1985**, *28*, 653−660.
(18) Dalby, N. O. GABA-level increasing and anticonvulsant effects of three different GABA uptake inhibitors. *Neuropharmacology* **2000**, *39*, 2399−2407.
(19) Borden, L. A.; Dhar, T. G. M.; Smith, K. E.; Weinshank, R. L.; Branchek, T. A.; Gluchowski, C. Tiagabine, SK&F 89976-A, CI-966, and NNC-711 are selective for the cloned GABA transporter GAT-1. *Eur. J. Pharmacol., Mol. Pharmacol. Sect.* **1994**, *269*, 219−224.
(20) Frey, H.-H.; Popp, C.; Loescher, W. Influence of the inhibitors of high affinity GABA uptake on seizure threshold in mice. *Neuropharmacology* **1979**, *18*, 581−590.
(21) Genton, P.; Guerrini, R.; Perucca, E. Tiagabine in clinical practice. *Epilepsia* **2001**, *42*, 42−45.
(22) Salat, K.; Podkowa, A.; Malikowska, N.; Kern, F.; Pabel, J.; Wojcieszak, E.; Kulig, K.; Wanner, K. T.; Strach, B.; Wyska, E. Novel, highly potent and in vivo active inhibitor of GABA transporter subtype 1 with anticonvulsant, anxiolytic, antidepressant and antinociceptive properties. *Neuropharmacology* **2017**, *113*, 331−342.
(23) Müller-Uri, C.; Singer, E. A.; Fleischhacker, W. Synthesis of alkyl-substituted arecoline derivatives as γ-aminobutyric acid uptake inhibitors. *J. Med. Chem.* **1986**, *29*, 125−132.
(24) Lapuyade, G.; Schlewer, G.; N'Goka, V.; Vernieres, J.-C.; Chambon, J.-P.; Lagrange, J.; Lagrange, P.; Wermuth, C. G. Alkyl and aryl derivatives of nipecotic acid: synthesis and inhibition of GABA uptake as a function of conformational parameters and bioavailability. *Eur. J. Med. Chem.* **1987**, *22*, 383−391.
(25) N'Goka, V.; Schlewer, G.; Linget, J.-M.; Chambon, J.-P.; Wermuth, C. G. GABA-uptake inhibitors: construction of a general pharmacophore model and successful prediction of a new representative. *J. Med. Chem.* **1991**, *34*, 2547−2557.
(26) Hoesl, C. E.; Höfner, G.; Wanner, K. T. First asymmetric syntheses of 6-substituted nipecotic acid derivatives. *Tetrahedron* **2004**, *60*, 307−318.
(27) N'Goka, V.; Bissantz, C.; Bisel, P.; Stenbøl, T. B.; Krogsgaard-Larsen, P.; Schlewer, G. Syntheses and GABA uptake properties of 6-ether- and 6-enol ether-substituted nipecotic acids. *Eur. J. Med. Chem.* **2004**, *39*, 633−638.
(28) N'Goka, V.; Stenbøl, T. B.; Krogsgaard-Larsen, P.; Schlewer, G. Synthesis and GABA uptake inhibitory properties of 6-aryl iminoxymethyl substituted nipecotic acids. *Eur. J. Med. Chem.* **2004**, *39*, 889−895.
(29) Hellenbrand, T.; Höfner, G.; Wein, T.; Wanner, K. T. Synthesis of 4-substituted nipecotic acid derivatives and their evaluation as potential GABA uptake inhibitors. *Bioorg. Med. Chem.* **2016**, *24*, 2072−2096.
(30) Yamashita, A.; Singh, S. K.; Kawate, T.; Jin, Y.; Gouaux, E. Crystal structure of a bacterial homologue of Na^+/Cl^--dependent neurotransmitter transporters. *Nature* **2005**, *437*, 215−223.
(31) Palló, A.; Bencsura, Á.; Héja, L.; Beke, T.; Perczel, A.; Kardos, J.; Simon, Á. Major human γ-aminobutyrate transporter: in silico prediction of substrate efficacy. *Biochem. Biophys. Res. Commun.* **2007**, *364*, 952−958.
(32) Wein, T.; Wanner, K. T. Generation of a 3D model for human GABA transporter hGAT-1 using molecular modeling and investigation of the binding of GABA. *J. Mol. Model.* **2010**, *16*, 155−161.
(33) Skovstrup, S.; Taboureau, O.; Bräuner-Osborne, H.; Jørgensen, F. S. Homology modelling of the GABA transporter and analysis of tiagabine binding. *ChemMedChem* **2010**, *5*, 986−1000.
(34) Wein, T.; Petrera, M.; Allmendinger, L.; Höfner, G.; Pabel, J.; Wanner, K. T. Different binding modes of small and large binders of GAT1. *ChemMedChem* **2016**, *11*, 509−518.
(35) Sindelar, M.; Wanner, K. T. Library screening by means of MS Binding Assays − exemplarily demonstrated for a pseudo-static library addressing GAT1. *ChemMedChem* **2012**, *7*, 1678−1690.
(36) Höfner, G.; Wanner, K. T. Competitive Binding Assays made easy with a native marker and mass spectrometric quantification. *Angew. Chem., Int. Ed.* **2003**, *42*, 5235−5237.
(37) Höfner, G.; Zepperitz, C.; Wanner, K. T. MS Binding Assays−An Alternative to Radioligand Binding. In *Mass Spectrometry in Medicinal Chemistry: Applications in Drug Discovery*, 1st ed.; Höfner, G., Wanner, K. T., Eds.; Wiley-VCH: Weinheim, 2007; pp 247−283.
(38) Zepperitz, C.; Höfner, G.; Wanner, K. T. MS-Binding Assays: kinetic, saturation and competitive experiments based on quantitation of bound marker − exemplified by the GABA transporter mGAT1. *ChemMedChem* **2006**, *1*, 208−217.
(39) Petrera, M.; Wein, T.; Allmendinger, L.; Sindelar, M.; Pabel, J.; Höfner, G.; Wanner, K. T. Development of highly potent GAT1 inhibitors: synthesis of nipecotic acid derivatives by Suzuki-Miyaura cross-coupling reactions. *ChemMedChem* **2016**, *11*, 519−538.
(40) Lutz, T.; Wein, T.; Höfner, G.; Wanner, K. T. Development of highly potent GAT1 inhibitors: synthesis of nipecotic acid derivatives with *N*-arylalkynyl substituents. *ChemMedChem* **2017**, *12*, 362−371.
(41) A synthesis of *rac*-**23** excluding analytical data is described in: Binch, H.; Hashimoto, M.; Mortimore, M.; Ohkubo, M.; Sunami, T. Novel Aminopyridine Derivatives Having Aurora Selective Inhibitory Action. US Patent US 2012/0015969 A1, Jan 1, 2012.
(42) A synthesis of **25** excluding analytical data is described in: Durón, S.; Campbell, D.; Ndubaku, C.; Rudolph, J. Serine/Threonine Kinase Inhibitors. US Patent 2014/0323478 A1, Oct 30, 2014.
(43) Smith, A. B.; Kim, D.-S. A general, convergent strategy for the construction of indolizidine alkaloids: total syntheses of (−)-indolizidine 223AB and alkaloid (−)-205B. *J. Org. Chem.* **2006**, *71*, 2547−2557.
(44) For chiral pool syntheses of enantiopure (3*S*,5*R*)-**20** (excluding analytical data) and enantiopure (3*S*,5*R*)-**27** (including analytical data), see: Mori, Y.; Iwamoto, M.; Mori, K.; Yoshida, M.; Honda, T.; Nagayama, T.; Nishi, T. An efficient synthesis of (3*S*,5*S*)-5-[3,3-dimethyl-1-(*o*-tolyl)-6-oxo-2*H*-pyridin-4-yl]piperidine-3-carboxamide as potent renin inhibitor. *Heterocycles* **2014**, *89*, 1413−1426.
(45) Brosse, N.; Pinto, M.-F.; Jamart-Grégoire, B. *N*-*tert*-Butoxycarbonylaminophthalimide, a versatile reagent for the conversion of alcohols into alkylated *tert*-butylcarbazates or hydrazines via the Mitsunobu protocol. *Tetrahedron Lett.* **2000**, *41*, 205−207.
(46) Brosse, N.; Pinto, M.-F.; Jamart-Grégoire, B. New synthesis of 1,1-substituted hydrazines by alkylation of *N*-acyl- or *N*-alkyloxycarbonylaminophthalimide using the Mitsunobu protocol. *J. Org. Chem.* **2000**, *65*, 4370−4374.
(47) Brosse, N.; Pinto, M.-F.; Jamart-Grégoire, B. Preparation of multiply protected alkylhydrazine derivatives by Mitsunobu and PTC approaches. *Eur. J. Org. Chem.* **2003**, *2003*, 4757−4764.

DOI: 10.1021/acs.jmedchem.8b01602
J. Med. Chem. 2018, 61, 10310−10332

(48) For asymmetric syntheses (including analytical data) of enantiopure (3*R*,5*R*)-**28** and enantiopure (3*S*,5*S*)-**28**, see: Iding, H.; Wirz, B.; Rodríguez Sarmiento, R.-M. Chemoenzymatic preparation of non-racemic *N*-Boc-piperidine-3,5-dicarboxylic acid 3-methyl esters and their 5-hydroxylmethyl derivatives. *Tetrahedron: Asymmetry* **2003**, *14*, 1541−1545.

(49) General note on hydrazine stability: The hydrazines *rac*-**11**−*rac*-**14** were prone for degradation, presumably to give corresponding hydrocarbons analogous to the observations in: Hoffman, R. V.; Kumar, A. Oxidation of hydrazine derivatives with arylsulfonyl peroxides *J. Org. Chem.* **1984**, *49*, 4014−4017. The hydrazines were thus isolated and used in further experiments as their more stable hydrochlorides. As shown by elemental analysis, all hydrazines were obtained with 3 equiv of HCl and 1 equiv of H_2O with exception of hydrazine *rac*-**11**, which had 2 equiv HCl and 1 H_2O. We performed control experiments in order to demonstrate that neither the use as hydrochloride nor the low hydrazine stability itself would affect the outcome of the screening experiments (data not shown). The buffer capacity in the bioassays was high enough to neutralize the HCl without affecting the pH. To guarantee hydrazine and hydrazone stability throughout the screening experiments the antioxidant sodium L-ascorbate (200 μM) was added to the incubation buffer.

(50) Fujimoto, T.; Imaeda, Y.; Konishi, N.; Hiroe, K.; Kawamura, M.; Textor, G. P.; Aertgeerts, K.; Kubo, K. Discovery of a tetrahydropyrimidin-2(1*H*)-one derivative (TAK-442) as a potent, selective, and orally active factor Xa inhibitor. *J. Med. Chem.* **2010**, *53*, 3517−3531.

(51) Sindelar, M.; Lutz, T. A.; Petrera, M.; Wanner, K. T. Focused pseudostatic hydrazone libraries screened by mass spectrometry Binding Assay: optimizing affinities toward γ-aminobutyric acid transporter 1. *J. Med. Chem.* **2013**, *56*, 1323−1340.

(52) Kern, F. T.; Wanner, K. T. Generation and screening of oxime libraries addressing the neuronal GABA transporter GAT1. *ChemMedChem* **2015**, *10*, 396−410.

(53) Irngartinger, H.; Escher, T. Strong electron acceptor properties of 3′-(pentafluorophenyl)isoxazolol[4′,5′:1,2][60]fullerene derivatives. *Tetrahedron* **1999**, *55*, 10753−10760.

(54) Likewise the hydrazines,[49] also the corresponding hydrazones (*rac*-**16**−*rac*-**19**) showed a low stability. The hydrazones were thus prepared in 10 mM solutions, in which they were directly used for full-scale competition experiments without additional drying or purification. The reactions were performed in deuterated solvents to demonstrate completeness of hydrazone formation by NMR and structures of the hydrazones in solution were confirmed by ^{1}H and ^{13}C NMR and HRMS prior to their use in the bioassays. Sodium deuteroxide was used to neutralize the hydrazine hydrochlorides and thus sodium chloride was obtained as side product (2 equiv NaCl for *rac*-**16** and 3 equiv NaCl for *rac*-**18**), which was not separated. We consider the presence of NaCl in the sample as negligible for the outcome of the bioassays; in the bioassays incubation buffers typically contain high salt concentrations and thus the additional, low-concentrated NaCl from the test substance is insignificant.

(55) Kragler, A.; Höfner, G.; Wanner, K. T. Synthesis and biological evaluation of aminomethylphenol derivatives as inhibitors of the murine GABA transporters mGAT1-GAT4. *Eur. J. Med. Chem.* **2008**, *43*, 2404−2411.

(56) Steffan, T.; Renukappa-Gutke, T.; Höfner, G.; Wanner, K. T. Design, synthesis and SAR studies of GABA uptake inhibitors derived from 2-substituted pyrrolidine-2-ylacetic acids. *Bioorg. Med. Chem.* **2015**, *23*, 1284−1306.

(57) Tsuruda, P. R.; Yung, J.; Martin, W. J.; Chang, R.; Mai, N.; Smith, J. A. M. Influence of ligand binding kinetics on functional inhibition of human recombinant serotonin and norepinephrine transporters. *J. Pharmacol. Toxicol. Methods* **2010**, *61*, 192−204.

(58) Hulme, E. C.; Trevethick, M. A. Ligand Binding Assays at equilibrium: validation and interpretation. *Br. J. Pharmacol.* **2010**, *161*, 1219−1237.

(59) Sarup, A.; Larsson, O. M.; Bolvig, T.; Frølund, B.; Krogsgaard-Larsen, P.; Schousboe, A. Effects of 3-hydroxy-4-amino-4,5,6,7-tetrahydro-1,2-benzisoxazol (*exo*-THPO) and its N-substituted analogs on GABA transport in cultured neurons and astrocytes and by the four cloned mouse GABA transporters. *Neurochem. Int.* **2003**, *43*, 445−451.

(60) Clausen, R. P.; Moltzen, E. K.; Perregaard, J.; Lenz, S. M.; Sanchez, C.; Falch, E.; Frølund, B.; Bolvig, T.; Sarup, A.; Larsson, O. M.; Schousboe, A.; Krogsgaard-Larsen, P. Selective inhibitors of GABA uptake: synthesis and molecular pharmacology of 4-*N*-methylamino-4,5,6,7-tetrahydrobenzo[*d*]isoxazol-3-ol analogues. *Bioorg. Med. Chem.* **2005**, *13*, 895−908.

(61) White, H. S.; Watson, W. P.; Hansen, S. L.; Slough, S.; Perregaard, J.; Sarup, A.; Bolvig, T.; Petersen, G.; Larsson, O. M.; Clausen, R. P.; Frølund, B.; Falch, E.; Krogsgaard-Larsen, P.; Schousboe, A. First demonstration of a functional role for central nervous system betaine/γ-aminobutyric acid transporter (mGAT2) based on synergistic anticonvulsant action among inhibitors of mGAT1 and mGAT2. *J. Pharmacol. Exp. Ther.* **2005**, *312*, 866−874.

(62) Timple, J. M. V.; Magalhães, L. G.; Souza Rezende, K. C.; Pereira, A. C.; Cunha, W. R.; Andrade e Silva, M. L.; Mortensen, O. V.; Fontana, A. C. K. The lignan (−)-hinokinin displays modulatory effects on human monoamine and GABA transporter activities. *J. Nat. Prod.* **2013**, *76*, 1889−1895.

(63) Christopoulos, A.; Changeux, J.-P.; Catterall, W. A.; Fabbro, D.; Burris, T. P.; Cidlowski, J. A.; Olsen, R. W.; Peters, J. A.; Neubig, R. R.; Pin, J.-P.; Sexton, P. M.; Kenakin, T. P.; Ehlert, F. J.; Spedding, M.; Langmead, C. J. International Union of Basic and Clinical Pharmacology. XC. multisite pharmacology: recommendations for the nomenclature of receptor allosterism and allosteric ligands. *Pharmacol. Rev.* **2014**, *66*, 918−947.

(64) Schmitt, S.; Höfner, G.; Wanner, K. T. MS Transport Assays for γ-aminobutyric acid transporters − an efficient alternative for radiometric assays. *Anal. Chem.* **2014**, *86*, 7575−7583.

(65) Schmitt, S.; Höfner, G.; Wanner, K. T. Application of MS Transport Assays to the four human γ-aminobutyric acid transporters. *ChemMedChem* **2015**, *10*, 1498−1510.

(66) Kragholm, B.; Kvist, T.; Madsen, K. K.; Jørgensen, L.; Vogensen, S. B.; Schousboe, A.; Clausen, R. P.; Jensen, A. A.; Bräuner-Osborne, H. Discovery of a subtype selective inhibitor of the human betaine/GABA transporter 1 (BGT-1) with a non-competitive pharmacological profile. *Biochem. Pharmacol.* **2013**, *86*, 521−528.

(67) Changeux, J.-P. The nicotinic acetylcholine receptor: a typical 'allosteric machine'. *Philos. Trans. R. Soc., B* **2018**, *373*, 20170174.

(68) Ballatore, C.; Huryn, D. M.; Smith, A. B., 3rd Carboxylic acid (bio)isosteres in drug design. *ChemMedChem* **2013**, *8*, 385−395.

(69) Lassalas, P.; Gay, B.; Lasfargeas, C.; James, M. J.; Tran, V.; Vijayendran, K. G.; Brunden, K. R.; Kozlowski, M. C.; Thomas, C. J.; Smith, A. B., 3rd; Huryn, D. M.; Ballatore, C. Structure property relationships of carboxylic acid isosteres. *J. Med. Chem.* **2016**, *59*, 3183−3203.

(70) *Anfärbereagenzien für Dünnschicht- und Papier-Chromatographie*; Merck: Darmstadt, 1970.

(71) Cushman, M.; Georg, G. I.; Holzgrabe, U.; Wang, S. Absolute quantitative ^{1}H NMR spectroscopy for compound purity determination. *J. Med. Chem.* **2014**, *57*, 9219.

(72) Pauli, G. F.; Chen, S. N.; Simmler, C.; Lankin, D. C.; Godecke, T.; Jaki, B. U.; Friesen, J. B.; McAlpine, J. B.; Napolitano, J. G. Importance of purity evaluation and the potential of quantitative ^{1}H NMR as a purity assay. *J. Med. Chem.* **2014**, *57*, 9220−9231.

(73) Aldrich, C.; Bertozzi, C.; Georg, G. I.; Kiessling, L.; Lindsley, C.; Liotta, D.; Merz, K.; Schepartz, A.; Wang, S. The ecstasy and agony of assay interference compounds. *J. Med. Chem.* **2017**, *60*, 2165−2168.

(74) Sterling, T.; Irwin, J. J. ZINC 15 − ligand discovery for everyone. *J. Chem. Inf. Model.* **2015**, *55*, 2324−2337.

(75) Peaks for the protons of OH and NH groups disappeared due to deuterium exchange. In the ^{1}H NMR spectra of compounds *rac*-**23**, *rac*-**27**, *rac*-**28**, *rac*-**32**, *rac*-**11**, *rac*-**12**, *rac*-**37**, (partly) *rac*-**38**, *rac*-**13**, *rac*-**14**, and all hydrazones *rac*-**16** or *rac*-**18** no corresponding signals were detectable.

(76) In addition to the signals listed ^{1}H NMR and ^{13}C NMR (and if applicable ^{19}F NMR) spectra showed signals of low intensity (3−17%) corresponding to the *Z*-isomer.

DOI: 10.1021/acs.jmedchem.8b01602
J. Med. Chem. 2018, 61, 10310−10332

(77) Zepperitz, C.; Höfner, G.; Wanner, K. T. Expanding the scope of MS Binding Assays to low-affinity markers as exemplified for mGAT1. *Anal. Bioanal. Chem.* **2008**, *391*, 309−316.
(78) Cheng, Y. C.; Prussoff, W. H. Relationship between the inhibition constant (K_i) and the concentration of inhibitor which causes 50% inhibition (IC_{50}) of an enzymatic reaction. *Biochem. Pharmacol.* **1973**, *22*, 3099−3108.

DOI: 10.1021/acs.jmedchem.8b01602
J. Med. Chem. 2018, 61, 10310−10332

Supporting Information.

Novel allosteric ligands of γ-aminobutyric acid transporter 1 (GAT1) by MS based screening of pseudostatic hydrazone libraries

*Tobias J. Hauke, Thomas Wein, Georg Höfner, Klaus T. Wanner**

Department of Pharmacy – Center of Drug Research, Ludwig-Maximilians-Universität München, Butenandtstrasse 5–13, 81377 Munich, Germany

Content:

1. Synthesis of aldehydes 15fd, 15ff, 15fh, 15fi, 15fn, 15fp, 15fs and 15gr

A. General procedure (GP) for the preparation of aldehydes 15fd, 15ff, 15fh, 15fi, 15fn, 15fp, 15fs and 15gr in a Suzuki-Miyaura reaction[1,2]

A mixture of toluene, ethanol and 2 M aqueous Na_2CO_3 (1:1:1, v/v/v, 12–15 mL) was flushed with Ar for 10 min. The desired bromoaryl aldehyde (1.0 equivalent), the boronic acid (1.0–1.2 equivalents) and the catalyst $Pd(PPh_3)_4$ (0.05 equivalents) were added and the mixture was heated to 80 °C. The reaction progress was monitored by TLC. After completion, the reaction mixture was cooled to rt, diluted with 10 mL H_2O and extracted with toluene or ethyl acetate (3 x 10 mL). The combined organic phases were dried over Na_2SO_4 or $MgSO_4$ and the solvent was removed in vacuum. The crude product was purified by flash flash chromatography on silica gel.

B. Detailed analytical data of aldehydes

4,5-Dichloro-2-phenylbenzaldehyde (15fd): According to **GP** from 2-bromo-4,5-dichlorobenzaldehyde (223 mg, 0.878 mmol), phenylboronic acid (132 mg, 1.05 mmol) and $Pd(PPh_3)_4$ (51 mg, 0.044 mmol). 16 h at 80 °C. After purification by flash chromatography (*iso*-hexanes/EtOAc = 98:2) **15fd** was obtained as white solid (150 mg; 60%). Mp 71 °C. ^{1}H NMR (400 MHz, $CDCl_3$, 25 °C): δ 7.39–7.33 (m, 2H), 7.43–7.54 (m, 3H), 7.57 (s, 1H), 8.09 (s, 1H), 9.87 (s, 1H) ppm. ^{13}C NMR (101 MHz, $CDCl_3$, 25 °C): δ 128.8, 128.9, 129.4, 129.9, 130.0, 132.6, 132.9, 135.4, 138.0, 145.0, 190.1 ppm. IR (KBr): $\tilde{\nu}$ 3061, 3031, 2876, 2763, 1693, 1585 cm^{-1}. HRMS (EI, 70 eV): M^+ calcd. for $C_{13}H_8Cl_2O$, 249.9952; found, 249.9942. Purity (qNMR: $CDCl_3$, 25 °C, dimethyl sulfone; m_S = 5.219 mg, m_{IC} = 6.034 mg): 96%.

2-(2-Fluoropyridin-3-yl)benzaldehyde (15ff): According to **GP** from 2-bromobenzaldehyde (159 mg, 0.842 mmol), (2-fluoropyridin-3-yl)boronic acid (121 mg, 0.859 mmol) and $Pd(PPh_3)_4$ (49 mg, 0.043 mmol). 3 h at 80 °C. After purification by flash chromatography (*n*-pentane/Et_2O = 1:1) **15ff** was obtained as orange solid (136 mg; 79%). Mp 84 °C. ^{1}H NMR (500 MHz, CD_2Cl_2, 25 °C): δ 7.35 (ddd, J = 7.0/4.9/1.9 Hz, 1 H), 7.41 (d, J = 7.6 Hz, 1 H), 7.62 (t, J = 7.6 Hz, 1 H), 7.72 (td, J = 7.6/1.5 Hz, 1 H), 7.79 (ddd, J = 9.5/7.3/2.0 Hz, 1 H), 8.01 (dd, J = 7.8/1.5 Hz, 1 H), 8.29 (ddd, J = 4.9/1.7/1.2 Hz, 1 H), 9.93 (d, J = 1.8 Hz, 1 H) ppm. ^{13}C NMR (126 MHz, CD_2Cl_2, 25 °C): δ 121.5 (d, J_{CF} = 31.6 Hz), 122.1 (d, J_{CF} = 4.4 Hz), 129.6, 130.0, 131.9, 134.3, 134.4, 136.7 (d, J_{CF} = 3.7 Hz), 142.4 (d, J_{CF} = 4.1 Hz), 148.0 (d, J_{CF} = 14.6 Hz), 160.7 (d, J_{CF} = 236.8 Hz), 191.3 (d, J_{CF} = 1.4 Hz) ppm. ^{19}F {^{1}H} NMR (376 MHz, CD_2Cl_2, 25 °C): δ -70.4 ppm. IR (KBr): $\tilde{\nu}$ 3076, 2929, 2867, 2752, 1684, 1630, 1593 cm^{-1}. HRMS (EI, 70 eV): M^+ calcd. for $C_{12}H_8FNO$, 201.0590; found, 201.0599. Purity (qNMR: $CDCl_3$, 25 °C, dimethyl sulfone; m_S = 5.576 mg, m_{IC} = 5.462 mg): 97%.

2-(6-Fluoropyridin-3-yl)benzaldehyde (15fh): According to **GP** from 2-bromobenzaldehyde (159 mg, 0.842 mmol), (6-fluoropyridin-3-yl)boronic acid (121 mg, 0.859 mmol) and $Pd(PPh_3)_4$ (53 mg, 0.045 mmol). 2 h at 80 °C. After purification by flash chromatography (*iso*-hexanes/EtOAc = 4:1) **15fh** was obtained as yellow solid (134 mg; 78%). Mp 59 °C. ^{1}H NMR (400 MHz, CD_2Cl_2, 25 °C): δ 7.07 (ddd, J = 8.4/3.0/0.7 Hz, 1 H), 7.43 (ddd, J = 7.7/1.2/0.5 Hz, 1 H), 7.56–7.64 (m, 1 H), 7.71 (td, J = 7.5/1.5 Hz, 1 H), 7.84 (ddd, J = 8.4/7.6/2.6 Hz, 1 H), 8.03 (ddd, J = 7.8/1.5/0.4 Hz, 1 H), 8.23 (dt, J = 2.5/0.8 Hz, 1 H), 9.97 (d, J = 0.6 Hz, 1 H) ppm. ^{13}C NMR (101 MHz, CD_2Cl_2, 25 °C): δ 109.5 (d, J_{CF} = 38.0 Hz), 129.2, 129.2, 131.6, 132.4 (d, J_{CF} = 4.5 Hz), 134.3, 134.4, 140.8 (d, J_{CF} = 1.1 Hz), 142.8 (d, J_{CF} = 8.2 Hz), 148.3 (d, J_{CF} = 15.3 Hz), 163.8 (d, J_{CF} = 239.3 Hz), 191.4 ppm. ^{19}F {^{1}H} NMR (376 MHz, CD_2Cl_2, 25 °C): δ -70.0 ppm. IR

(KBr): $\tilde{\nu}$ 3065, 2864, 2783, 1693, 1597 cm^{-1}. HRMS (EI, 70 eV): M^+ calcd. for $C_{12}H_8FNO$, 201.0590; found, 201.0578. Purity (qNMR: $CDCl_3$, 25 °C, dimethyl sulfone; m_S = 5.050 mg, m_{IC} = 5.173 mg): 96%.

2-(2-Methoxypyridin-3-yl)benzaldehyde (15fi): According to **GP** from 2-bromobenzaldehyde (159 mg, 0.842 mmol), (2-methoxypyridin-3-yl)boronic acid (131 mg, 0.856 mmol) and $Pd(PPh_3)_4$ (52 mg, 0.045 mmol). 4 h at 80 °C. After purification by flash chromatography (*iso*-hexanes/EtOAc = 4:1) **15fi** was obtained as yellow solid (156 mg; 85%). Mp 103 °C. ^{1}H NMR (400 MHz, CD_2Cl_2, 25 °C): δ 3.86 (s, 3 H), 7.04 (dd, *J* = 7.2/5.0 Hz, 1 H), 7.35 (ddd, *J* = 7.6/1.3/0.6 Hz, 1 H), 7.49–7.55 (m, 1 H), 7.59 (dd, *J* = 7.2/1.9 Hz, 1 H), 7.67 (td, *J* = 7.5/1.5 Hz, 1 H), 7.96 (ddd, *J* = 7.7/1.4/0.4 Hz, 1 H), 8.24 (dd, *J* = 5.0/1.9 Hz, 1 H), 9.80 (d, *J* = 0.8 Hz, 1 H) ppm. ^{13}C NMR (101 MHz, CD_2Cl_2, 25 °C): δ 53.8, 117.5, 121.7, 127.7, 128.7, 131.7, 134.1, 134.5, 140.0, 140.3, 147.6, 161.4, 191.8 ppm. IR (KBr): $\tilde{\nu}$ 3060, 3019, 2980, 2947, 2869, 2758, 1687, 1595 cm^{-1}. HRMS (EI, 70 eV): M^+ calcd. for $C_{13}H_{11}NO_2$, 213.0790; found, 213.0785. Purity (qNMR: $CDCl_3$, 25 °C, dimethyl sulfone; m_S = 5.359 mg, m_{IC} = 5.350 mg): ≥ 99%

2-(2-Methoxypyrimidin-5-yl)benzaldehyde (15fn): According to **GP** from 2-bromobenzaldehyde (159 mg, 0.842 mmol), (2-methoxypyrimidin-5-yl)boronic acid (132 mg, 0.859 mmol) and $Pd(PPh_3)_4$ (50 mg, 0.043 mmol). 6.5 h at 80 °C. After purification by flash chromatography (*n*-pentane/Et_2O = 1:1) **15fn** was obtained as yellow solid (143 mg; 78%). Mp 78 °C. ^{1}H NMR (500 MHz, CD_2Cl_2, 25 °C): δ 4.06 (s, 3 H), 7.41 (dd, *J* = 7.6/1.2 Hz, 1 H), 7.61 (tdd, *J* = 8.1/1.1/0.7 Hz, 1 H), 7.72 (td, *J* = 7.6/1.5 Hz, 1 H), 8.03 (dd, *J* = 7.8/1.4 Hz, 1 H), 8.54 (s, 2 H), 10.01 (d, *J* = 0.6 Hz, 1 H) ppm. ^{13}C NMR (126 MHz, CD_2Cl_2, 25 °C): δ 55.5, 126.0, 129.3, 130.1, 131.7, 134.3, 134.4, 138.3, 159.6, 159.6, 165.8, 191.3 ppm. IR (KBr): $\tilde{\nu}$ 3060, 3031, 3000, 2954, 2884, 2770, 1690, 1593, 1545 cm^{-1}. HRMS (EI, 70 eV): M^+ calcd. for $C_{12}H_{10}N_2O_2$, 214.0742; found, 214.0728. Purity (qNMR: $CDCl_3$, 25 °C, dimethyl sulfone; m_S = 7.818 mg, m_{IC} = 5.478 mg): 98%.

2-(2,4-Dimethoxypyrimidin-5-yl)benzaldehyde (15fp): According to **GP** from 2-bromobenzaldehyde (159 mg, 0.842 mmol), (2,4-dimethoxypyrimidin-5-yl)boronic acid (158 mg, 0.860 mmol) and $Pd(PPh_3)_4$ (50 mg, 0.043 mmol). 4 h at 80 °C. After purification by flash chromatography (*n*-pentane/Et_2O = 1:1) **15fp** was obtained as white solid (124 mg; 59%). Mp 131 °C. ^{1}H NMR (500 MHz, CD_2Cl_2, 25 °C): δ 3.92 (s, 3 H), 4.03 (s, 3 H), 7.34 (ddd, *J* = 7.6/1.2/0.5 Hz, 1 H), 7.55 (tdd, *J* = 7.6/1.1/0.7 Hz, 1 H), 7.67 (td, *J* = 7.5/1.4 Hz, 1 H), 7.96 (dd, *J* = 7.7/1.4 Hz, 1 H), 8.19 (s, 1 H), 9.85 (d, *J* = 0.6 Hz, 1 H) ppm. ^{13}C NMR (126 MHz, CD_2Cl_2, 25 °C): δ 54.5, 55.3, 113.5, 128.8, 129.0, 131.9, 134.3, 134.8, 136.6, 158.8, 166, 168.8, 191.5 ppm. IR (KBr): $\tilde{\nu}$ 3025, 2994, 2957, 2871, 2770, 1693, 1597, 1574, 1554 cm^{-1}. HRMS (EI, 70 eV): M^+ calcd. for $C_{13}H_{12}N_2O_3$, 244.0848; found, 244.0835. Purity (qNMR: $CDCl_3$, 25 °C, dimethyl sulfone; m_S = 5.882 mg, m_{IC} = 5.196 mg): 98%.

2-(2,3-Dihydro-1,4-benzodioxin-6-yl)benzaldehyde (15fs): According to **GP** from 2-bromobenzaldehyde (159 mg, 0.834 mmol), (2,3-dihydro-1,4-benzodioxin-6-yl)boronic acid (150 mg, 0.834 mmol) and $Pd(PPh_3)_4$ (48 mg, 0.042 mmol). 4 h at 80 °C. After purification by flash chromatography (*n*-pentane/Et_2O = 2:1) **15fs** was obtained as colorless oil (194 mg; 97%). ^{1}H NMR (500 MHz, $CDCl_3$, 25 °C): δ 4.32 (s, 4 H), 6.83 (dd, *J* = 8.2/2.1 Hz, 1 H), 6.91 (d, *J* = 2.1 Hz, 1 H), 6.95 (d, *J* = 8.2 Hz, 1 H), 7.42 (dd, *J* = 7.6/1.1 Hz, 1 H), 7.44–7.48 (m, 1 H), 7.61 (td, *J* = 7.6/1.4 Hz, 1 H), 7.99 (dd, *J* = 7.8/1.4 Hz, 1 H), 10.02 (d, *J* = 0.8 Hz, 1 H) ppm. ^{13}C NMR (126 MHz, $CDCl_3$, 25 °C): δ 64.4, 64.5, 117.2, 118.9, 123.5, 127.5, 127.5, 130.7, 131.0, 133.5, 133.7, 143.4, 143.8, 145.4, 192.6 ppm. IR (KBr): $\tilde{\nu}$ 3059, 2878, 2751, 1690, 1509 cm^{-1}. HRMS (EI, 70

eV): M^+ calcd. for $C_{15}H_{12}O_3$, 240.0787; found, 240.0788. Purity (qNMR: $CDCl_3$, 25 °C, dimethyl sulfone; m_S = 5.715 mg, m_{IC} = 10.646 mg): 98%.

2-(2-Aminopyrimidin-5-yl)benzaldehyde (15gr): According to **GP** from 2-bromobenzaldehyde (159 mg, 0.842 mmol), (2-aminopyrimidin-5-yl)boronic acid (116 mg, 0.834 mmol) and $Pd(PPh_3)_4$ (48 mg, 0.042 mmol). 5 h at 80 °C. After purification by flash chromatography (*n*-pentane/Et_2O = 1:1 + 5% NEt_3) **15gr** was obtained as white solid (127 mg; 77%). Mp 152 °C. ^{1}H NMR (400 MHz, DMSO-d_6, 25 °C): δ 6.92 (br s, 2 H), 7.51 (dd, J = 7.7/0.8 Hz, 1 H), 7.54–7.60 (m, 1 H), 7.74 (td, J = 7.5/1.5 Hz, 1 H), 7.93 (dd, J = 7.8/1.2 Hz, 1 H), 8.33 (s, 2 H), 9.96 (d, J = 0.6 Hz, 1 H) ppm. ^{13}C NMR (101 MHz, DMSO-d_6, 25 °C): δ 119.5, 127.8, 128.7, 130.8, 133.0, 134.0, 139.1, 158.1, 162.9, 191.6 ppm. IR (KBr): $\tilde{\nu}$ 3374, 3175, 2848, 2722, 1681, 1595 cm^{-1}. HRMS (EI, 70 eV): M^+ calcd. for $C_{11}H_9N_3O$, 199.0747; found, 199.0749. Purity (qNMR: DMSO-d_6, 25 °C, dimethyl sulfone; m_S = 4.610 mg, m_{IC} = 11.821 mg): 95%.

2. Monitoring of reaction progress

Control experiments in the absence of the target were performed to verify that the formation of hydrazones *rac*-**16**–*rac*-**19** from hydrazines *rac*-**11**–*rac*-**14** and appropriate aldehydes **15** basically proceeds in the same time and to the same extent as evaluated previously.[3] Therefore, both NMR and UV experiments were utilized for monitoring the reaction progress. The latter has the advantage that it is sensitive enough to apply concentrations as it is desired in the actual generation and screening of the hydrazone libraries in presence of the target. Herein, the UV-monitored formations of hydrazones *rac*-**16s** and *rac*-**16w** from hydrazine *rac*-**11** and aldehydes **15s** and **15w**, respectively, are exemplarily shown. Aldehydes **15s** and **15w** were already included in the previous approach[3] due to their electronic and UV characteristics and were thus chosen herein for comparing the reaction progresses in the previous[3] and the present approach. Aldehyde **15s** is a fast to average reacting aldehyde and hydrazone formation was completed within 2 h of reaction time. In contrast, **15w** is an extraordinarily slow reacting aldehyde and near complete hydrazone formation required slightly more than 4 h. The times needed for the conversions of aldehydes **15s** and **15w** are in line with the observations in Sindelar and Wanner[3] after the concentrations of the hydrazines and aldehydes were modified accordingly (the hydrazine concentration was doubled as with the initial 100 µM concentration the reactions did not reach the plateaus within the given time). Hence, it was concluded that under these conditions (including 200 µM hydrazine concentration and 8 µM total aldehyde concentration) an incubation period of 4 h is still appropriate for the generation of the libraries in the final experiments (i.e. during the screening experiments in the presence of the target).

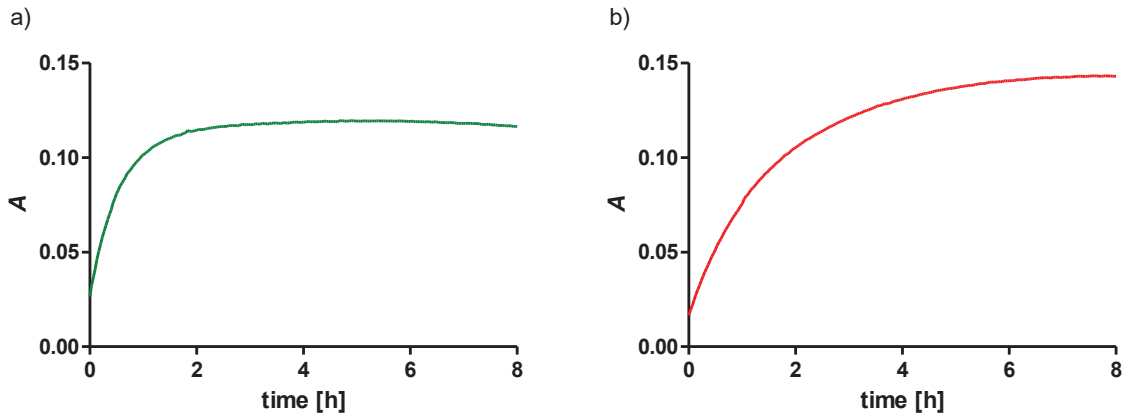

Figure S1. Absorbance (*A*) versus time for the reaction of hydrazine *rac*-**11** (200 µM; applied as the corresponding hydrochloride) with aldehydes a) **15s** and b) **15w** (each 8 µM) in incubation puffer at pH = 7.1 and 37 °C. Reactions were monitored by UV: ε_{356nm} *rac*-**11**: 45 $L \cdot mol^{-1} \cdot cm^{-1}$, ε_{356nm} **15s**: 875 $L \cdot mol^{-1} \cdot cm^{-1}$, ε_{356nm} **15w**: 250 $L \cdot mol^{-1} \cdot cm^{-1}$, ε_{356nm} *rac*-**16s**: 9675 $L \cdot mol^{-1} \cdot cm^{-1}$, ε_{356nm} *rac*-**16w**: 12175 $L \cdot mol^{-1} \cdot cm^{-1}$.

The experimental conditions were identical to the ones previously described[3] apart from the following adaptions: The reactions were performed in quartz glass cuvettes (3.5 mL; Hellma) in a total volume of 3.0 mL. Sodium L-ascorbate (200 µM) was added to the incubation buffer and the concentrations of the hydrazines and aldehydes were modified as described above.

3. Control experiments for library screening with individual building blocks

Control experiments with hydrazines *rac*-**11**–*rac*-**14** and the 28 libraries of aldehydes **15a**–**15hp** were performed in order to demonstrate that none of the single building blocks required for the generation of the hydrazone libraries (*rac*-**16**–*rac*-**19**) alone affected the remaining binding of MS marker **6** in the applied concentrations to a remarkable extent.

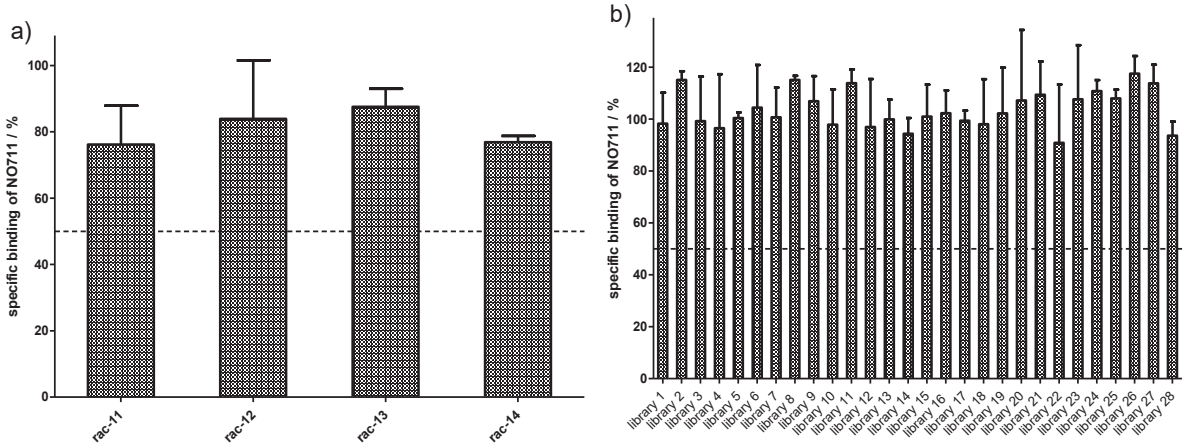

Figure S2. Screening of a) hydrazines *rac*-**11**–*rac*-**14** (each 200 µM; applied as their corresponding hydrochlorides) and b) libraries 1–28 of aldehydes **15a**–**15hp** (each library containing eight aldehydes in a concentration of 1 µM). The bars indicate the percentage of remaining specific binding of NO711 (**6**) after an incubation time of 4 h and additionally 40 min for marker binding to mGAT1; data represent means±SD of four replicates. The "activity criterion" was defined as 50% remaining marker binding (indicated by the dashed line).

The experimental conditions were identical to the conditions applied for the generation and screening with the exception that only one of the two building blocks required for hydrazone formation was applied. None of the individually applied building blocks reduced remaining marker binding below 50% or even close to this value that was set as the limit for further analysis.

4. Control experiments for hydrazone stability in incubation buffers

One potential explanation for the observed discrepancies in binding affinities (pK_i values) and inhibition of GABA uptake (pIC_{50} values) could involve a higher lability of the hydrazones in the incubation buffer used for uptake experiments than in the one used for MS Binding Assays. In the uptake assays "Krebs" buffer (containing salts, glucose and Tris; pH = 7.2)[4] was used and sodium L-ascorbate (200 µM; final concentration in the assay) was added to all samples, while in the binding experiments phosphate buffer containing sodium chloride and sodium L-ascorbate (pH = 7.1) was used. To demonstrate whether the used buffer has an influence on hydrazone stability the hydrazone stock solution (10 mM in DMSO-d_6/D_2O = 9:1) was diluted 1:10 in the corresponding buffer as for the sample preparation during the corresponding bio assays and the solution was monitored by ^{1}H NMR at 37 °C over 2.5 h. For these experiments *rac*-**16gg** was chosen as this hydrazone showed the highest difference between pK_i and pIC_{50} values. During the kinetic experiments no degradation of hydrazone *rac*-**16gg** could be observed and *rac*-**16gg** appeared stabile at 37 °C over the observation period (2.5 h). Thus, it was concluded that the used puffer system had no influence on the hydrazone stability.

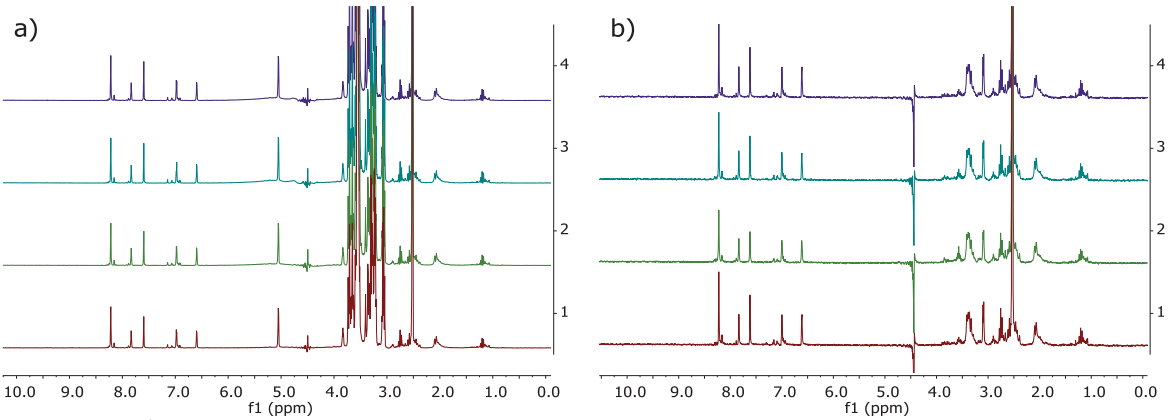

Figure S3. ^{1}H NMR spectra of hydrazone *rac*-**16gg** diluted 1:10 to 1 mM in a) "Krebs" puffer (pH = 7.2; and 2 mM sodium L-ascorbate were added) and b) phosphate buffer containing sodium chloride and sodium L-ascorbate (pH = 7.1). The spectra were recorded 5 min (1), 30 min (2), 90 min (3) and 150 min (4) after sample preparation. The kinetic experiments were performed at 37 °C.

All NMR spectra were measured with an Avance III HD Bruker BioSpin (Bruker; 500 MHz). The respective water resonance was presaturated and spectra were recorded with 64 transients and a relaxation delay of 1 s. The first NMR spectrum was measured 5 min after sample preparation and a 5 min time increment was chosen for further measurements.[3]

Sample preparation in "Krebs" buffer. To 480 µL "Krebs" buffer (119 mM NaCl, 2.5 mM $CaCl_2$, 1.2 mM $MgSO_4$, 1.2 mM KH_2PO_4, 4.7 mM KCl, 11 mM glucose, 25 mM Tris; pH = 7.2)[4] 60 µL of a 20 mM solution of sodium L-ascorbate in H_2O and 60 µL of a 10 mM solution of *rac*-**16gg** in DMSO-d_6/D_2O (= 9:1) were added. The monitoring was started after the addition of the hydrazone.

Sample preparation in phosphate buffer. To 540 µL phosphate buffer containing sodium chloride and sodium L-ascorbate (1 M NaCl, 12.5 mM Na_2HPO_4, 12.5 mM NaH_2PO_4, 200 µM sodium L-ascorbate; pH = 7.1) 60 µL of a 10 mM solution of *rac*-**16gg** in DMSO-d_6/D_2O (= 9:1) was added. The monitoring was started after the addition of the hydrazone.

5. Control experiments for investigation of test compounds' mode of interaction

While the initial experiments (including the screening and deconvolution experiments as well as the hit verification and MS binding saturation experiments) were based on the murine GABA transporter mGAT1, the latter saturation experiments by means of MS Transport Assays[5,6] were based on the human equivalent hGAT1. In order to ensure that the results obtained with mGAT1 and hGAT1, respectively, are equivalent, binding affinities (pK_i values) from MS Binding Assays and inhibitory potencies (pIC_{50} values) from [^{3}H]GABA uptake assays were established for the six most potent hydrazones also utilizing HEK cells stably expressing hGAT1. The results obtained thereby are summarized in Table S1. Although individual values might differ slightly from those determined at mGAT1 (see Tables 2 and 3), they are generally in a similar order of magnitude. Accordingly, it was concluded that the results obtained at hGAT1 are comparable to those obtained at mGAT1.

Table S1. Binding affinities (pK_i) from MS Binding Assays and inhibitory potencies (pIC_{50}) from [^{3}H]GABA uptake experiments using HEK cells stably expressing hGAT1

entry	compd	pK_i (hGAT1)[a]	pIC_{50} (hGAT1)[b]
1	*rac*-**16e**	5.99±0.09	4.27±0.05
2	*rac*-**16ga**	6.07±0.03	4.09±0.03
3	*rac*-**16gf**	6.25±0.09	4.50±0.08
4	*rac*-**16gg**	6.22±0.03	4.15±0.08
5	*rac*-**18e**	5.91±0.06	4.44±0.05
6	*rac*-**18fy**	6.07±0.05	4.52±0.07
7	tiagabine (**5**)	7.51±0.16	6.42±0.01
8	NO711 (**6**)	-[c]	6.82±0.08

[a]Results of competitive MS Binding Assays performed with HEK cells stably expressing hGAT1; pK_i values are given as means±SEM of at least three independent experiments. [b]Results of [^{3}H]GABA uptake assays performed with HEK cells stably expressing hGAT1; pIC_{50} values are given as means±SEM of at least three independent experiments. [c]not determined.

The experimental conditions were exactly the same as described in the paper for the competitive MS Binding Assays and the [^{3}H]GABA uptake assays, respectively, except that HEK cells stably expressing the human transporter hGAT1 were utilized.

In order to support an allosteric mode of interaction and to rule out kinetic phenomena as explanation of the noncompetitive behavior observed during the saturation experiments, the inhibitory potencies (pIC_{50} values) for the six most potent hydrazones at hGAT1 were established by means of MS Transport Assays[5,6] whereupon the time periods chosen for the preincubation step (after adding the test compounds to the sample containing the hGAT1-COS cells) varied: Besides the usual 25 min preincubation time, the experiments were also performed without preincubation (0 min). The results obtained thereby are summarized in Table S2. There appears to be a tendency that the experimentally determined pIC_{50} values slightly increase with the duration of the preincubation. However, the observed differences are minor and not significant. Furthermore, this tendency was also observed for the reference compound NO711 (**6**), which was shown to exhibit the same competitive interaction mode as tiagabine (**5**). Accordingly, it was concluded that the noncompetitive behavior observed for the herein introduced hydrazones is not caused by very slow off-rates or even covalent binding.

Table S2. Comparison of inhibitory potencies (pIC_{50}) at hGAT1 from MS Transport Assays using different time periods for preincubation

		pIC_{50} (hGAT1)[a]	
entry	**Compd**	**0 min**	**25 min**
1	*rac*-**16e**	4.05±0.07	4.16±0.11
2	*rac*-**16ga**	3.93±0.18	4.18±0.23
3	*rac*-**16gf**	4.18±0.19	4.37±0.07
4	*rac*-**16gg**	4.17±0.25	3.87±0.03
5	*rac*-**18e**	3.77±0.13	4.20±0.14
6	*rac*-**18fy**	4.57±0.23	4.51±0.08
7	NO711 (**6**)	6.53±0.16	6.74±0.15

[a]Results of MS Transport Assays performed with COS cells stably expressing hGAT1 and different time periods for preincubation; pIC_{50} values are given as means±SEM of three independent experiments.

The experimental conditions were exactly the same as described in literature[5] (with the exception that 200 µM sodium L-ascorbate was additionally present in each sample for incubation as described in this paper) for the competitive MS Transport Assays except that after adding the test compounds to the samples besides the usual 25 min time period for preincubation also no preincubation (0 min) was utilized.

6. Settings of the API 3200 and API 3200 Q TRAP triple-quadrupole mass spectrometers

API 3200: Mass transitions (NO711: 351.1 → 180.1 *m/z*; d_{10}-NO711: 361.2 → 190.2 *m/z*); Q1 and Q3 were set to low resolution. Compound-dependent parameters: declustering potential 50 V (NO711) and 40 V (d_{10}-NO711), entrance potential 5 V (NO711 and d_{10}-NO711), collision energy 28 V (NO711 and d_{10}-NO711), collision cell exit potential 5 V (NO711 and d_{10}-NO711). Source-dependent parameters: source temperature 650 °C, ion-spray voltage 2000 V, curtain gas (N_2) 20 psi, auxiliary gas and nebulizing gas (N_2) 50 and 30 psi, respectively, collision gas (N_2) 3 psi.

API 3200 Q TRAP: Mass transitions (NO711: 351.2 → 180.2 *m/z*; d_{10}-NO711: 361.2 → 190.2 *m/z*); Q1 and Q3 were set to low resolution. Compound-dependent parameters: declustering potential 51 V (NO711 and d_{10}-NO711), entrance potential 6 V (NO711 and d_{10}-NO711), collision energy 25 V (NO711 and d_{10}-NO711), collision cell exit potential 4 V (NO711 and d_{10}-NO711). Source-dependent parameters: source temperature 700 °C, ion-spray voltage 2500 V, curtain gas (N_2) 20 psi, auxiliary gas and nebulizing gas (N_2) 40 and 60 psi, respectively, collision gas (N_2) 3 psi.

7. NMR spectra of compounds

1H NMR of rac-23 (400 MHz, tetrachlorethane-d2, 80 °C)

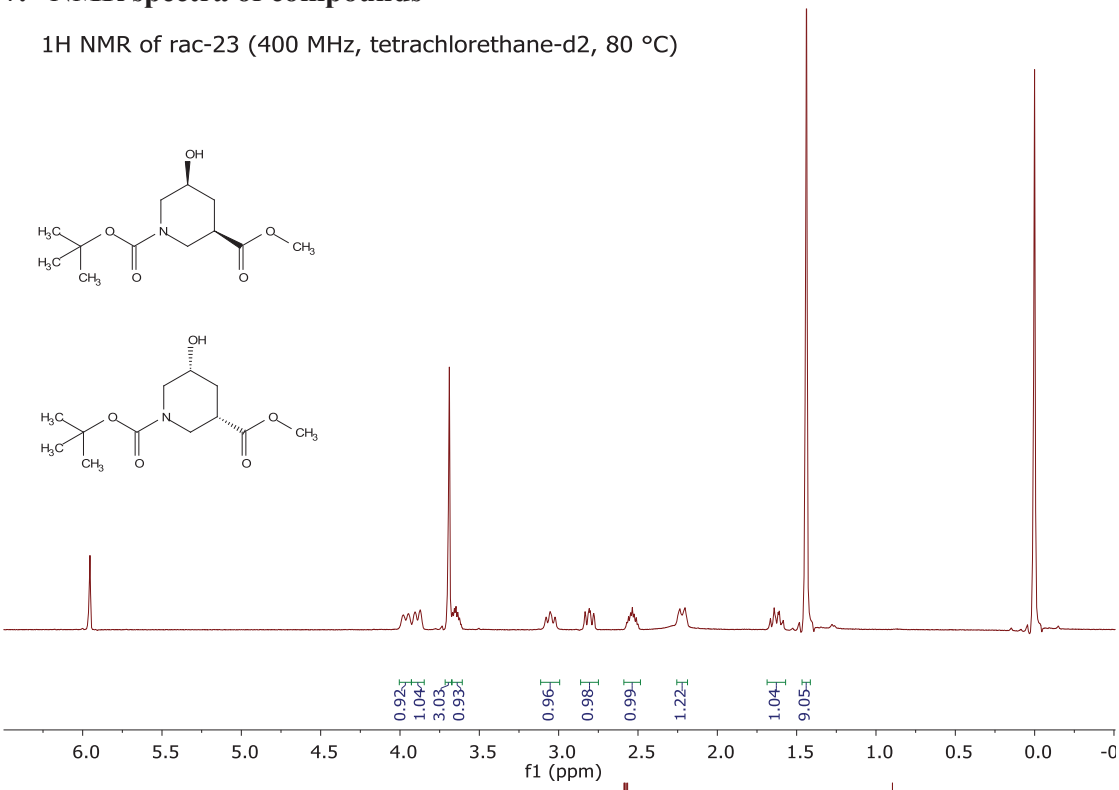

13C NMR of rac-23 (101 MHz, tetrachlorethane-d2, 80 °C)

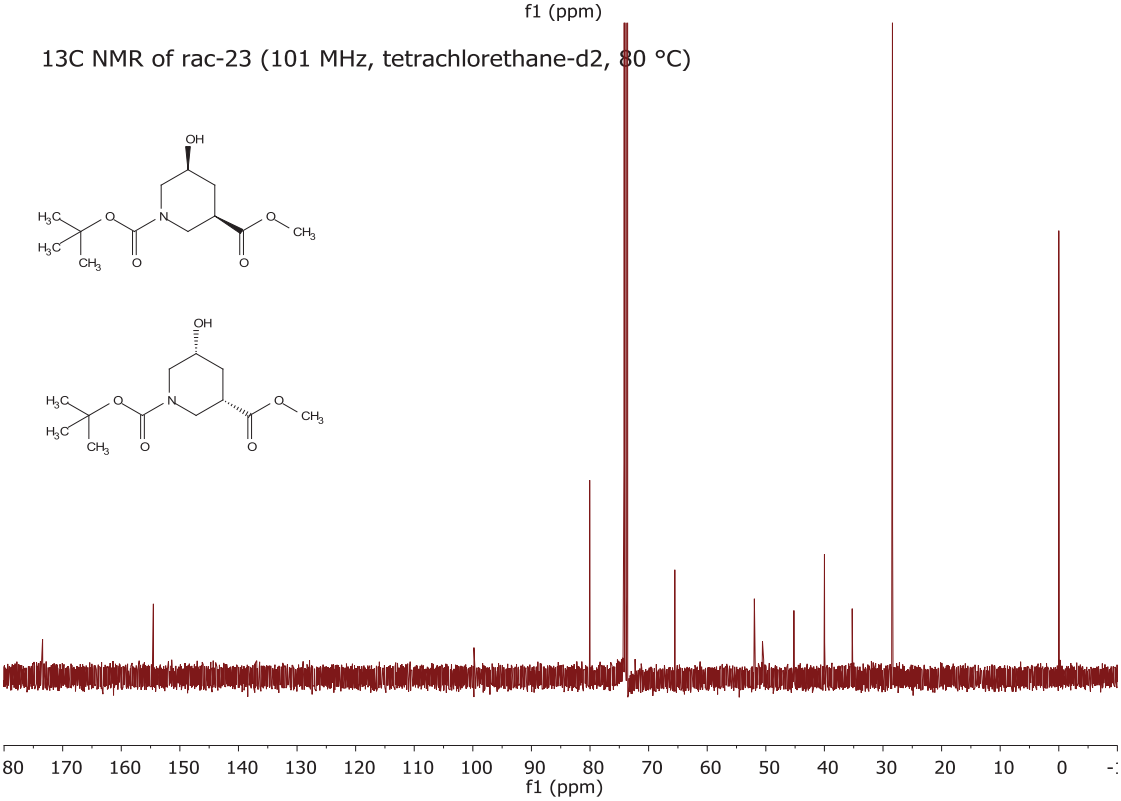

1H NMR of rac-24 (400 MHz, tetrachlorethane-d2, 80 °C)

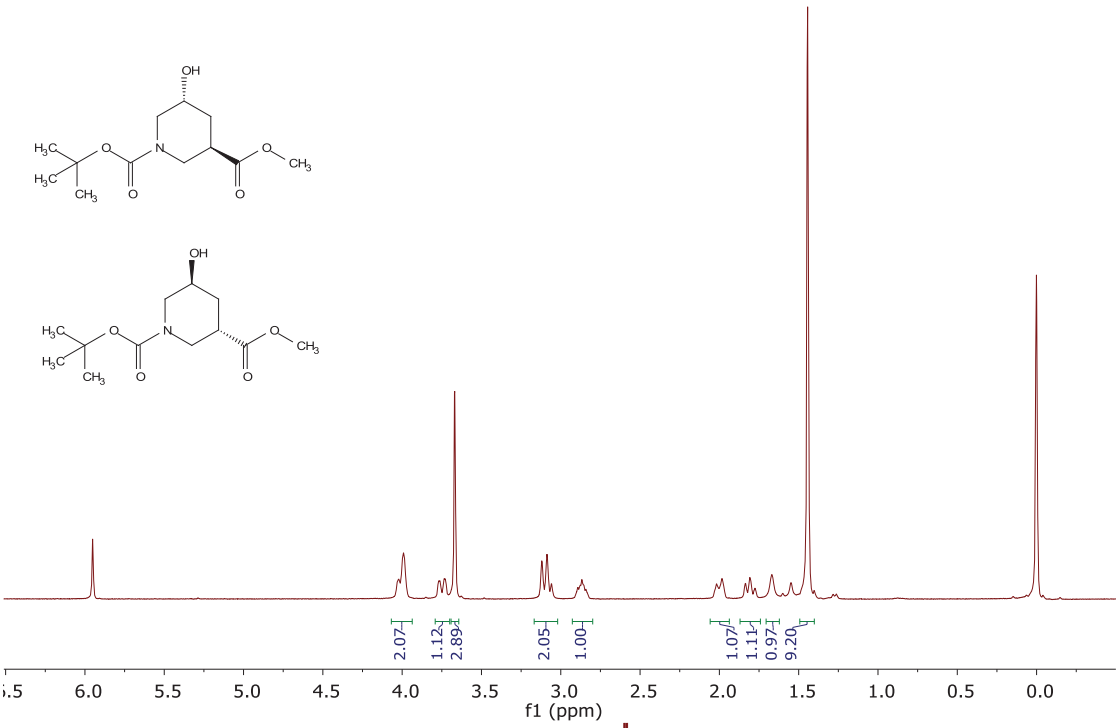

13C NMR of rac-24 (101 MHz, tetrachlorethane-d2, 80 °C)

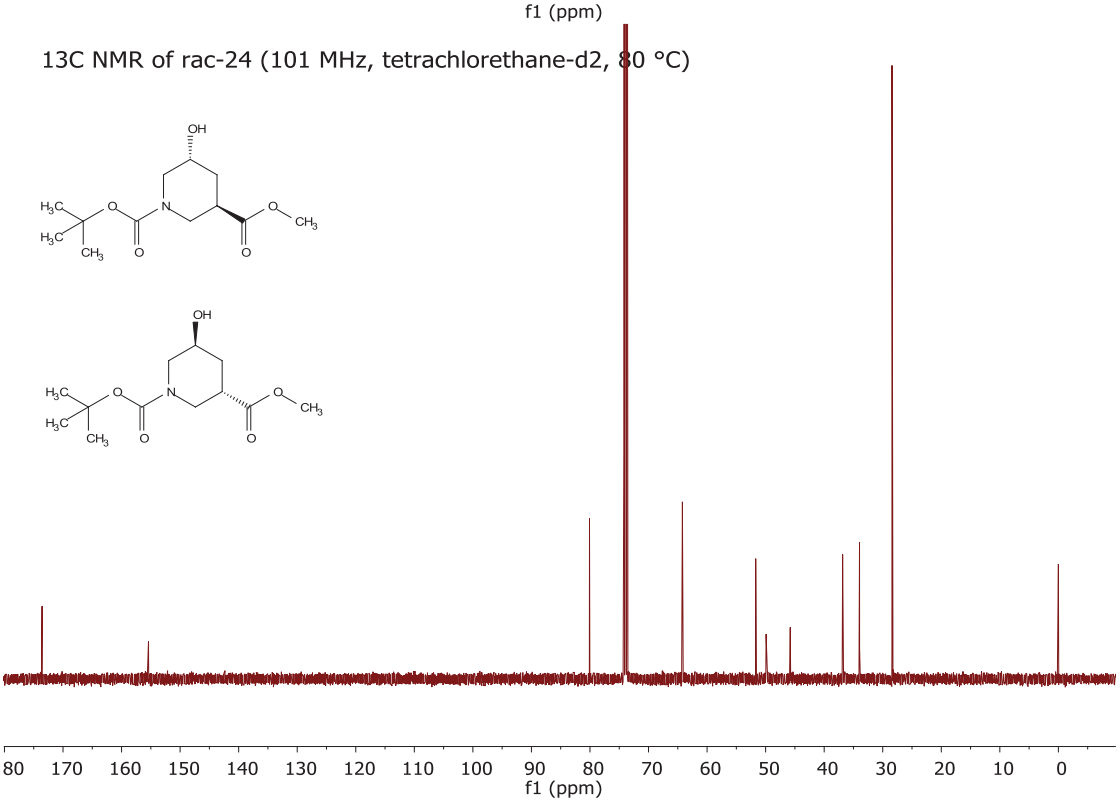

1H NMR of 25 (400 MHz, tetrachlorethane-d2, 80 °C)

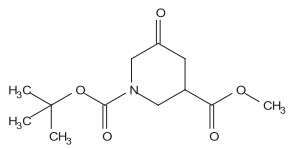

13C NMR of 25 (101 MHz, tetrachlorethane-d2, 80 °C)

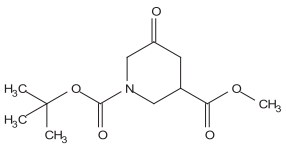

1H NMR of 26 (400 MHz, tetrachlorethane-d2, 80 °C)

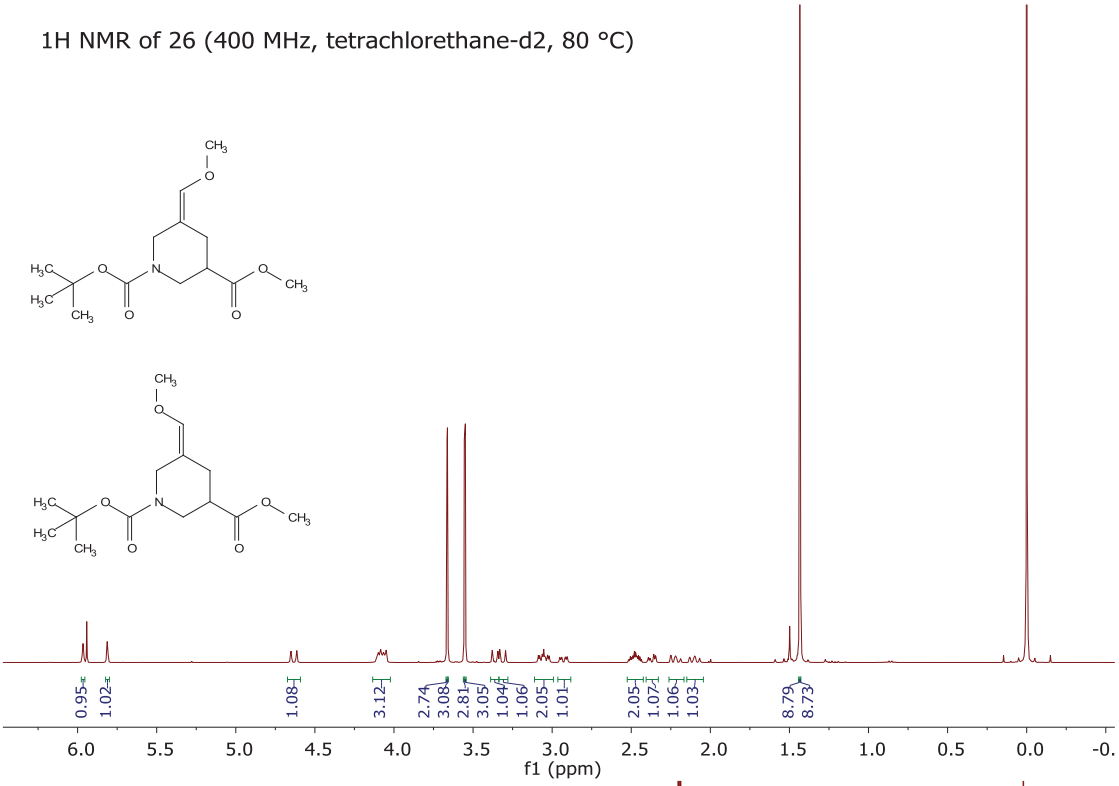

13C NMR of 26 (101 MHz, tetrachlorethane-d2, 80 °C)

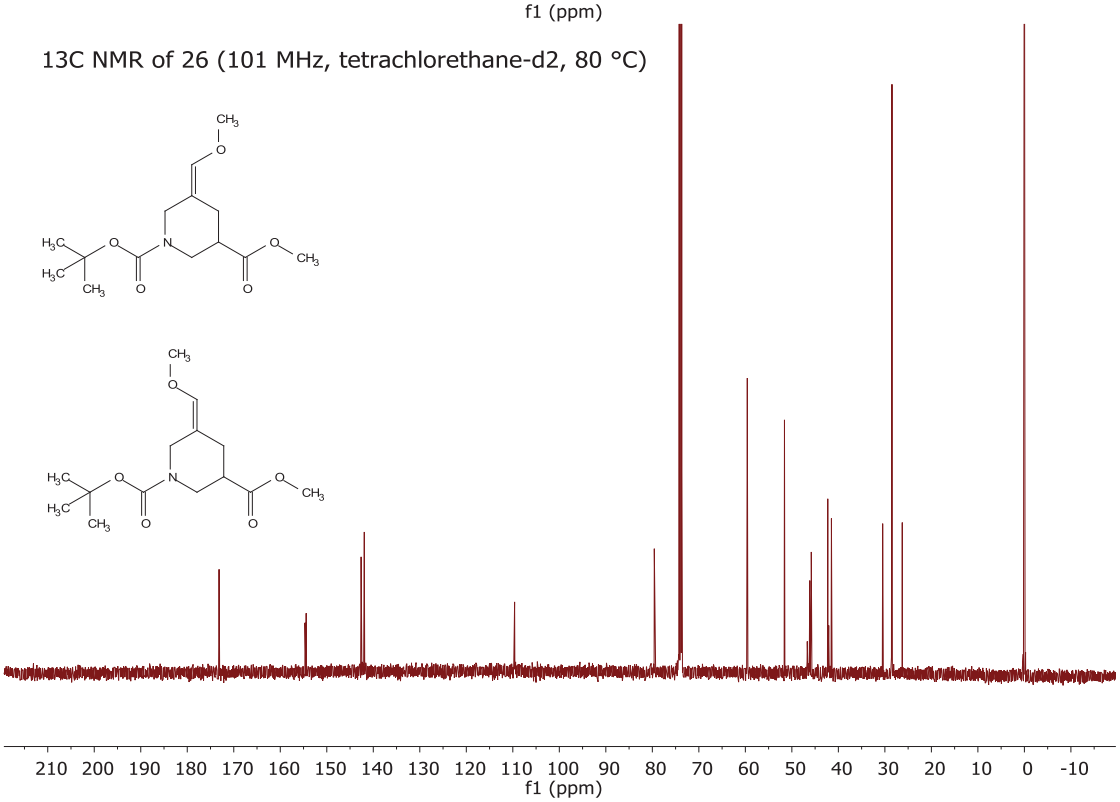

1H NMR of rac-20 & rac-21 (400 MHz, tetrachlorethane-d2, 80 °C)

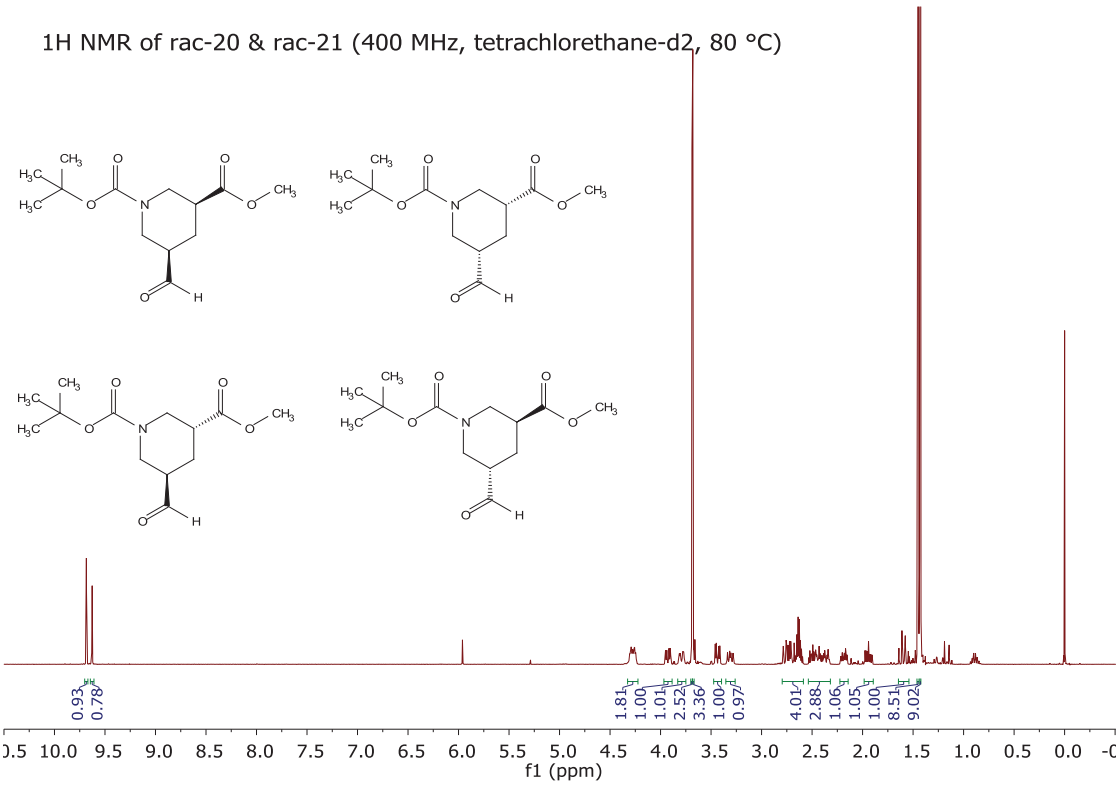

13C NMR of rac-20 & rac-21 (101 MHz, tetrachlorethane-d2, 80 °C)

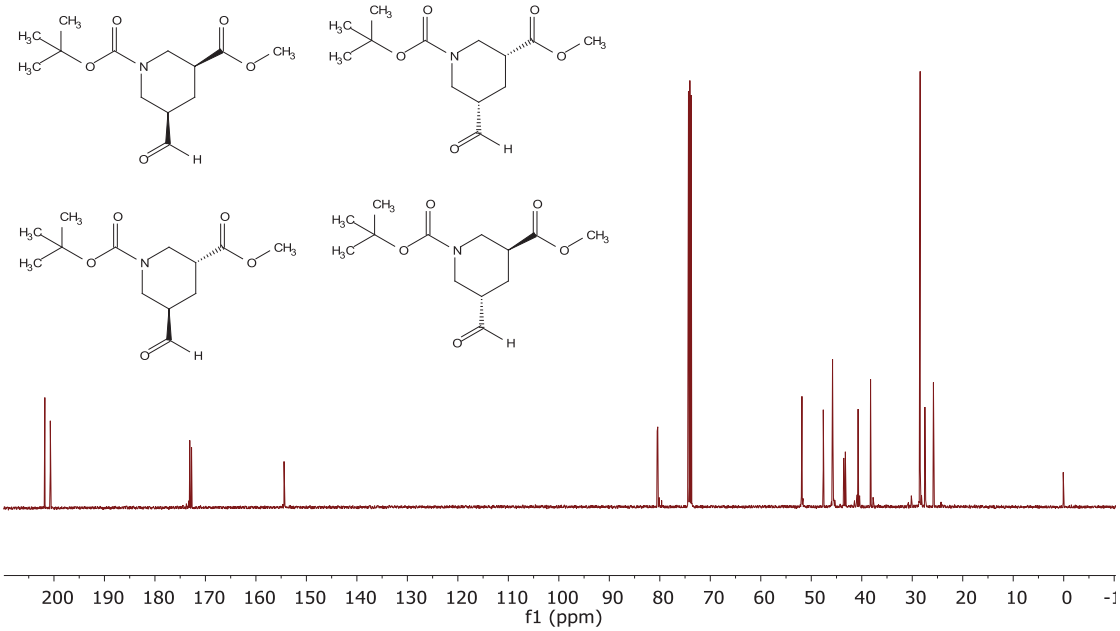

1H NMR of rac-27 & rac-28 (400 MHz, tetrachlorethane-d2, 80 °C)

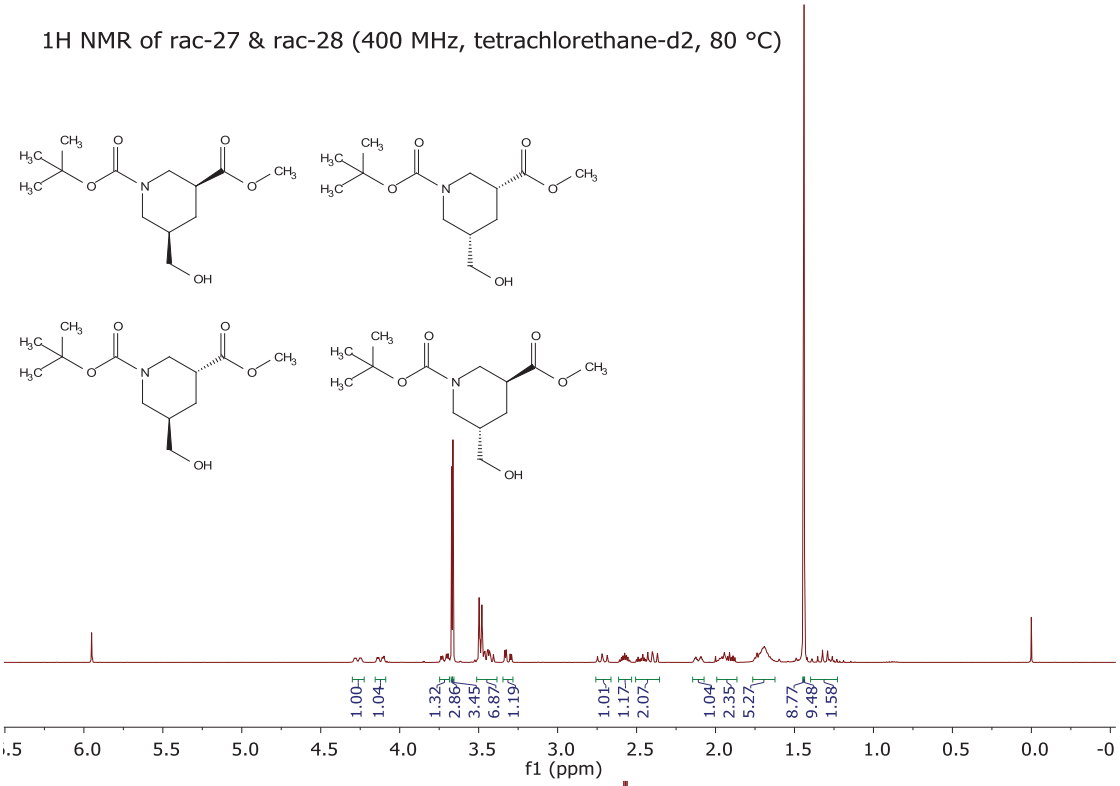

13C NMR of rac-27 & rac-28 (101 MHz, tetrachlorethane-d2, 80 °C)

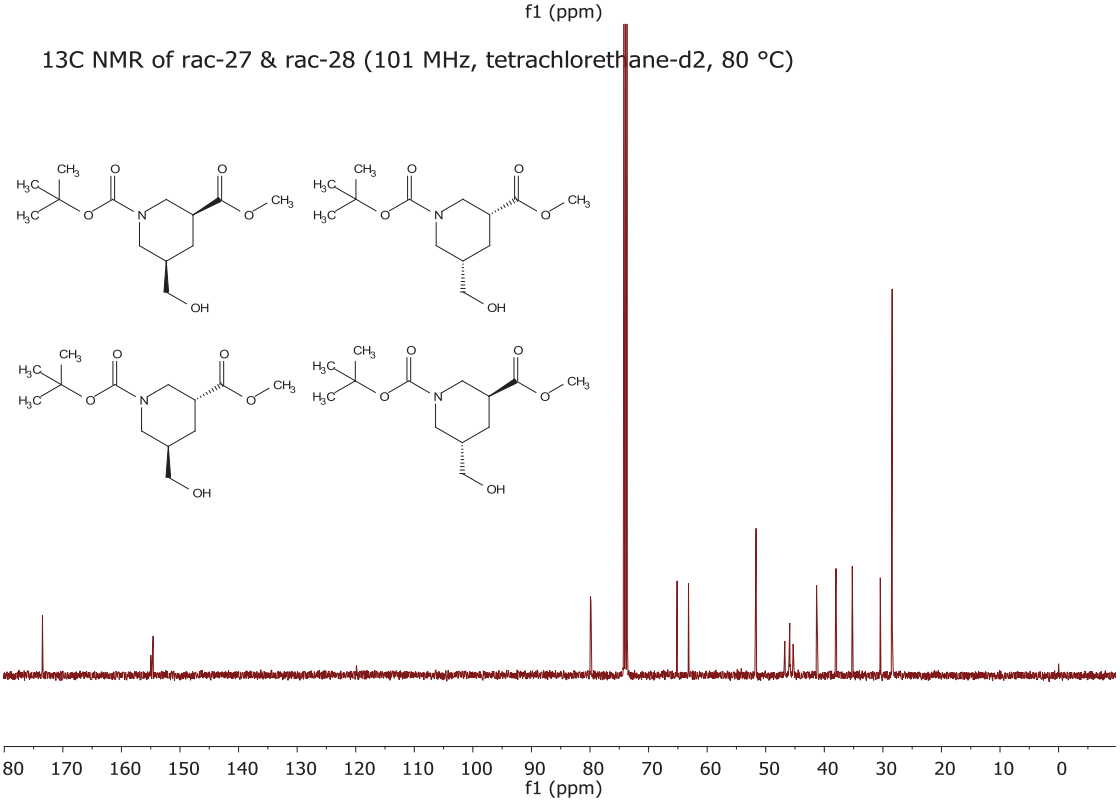

1H NMR of rac-30 (400 MHz, tetrachlorethane-d2, 80 °C)

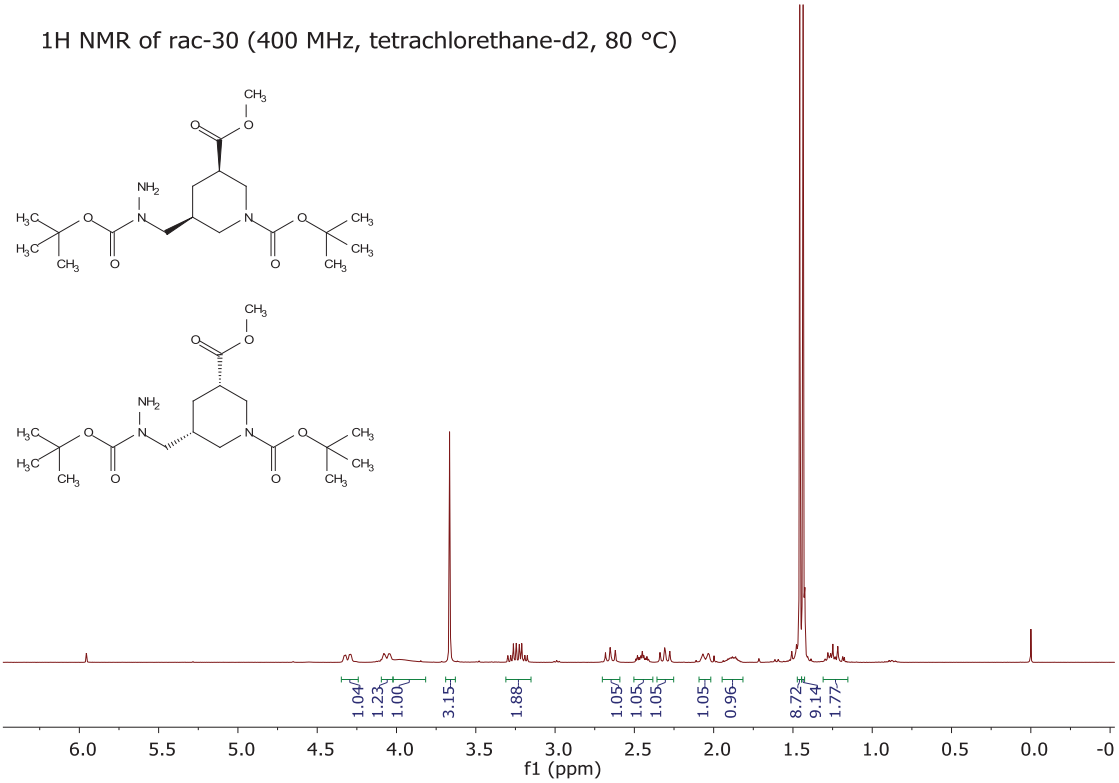

13C NMR of rac-30 (101 MHz, tetrachlorethane-d2, 80 °C)

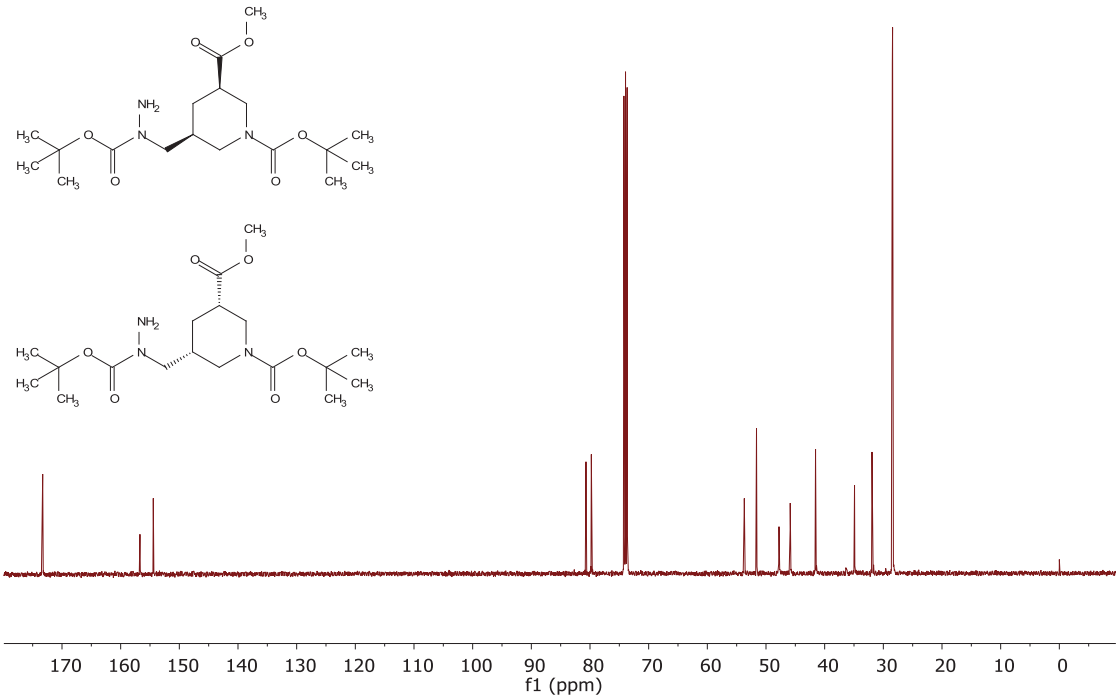

1H NMR of rac-31 (400 MHz, tetrachlorethane-d2, 80 °C)

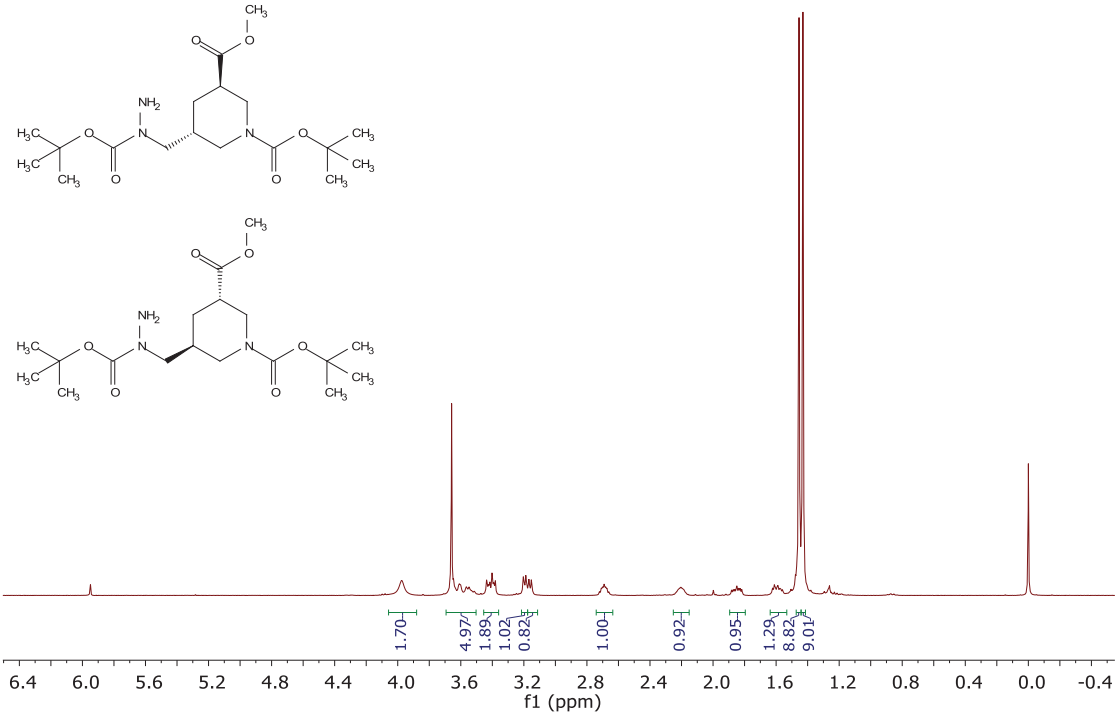

13C NMR of rac-31 (101 MHz, tetrachlorethane-d2, 80 °C)

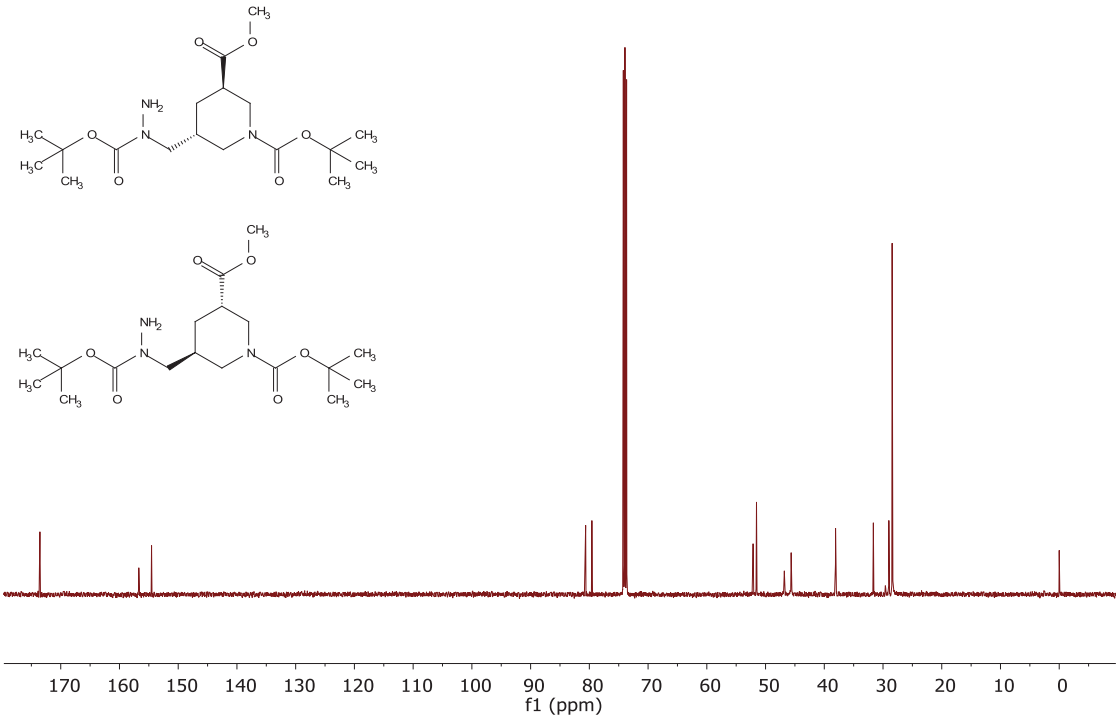

1H NMR of rac-32 (400 MHz, tetrachlorethane-d2, 80 °C)

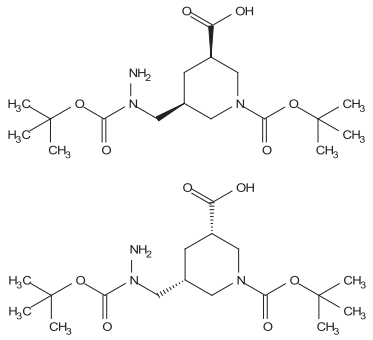

13C NMR of rac-32 (101 MHz, tetrachlorethane-d2, 80 °C)

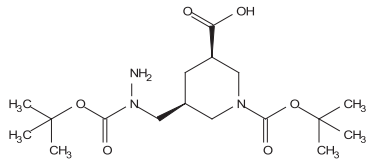

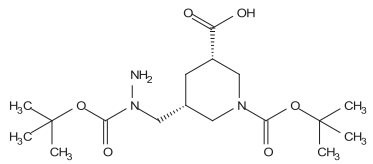

1H NMR of rac-11 x HCl (500 MHz, sodium deuteroxide in deuterium oxide, 25 °C)

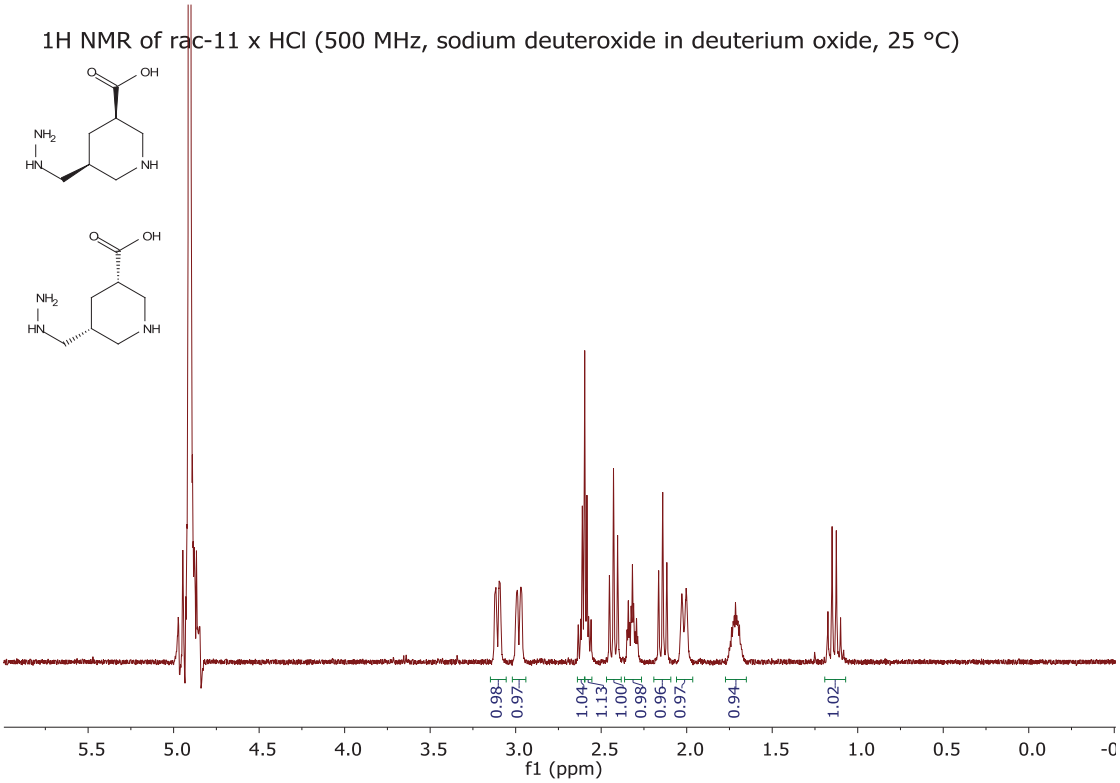

13C NMR of rac-11 x HCl (126 MHz, sodium deuteroxide in deuterium oxide, 25 °C)

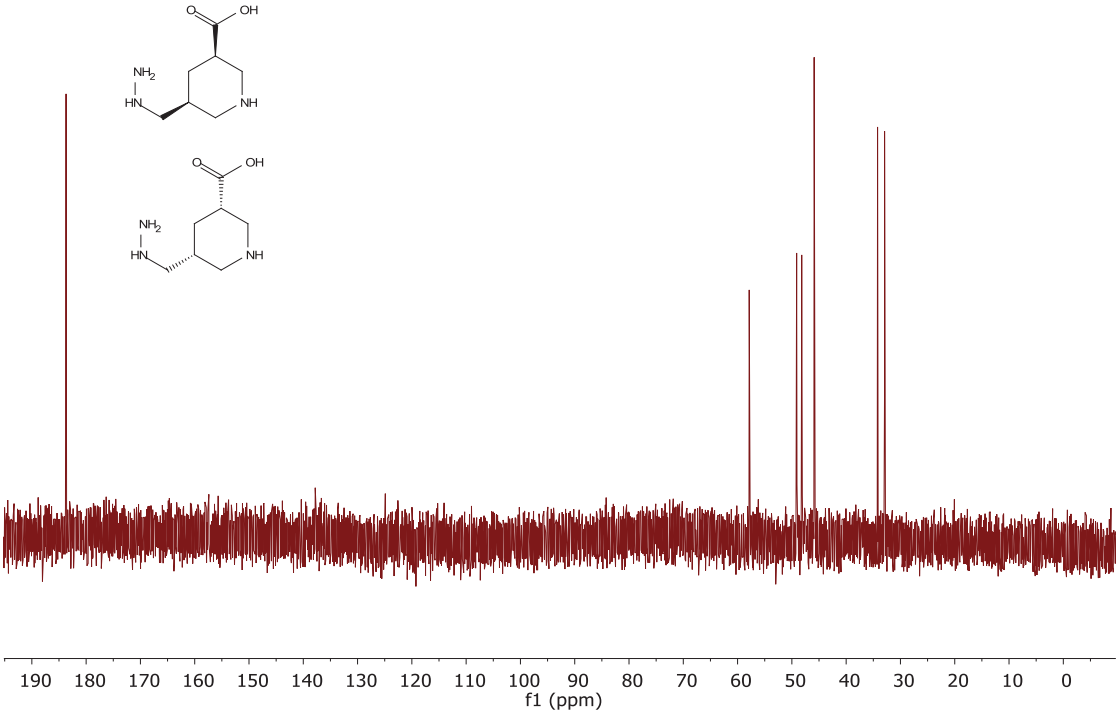

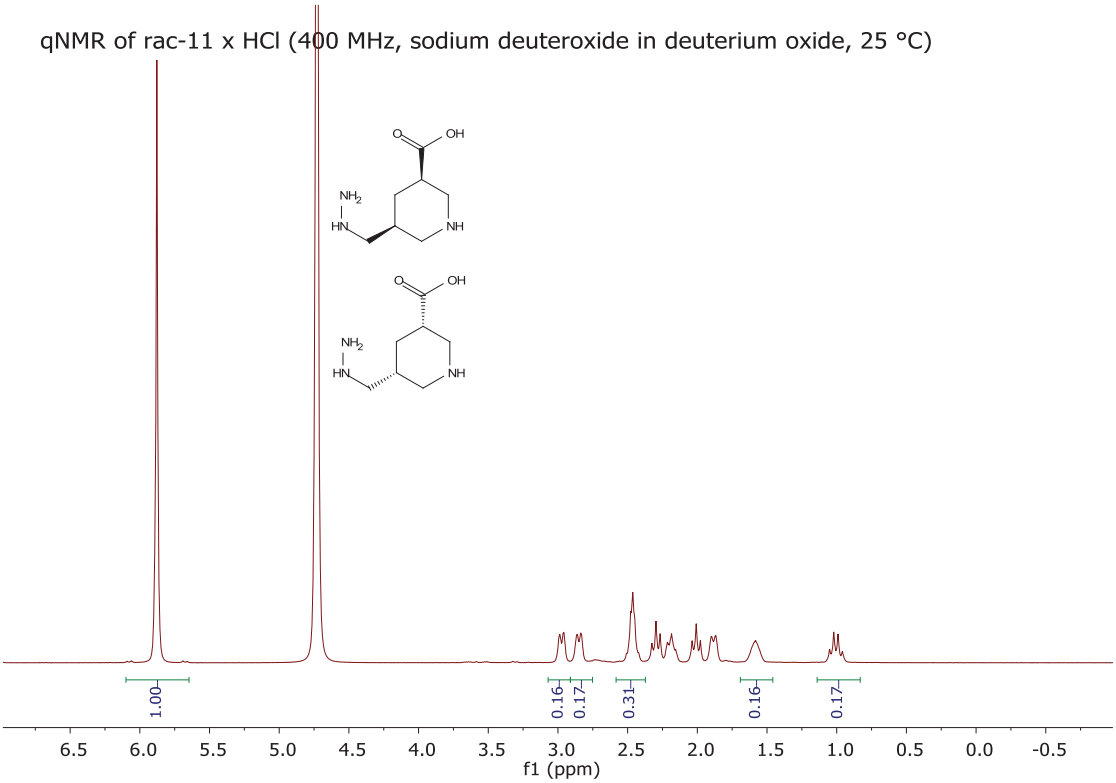

For the purity determination the sample weight was 6.951 mg and the assumed molecular weight 264.14 g/mol (calculated for the dihydrochloride monohydrate of the hydrazine). Maleic acid was used as internal calibrant with a weight of 9.117 mg, a molecular weight of 116.07 g/mol and a purity of 99.94%. A purity of 96.3% was calculated for the sample using the MestReNova NMR software.

1H NMR of rac-12 x HCl (400 MHz, sodium deuteroxide in deuterium oxide, 25 °C)

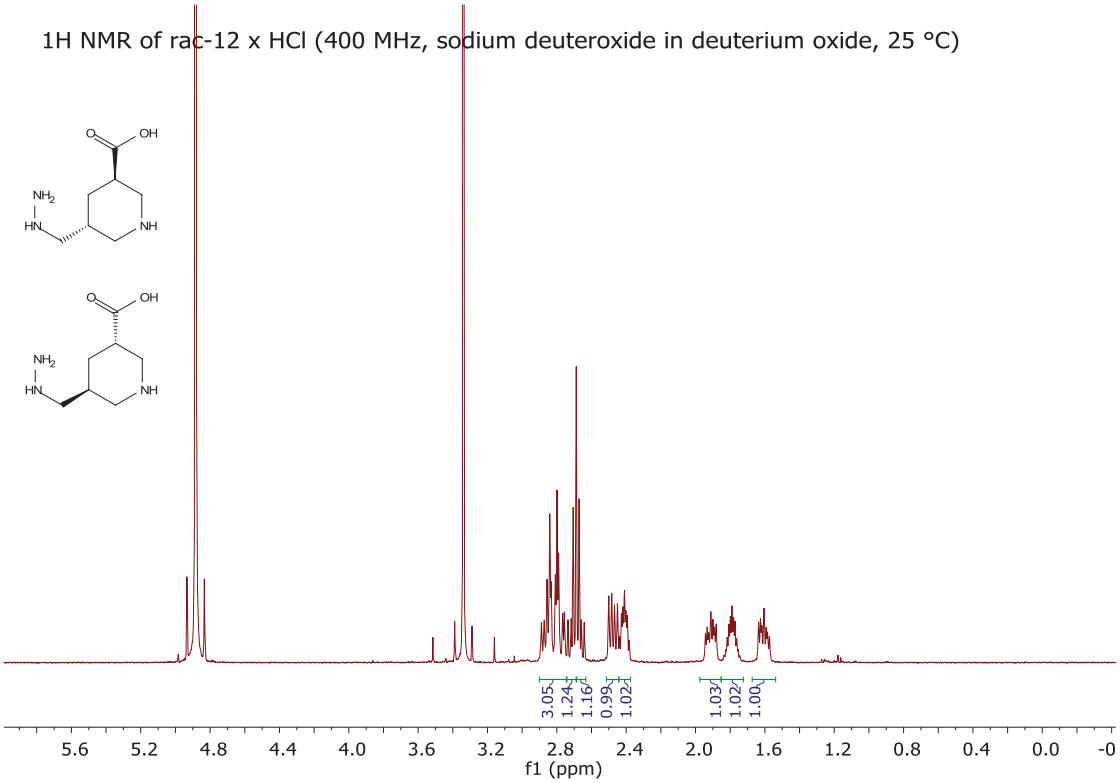

13C NMR of rac-12 x HCl (101 MHz, sodium deuteroxide in deuterium oxide, 25 °C)

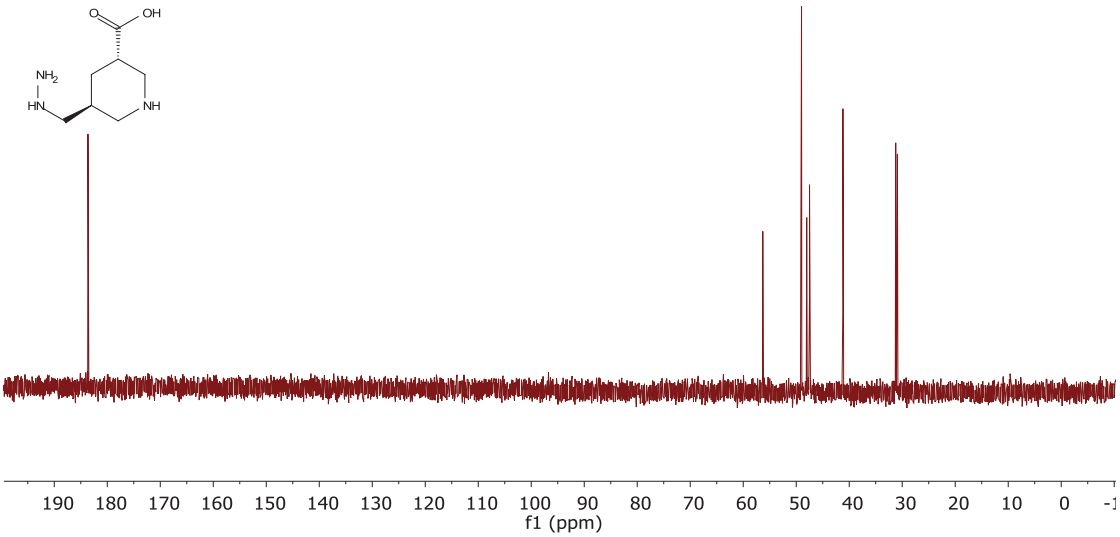

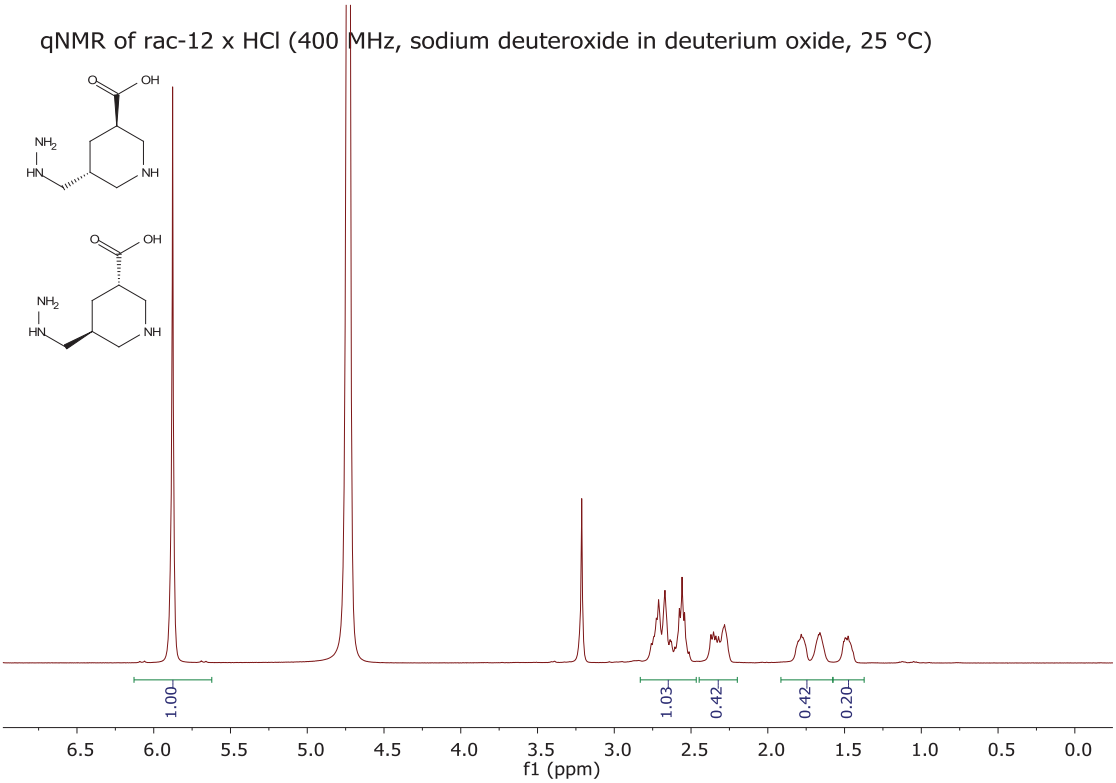

For the purity determination the sample weight was 6.166 mg and the assumed molecular weight 300.61 g/mol (calculated for the trihydrochloride monohydrate of the hydrazine). Maleic acid was used as internal calibrant with a weight of 5.709 mg, a molecular weight of 116.07 g/mol and a purity of 99.94%. A purity of 97.6% was calculated for the sample using the MestReNova NMR software.

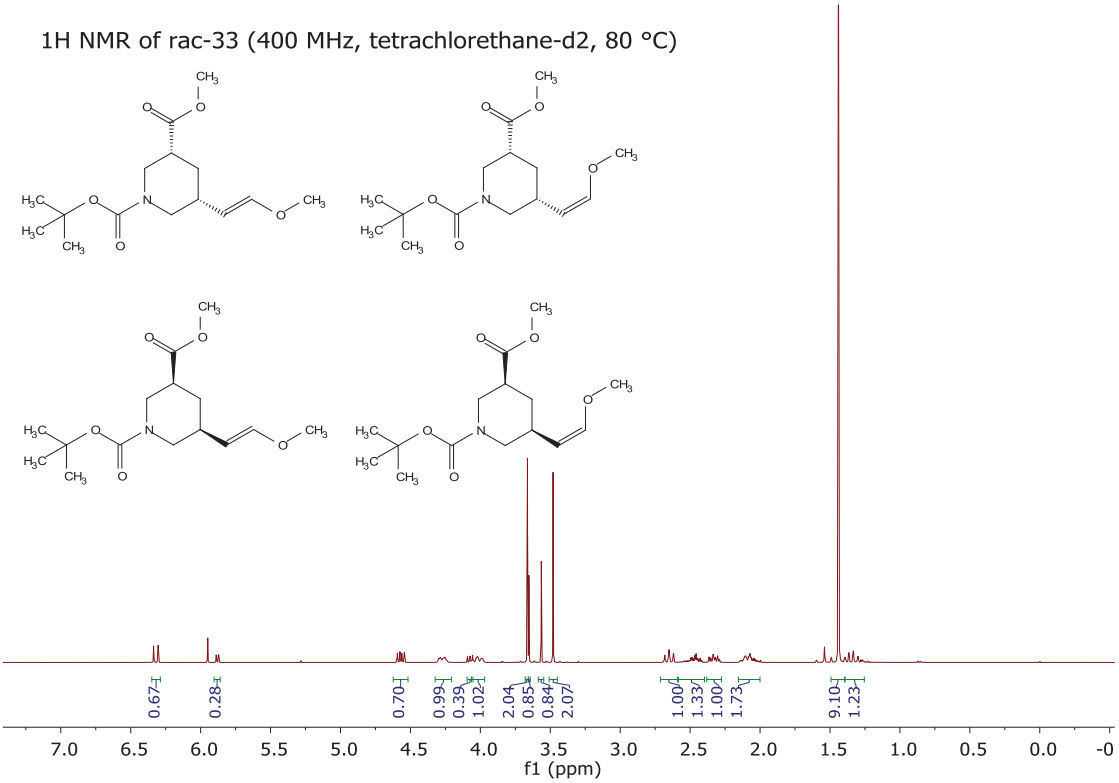
1H NMR of rac-33 (400 MHz, tetrachlorethane-d2, 80 °C)
0.67
0.28
0.70
0.99
0.39
1.02
2.04
0.85
0.84
2.07
1.00
1.33
1.00
1.73
9.10
1.23
7.0 6.5 6.0 5.5 5.0 4.5 4.0 3.5 3.0 2.5 2.0 1.5 1.0 0.5 0.0 -0
f1 (ppm)

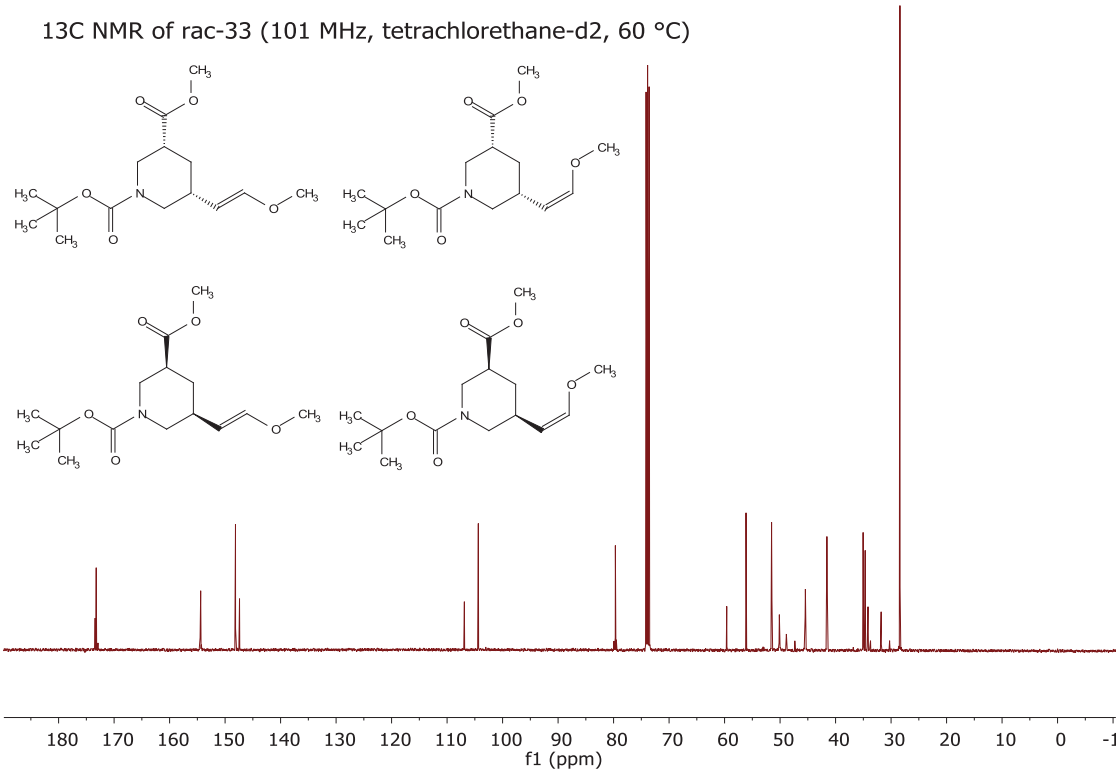
13C NMR of rac-33 (101 MHz, tetrachlorethane-d2, 60 °C)
180 170 160 150 140 130 120 110 100 90 80 70 60 50 40 30 20 10 0 -1
f1 (ppm)

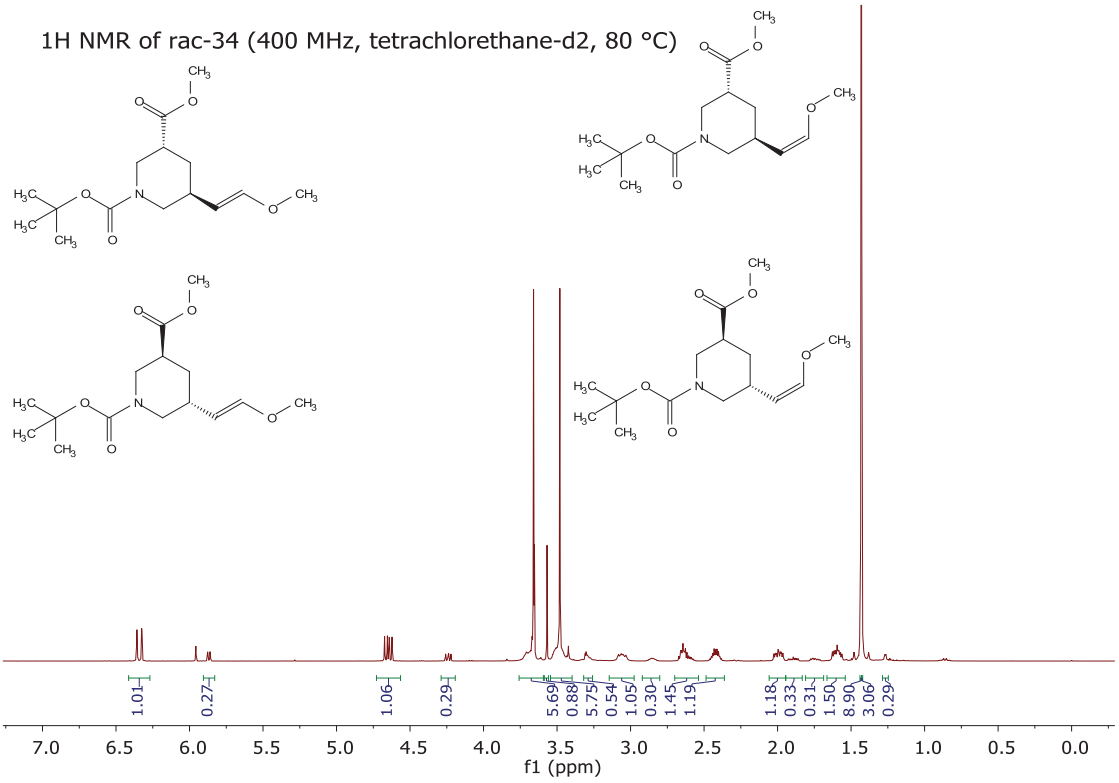
1H NMR of rac-34 (400 MHz, tetrachlorethane-d2, 80 °C)
1.01
0.27
1.06
0.29
5.69
0.88
5.75
0.54
1.05
0.30
1.45
1.19
1.18
0.33
0.31
1.50
8.90
3.06
0.29
7.0 6.5 6.0 5.5 5.0 4.5 4.0 3.5 3.0 2.5 2.0 1.5 1.0 0.5 0.0
f1 (ppm)

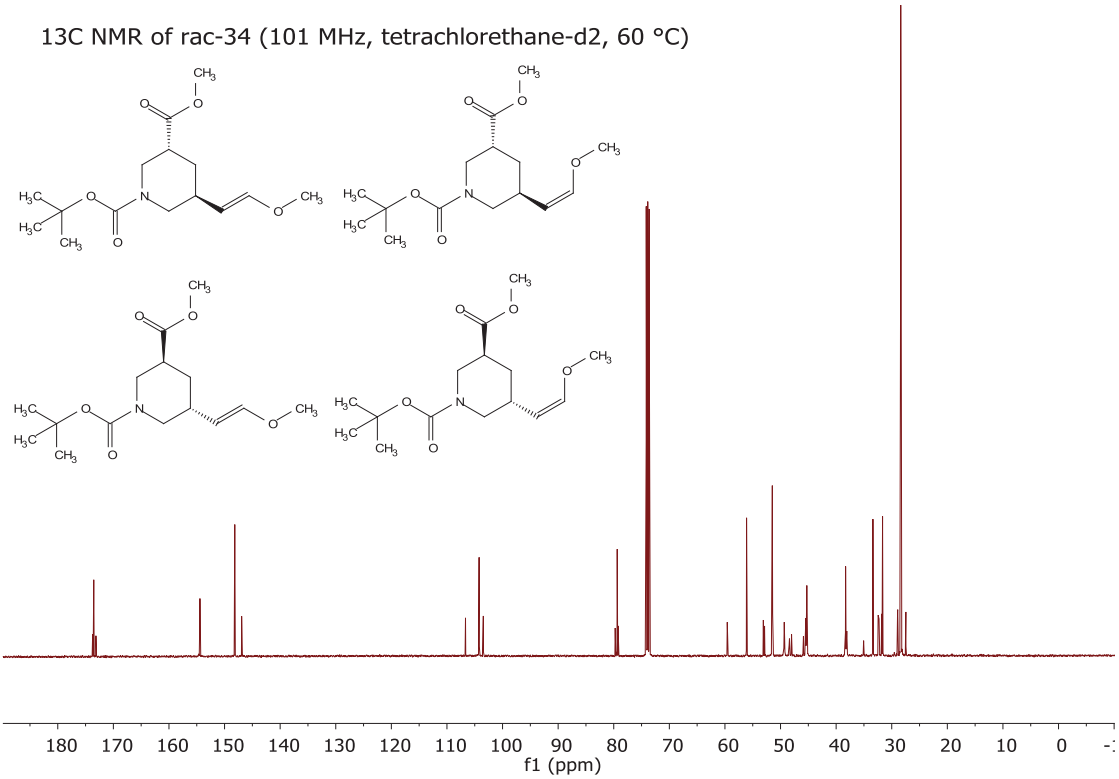
13C NMR of rac-34 (101 MHz, tetrachlorethane-d2, 60 °C)
180 170 160 150 140 130 120 110 100 90 80 70 60 50 40 30 20 10 0
f1 (ppm)

1H NMR of rac-35 (400 MHz, tetrachlorethane-d2, 80 °C)

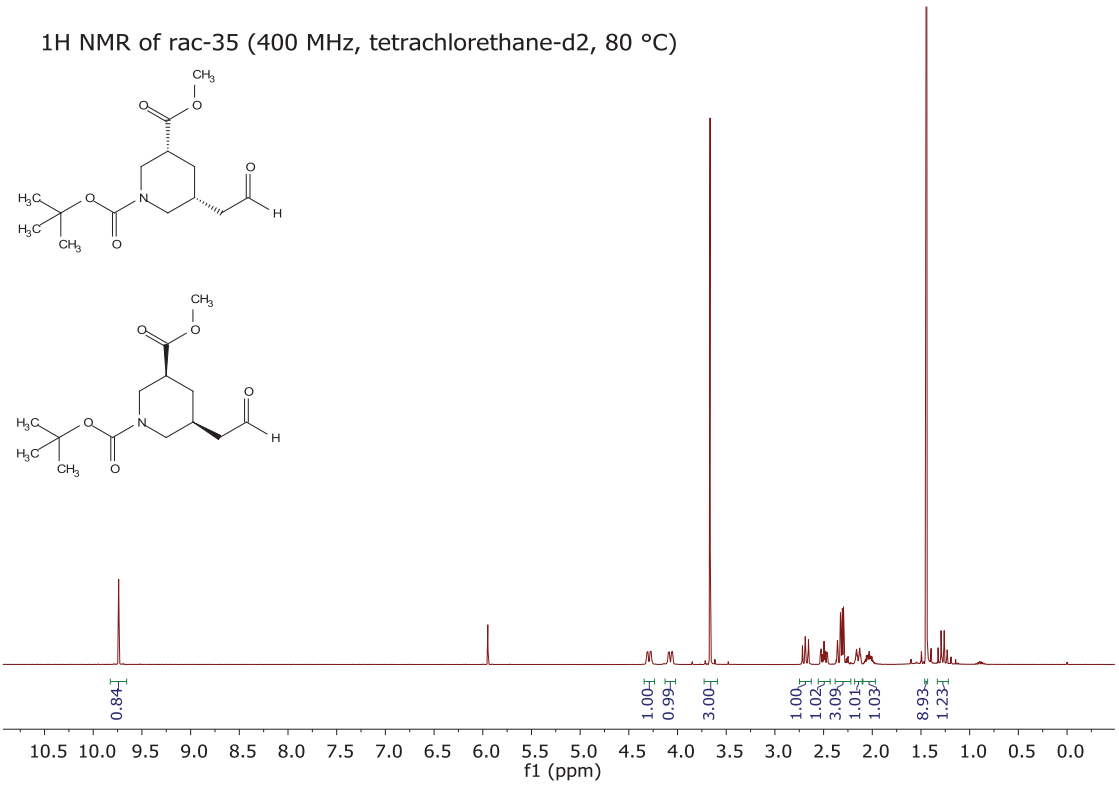

13C NMR of rac-35 (101 MHz, tetrachlorethane-d2, 80 °C)

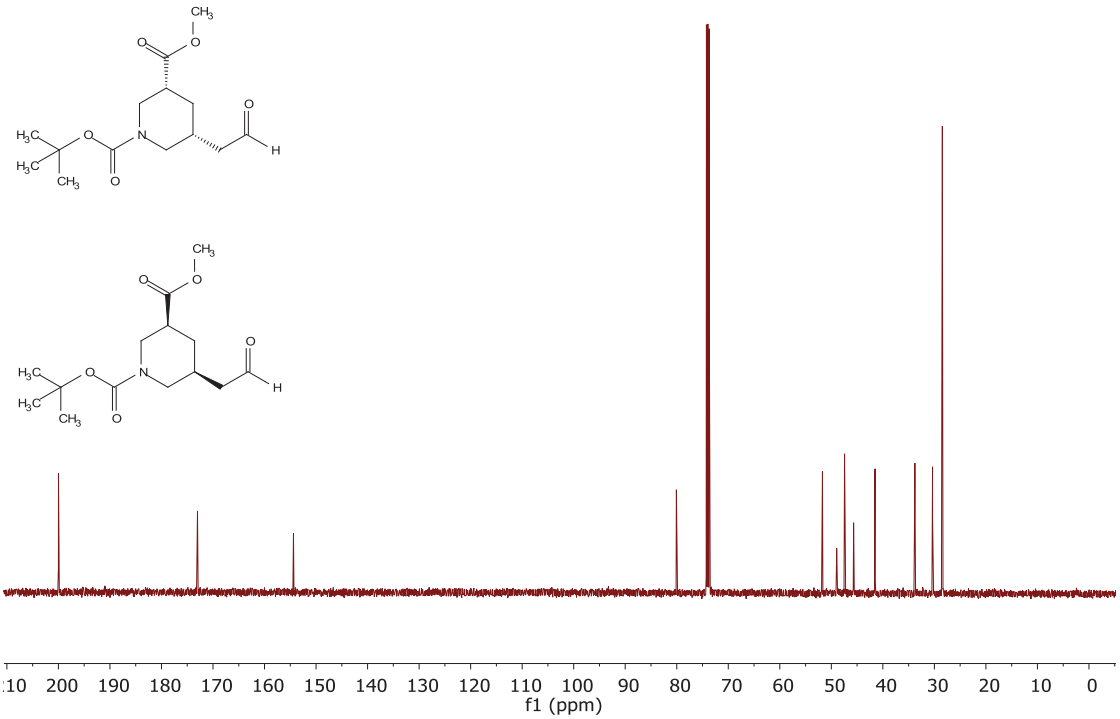

1H NMR of rac-36 (400 MHz, tetrachlorethane-d2, 120 °C)

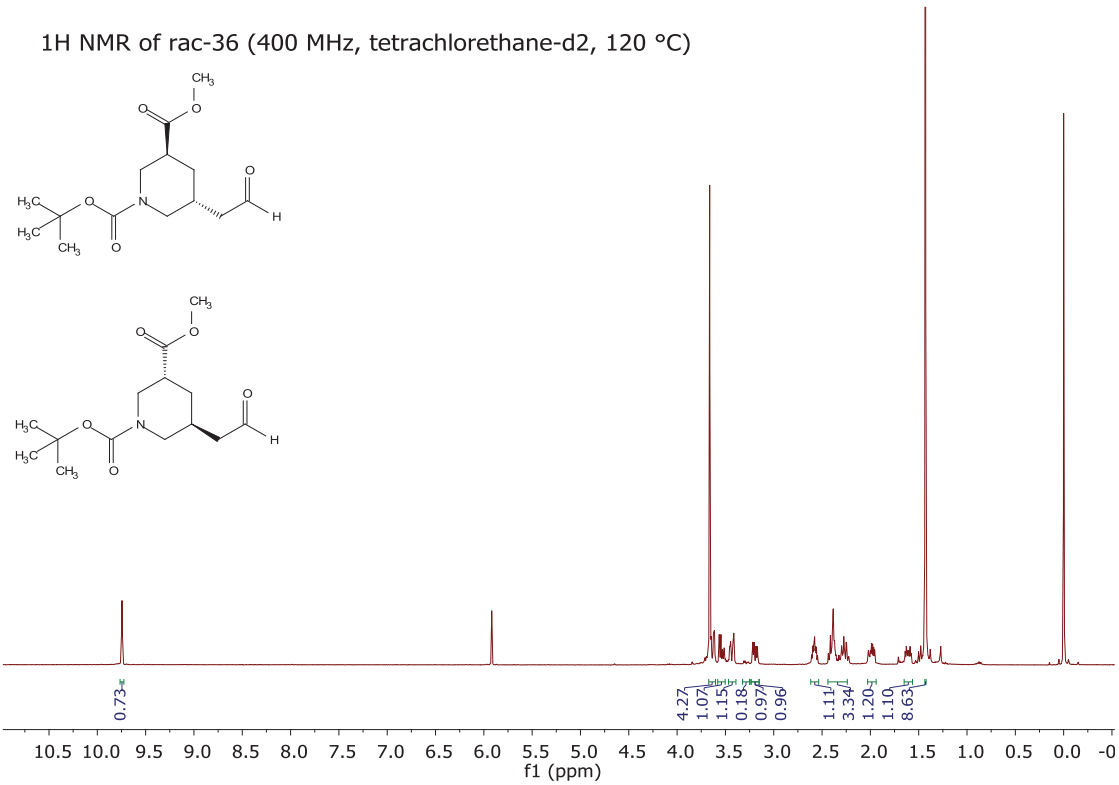

13C NMR of rac-36 (101 MHz, tetrachlorethane-d2, 80 °C)

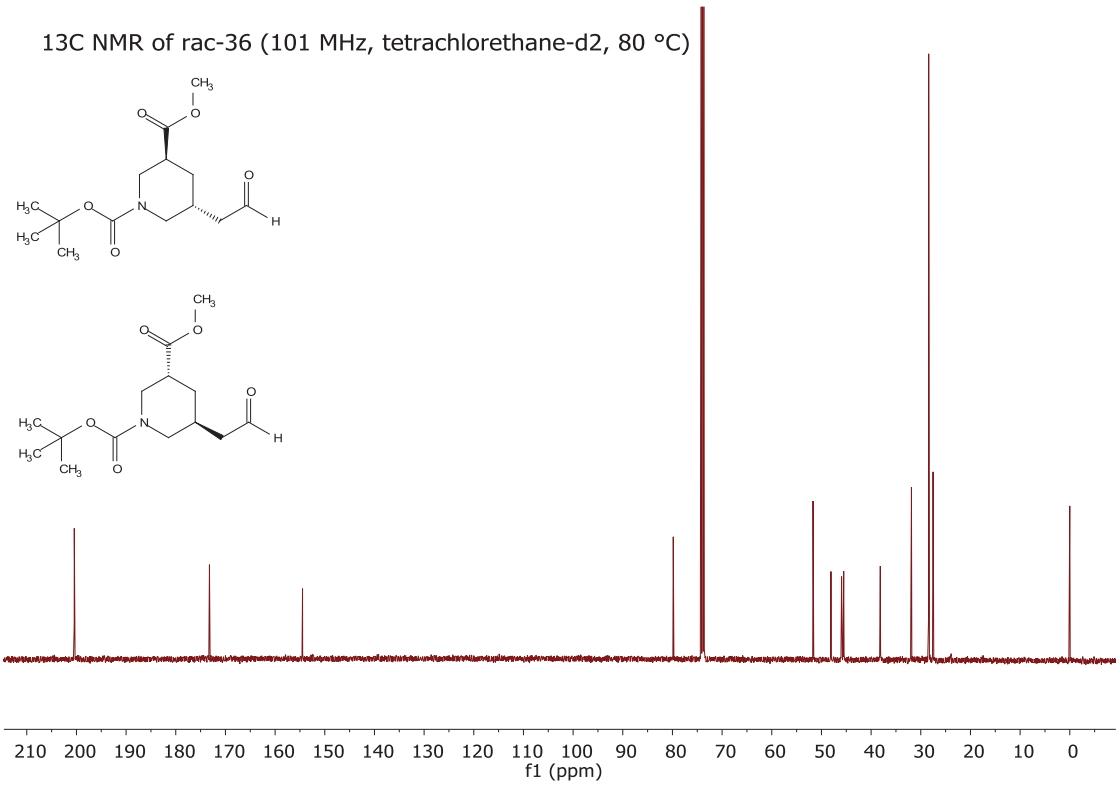

1H NMR of rac-37 (400 MHz, tetrachlorethane-d2, 80 °C)

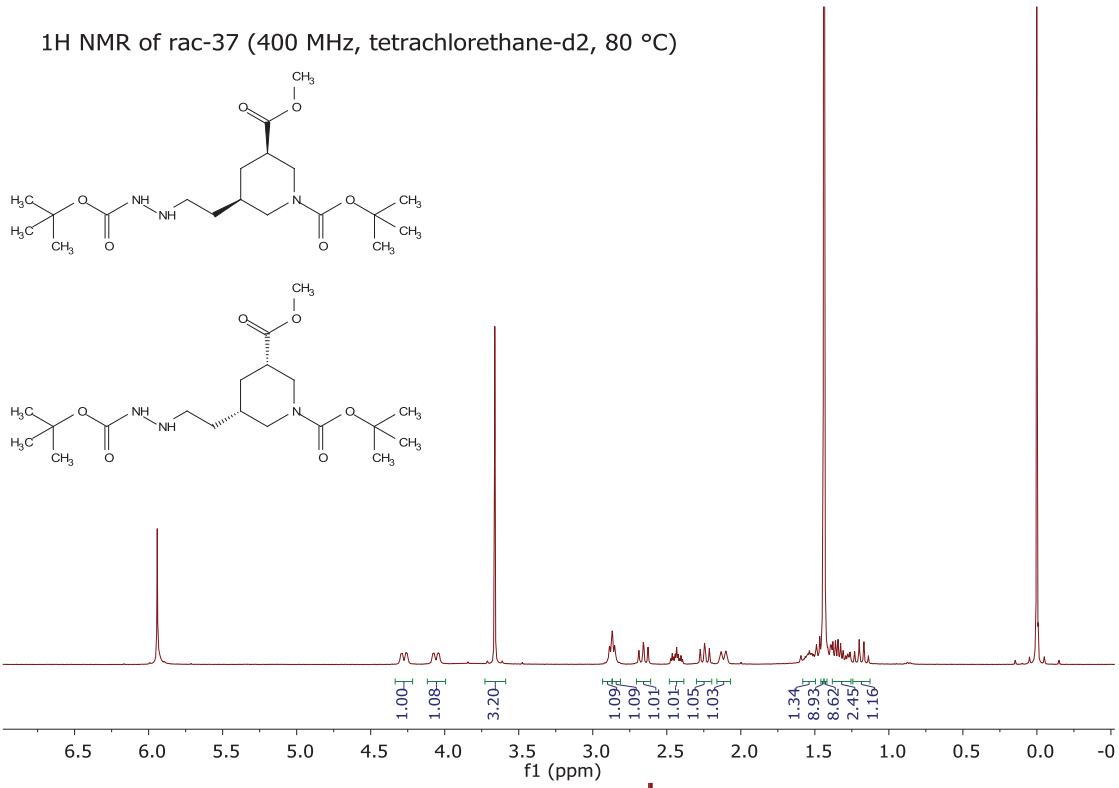

13C NMR of rac-37 (101 MHz, tetrachlorethane-d2, 80 °C)

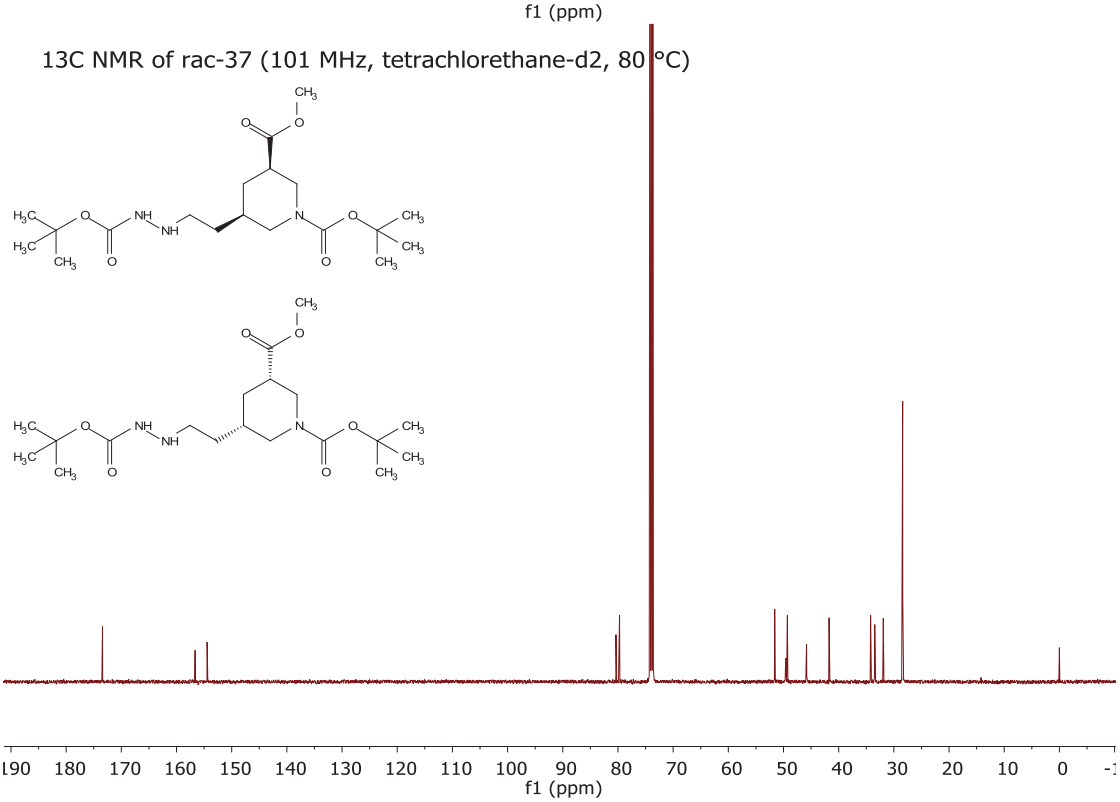

1H NMR of rac-38 (400 MHz, tetrachlorethane-d2, 120 °C)

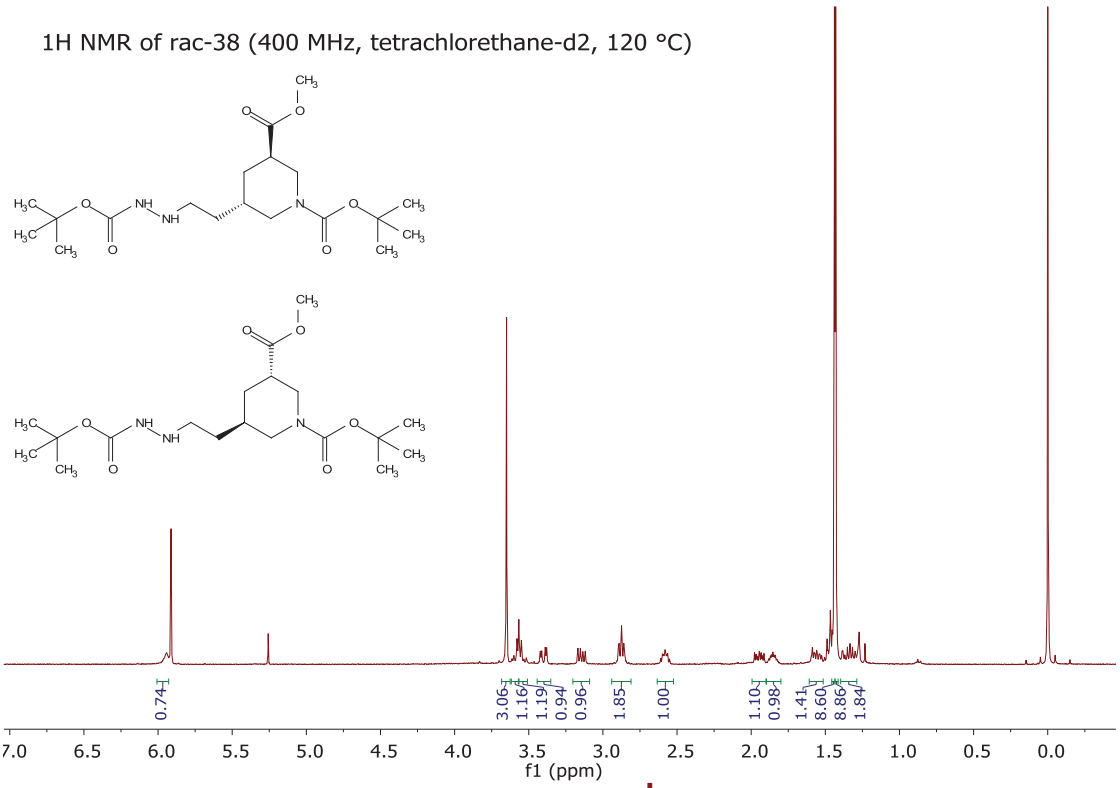

13C NMR of rac-38 (101 MHz, tetrachlorethane-d2, 80 °C)

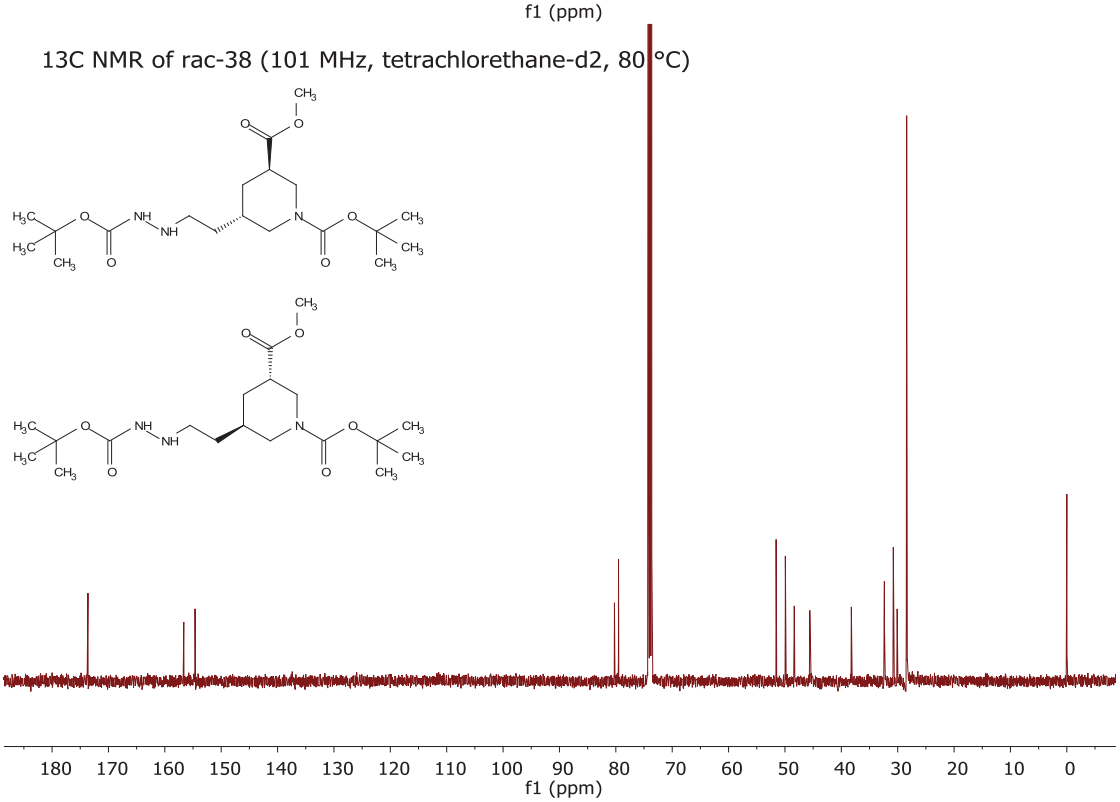

1H NMR of rac-13 x HCl (500 MHz, sodium deuteroxide in deuterium oxide, 25 °C)

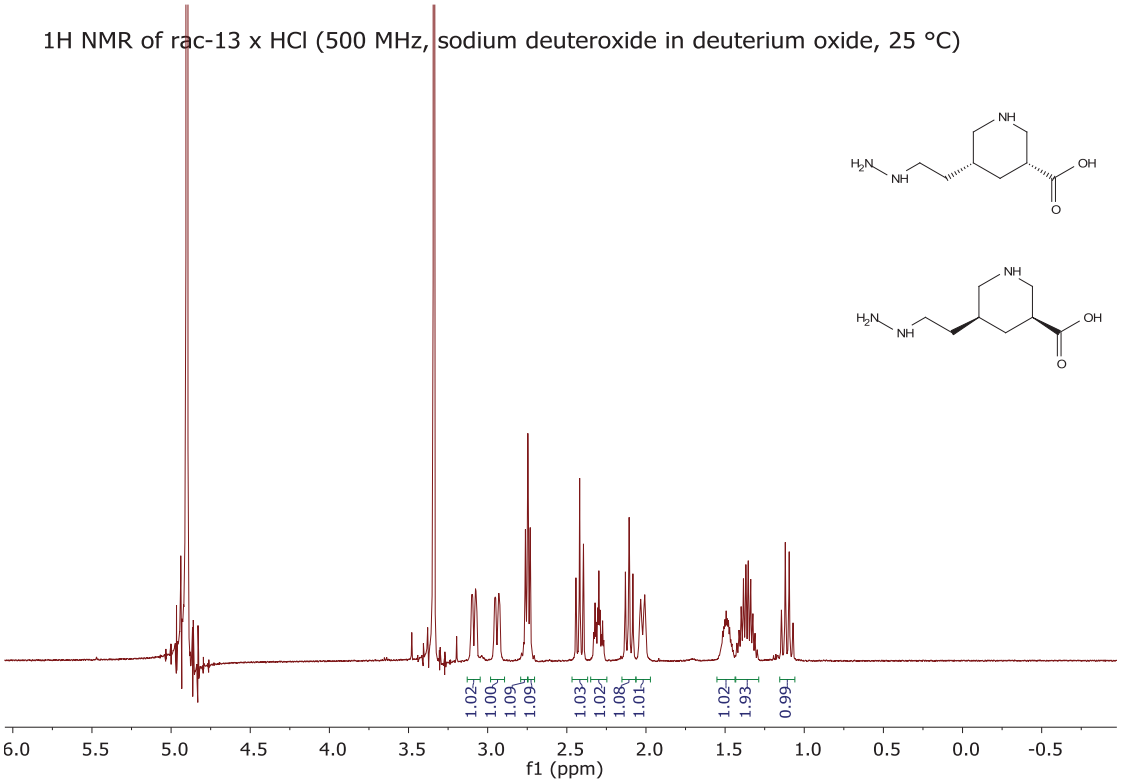

13C NMR of rac-13 x HCl (126 MHz, sodium deuteroxide in deuterium oxide, 25 °C)

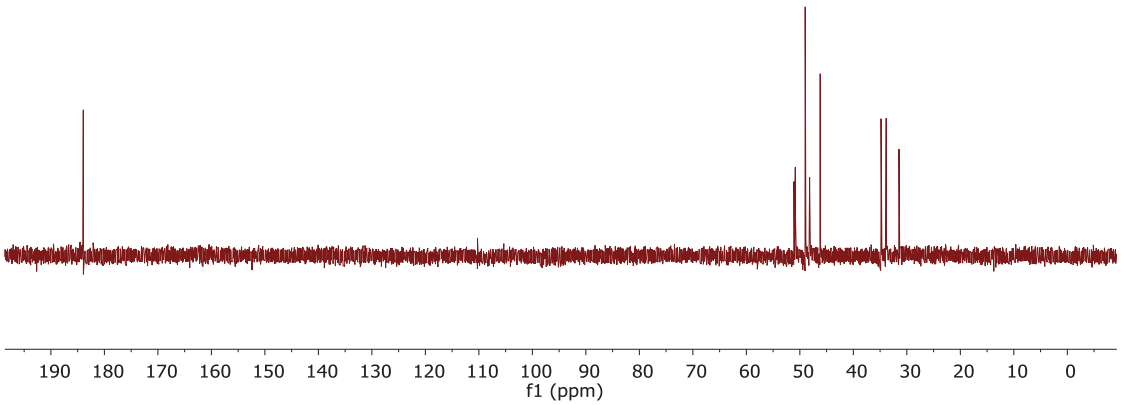

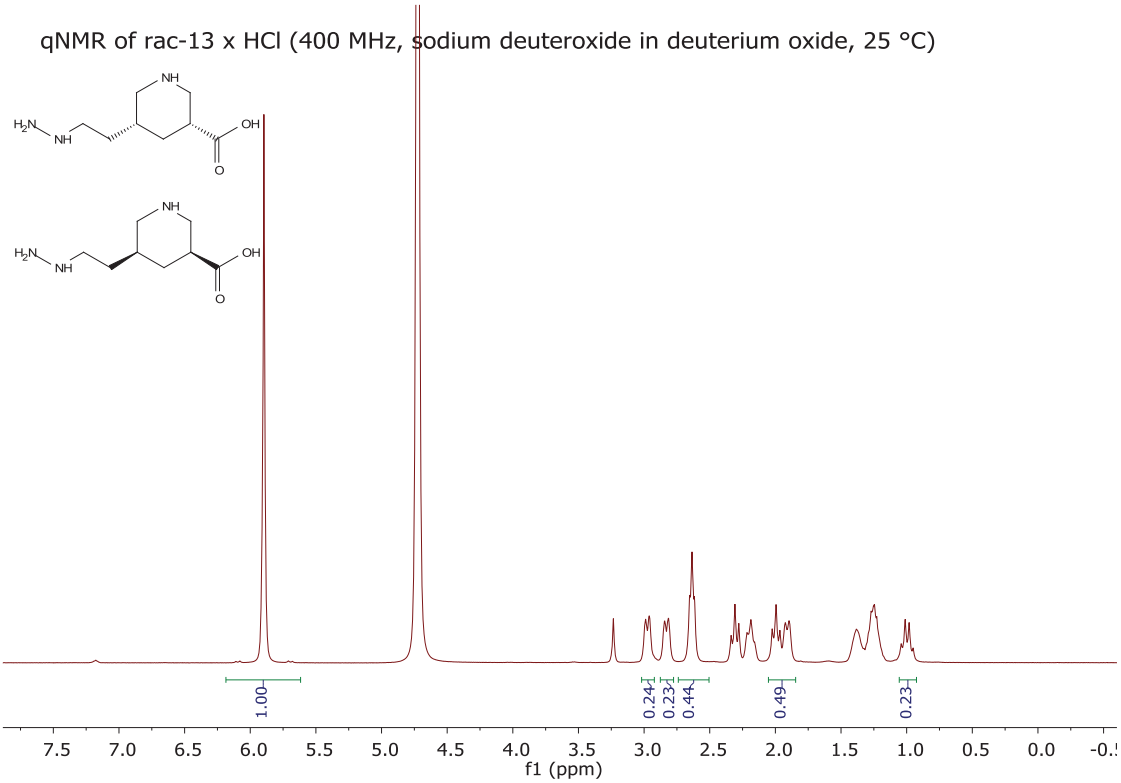

For the purity determination the sample weight was 11.26 mg and the assumed molecular weight 314.63 g/mol (calculated for the trihydrochloride monohydrate of the hydrazine). Maleic acid was used as internal calibrant with a weight of 8.962 mg, a molecular weight of 116.07 g/mol and a purity of 99.94%. A purity of 100.9% was calculated for the sample using the MestReNova NMR software.

1H NMR of rac-14 x HCl (400 MHz, sodium deuteroxide in deuterium oxide, 25 °C)

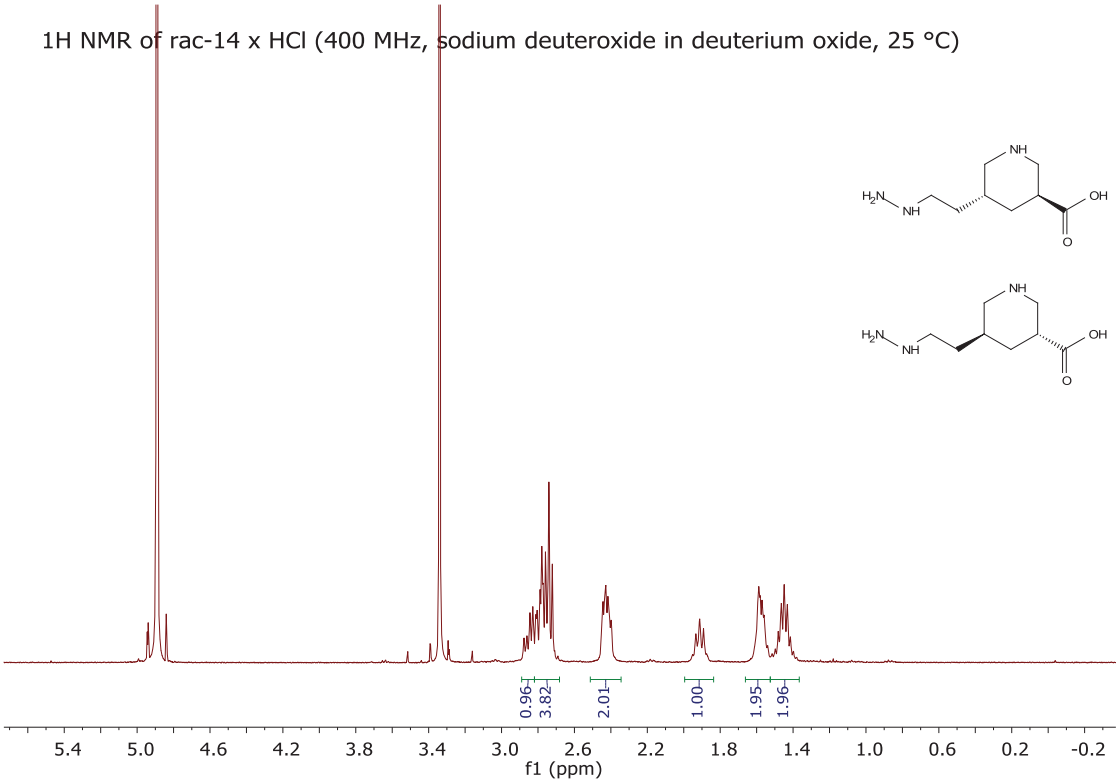

13C NMR of rac-14 x HCl (101 MHz, sodium deuteroxide in deuterium oxide, 25 °C)

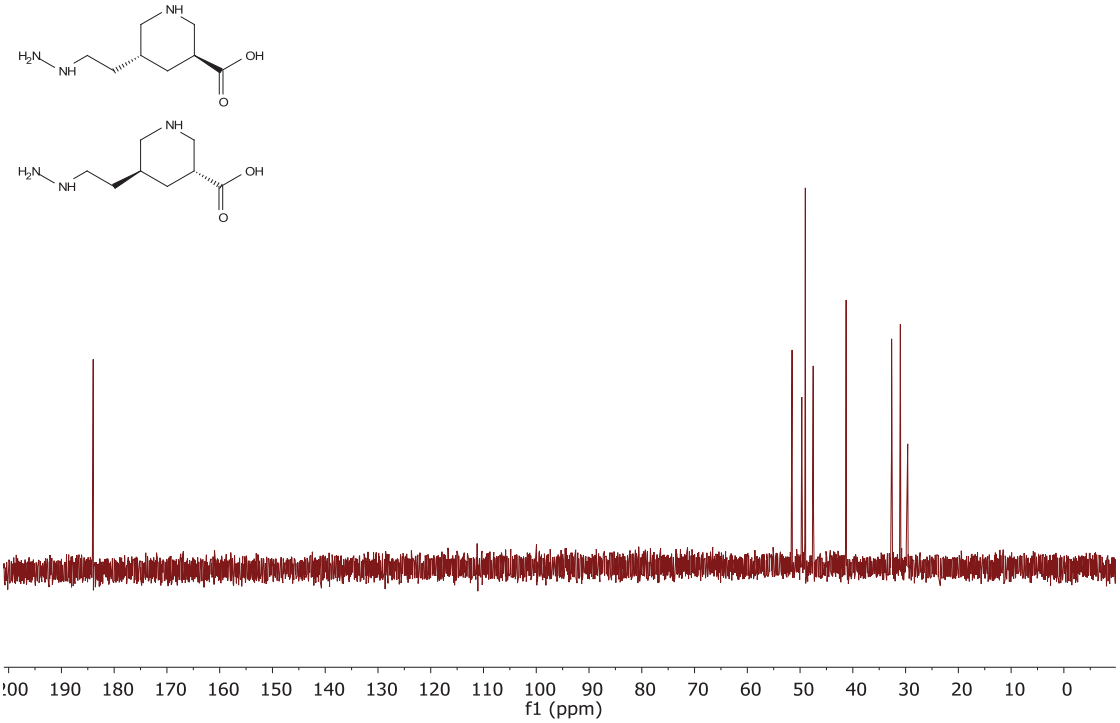

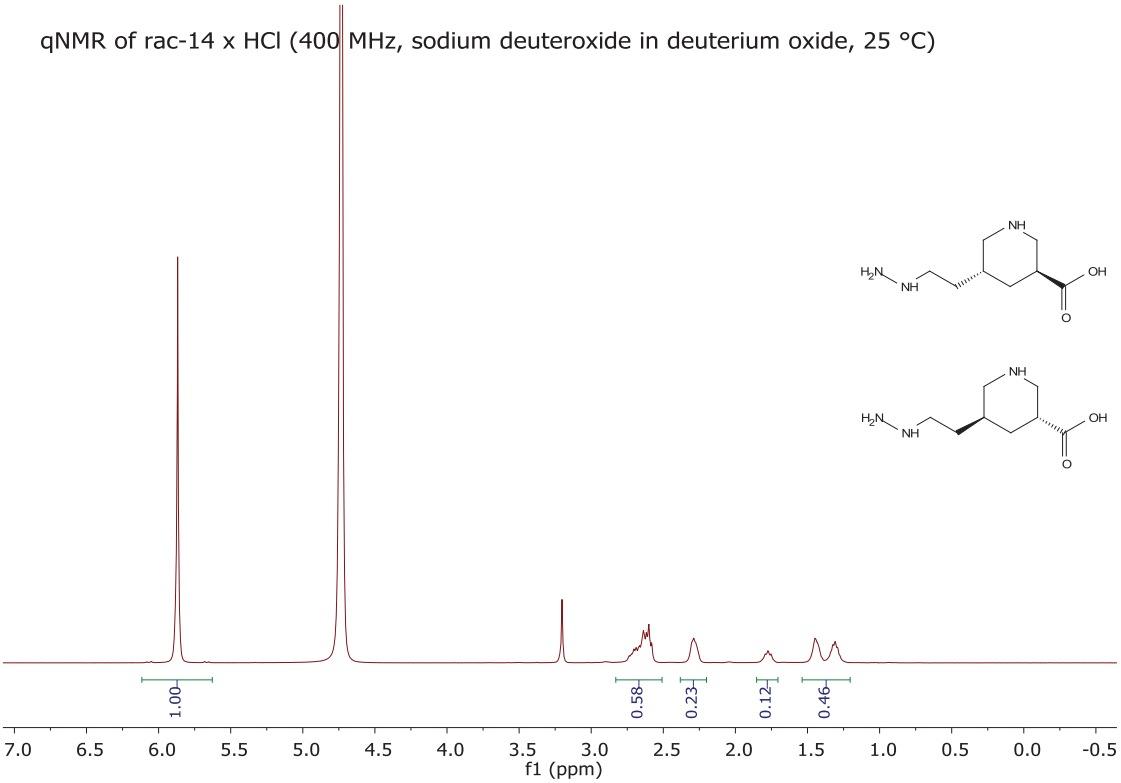

For the purity determination the sample weight was 5.076 mg and the assumed molecular weight 314.63 g/mol (calculated for the trihydrochloride monohydrate of the hydrazine). Maleic acid was used as internal calibrant with a weight of 7.986 mg, a molecular weight of 116.07 g/mol and a purity of 99.94%. A purity of 99.2% was calculated for the sample using the MestReNova NMR software.

1H NMR of rac-16e (500 MHz, DMSO-d6/deuterium oxide, 25 °C)

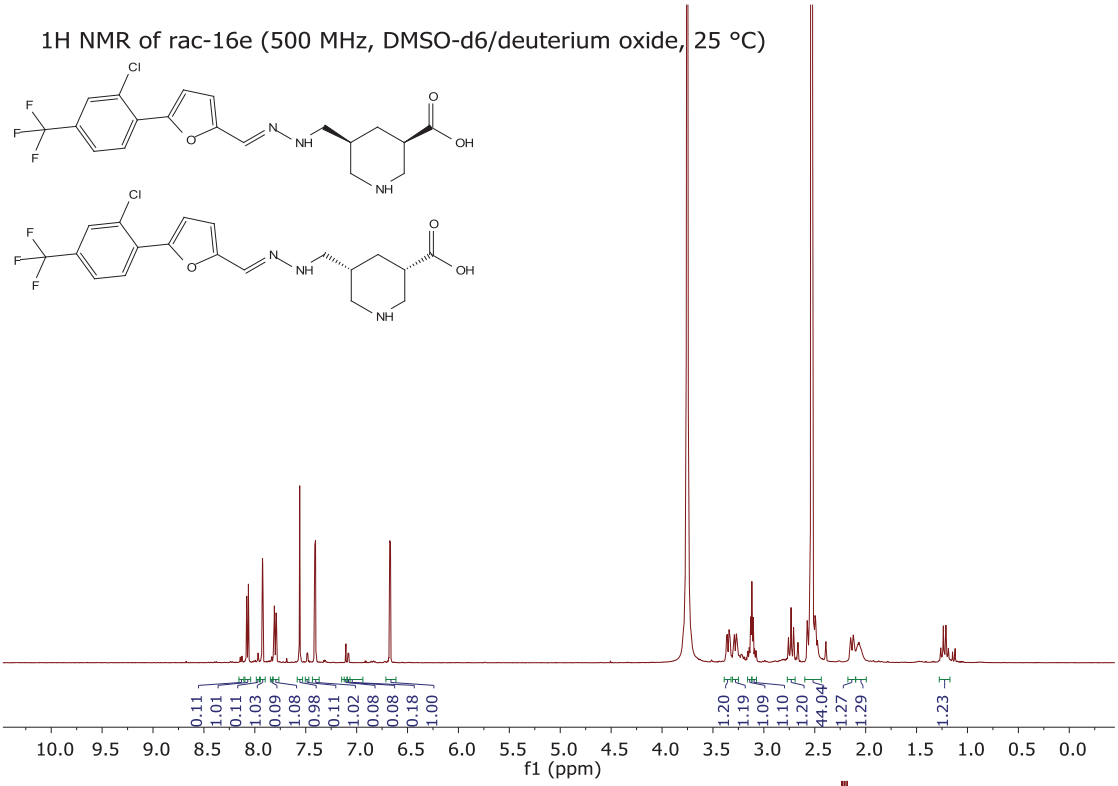

13C NMR of rac-16e (126 MHz, DMSO-d6/deuterium oxide, 25 °C)

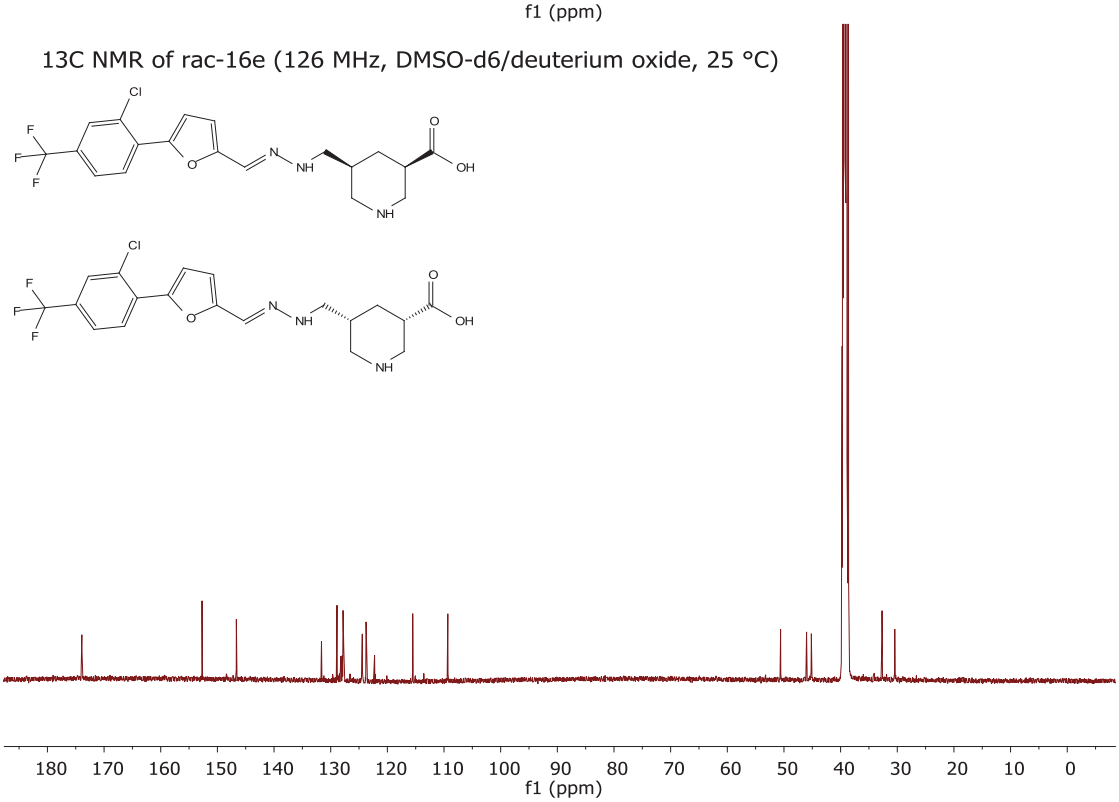

1H NMR of rac-16r (500 MHz, DMSO-d6/deuterium oxide, 25 °C)

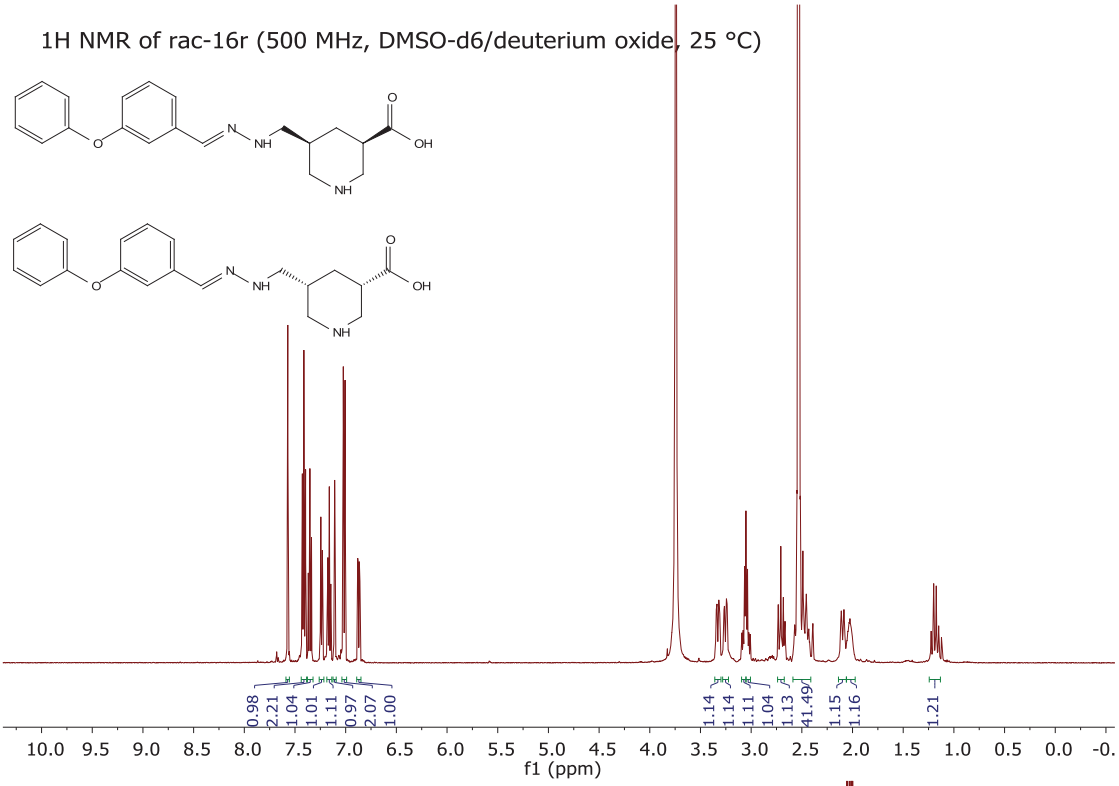

13C NMR of rac-16r (126 MHz, DMSO-d6/deuterium oxide, 25 °C)

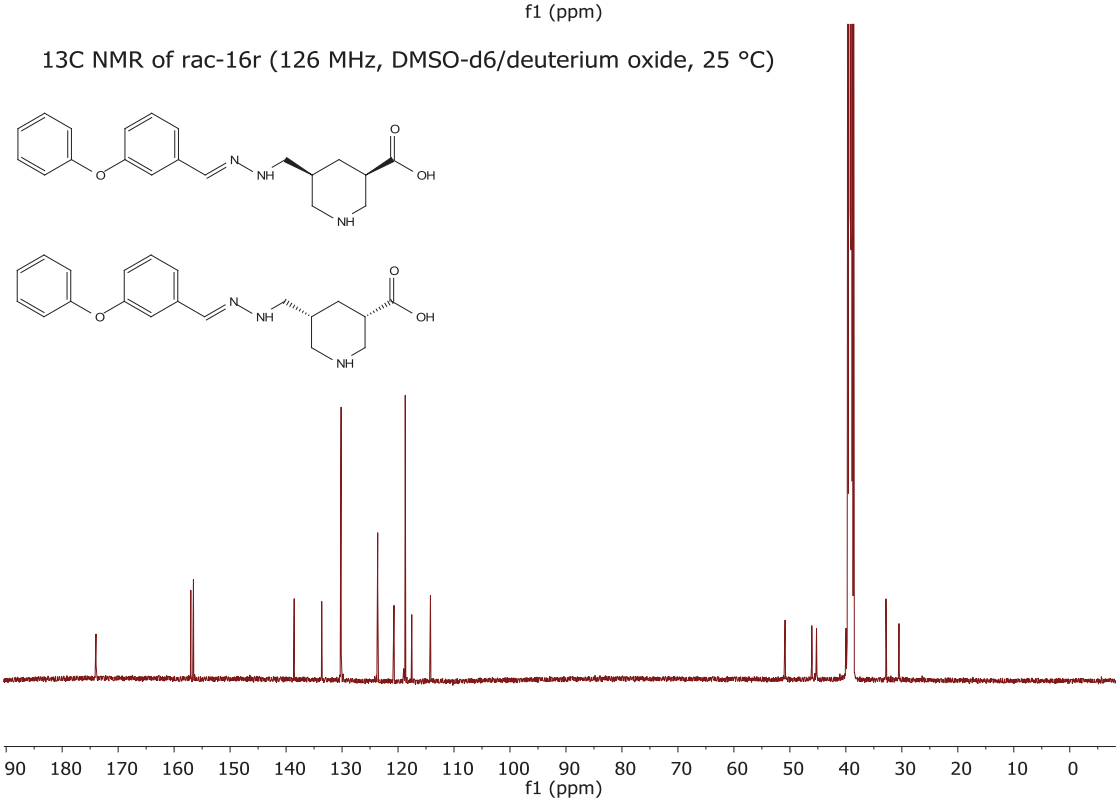

1H NMR of rac-16fv (500 MHz, DMSO-d6/deuterium oxide, 25 °C)

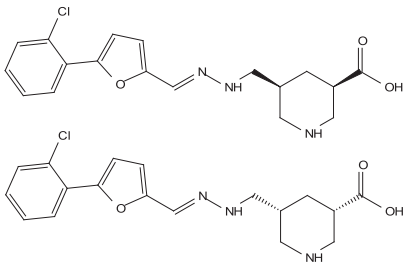

13C NMR of rac-16fv (126 MHz, DMSO-d6/deuterium oxide, 25 °C)

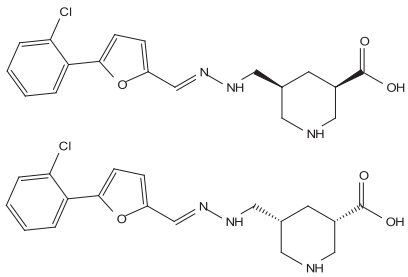

1H NMR of rac-16fw (500 MHz, DMSO-d6/deuterium oxdie, 25 °C)

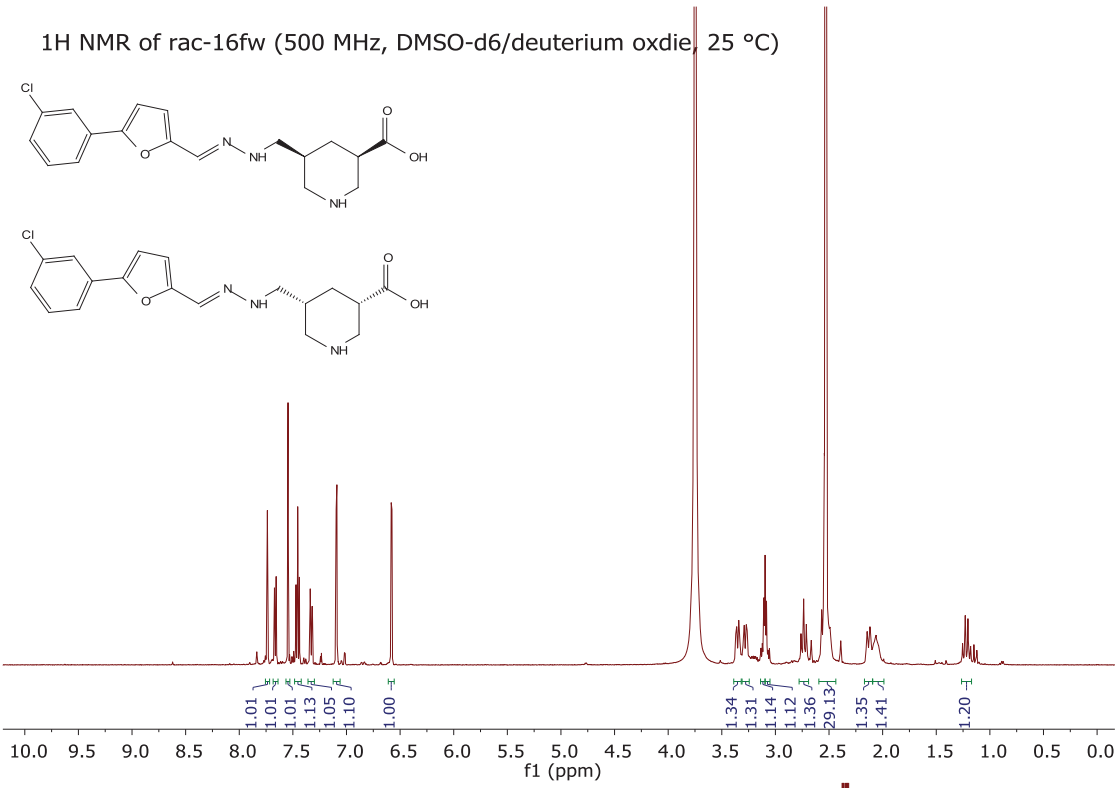

13C NMR of rac-16fw (126 MHz, DMSO-d6/deuterium oxide, 25 °C)

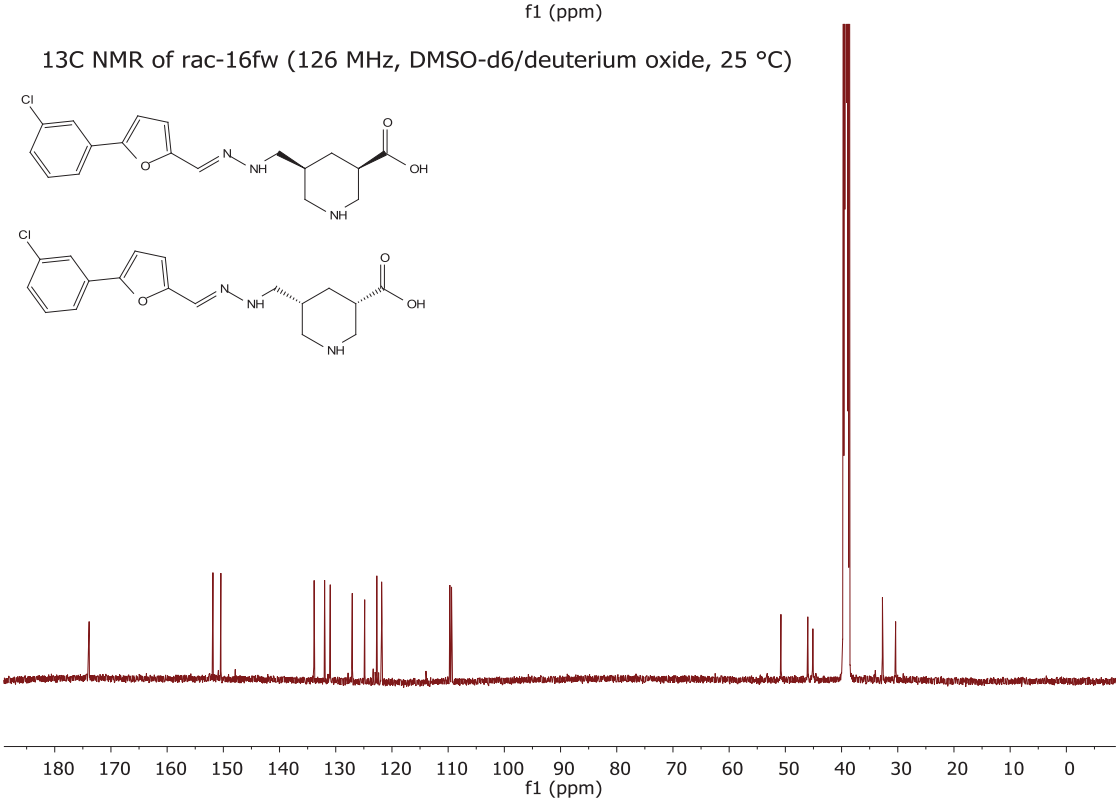

1H NMR of rac-16fy (500 MHz, DMSO-d6/deuterium oxide, 25 °C)

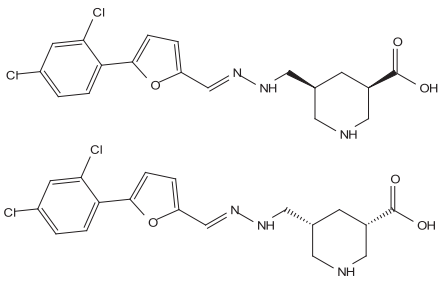

13C NMR of rac-16fy (126 MHz, DMSO-d6/deuterium oxide, 25 °C)

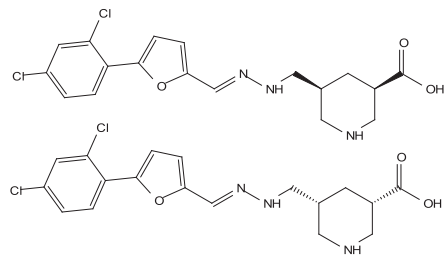

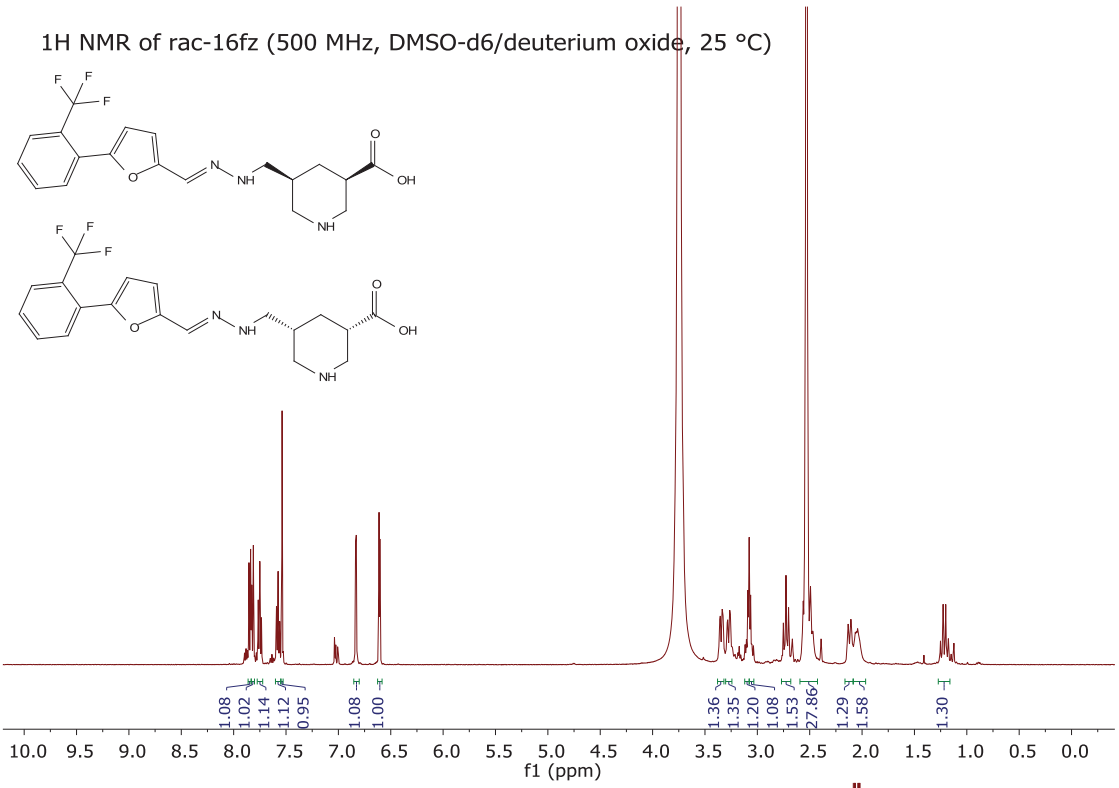
1H NMR of rac-16fz (500 MHz, DMSO-d6/deuterium oxide, 25 °C)
1.08
1.02
1.14
1.12
0.95
1.08
1.00
1.36
1.35
1.20
1.08
1.53
27.86
1.29
1.58
1.30
10.0 9.5 9.0 8.5 8.0 7.5 7.0 6.5 6.0 5.5 5.0 4.5 4.0 3.5 3.0 2.5 2.0 1.5 1.0 0.5 0.0
f1 (ppm)

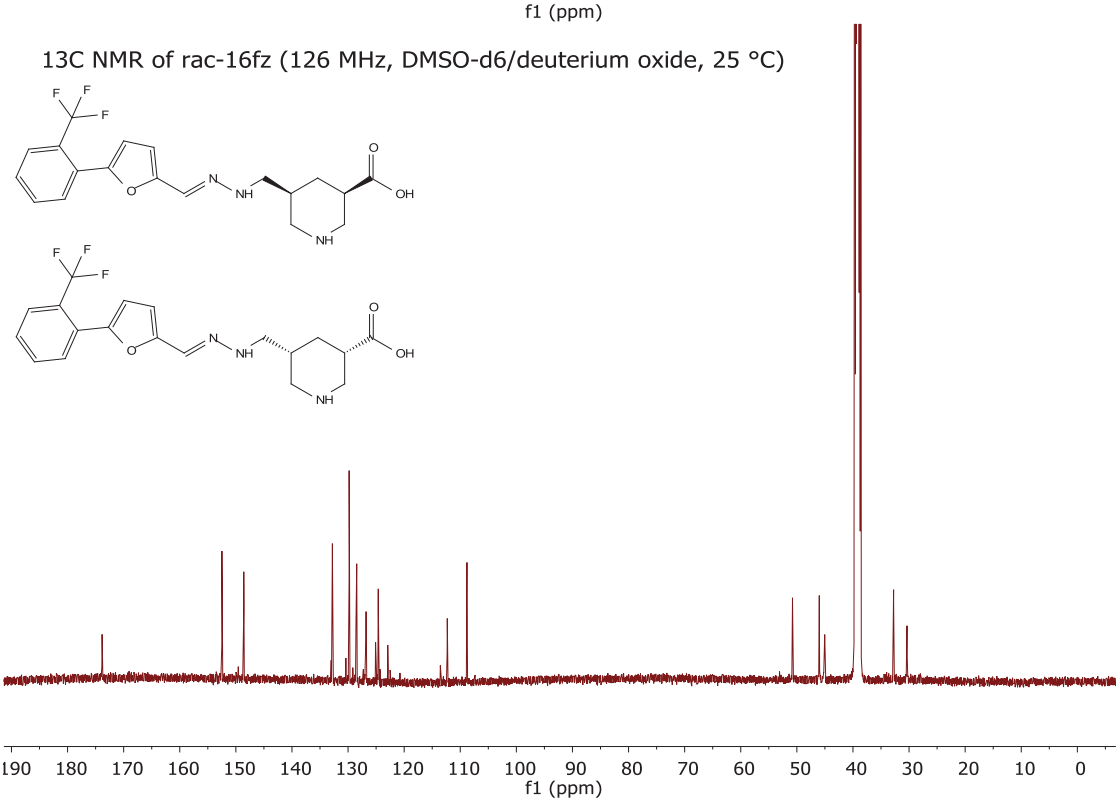
13C NMR of rac-16fz (126 MHz, DMSO-d6/deuterium oxide, 25 °C)
190 180 170 160 150 140 130 120 110 100 90 80 70 60 50 40 30 20 10 0
f1 (ppm)

1H NMR of rac-16ga (500 MHz, DMSO-d6/deuterium oxide, 25 °C)

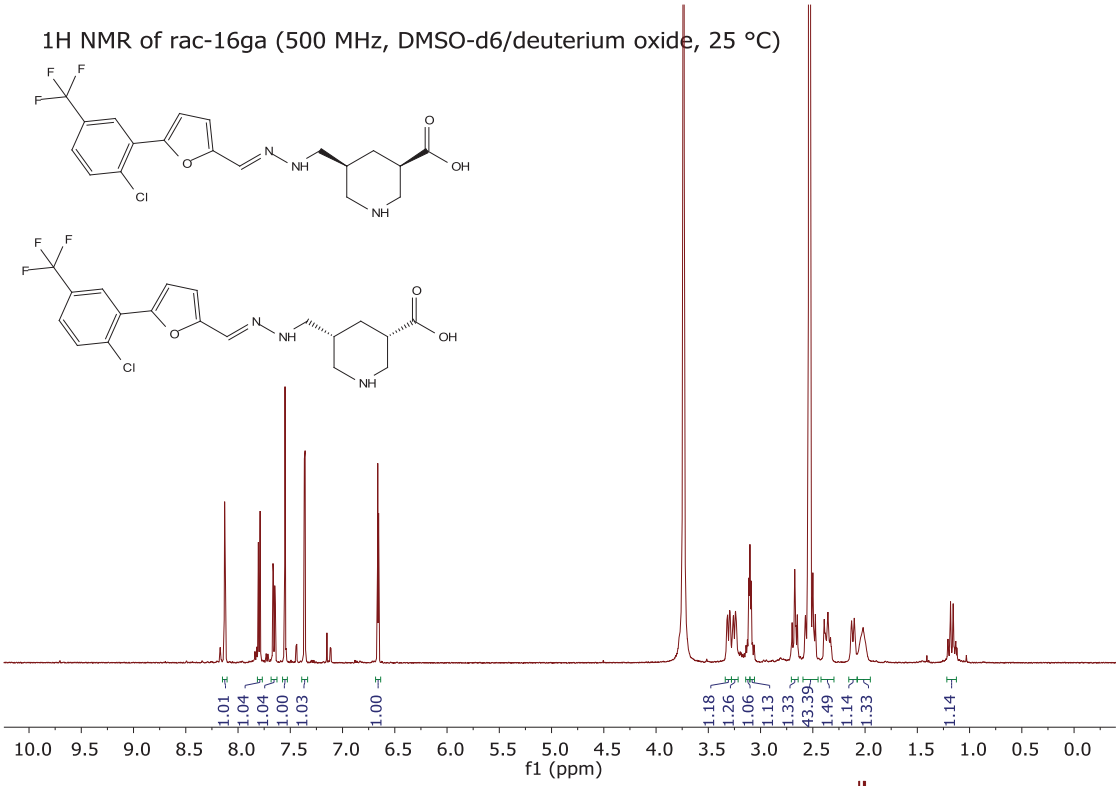

13C NMR of rac-16ga (126 MHz, DMSO-d6/deuterium oxide, 25 °C)

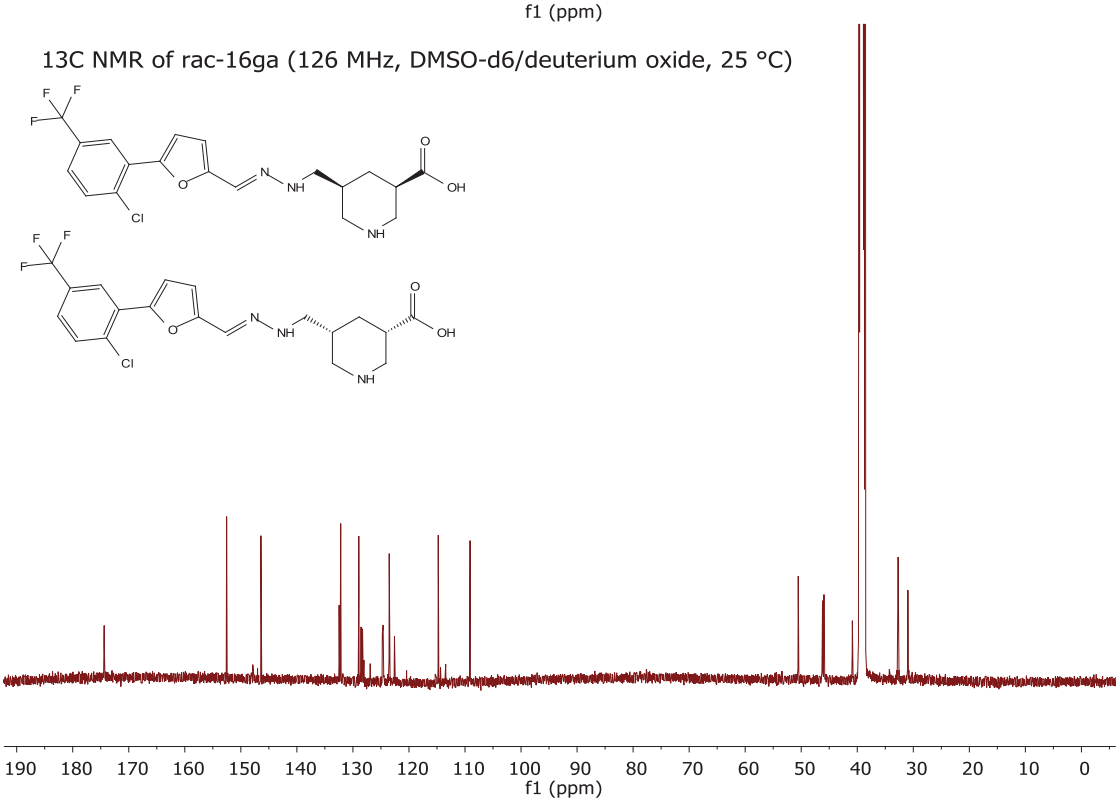

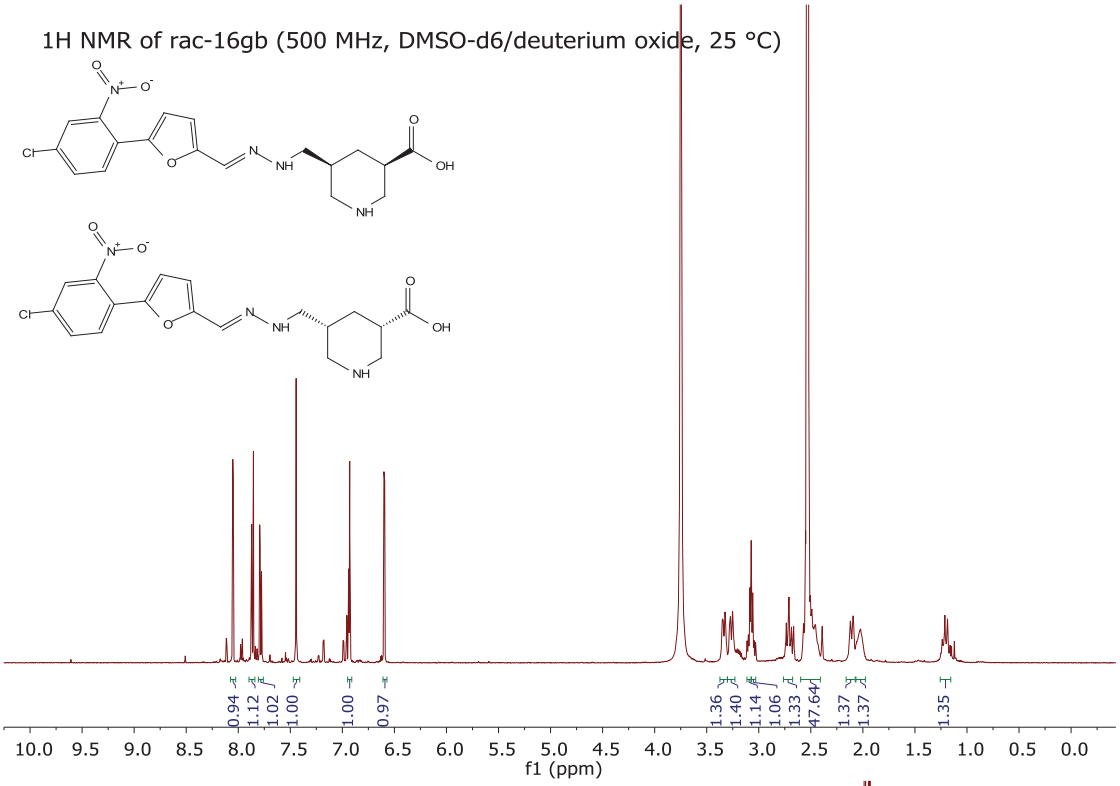
1H NMR of rac-16gb (500 MHz, DMSO-d6/deuterium oxide, 25 °C)
0.94
1.12
1.02
1.00
1.00
0.97
1.36
1.40
1.14
1.06
1.33
47.64
1.37
1.37
1.35
10.0 9.5 9.0 8.5 8.0 7.5 7.0 6.5 6.0 5.5 5.0 4.5 4.0 3.5 3.0 2.5 2.0 1.5 1.0 0.5 0.0
f1 (ppm)

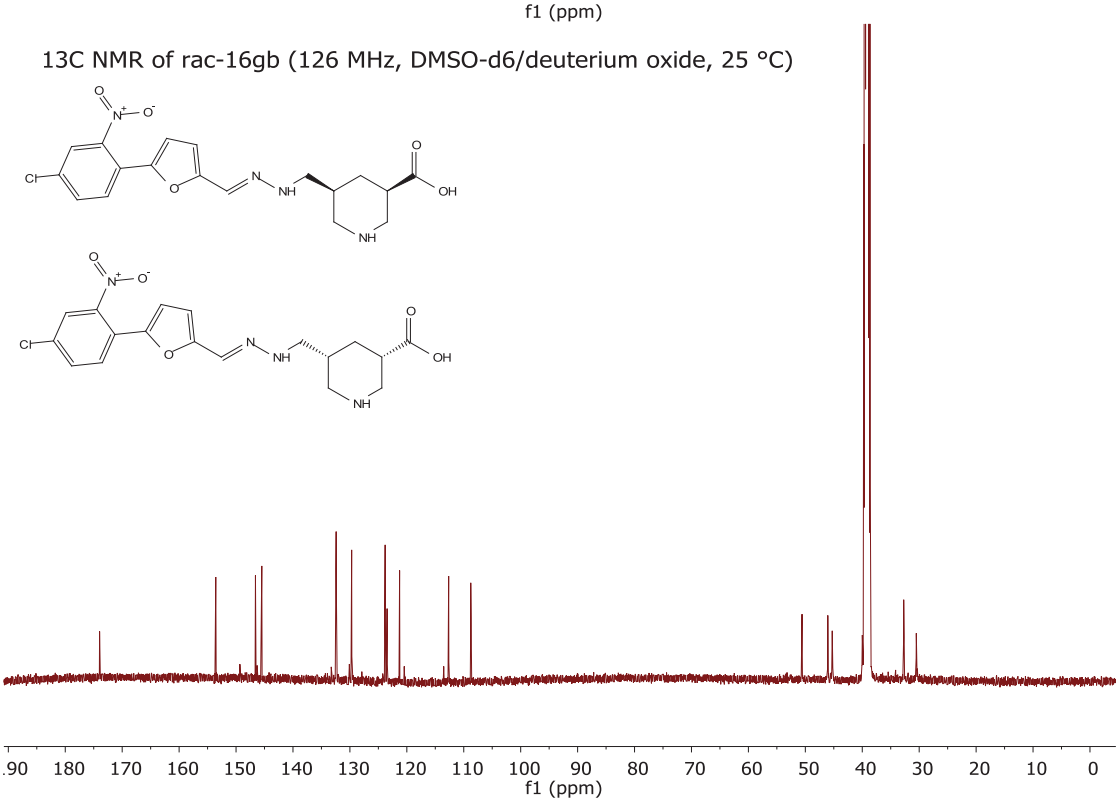
13C NMR of rac-16gb (126 MHz, DMSO-d6/deuterium oxide, 25 °C)
.90 180 170 160 150 140 130 120 110 100 90 80 70 60 50 40 30 20 10 0
f1 (ppm)

1H NMR of rac-16gc (500 MHz, DMSO-d6/deuterium oxide, 25 °C)

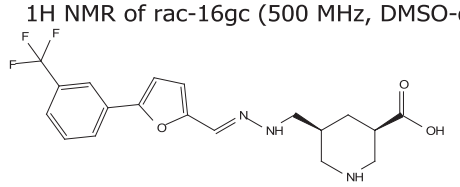

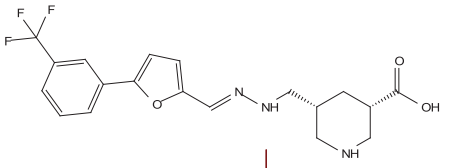

13C NMR of rac-16gc (126 MHz, DMSO-d6/deuterium oxide, 25 °C)

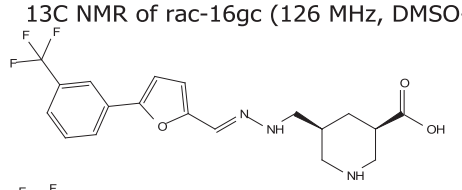

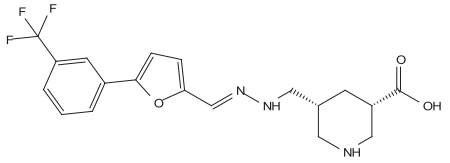

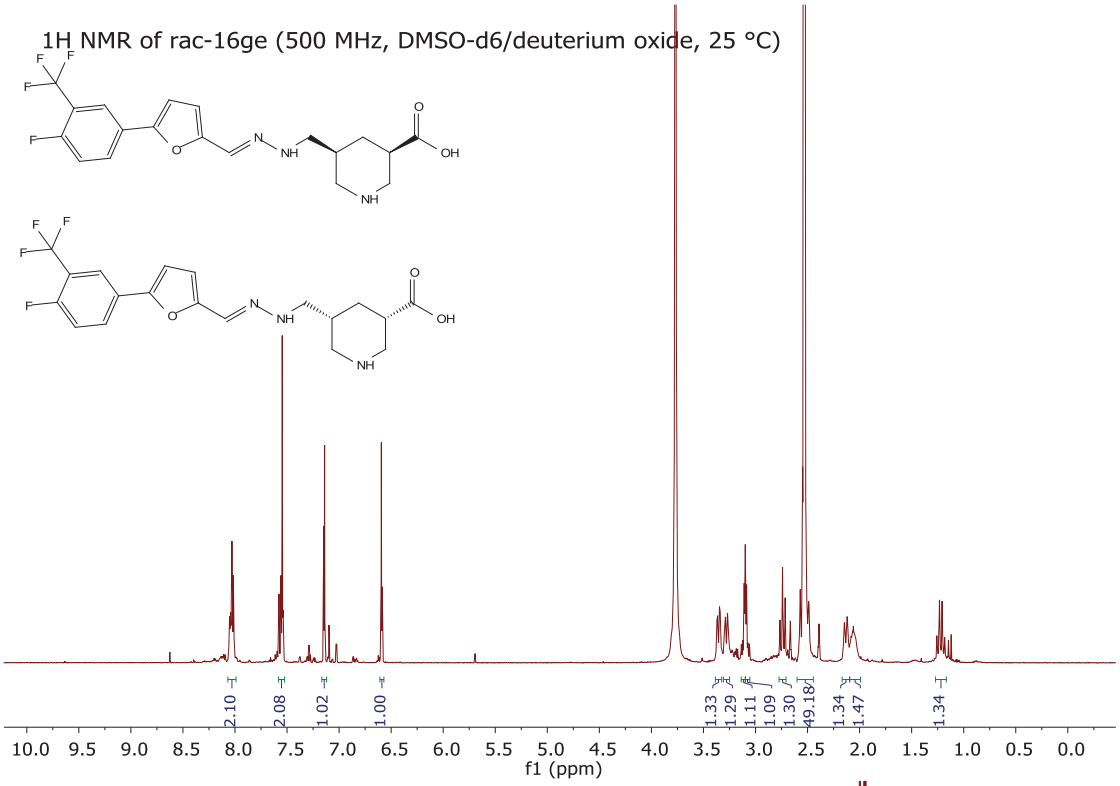
1H NMR of rac-16ge (500 MHz, DMSO-d6/deuterium oxide, 25 °C)
2.10
2.08
1.02
1.00
1.33
1.29
1.11
1.09
1.30
49.18
1.34
1.47
1.34
10.0 9.5 9.0 8.5 8.0 7.5 7.0 6.5 6.0 5.5 5.0 4.5 4.0 3.5 3.0 2.5 2.0 1.5 1.0 0.5 0.0
f1 (ppm)

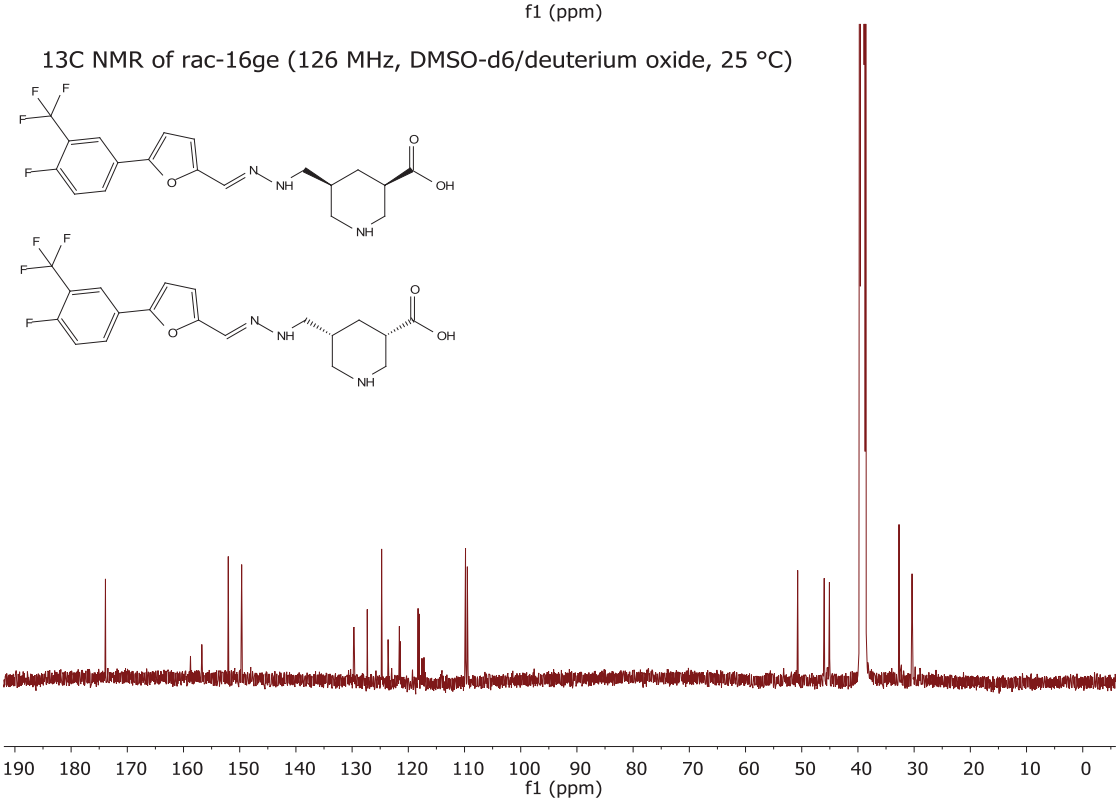
13C NMR of rac-16ge (126 MHz, DMSO-d6/deuterium oxide, 25 °C)
190 180 170 160 150 140 130 120 110 100 90 80 70 60 50 40 30 20 10 0
f1 (ppm)

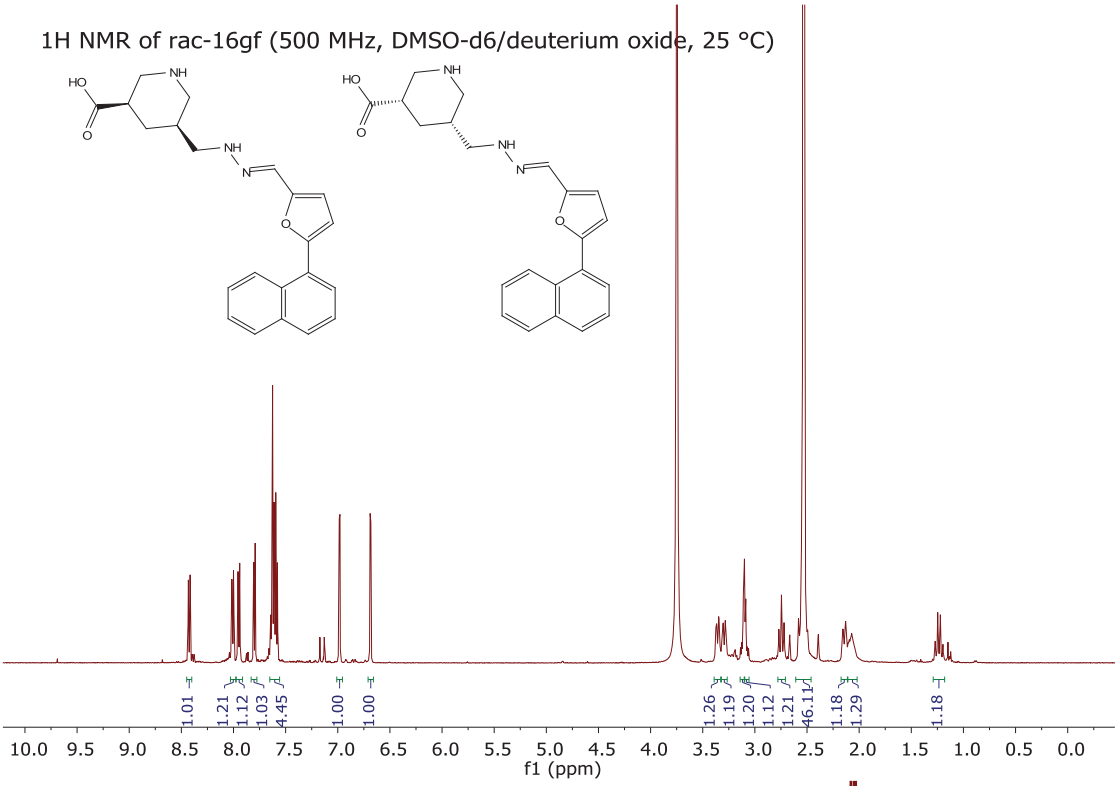
1H NMR of rac-16gf (500 MHz, DMSO-d6/deuterium oxide, 25 °C)
HO
O
NH
NH
N
O
1.01
1.21
1.12
1.03
4.45
1.00
1.00
1.26
1.19
1.20
1.12
1.21
46.11
1.18
1.29
1.18
10.0 9.5 9.0 8.5 8.0 7.5 7.0 6.5 6.0 5.5 5.0 4.5 4.0 3.5 3.0 2.5 2.0 1.5 1.0 0.5 0.0
f1 (ppm)

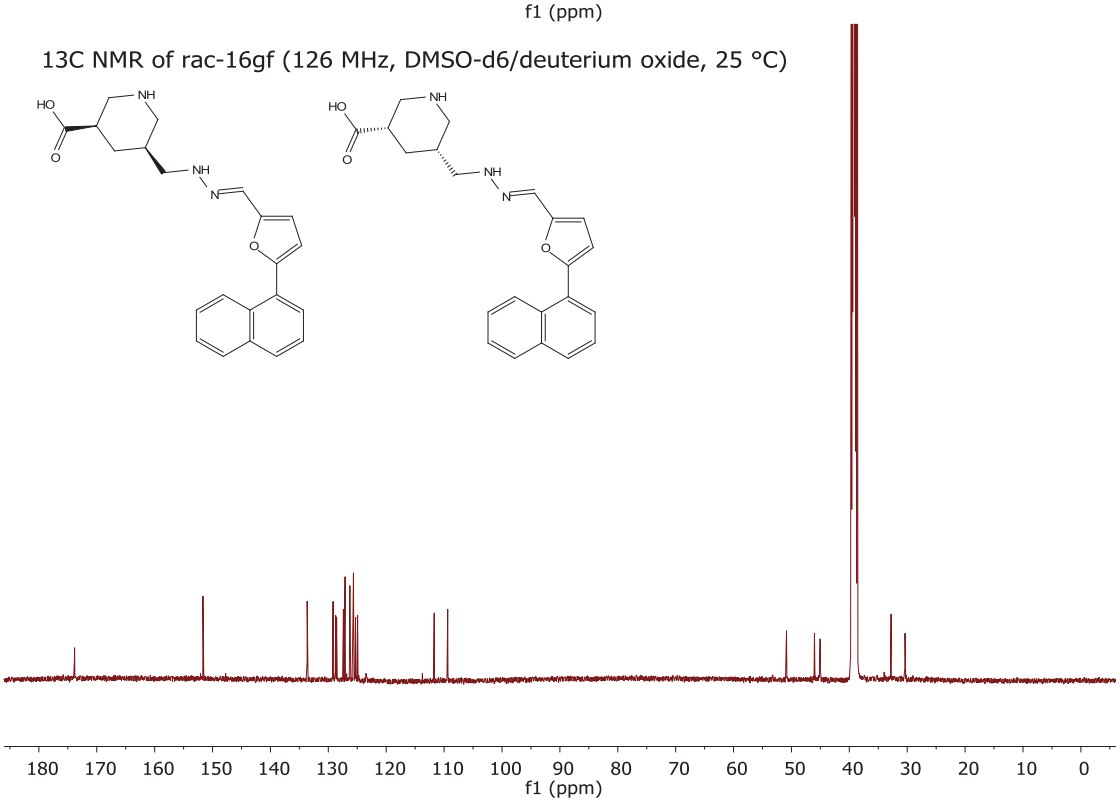
13C NMR of rac-16gf (126 MHz, DMSO-d6/deuterium oxide, 25 °C)
HO
O
NH
NH
N
O
180 170 160 150 140 130 120 110 100 90 80 70 60 50 40 30 20 10 0
f1 (ppm)

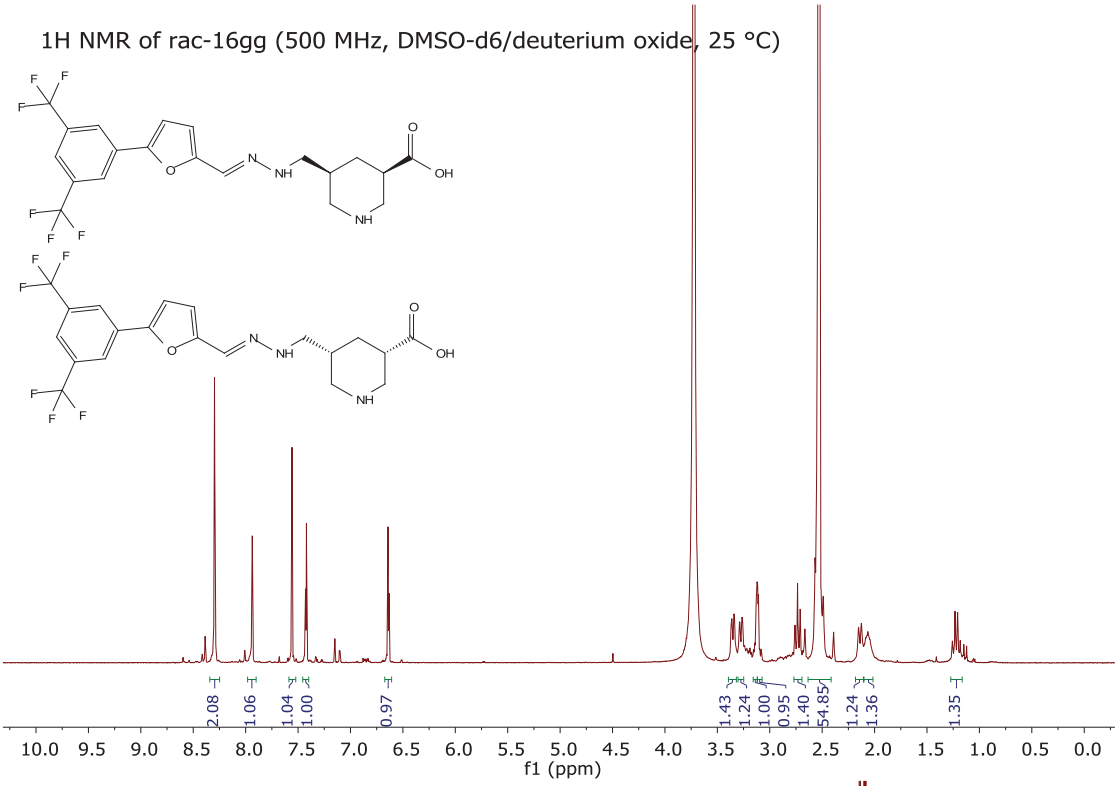
1H NMR of rac-16gg (500 MHz, DMSO-d6/deuterium oxide, 25 °C)
2.08
1.06
1.04
1.00
0.97
1.43
1.24
1.00
0.95
1.40
54.85
1.24
1.36
1.35
10.0 9.5 9.0 8.5 8.0 7.5 7.0 6.5 6.0 5.5 5.0 4.5 4.0 3.5 3.0 2.5 2.0 1.5 1.0 0.5 0.0
f1 (ppm)

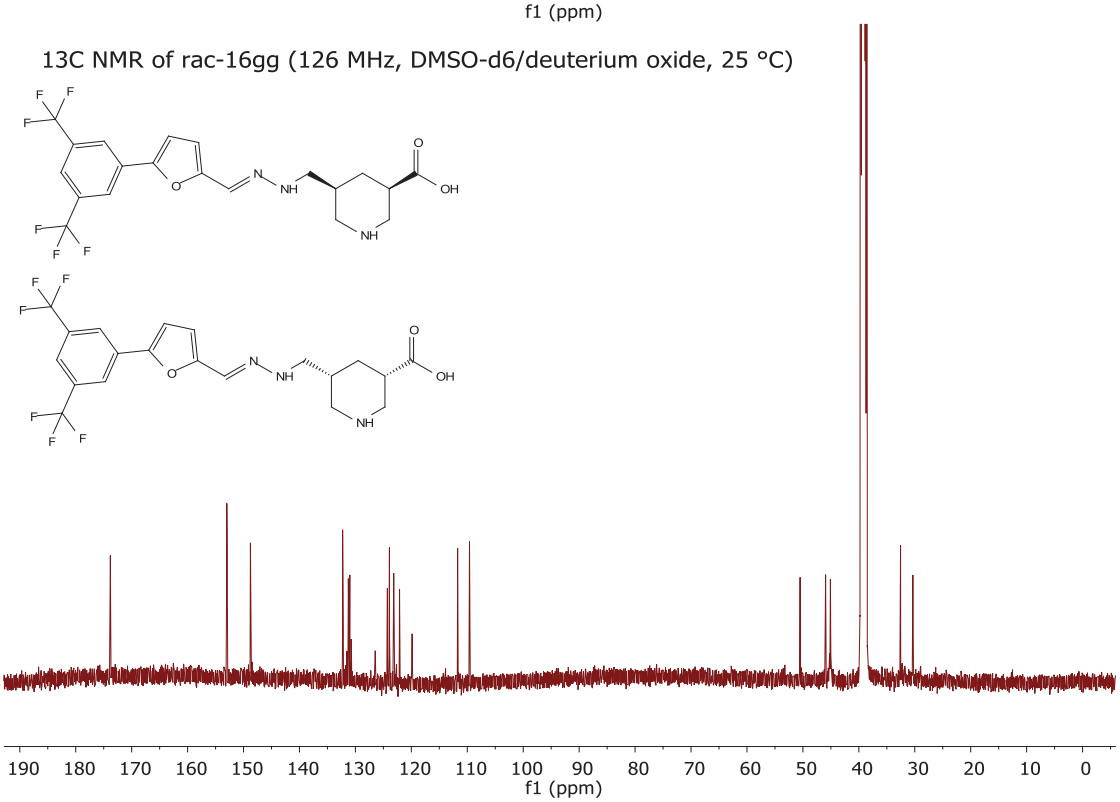
13C NMR of rac-16gg (126 MHz, DMSO-d6/deuterium oxide, 25 °C)
190 180 170 160 150 140 130 120 110 100 90 80 70 60 50 40 30 20 10 0
f1 (ppm)

1H NMR of rac-16gk (500 MHz, DMSO-d6/deuterium oxide, 25 °C)

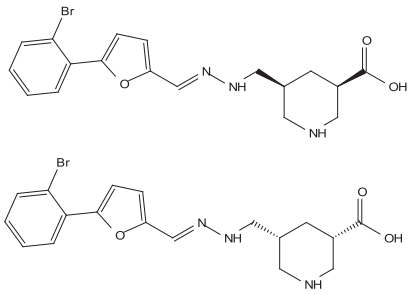

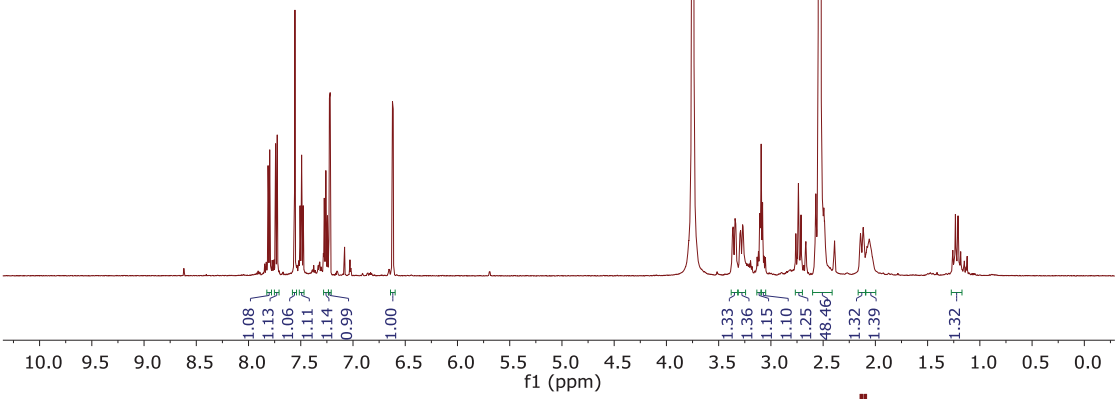

13C NMR of rac-16gk (126 MHz, DMSO-d6/deuterium oxide, 25 °C)

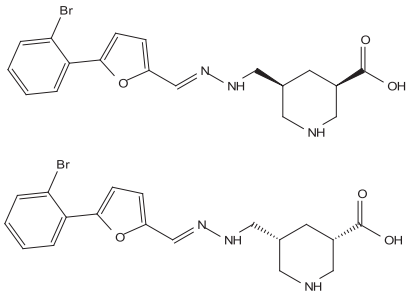

1H NMR of rac-16ho (500 MHz, DMSO-d6/deuterium oxide, 25 °C)

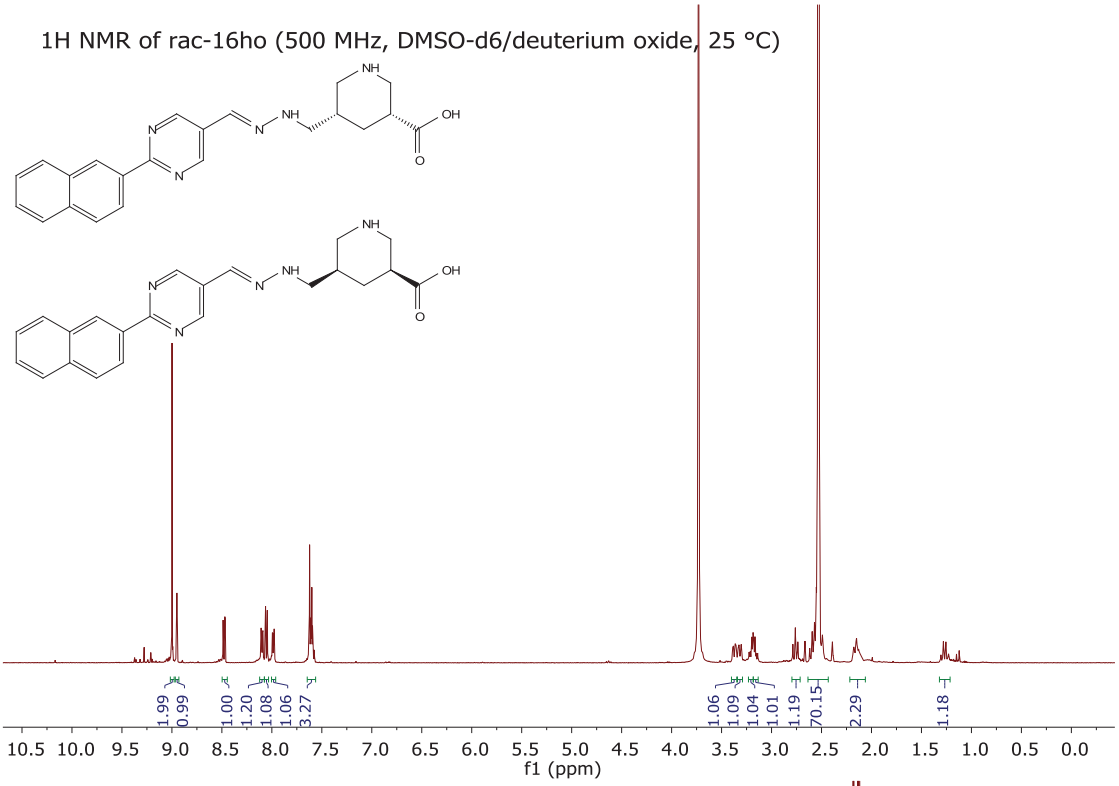

13C NMR of rac-16ho (126 MHz, DMSO-d6/deuterium oxide, 25 °C)

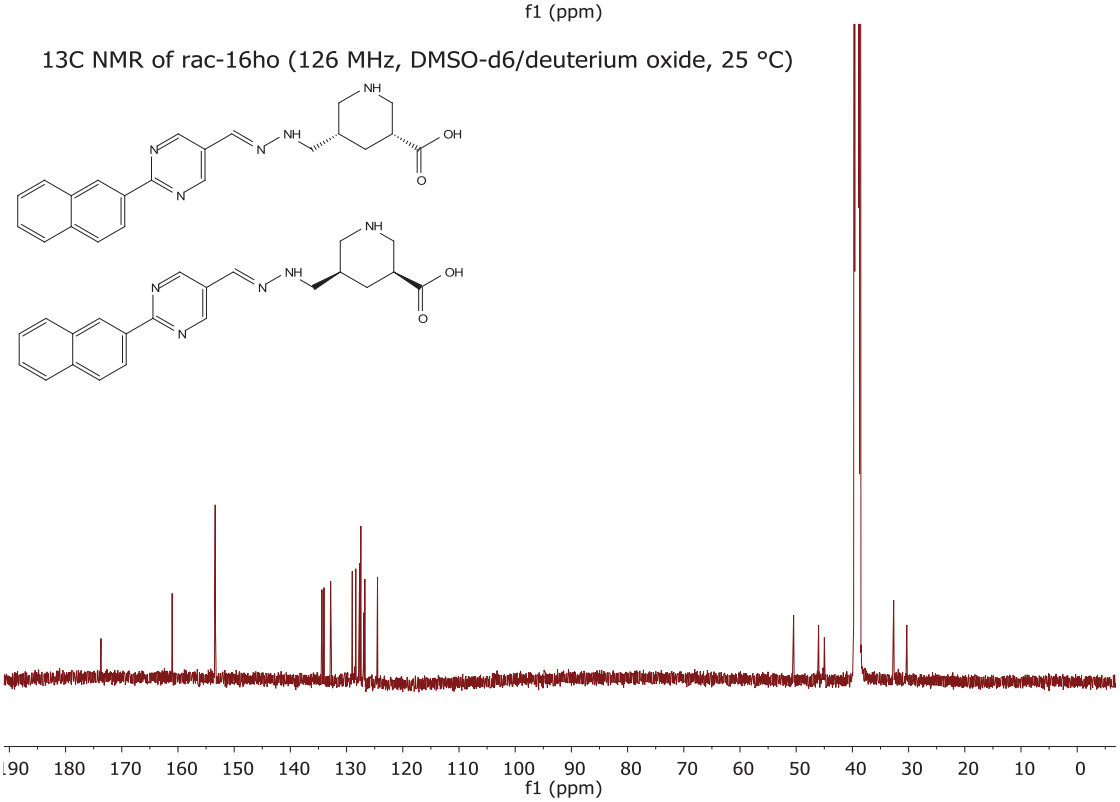

1H NMR of rac-18e (500 MHz, DMSO-d6/deuterium oxide, 25 °C)

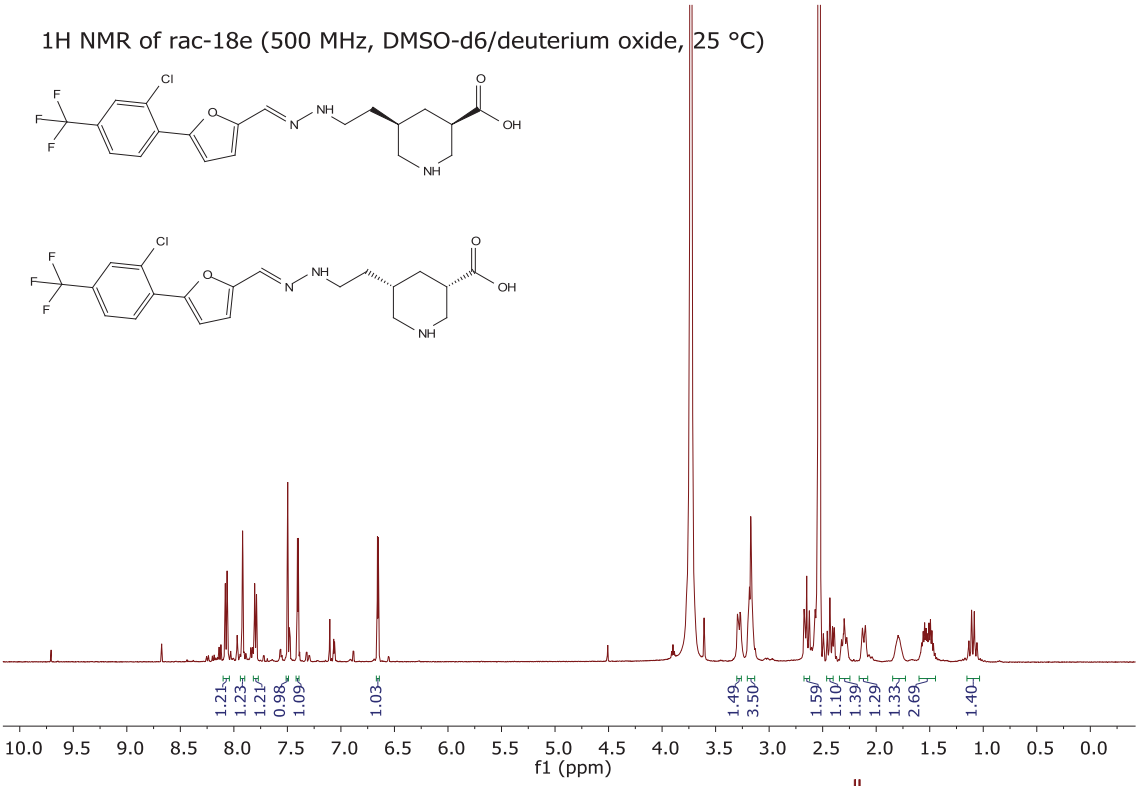

13C NMR of rac-18e (126 MHz, DMSO-d6/deuterium oxide, 25 °C)

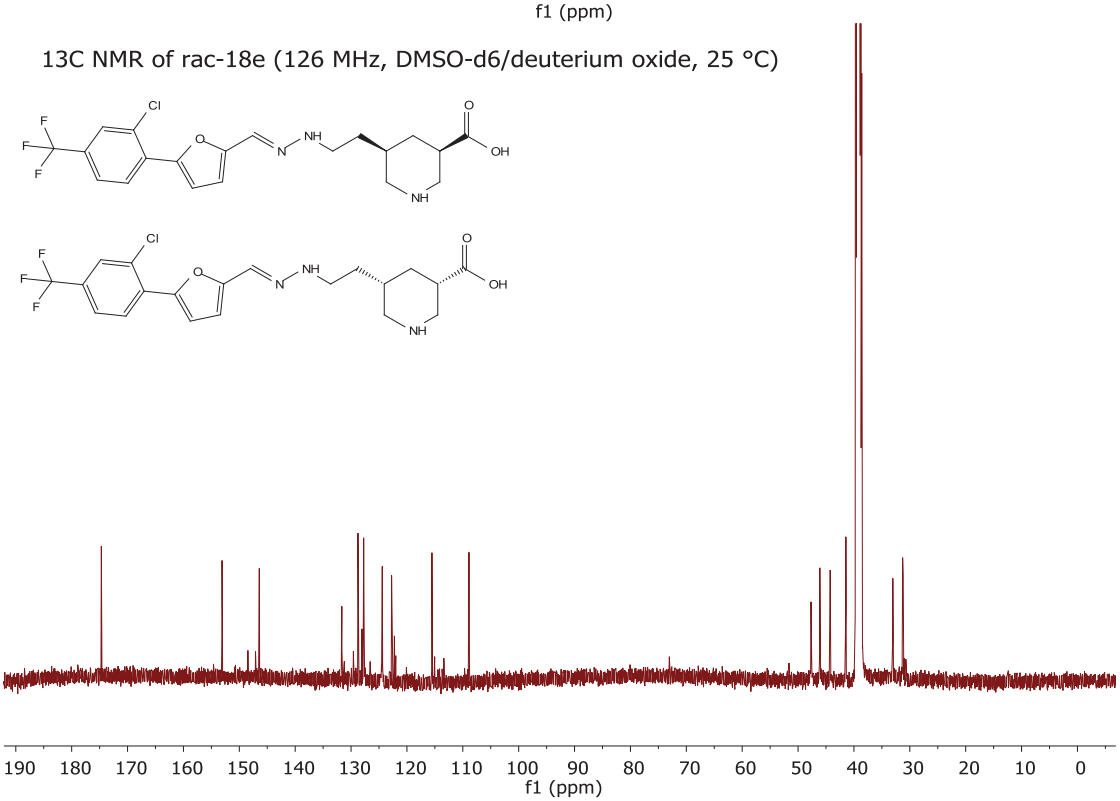

1H NMR of rac-18fy (500 MHz, DMSO-d6/deuterium oxide, 25 °C)

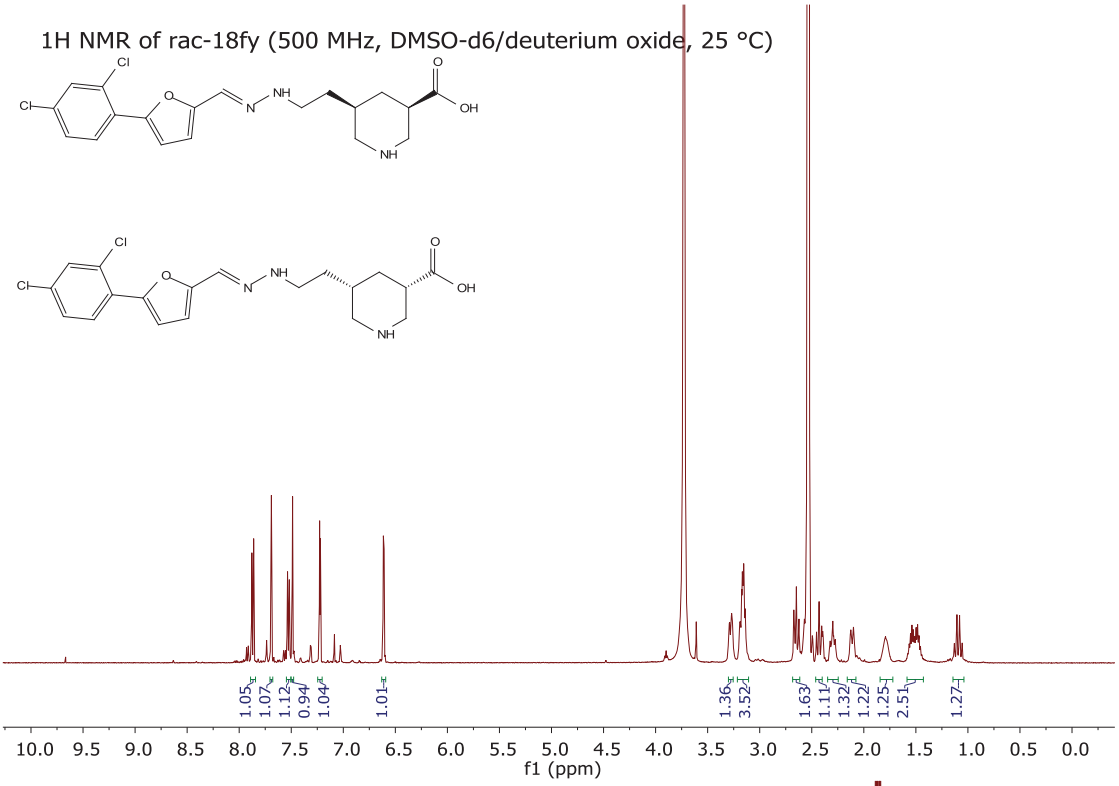

13C NMR of rac-18fy (126 MHz, DMSO-d6/deuterium oxide, 25 °C)

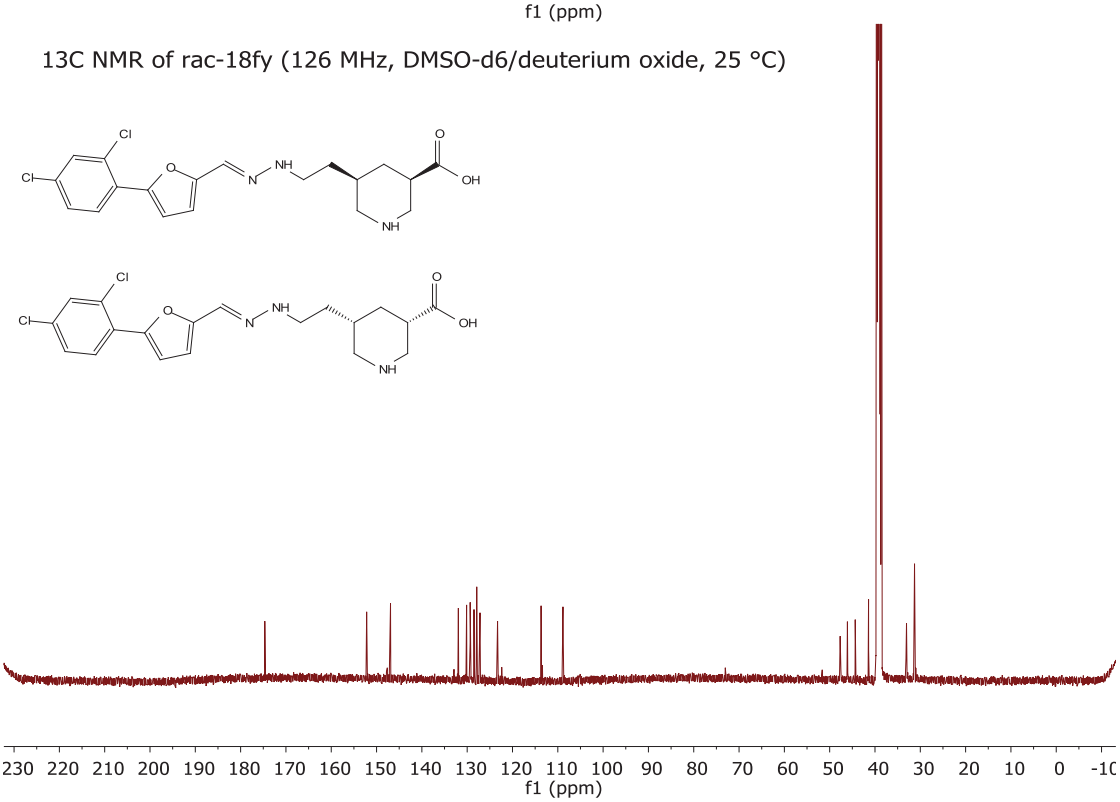

1H NMR of 15fd (400 MHz, chloroform-d, 25 °C)

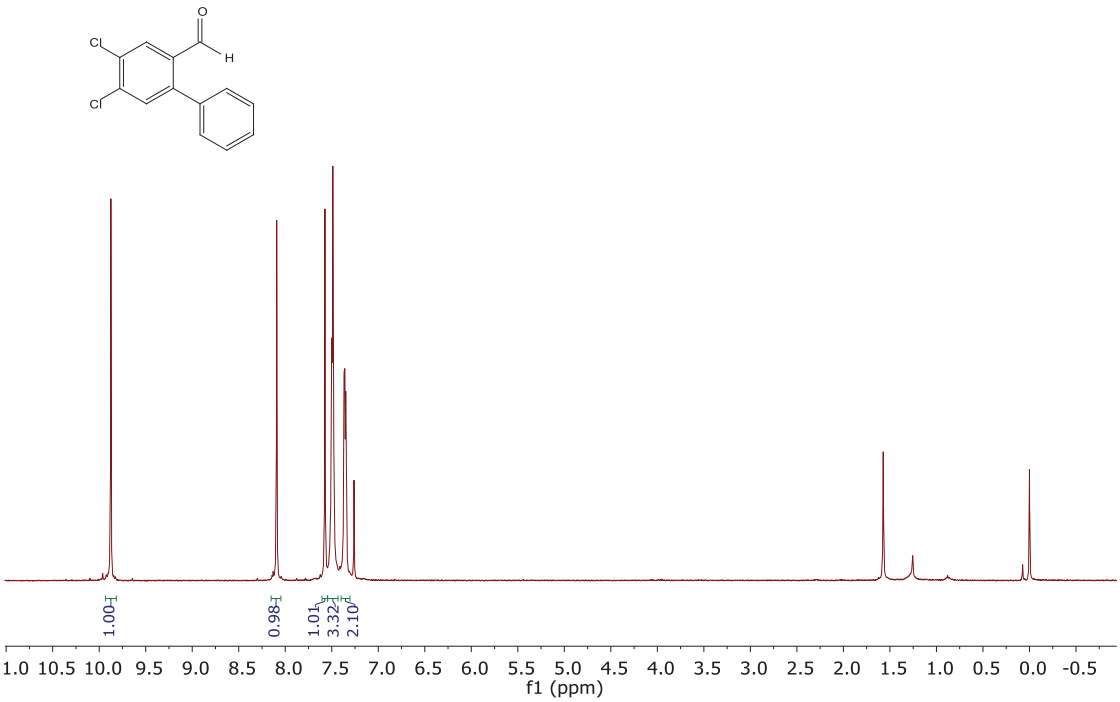

13C NMR of 15fd (101 MHz, chloroform-d, 25 °C)

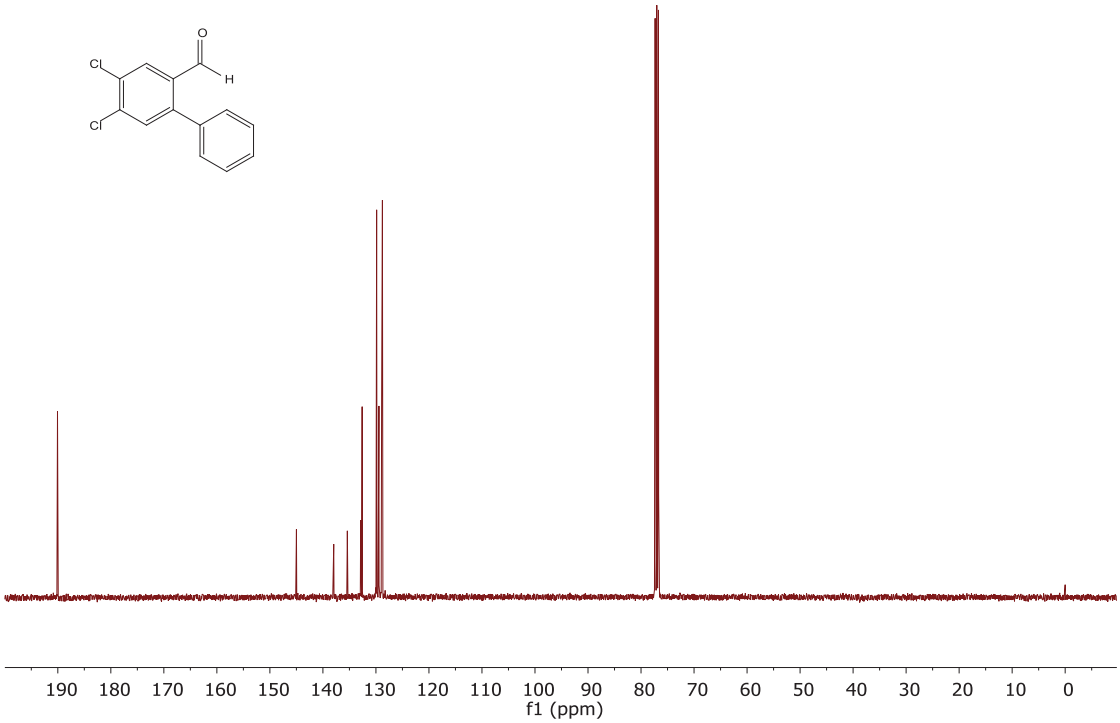

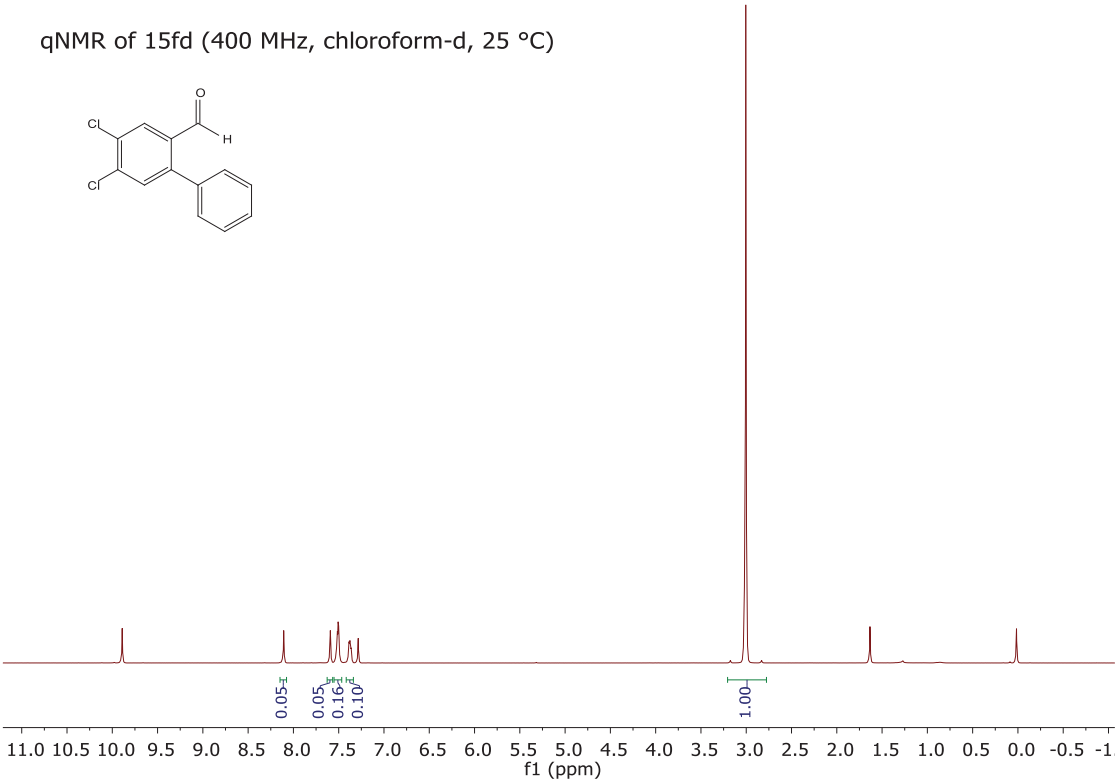

For the purity determination the sample weight was 5.219 mg and the assumed molecular weight 251.11 g/mol. Dimethyl sulfone was used as internal calibrant with a weight of 6.034 mg, a molecular weight of 94.3 g/mol and a purity of 99.73%. A purity of 95.6% was calculated for the sample using the MestReNova NMR software.

1H NMR of 15ff (500 MHz, dichloromethane-d2, 25 °C)

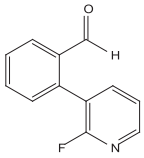

13C NMR of 15ff (126 MHz, dichloromethane-d2, 25 °C)

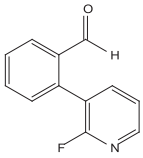

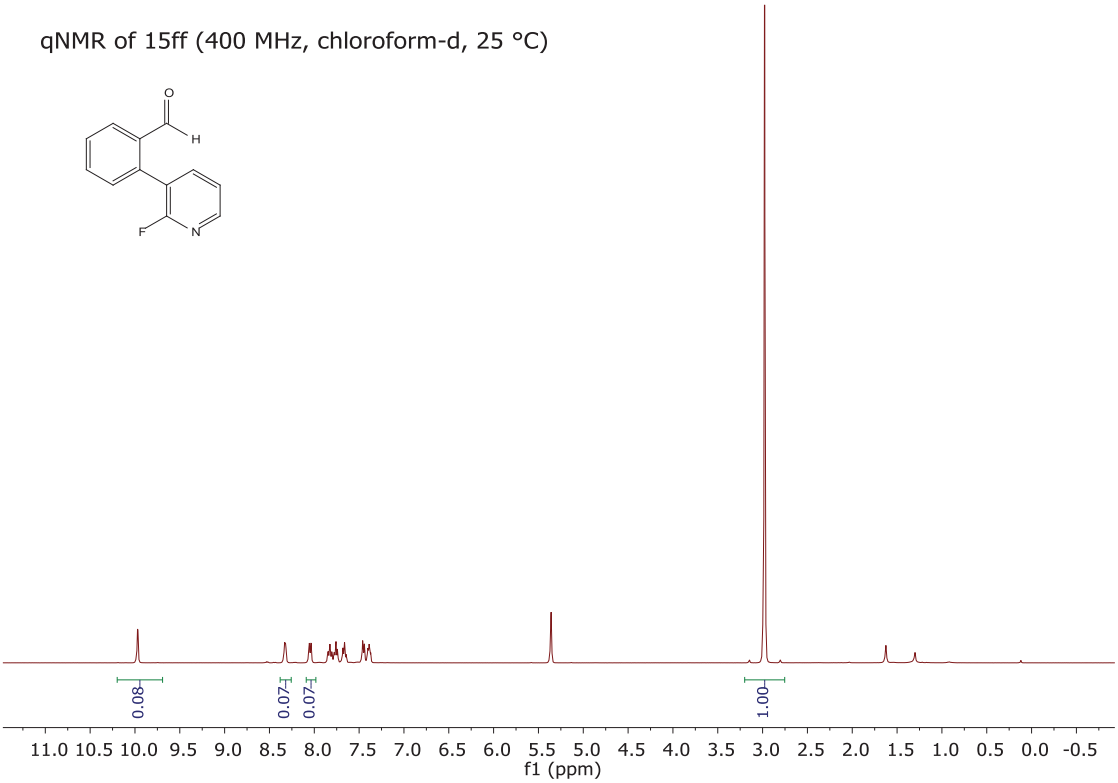

For the purity determination the sample weight was 5.576 mg and the assumed molecular weight 201.2 g/mol. Dimethyl sulfone was used as internal calibrant with a weight of 5.462 mg, a molecular weight of 94.3 g/mol and a purity of 99.73%. A purity of 97.3% was calculated for the sample using the MestReNova NMR software.

1H NMR of 15fh (400 MHz, dichloromethane-d2, 25 °C)

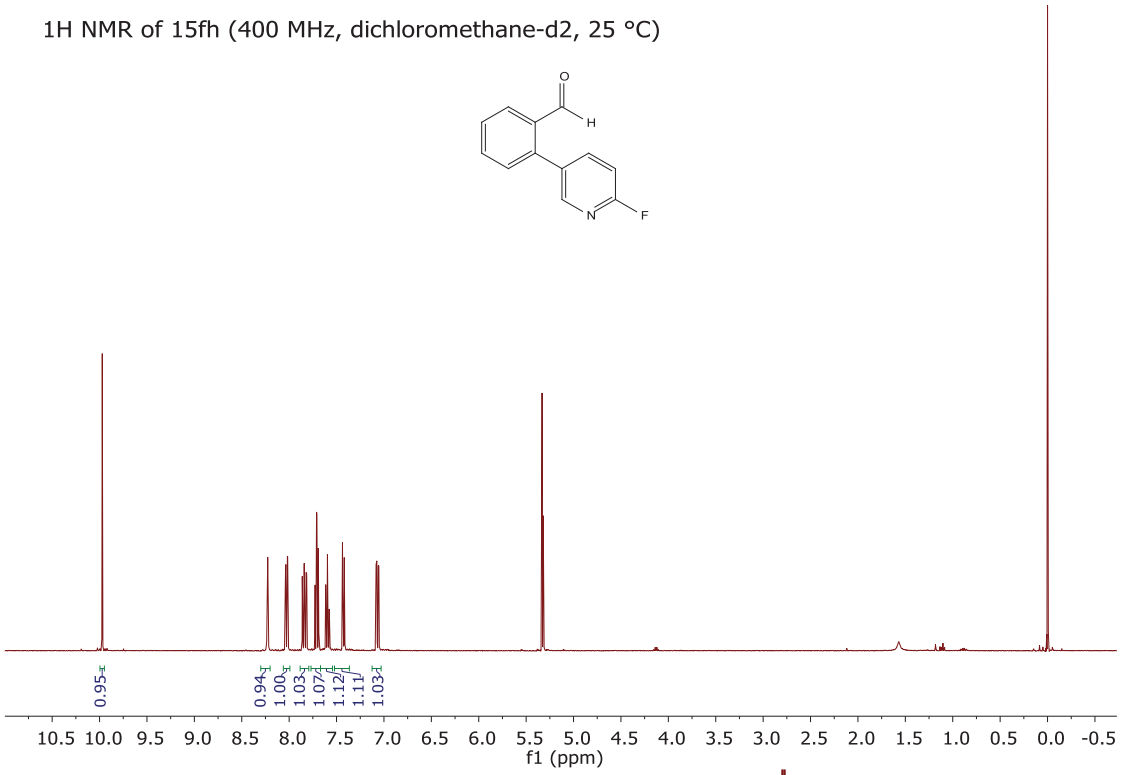

13C NMR of 15fh (101 MHz, dichloromethane-d2, 25 °C)

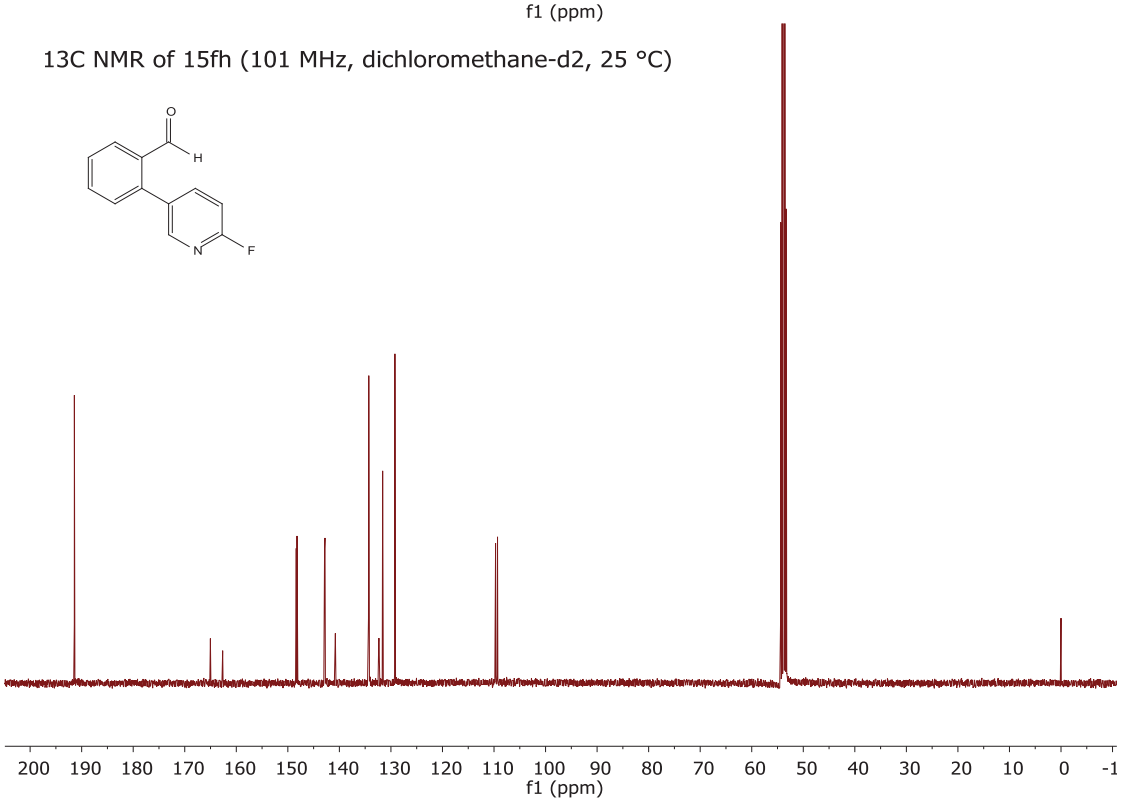

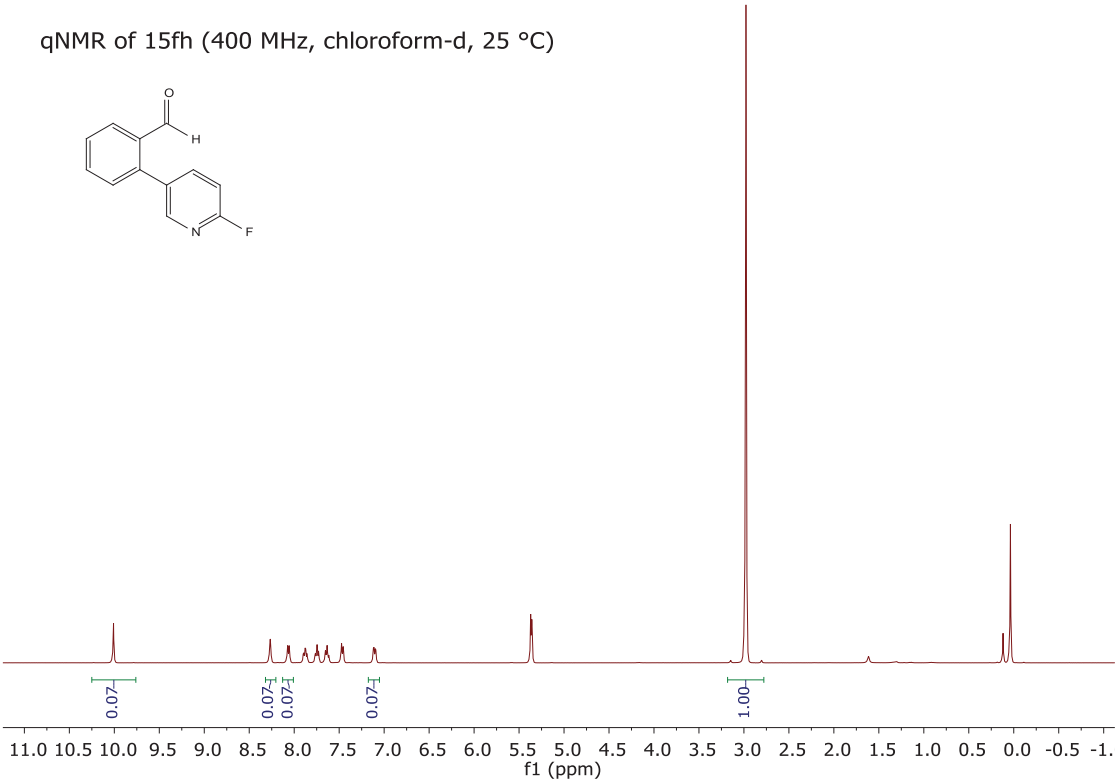

For the purity determination the sample weight was 5.050 mg and the assumed molecular weight 201.2 g/mol. Dimethyl sulfone was used as internal calibrant with a weight of 5.173 mg, a molecular weight of 94.3 g/mol and a purity of 99.73%. A purity of 96.3% was calculated for the sample using the MestReNova NMR software.

1H NMR of 15fi (400 MHz, dichloromethane-d2, 25 °C)

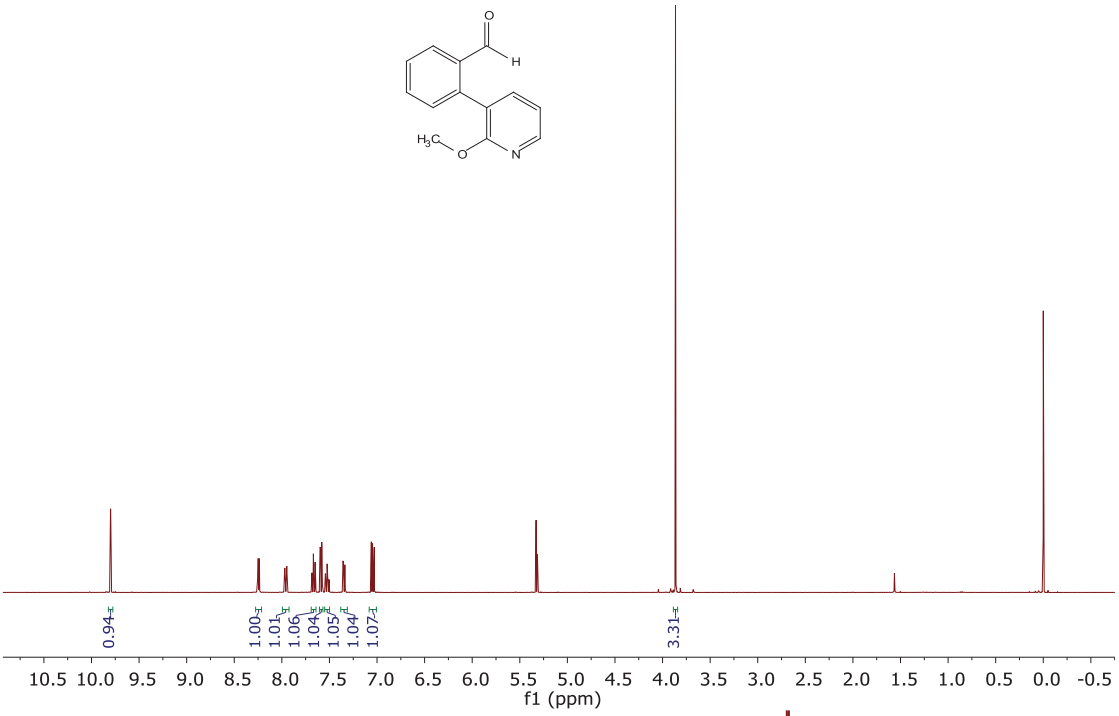

13C NMR of 15fi (101 MHz, dichloromethane-d2, 25 °C)

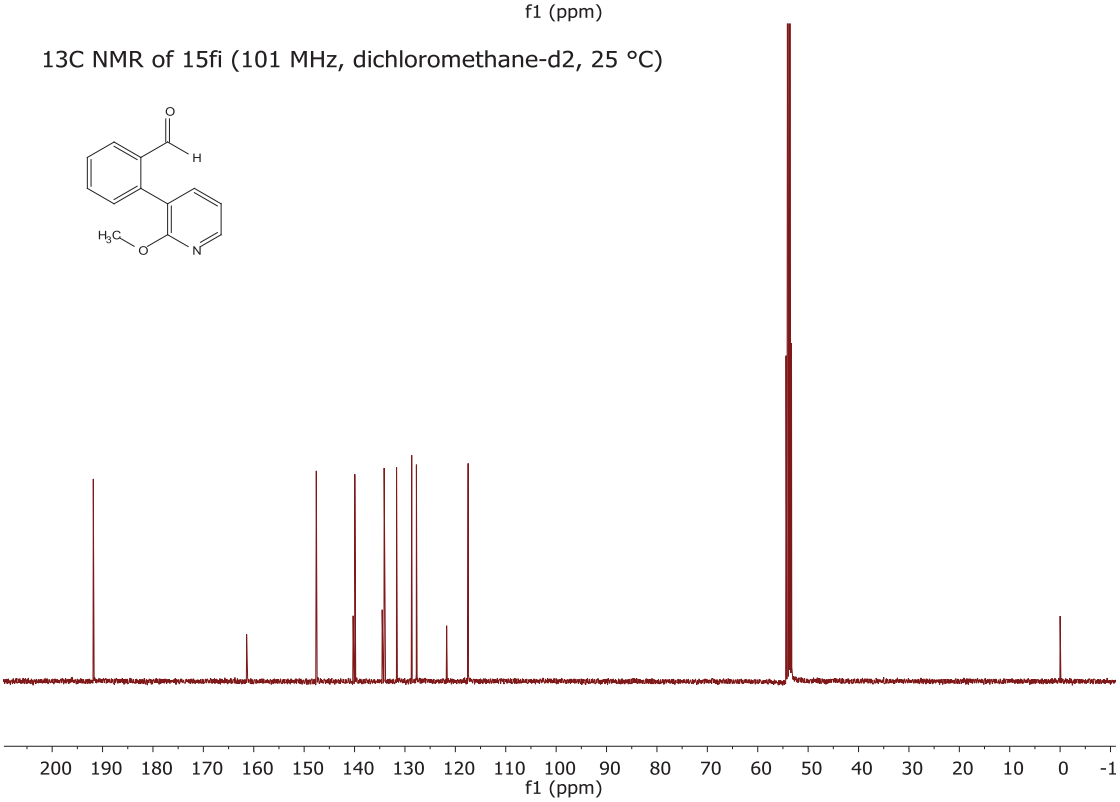

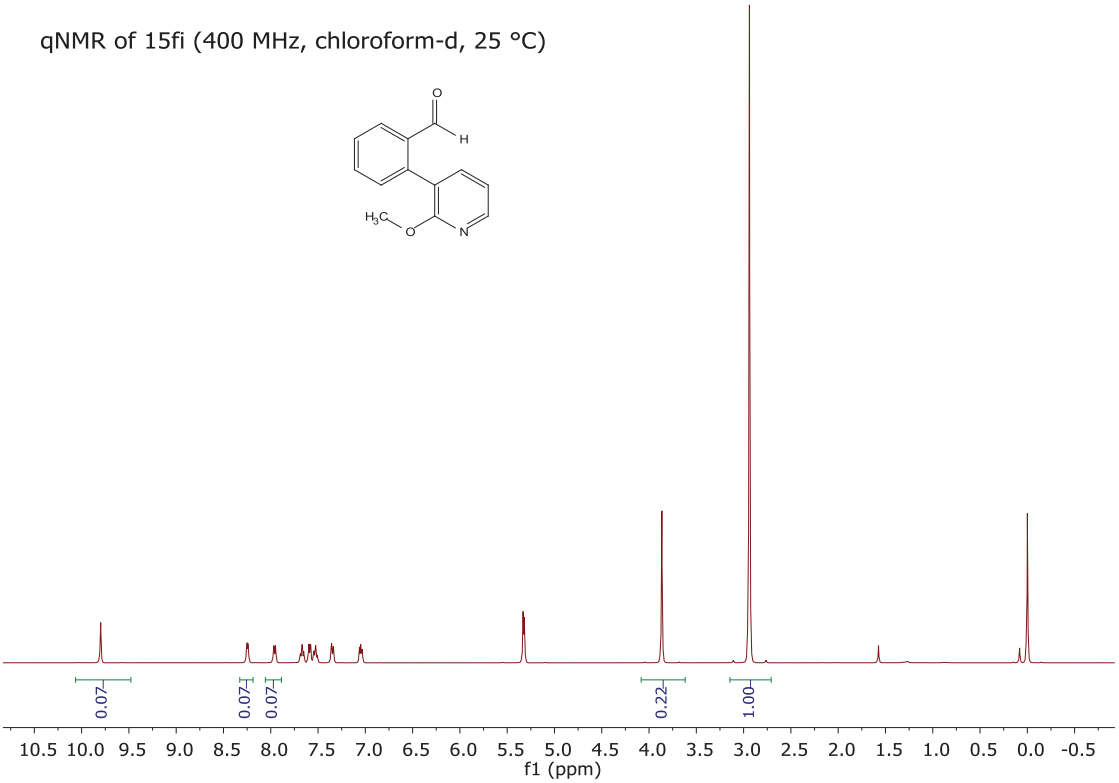

For the purity determination the sample weight was 5.359 mg and the assumed molecular weight 213.2 g/mol. Dimethyl sulfone was used as internal calibrant with a weight of 5.350 mg, a molecular weight of 94.3 g/mol and a purity of 99.73%. A purity of 99.5% was calculated for the sample using the MestReNova NMR software.

1H NMR of 15fn (500 MHz, dichloromethane-d2, 25 °C)

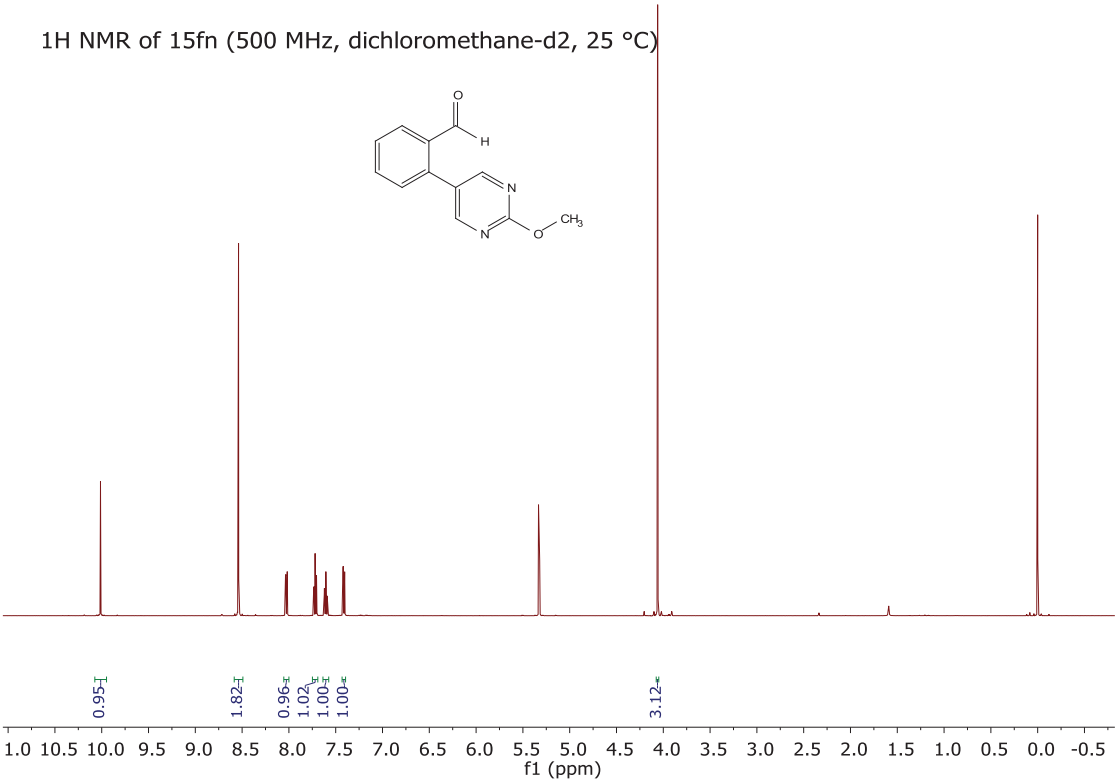

13C NMR of 15fn (126 MHz, dichloromethane-d2, 25 °C)

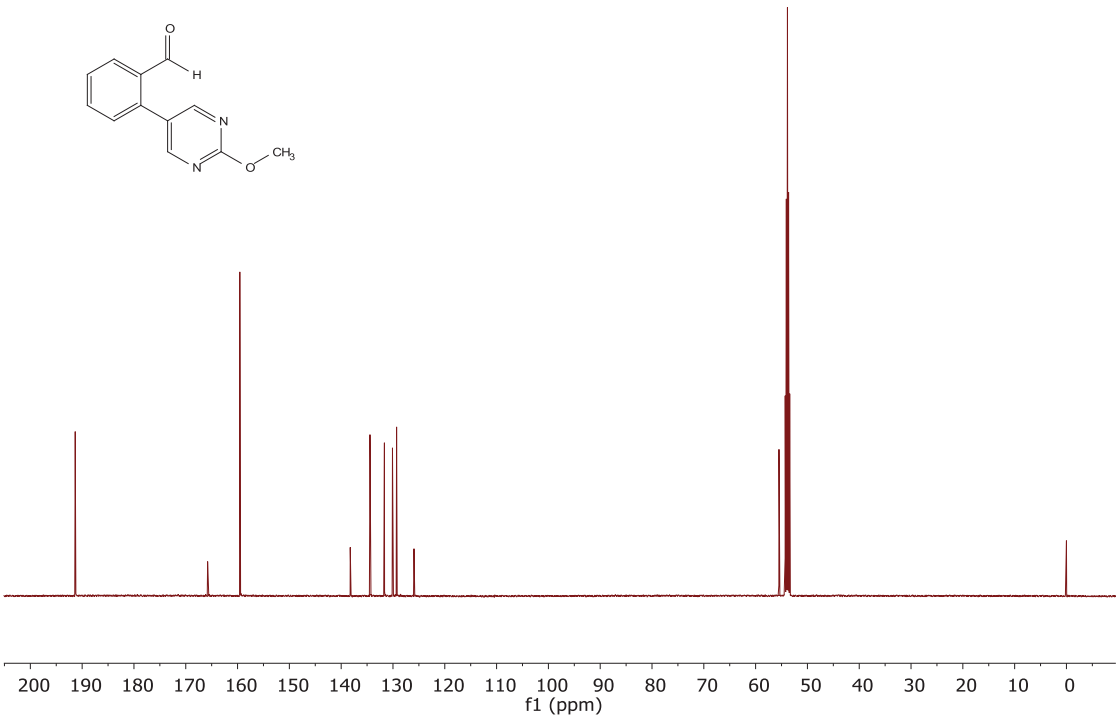

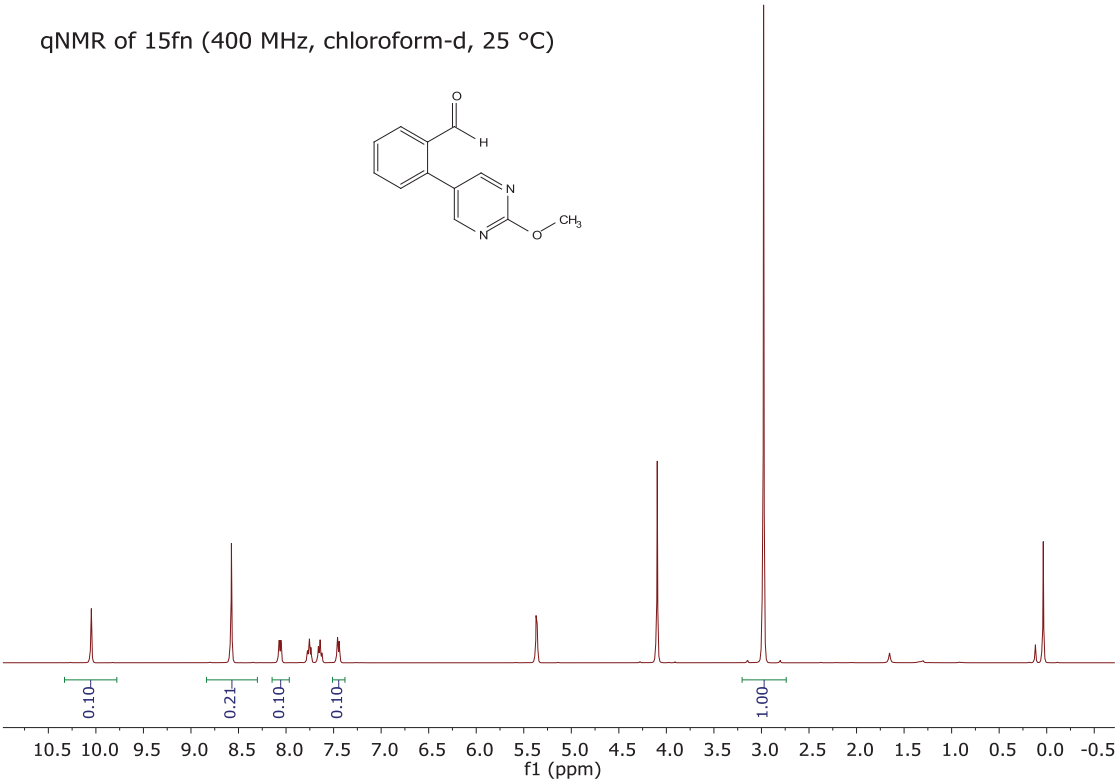

For the purity determination the sample weight was 7.818 mg and the assumed molecular weight 214.2 g/mol. Dimethyl sulfone was used as internal calibrant with a weight of 5.478 mg, a molecular weight of 94.3 g/mol and a purity of 99.73%. A purity of 98.2% was calculated for the sample using the MestReNova NMR software.

1H NMR of 15fp (500 MHz, dichloromethane-d2, 25 °C)

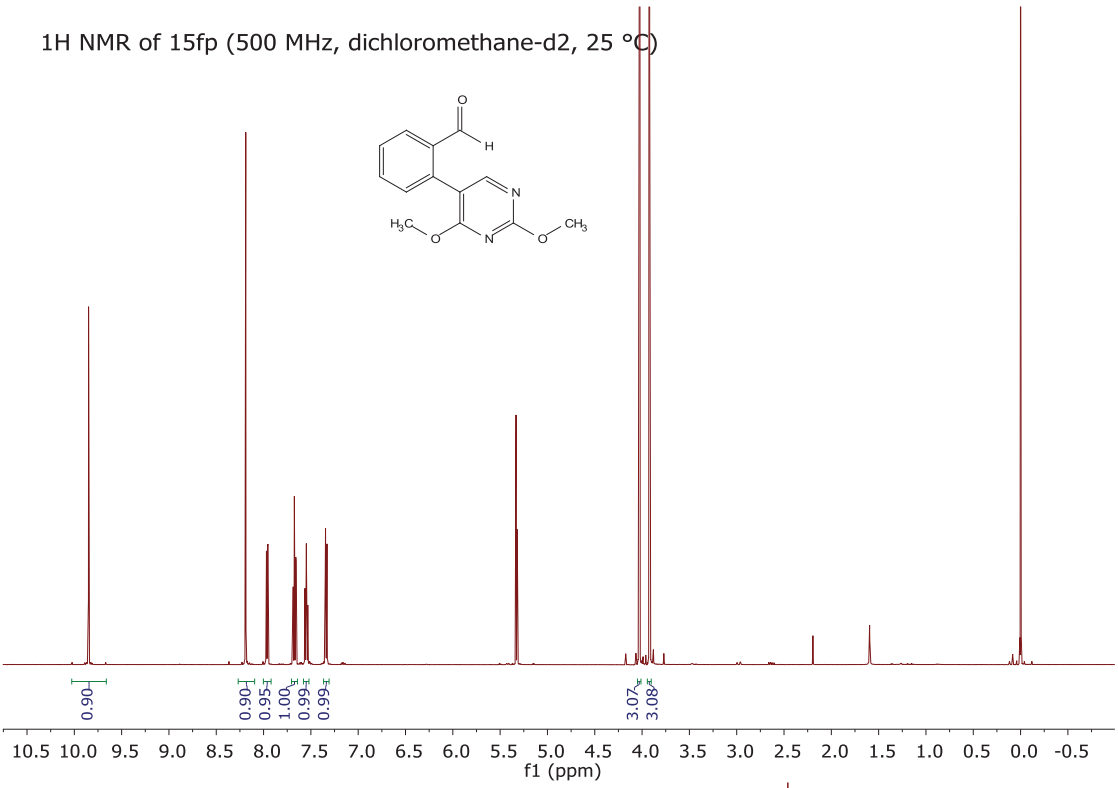

13C NMR of 15fp (126 MHz, dichloromethane-d2, 25 °C)

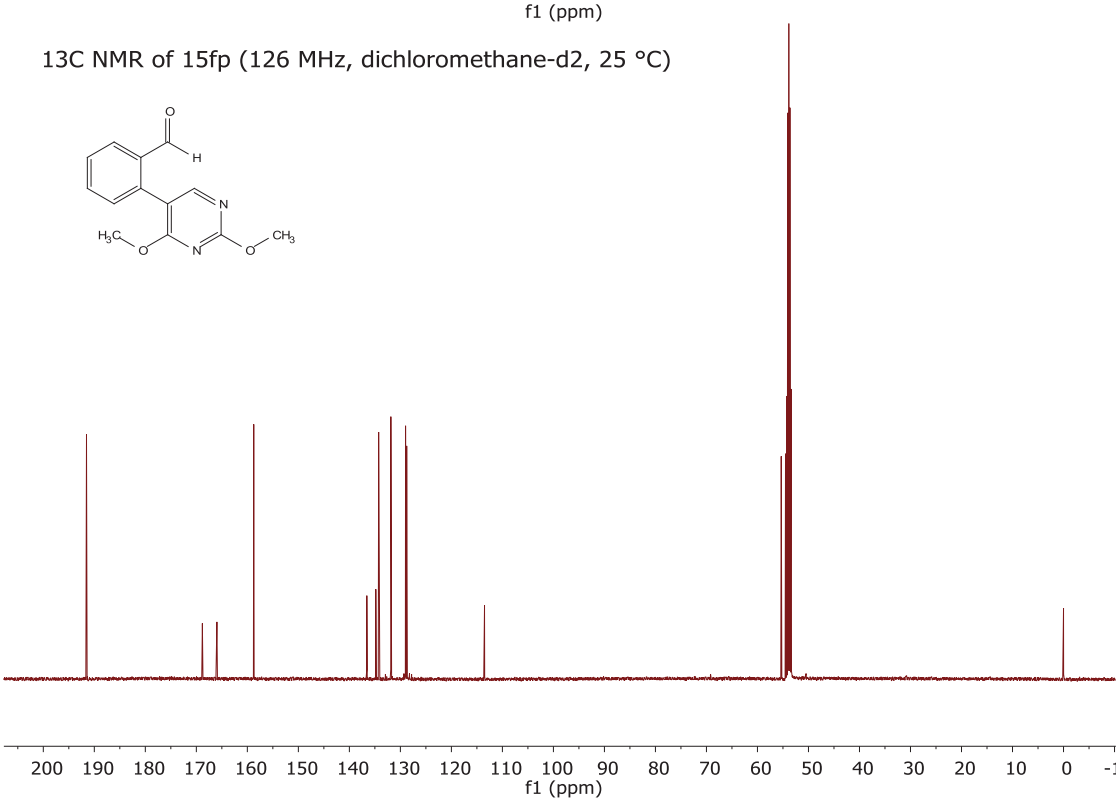

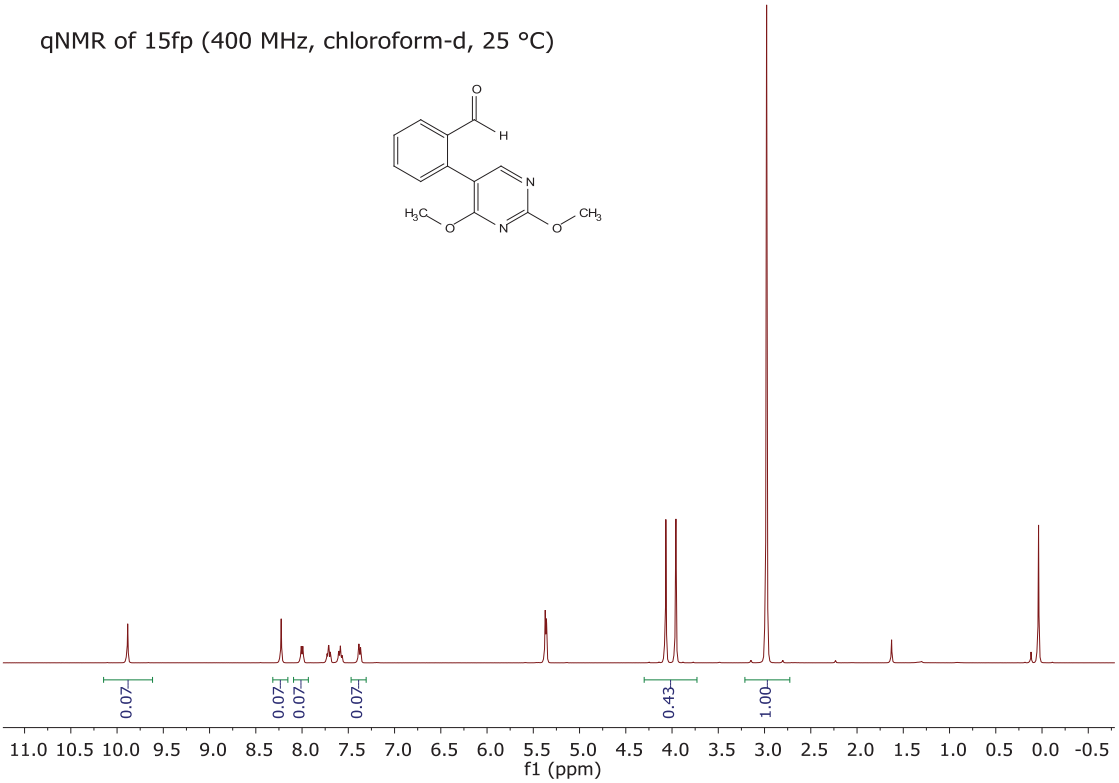

For the purity determination the sample weight was 5.882 mg and the assumed molecular weight 244.3 g/mol. Dimethyl sulfone was used as internal calibrant with a weight of 5.196 mg, a molecular weight of 94.3 g/mol and a purity of 99.73%. A purity of 97.5% was calculated for the sample using the MestReNova NMR software.

1H NMR of 15fs (500 MHz, chloroform-d, 25 °C)

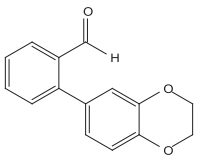

13C NMR of 15fs (126 MHz, chloroform-d, 25 °C)

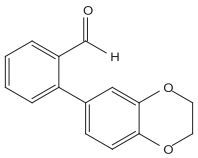

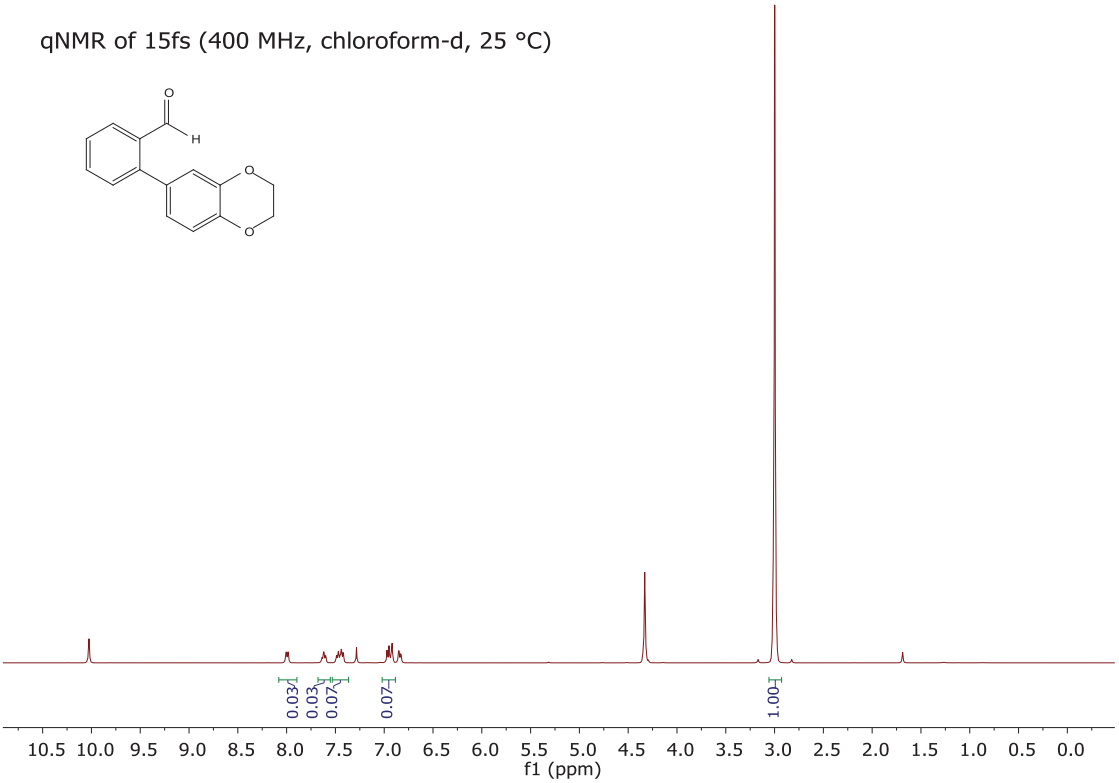

For the purity determination the sample weight was 5.715 mg and the assumed molecular weight 240.3 g/mol. Dimethyl sulfone was used as internal calibrant with a weight of 10.646 mg, a molecular weight of 94.3 g/mol and a purity of 99.73%. A purity of 97.7% was calculated for the sample using the MestReNova NMR software.

1H NMR of 15gr (400 MHz, DMSO-d6, 25 °C)

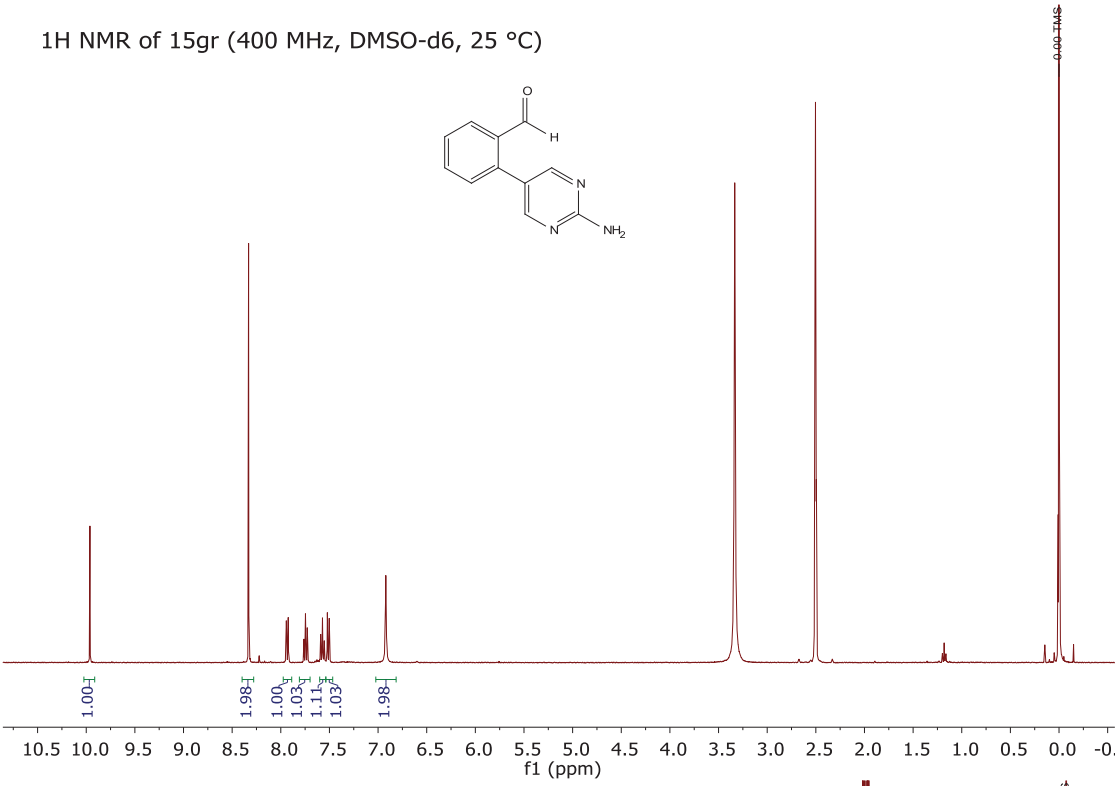

13C NMR of 15gr (101 MHz, DMSO-d6, 25 °C)

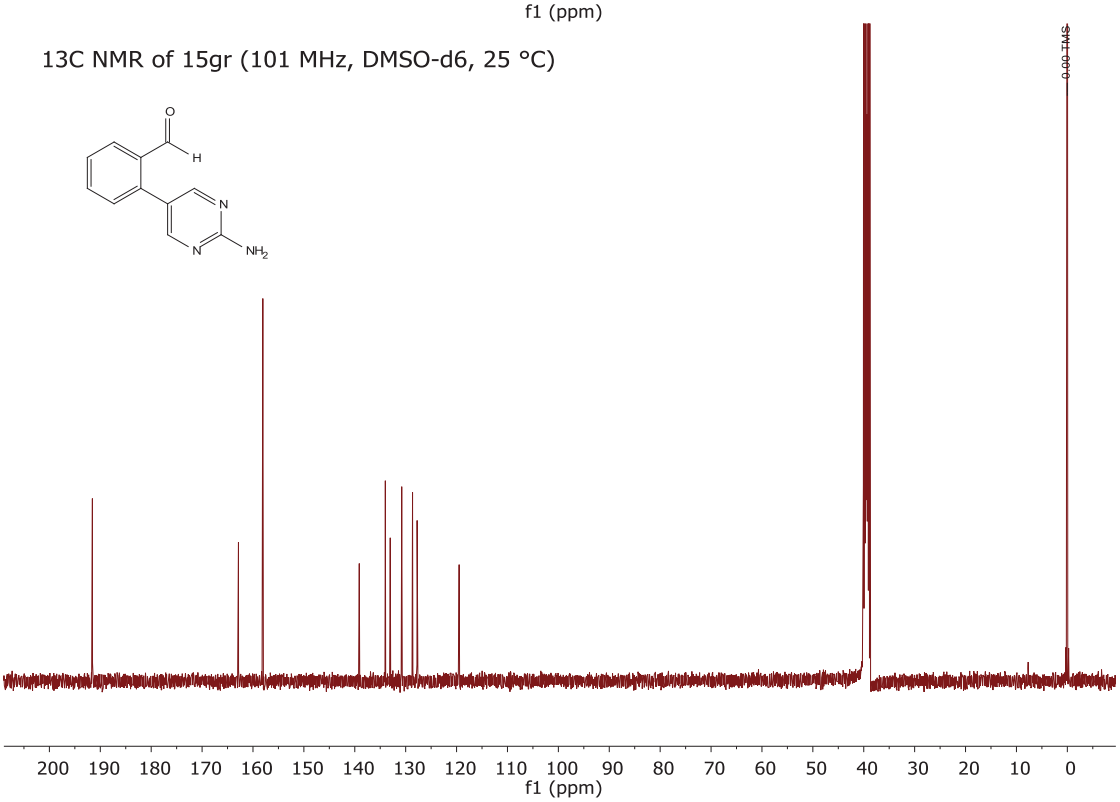

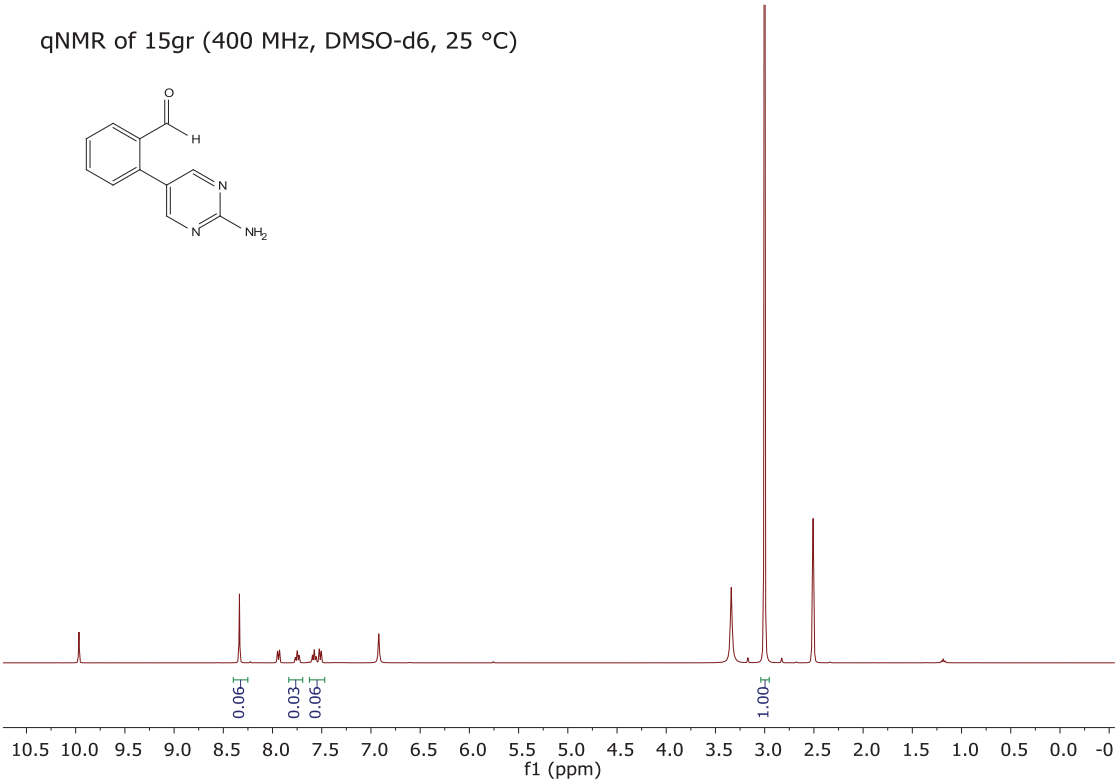

For the purity determination the sample weight was 4.610 mg and the assumed molecular weight 199.2 g/mol. Dimethyl sulfone was used as internal calibrant with a weight of 11.821 mg, a molecular weight of 94.3 g/mol and a purity of 99.73%. A purity of 94.8% was calculated for the sample using the MestReNova NMR software.

8. References

(1) Sindelar, M.; Lutz, T. A.; Petrera, M.; Wanner, K. T. Focused pseudostatic hydrazone libraries screened by mass spectrometry binding assay: Optimizing affinities toward γ-aminobutyric acid transporter 1. *J. Med. Chem*. **2013**, *56*, 1323−1340.

(2) Irngartinger, H.; Escher, T. Strong electron acceptor properties of 3'-(pentafluorophenyl)isoxazolol[4',5':1,2][60]fullerene derivatives. *Tetrahedron* **1999**, *55*, 10753−10760.

(3) Sindelar, M.; Wanner, K. T. Library screening by means of MS Binding Assays – exemplarily demonstrated for a pseudo-static library addressing GAT1. *ChemMedChem* **2012**, *7*, 1678−1690.

(4) Kragler, A.; Höfner, G.; Wanner, K. T. Synthesis and biological evaluation of aminomethylphenol derivatives as inhibitors of the murine GABA transporters mGAT1−GAT4. *Eur. J. Med. Chem*. **2008**, *43*, 2404−2411.

(5) Schmitt, S.; Höfner, G.; Wanner, K. T. MS Transport Assays for γ-aminobutyric acid transporters – an efficient alternative for radiometric assays. *Anal. Chem*. **2014**, *86*, 7575–7583.

(6) Schmitt, S.; Höfner, G.; Wanner, K. T. Application of MS Transport Assays to the four human γ-aminobutyric acid transporters. *ChemMedChem* **2015**, *10*, 1498–1510.

WILEY-VCH

FULL PAPER

MS based screening of 5-substituted nipecotic acid derived hydrazone libraries as ligands of the GABA transporter 1

Tobias J. Hauke, Georg Höfner and Klaus T. Wanner*[a]

[a] T. J. Hauke (ORCID: http://orcid.org/0000-0003-1737-9945), Dr. Georg Höfner, Prof. Dr. K. T. Wanner (ORCID: https://orcid.org/0000-0003-4399-1425)
Department of Pharmacy – Center for Drug Research
Ludwig-Maximilians-Universität München
Butenandtstr. 5–13, 81377 Munich, Germany
E-mail: klaus.wanner@cup.uni-muenchen.de

Supporting Information for this article is given via a link at the end of the document.

Abstract: A screening of compound libraries based on nipecotic acid derivatives with lipophilic residues attached to the scarcely explored 5-position of the core structure was utilized for the search of new inhibitors of the γ-aminobutyric acid (GABA) transporter 1 (mGAT1). The generated compound libraries, which were based on hydrazone chemistry commonly employed in dynamic combinatorial chemistry but rendered pseudostatic, were screened for their binding affinities towards mGAT1 by means of MS Binding Assays. With hydrazone *rac*-**16h** one hit was found and evaluated displaying submicromolar potency ($pK_i = 6.62 \pm 0.04$) and a noncompetitive interaction mode at mGAT1. By bearing a 5-(2-phenylethynyl)thiophen-2-yl residue attached to the 5-position of nipecotic acid (**6**) via a three atom spacer, compound *rac*-**16h** contains a structural moiety so far unprecedented for this kind of bioactive molecules and complements novel, 5-substituted nipecotic acid derived ligands of mGAT1 revealed in a recently published screening campaign. This new class of ligands with an inhibition mode distinctly different from that of bench mark mGAT1 inhibitors could serve as research tools for investigations of the mGAT1 mediated GABA transport.

Introduction

The neurotransmitter transporters of the solute carrier 6 (SLC6) gene family are widely expressed in the mammalian brain and play an important role in the regulation of neurotransmission that is involved in many physiological responses. These membrane bound transporters remove several monoamine or amino acid neurotransmitters from the synaptic cleft by utilizing a sodium- and chloride-dependent reuptake into presynaptic neurons and glial cells. The transporters can thus effectively reduce the neurotransmitter concentration available for postsynaptic receptors and finally terminate downstream neurotransmitter signaling.[1] The amino acid γ-aminobutyric acid (GABA; **1**; Figure 1) is the most important inhibitory neurotransmitter in the CNS and the four GABA uptake transporter subtypes GAT1, BGT1, GAT2 and GAT3 (as suggested by HUGO and designated as mGAT1, mGAT2, mGAT3 and mGAT4 when expressed in mice) are members of the SLC6 gene family.[2,3] In the past years, particularly GAT1 emerged as a well-known drug target for the treatment of epilepsy and other neurological or psychiatric diseases, as for example anxiety disorders.[4] So far, tiagabine (**2**) is the only GAT1-selective GABA uptake inhibitor in clinical use and it was approved as add-on treatment of partial-onset seizures.[5,6] Furthermore, several experimental GAT1 inhibitors such as SK&F-89976A (**3**), NO711 (**4**) or DDPM-2571 (**5**) have been synthesized and characterized with respect to their biological activities including anticonvulsant, anxiolytic, antidepressant or antinociceptive effects.[7,8,9,10] GAT1-selective inhibitors are usually derivatives of small cyclic amino acids, particularly nipecotic acid (**6**) or guvacine (**7**). These small cyclic amino acids, **6** and **7**, already possess a reasonable inhibitory potency towards GAT1 *in vitro*, but due to their polarity they have a limited blood brain barrier permeability and display hardly any anticonvulsant effects *in vivo*.[11] The substitution of the amino group of the cyclic amino acids **6** or **7** with a spacer and an aromatic residue is a common approach to increase lipophilicity and to improve the capability of crossing the blood brain barrier and thus to obtain compounds such as **2**–**5** that mediate potent anticonvulsant effects *in vivo*.[7,8,9,10]

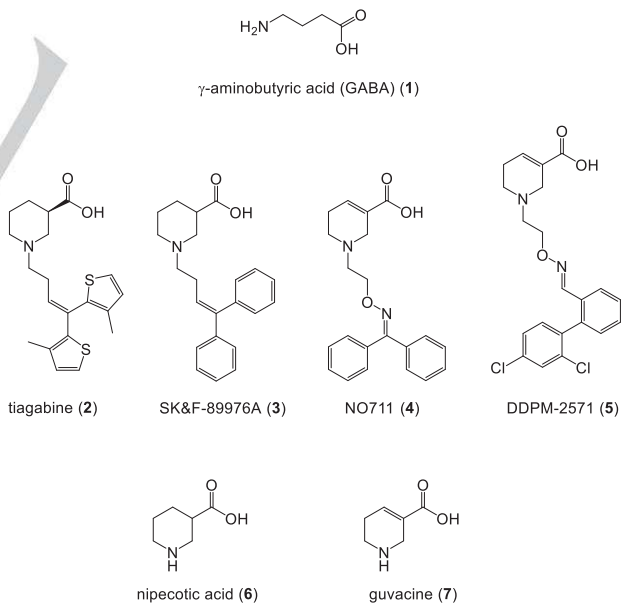

Figure 1. Structures of GABA and GAT1 inhibitors.

Besides these N-substituted GABA uptake inhibitors also analogs showing different substitution patterns at the cyclic amino acids were synthesized and tested for their biological activity towards GAT1 (Figure 2). For instance, Müller-Uri et al.[12] synthesized 5-substituted arecoline derivatives as well as the *N*-methyl guvacine derivative **8**. Lapuyade et al.[13] prepared nipecotic acid (**6**) derivatives substituted at the positions 2, 3, 4, 5, or 6 with a methyl

or phenyl residue (e.g. compound **9**) and tested their inhibitory potencies of the GABA transport in synaptosomes. N'Goka et al.[14] synthesized 6-substituted guvacine (**7**) derivatives of which compound **10** showed an *in vitro* inhibitory potency of the GABA uptake comparable to those of compounds **2**–**4**. Furthermore, Hoesl et al.[15] and N'Goka et al.[16,17] synthesized 6-substituted nipecotic acid (**6**) derivatives (e.g. compound **11**).

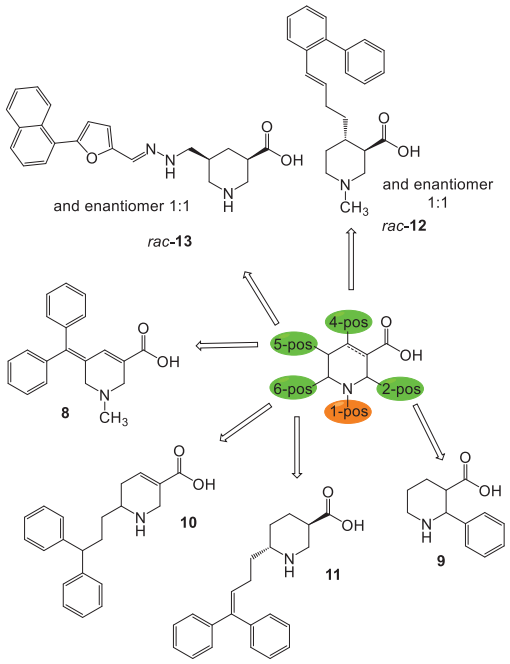

Figure 2. Structures of differentially substituted analogs of known GAT1 inhibitors.

However, none of these approaches revealed GABA uptake inhibitors as effective as compounds **2**–**5** except for compound **10**. As already indicated, the latter showed a biological activity comparable to those of known GAT1-selective inhibitors **2**–**4** in *in vitro* assays, but was nearly inactive in classical *in vivo* screening models for anticonvulsants, which is possibly due to an insufficient blood-brain barrier penetration.[14]

Despite these failures, the substitution of positions different from the amino function (e.g. in compounds **6** and **7**) appears as interesting means for the development of potentially new GABA uptake inhibitors. Based on molecular modeling the unsubstituted (*R*)-nipecotic acid [(*R*)-**6**] preferably adopts a binding pose in which the piperidine nitrogen is facing to the intracellular side, while for the larger inhibitor tiagabine (**2**) the binding pose of the piperidine ring is switched with the nitrogen and the attached arylalkyl residue facing to the extracellular side of the transporter.[18] On the basis of these results, we concluded that substitutions particularly in positions 4 or 5 with an appropriate spacer and lipophilic residue could potentially yield GABA uptake inhibitors in which the binding pose of the piperidine ring is retained compared to that of unsubstituted (*R*)-**6**.[19,20] Such compounds could hopefully bring new insights in the interactions between the ligand and target molecules or could even lead to novel GABA uptake inhibitors with higher potencies. Initial experiments exploiting nipecotic acid (**6**) and *N*-methyl nipecotic acid derivatives substituted in the 4-position (e.g. compound *rac*-**12**) did not yet reveal any new GABA uptake inhibitors with striking activity.[19] However, more recently, we reported on an approach that led to 5-substitituted nipecotic acid derivatives with interesting biological activities. A screening of pseudostatic dynamic combinatorial libraries containing nearly 900 compounds by means of competitive mass spectrometry (MS) based binding assays (MS Binding Assays) revealed new ligands of mGAT1 with submicromolar potency, of which hydrazone *rac*-**13** displayed the highest binding affinity. Surprisingly, despite the good binding affinity, *rac*-**13** and the other hydrazones synthesized in this approach only showed a low to moderate functional activity in GABA uptake experiments. Additional experiments indicated these compounds to be noncompetitive inhibitors of GAT1 addressing a so far uncharacterized, allosteric binding site.[20] To our knowledge, the compounds of this series represent the first noncompetitive ligands of GAT1 containing a nipecotic acid (**6**) moiety, while the few other noncompetitive inhibitors known for GAT1 are structurally more dissimilar from GAT1-selective inhibitors **2**–**5**.[21,22,23] In this previous screening approach, *cis*- and *trans*-configurated 5-substituted nipecotic acid derived hydrazines with both one ("C1") and two C-atoms ("C2") between the piperidine ring and a hydrazine function were included. These four nipecotic acid derived hydrazines were individually reacted with more than 220 aldehydes, **14**, grouped in 28 libraries to form corresponding hydrazone libraries (one of which included compound *rac*-**13**), which were finally screened for their binding affinities towards mGAT1 in MS Binding Assays. The results of the screening experiments indicated that the *cis*-configuration of the 3,5-disubstituted piperidine ring is basically more favorable than the *trans*-configuration for high binding affinities. Furthermore, it was found that compounds with the shorter chain length, i.e. those derived from the "C1" hydrazine building block, display a higher potency than the longer chained "C2" hydrazones. Prompted by these results, we decided to explore the *cis*-configurated, "C0" nipecotic acid derived hydrazine *rac*-**15** as a building block for the present study since it was concluded that this compound might represent another interesting building block for the generation of hydrazone libraries; hydrazine *rac*-**15** is a shorter chained analog (i.e. without a C-atom in the side chain) of the "C1" hydrazines that led to the formation of "most active" hydrazones reported previously (see e.g. *rac*-**13**).[20] A conversion of this "C0" hydrazine, *rac*-**15**, with appropriate aldehydes **14** would lead to hydrazones with a total spacer length of three atoms and thus complement the yet described series of hydrazones with a spacer between the 5-position of the nipecotic acid and the lipophilic moiety comprising four (see e.g. *rac*-**13**) and five atoms. Herein, we describe the synthesis of *rac*-**15** and its application as a building block for the generation of hydrazone libraries *rac*-**16** (Scheme 1), the latter of which were then screened towards the target mGAT1 in competitive MS Binding Assays.[20,24,25] Potential hits were identified in deconvolution experiments of the most active libraries and verified by individually resynthesizing corresponding hydrazones followed by determination of their binding affinities (pK_i values) in full-scale competitive binding assays. After that, potential hits were examined for their functional activities at the different GABA transporter subtypes and characterized with respect to their mode of inhibition at mGAT1.

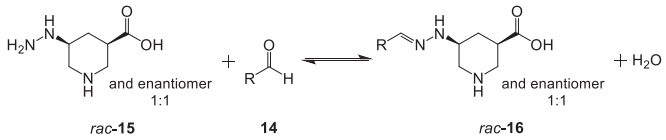

Scheme 1. Condensation of nipecotic acid derived hydrazine *rac*-**15** with diverse aldehydes **14** to afford hydrazones with the general structure *rac*-**16**.

Results and Discussion

Chemistry

The hydrazine *rac*-**15** was synthesized as shown in Scheme 2. To this end, ketone **17**[20] was reacted with *tert*-butyl carbazate in the presence of sodium cyanoborohydride and acetic acid to yield the doubly *tert*-butyloxycarbonyl (Boc) protected hydrazine precursor *rac*-**18** following a protocol for an analogous reaction from literature.[26] This reductive hydrazine formation reaction exclusively led to the synthesis of the desired *cis*-configured *rac*-**18** (79% yield); no *trans*-configured isomer could be recovered. By refluxing *rac*-**18** in aqueous HCl, simultaneous ester hydrolysis and Boc cleavage could be achieved leading to hydrazine *rac*-**15**, which was isolated as hydrochloride[27] in a yield of 96%.

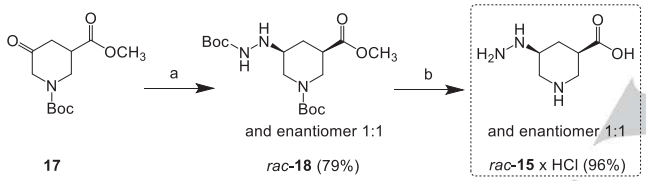

Scheme 2. Synthesis of hydrazine *rac*-**15**. *Reagents and conditions*: a) Boc-$NHNH_2$, NaH_3BCN, AcOH, MeOH, 40 min at 0 °C and 16 h at rt, 17 h; b) aq. HCl (1 M), H_2O, reflux, 1.5 h.

The individual hydrazone required for full-scale competitive MS Binding Assays was synthesized as exemplified in Scheme 1 in analogy to the previously described procedure.[20] To this end, 1.0 equivalent of aldehyde (**14**) was combined with 1.1 equivalents of hydrazine (*rac*-**15**) and 2.0 equivalents of sodium deuteroxide. For practical reasons, synthesis was performed in deuterated solvents (DMSO-d_6/D_2O 9:1) to be able to monitor the progress of the reaction and to confirm the structure by NMR. The resulting 10 mM solution was used in all further experiments without additional purification or drying.[28] The reaction equilibrium was not completely on the hydrazone side and thus small amounts of the starting materials (hydrazine and aldehyde) remained in the reaction mixture, which, however, did not affect the outcome of the biological evaluation (see Supporting Information).

Generation and screening of hydrazone libraries

For hydrazone library generation, hydrazine *rac*-**15**, which had been synthesized as described above and was used as hydrochloride,[27] was individually incubated with each aldehyde library (Scheme 3). In order to facilitate assay performance, the hydrazone formation was carried out in the presence of the target mGAT1 in phosphate buffer, of which the pH had been adjusted to 7.1 to be compatible with the proteins. A first incubation period was set to four hours to allow complete conversion. Subsequent to library generation, competitive MS binding experiments were performed by directly adding NO711 (**4**), an MS marker, to the incubation mixtures to determine the activities of the libraries.[29] When a second incubation period of 40 min for equilibration had passed, the amount of specifically bound MS marker **4** (after liberation from the target) was quantified by LC-ESI-MS/MS. This experimental procedure was basically in accordance with a formerly published protocol for the generation and screening of pseudostatic combinatorial hydrazone libraries towards the membrane bound transport protein mGAT1 by means of MS Binding Assays[24,30] (with certain adaptions as described in reference[20]).

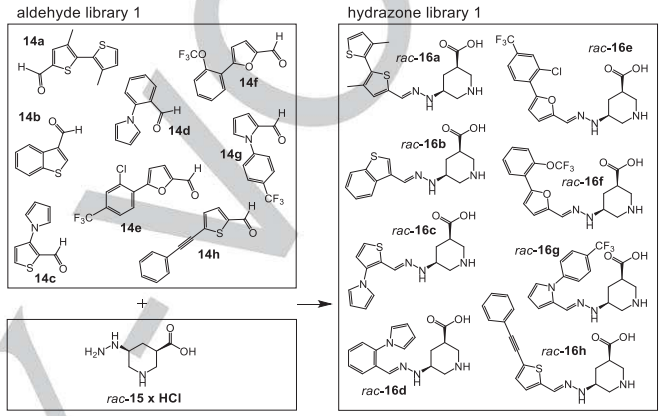

Scheme 3. Example for the conversion of aldehyde library 1 with hydrazine *rac*-**15** into hydrazone library 1 (note that the hydrazine and each hydrazone was obtained as racemate as indicated in Scheme 1; for the sake of simplicity, only one enantiomer is depicted in this scheme).

For the library generation, hydrazine *rac*-**15** was used in large excess compared to aldehydes to render the hydrazone libraries "pseudostatic", that is to achieve an almost constant composition of the libraries, which are still dynamic in nature.[24,30] As in the recently reported screening protocol,[20] hydrazine *rac*-**15** was applied in a concentration of 200 µM and aldehyde libraries consisted of eight individual aldehydes, each present in a concentration of 1.0 µM. Hence, a 24-fold excess of the hydrazine compared to the total aldehyde concentration was used for the generation of each hydrazone library. These concentrations appeared appropriate to warrant an almost complete hydrazone formation within the set time frame. Exemplarily, also kinetic experiments in the absence of the target mGAT1 were performed to control the reaction progress. Therefore, the hydrazone formation for the conversion of hydrazine *rac*-**15** with aldehydes **14s** and **14w**, respectively, was monitored by UV (Figure 3).

Due to their electronic and UV characteristics, hydrazone formation of these two aldehydes had already been studied previously in related approaches.[20,24] From these studies, compound **14s** is known to be a rather fast and **14w** a rather slowly reacting aldehyde. Still, in the present case formation of both hydrazones *rac*-**16s** and *rac*-**16w** went to completion with the set four-hour incubation time, hence demonstrating the suitability of the used reaction conditions.

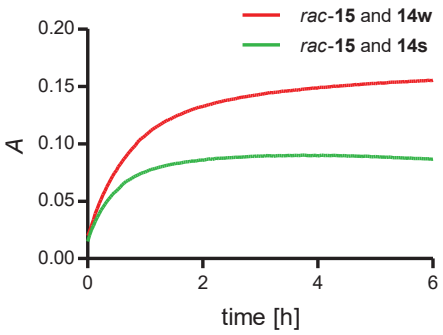

Figure 3. Absorbance (*A*) versus time for the reaction of hydrazine *rac*-**15** (200 µM) with aldehydes **14s** (green line) and **14w** (red line) (each 8 µM) in incubation puffer at pH = 7.1 and 37 °C. Reactions were monitored by UV at 356 nm: ε_{356nm} *rac*-**15**: 95 L·mol^{-1}·cm^{-1}, ε_{356nm} **14s**: 875 L·mol^{-1}·cm^{-1}, ε_{356nm} **14w**: 250 L·mol^{-1}·cm^{-1}, ε_{356nm} *rac*-**16s**: 5095 L·mol^{-1}·cm^{-1}, ε_{356nm} *rac*-**16w**: 12350 L·mol^{-1}·cm^{-1}.

For the screening, a total of 28 aldehyde libraries, each consisting of eight individual aldehydes in a concentration of 1 µM (constituted as described in reference;[20] see Figure 4), was employed, in order to screen exclusively for ligands with low micromolar to submicromolar affinity. For the assumed complete conversion of the aldehydes with hydrazine *rac*-**15** employed in excess to the corresponding hydrazones *rac*-**16**, each hydrazone will be present in a concentration of 1 µM in the competitive MS binding experiments. As mentioned above, in this study it is aimed to screen exclusively for compounds with low micromolar to submicromolar affinity; accordingly, a library (with its components being present in a concentration of 1 µM) is considered "active", if it reduces remaining MS marker binding below 50%. The minimum affinity of the test compounds defined by these conditions would equal an $IC_{50} \leq 1$ µM provided the activity of the library is due to a single constituent.

Libraries reducing remaining marker binding below 50% and hence fulfilling the "activity criterion" should be further examined in deconvolution experiments, in which single hydrazones are employed in order to identify the contained most active components. For these deconvolution experiments, the experimental conditions were set identical to those of the library screening experiments except that only single aldehydes were employed in the test procedure instead of libraries containing eight aldehydes (single aldehydes in a concentration of 1 µM were incubated with hydrazine *rac*-**15** in a concentration of 200 µM).

Results of screening and deconvolution experiments

The results of the screening of hydrazone libraries 1–28 towards mGAT1 by means of a competitive MS Binding Assay with NO711 (**4**) as MS marker are shown in Figure 5a, i.e. given as percentages of remaining specific binding of MS marker NO711 (**4**). Notably, amongst the 28 hydrazone libraries only one fulfilled the "activity criterion" of reducing the remaining marker binding below 50% (by mean values of four replicates), that is hydrazone library 1 with 37% remaining marker binding. Accordingly, hydrazone library 1 was subjected to deconvolution in order to elucidate its most active components. The results obtained thereby are shown in Figure 5b. With hydrazone *rac*-**16h** one component from hydrazone library 1 reduced remaining MS marker binding below 50% (i.e. to 46%), while all other hydrazones, *rac*-**16a**–*rac*-**16g**, did not show any striking activity at mGAT1 (with remaining marker bindings ≥ 87%). Besides, none of the individual building blocks required for hydrazone formation, i.e. neither hydrazine *rac*-**15** (nominal remaining marker binding was 102% when applied in a concentration of 200 µM; Figure 5b) nor aldehyde libraries and individual aldehydes, respectively (see literature reference[20]), alone showed any notable activity in additionally performed control experiments. By exhibiting an IC_{50} below 1 µM in the deconvolution experiments, hydrazone *rac*-**16h** as the only hit from the library screening was considered worthwhile to be subjected to further analysis for verifying its biological activity.

Figure 4. Aldehyde libraries 1–28 employed for the screening experiments (containing compounds **14a**–**14hp**[20]).

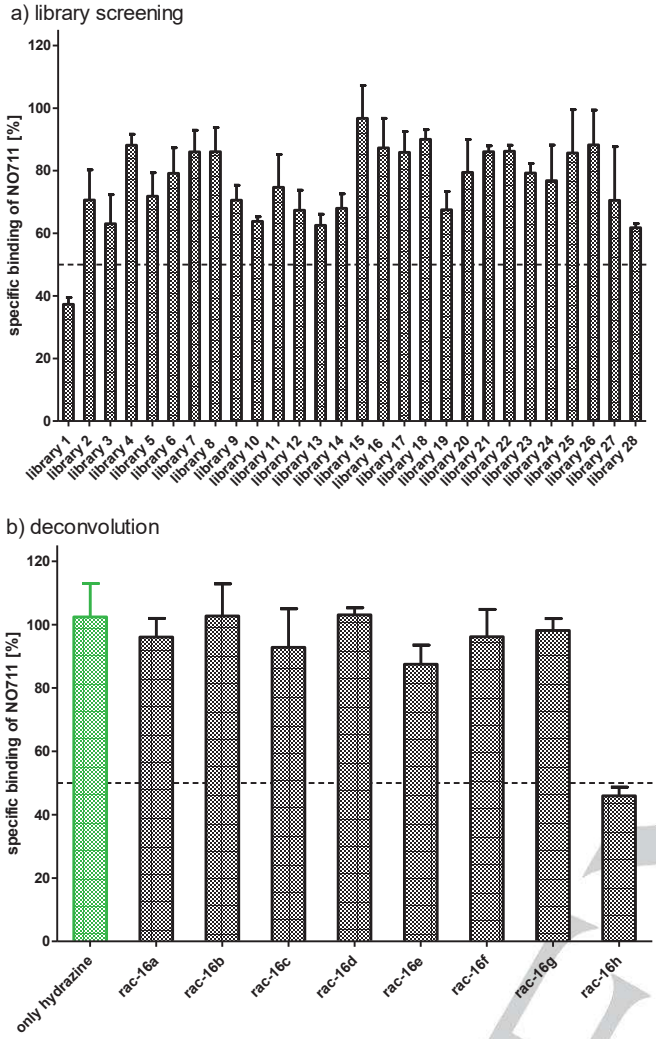

Figure 5. Screening of a) hydrazone libraries 1–28 and b) single hydrazones *rac*-**16** for deconvolution of active libraries. Formation of hydrazone libraries and single hydrazones was accomplished by incubating hydrazine *rac*-**15** (200 µM) with corresponding aldehyde libraries (containing eight aldehydes, each in a concentration of 1 µM) and single aldehydes (1 µM), respectively (and for control, pure hydrazine *rac*-**15** was applied in a concentration of 200 µM; Figure 5b; green bar). The specific binding of MS marker NO711 (**4**) without any additional inhibitor (i.e. in the absence of hydrazone libraries and single hydrazones, respectively) was defined as 100%. The bars indicate the percentage of remaining specific binding of NO711 (**4**) after an incubation time of 4 h for hydrazone formation and 40 min for marker binding to mGAT1; data represent means ± SD of four replicates. The limit for further analysis was defined as 50% remaining marker binding (indicated by the dashed line).

Hit verification

For hit verification, hydrazone *rac*-**16h**, the most active compound from deconvolution experiments, was synthesized in pure form[28] and examined in full-scale competitive MS binding experiments in order to establish its binding affinity (denoted as pK_i value) at mGAT1. The results of these experiments as well as a comparison of biological activities with those of selected GAT1 inhibitors from literature are shown in Table 1. For hydrazone *rac*-**16h**, a pK_i of 6.62 ± 0.04 was established, thus displaying submicromolar potency at mGAT1 (Table 1, entry 1). In hydrazone *rac*-**16h**, the lipophilic domain is represented by a 5-(2-phenylethynyl)thiophen-2-yl residue that to our knowledge is not known so far for other compounds inhibiting GABA transport proteins. Notably, the binding affinity of *rac*-**16h** is similar to that of hydrazone *rac*-**13** (pK_i = 6.67 ± 0.03), which was found to be the most potent compound in our recently described screening campaign,[20] and compared to tiagabine (**2**; pK_i = 7.56 ± 0.06[20]) as an example of an established, potent GAT1 inhibitor the nominal difference of the pK_i values is less than one log unit. Furthermore, the binding affinity of 5-substituted nipecotic acid derived hydrazone *rac*-**16h** alike that of *rac*-**13** is distinctly higher than those of known 4-substituted nipecotic acid derivatives such as compound *rac*-**12** (pK_i = 4.85[19]). This implies that the 5-position represents a more favored substitution pattern as compared to the 4-position leading to potent ligands of GAT1. However, such conclusions require further examinations as for 4-substituted nipecotic acid derivatives only a limited range of aromatic residues attached to the hydrophilic moiety via a spacer has been explored so far (e.g. biphen-2-yl or 2-benzylphenyl residues as described in reference[19]). In contrast, generation of pseudostatic hydrazone libraries so far only applied for 1- and 5-substituted nipecotic acid derivatives is to be considered as a powerful tool in drug research allowing to screen for a vast diversity of aromatic residues (as described herein and previously[20,24,30]). In fact, these screening approaches did reveal new aromatic moieties for 5-substituted nipecotic acid derivatives so far unprecedented for GAT1 inhibitors, that is the 3-phenoxyphenyl, 2-(2-naphthyl)pyrimidin-5-yl, 5-(1-naphthyl)furan-2-yl, 5-phenylfuran-2-yl, and 5-(2-phenylethynyl)thiophen-2-yl residue.

Table 1. Binding affinity (pK_i) and inhibitory potencies (pIC_{50}) of hydrazone *rac*-**16h** synthesized in pure form[27] at different GABA transporter subtypes and a comparison with reference compounds from literature.[a]

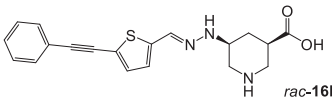

and enantiomer 1:1

rac-**16h**

compd	pK_i[b] (mGAT1)	pIC_{50}[c] (mGAT1)	pIC_{50}[c] (mGAT2)	pIC_{50}[c] (mGAT3)	pIC_{50}[c] (mGAT4)
rac-**16h**	6.62 ± 0.04	4.36 ± 0.08	58%	4.49 ± 0.06	4.41 ± 0.13
rac-**13**	6.67 ± 0.03[d]	4.64 ± 0.01[d]	64%[d]	4.48 ± 0.09[d]	4.12 ± 0.08[d]
rac-**12**	4.85[e]	4.58 ± 0.10[e]	108%[e]	68%[e]	76%[e]
2	7.56 ± 0.06[d]	6.88 ± 0.12[f]	52%[f]	64%[f]	73%[f]

[a] Binding affinity (pK_i) was determined in MS Binding Assays at mGAT1 and inhibitory potencies (pIC_{50}) were determined in [^{3}H]GABA uptake experiments at mGAT1–mGAT4. [b] pK_i values are given as means ± SEM of at least three different experiments (except for compound *rac*-**12**, for which no SEM was available from literature[19]). [c] pIC_{50} values are given as means ± SEM of at least three different experiments. In case of low inhibitory potencies percentages are given that represent remaining GABA uptake in presence of 100 µM test compound. [d] Values are taken from reference literature.[20] [e] Values are taken from reference literature.[19] [f] Values are taken from reference literature.[31]

Interestingly, the 5-(2-phenylethynyl)thiophen-2-yl residue of *rac*-**16h** with a three atom spacer was not present amongst the most potent hits from the previous study examining derivatives with

longer spacers. And conversely, none of the aromatic residues (i.e. 3-phenoxyphenyl, 2-(2-naphthyl)pyrimidin-5-yl, 5-(1-naphthyl)furan-2-yl, 5-phenylfuran-2-yl) of the most potent hits from 5-substituted nipecotic acid derivatives with four and five atom spacers led to compounds with striking activity at mGAT1 containing a three atom spacer.

After characterizing the binding affinity, the functional activities of hydrazone *rac*-**16h** were examined at the four different GABA transporter subtypes. To this end, the inhibitory potencies (denoted as pIC_{50} values; Table 1) were determined in [^{3}H]GABA uptake assays with HEK cells stably expressing mGAT1–mGAT4.[31] The pIC_{50} value found for *rac*-**16h** at mGAT1 was 4.36, which is considerably low compared to the inhibitory potency of bench mark GAT1 inhibitor tiagabine (**2**; pIC_{50} = 6.88 at mGAT1[31]) for example. Furthermore, with pIC_{50} values of 4.49 and 4.41 at mGAT3 and mGAT4, respectively, inhibitory potencies at other GABA transporter subtypes are similar to that at mGAT1 thus implying a poor subtype selectivity of *rac*-**16h**; only at mGAT2 the activity is clearly lower since *rac*-**16h** did not show an inhibitory potency high enough for reliable determination of a pIC_{50} value in concentrations up to 100 µM at this transporter subtype. There is a remarkable difference in the pIC_{50} value from uptake experiments and the pK_i value from binding experiments at mGAT1 for hydrazone *rac*-**16h**, which nominally amounts to more than two log units. Such a high discrepancy was already observed for hydrazone *rac*-**13** and related 5-substituted nipecotic acid derived hydrazones with four and five atom spacers reported previously.[20] As already mentioned above, for *rac*-**13** a noncompetitive interaction mode at GAT1 could be demonstrated and further experiments revealed an allosteric modulation; accordingly, it had to be concluded that the mode of action of 5-substituted nipecotic acid derived hydrazones is distinctly different to that of the established, N-substituted GAT1 inhibitor tiagabine (**2**). Although the discrepancies observed between the pK_i values from the binding experiments and the pIC_{50} values from uptake experiments can hardly be explained by the allosteric mode of action of the hydrazone inhibitors alone, we believe that the contradicting results obtained from the two different test systems (i.e. GABA uptake assays and MS Binding Assays) might at least be partly associated to the yet hardly explored allosteric modulation of GAT1 proteins as well as to different experimental conditions employed in the respective test system (as discussed in more detail in reference[20]). Hence, the distinct numerical differences could be the consequence of several, cumulating factors, which on their own have only minor effects, rather than due to a single cause. However, further studies are necessary to elucidate this issue.

In order to evaluate, if hydrazone *rac*-**16h** described herein is also exhibiting a noncompetitive inhibition mode, further binding experiments were conducted. To this end, MS based saturation experiments with NO711 (**4**) as reporter ligand for mGAT1 were performed in the presence and absence (for control) of fixed concentrations of *rac*-**16h**. According to Hulme and Trevethick[32] saturation isotherms as well as Schild-like coefficients were determined from the data (see Table 2; the Schild-like coefficients were calculated as described recently;[20] values different from 1.0 are indicators for a noncompetitive interaction mode). In the presence of hydrazone *rac*-**16h** the densities of binding sites at mGAT1 (i.e. the B_{max} values) were distinctly decreased in both concentrations studied, i.e. at 1 µM and 10 µM, and the apparent affinities for the reporter ligand **4** in presence of the test compound *rac*-**16h** were also decreased (i.e. higher K_{d_app} values). Furthermore, with a mean value of 0.55 the calculated Schild-like coefficient was distinctly different from 1.0. Accordingly, the result strongly support a noncompetitive interaction mode between hydrazone *rac*-**16h** and the reporter ligand NO711 (**4**) at mGAT1, similar to that of hydrazone *rac*-**13** and opposite to that of tiagabine (**2**), for the latter of which a competitive interaction mode was demonstrated in this kind of experiments.[20] Hence, it can be concluded that the inhibition mode of compound *rac*-**16h** in accordance with that of other, recently described 5-substituted nipecotic acid derived hydrazones (including *rac*-**13**, see literature reference[20]) at GAT1 is distinctly different to that of well-known, N-substituted GAT1 inhibitors such as tiagabine (**2**) or NO711 (**4**). In regard to the modulation of GABA transporter mGAT1, it is likely that hydrazone *rac*-**16h** addresses the same allosteric binding site as the previously evaluated hydrazones. Consequently, the inhibitory potency of *rac*-**16h** determined in functional assays cannot be assessed by a comparison with classical, competitive GAT1 inhibitors such as compounds **2**–**4**, but rather with the few other noncompetitive inhibitors reported in literature.[20,21,22,23] With those, it shares a pIC_{50} value in a similar order of magnitude. Still, further investigations are necessary in order to elucidate the pharmacological importance of the noncompetitive interaction characteristics and hopefully to obtain new insights of GAT1 mediated GABA transport in general.

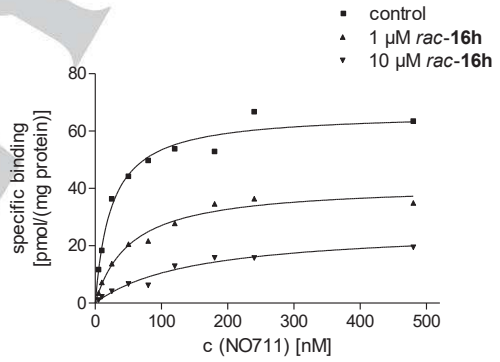

Figure 6. Saturation isotherms for NO711 (**4**) as reporter ligand addressing mGAT1. Data points represent specific binding (means from triplicates) obtained in the presence of hydrazone *rac*-**16h** in different fixed concentrations (as indicated) and for control also in the absence of any additional test compound.

Table 2. Characterization of the interaction mode between hydrazone *rac*-**16h** and the reporter ligand NO711 (**4**) at mGAT1.[a]

para-meters	0 µM *rac*-**16h**[b]	1 µM *rac*-**16h**[b]	10 µM *rac*-**16h**[b]	coefficient[c]	conclusion
B_{max} [%]	100[d]	76 ± 9	55 ± 11*[e]	0.55 ± 0.05	non-competitive
K_{d_app} [nM]	28.6 ± 2.2	67.9 ± 9.3*[f]	165.8 ± 23.8*[f]		

[a] Determined in MS based saturation experiments using NO711 (**4**) as reporter ligand for mGAT1. [b] Saturation experiments were performed in the presence (in fixed concentrations of 1 µM and 10 µM, respectively) and absence (for control; "0 µM") of *rac*-**16h**. [c] Schild-like coefficient calculated according to Hulme and Trevethick.[32] [d] The B_{max} value in the absence of the inhibitor was 42.4 ± 12.2 pmol/(mg protein). All results are presented as means ± SEM from three independently performed experiments. Statistically significant (with α = 0.05) differences from control values ("0 µM") are indicated by asterisks ([e] according to one-sample one-tailed Student's *t*-tests; [f] according to two-sample one-tailed Student's *t*-tests).

Conclusions

In summary, by complementing a larger, recently described screening campaign,[20] the search for novel GABA uptake inhibitors based on nipecotic acid derivatives with an uncommon substitution pattern was continued. To this end, the nipecotic acid derivative *rac*-**15** bearing a hydrazine function directly attached to the 5-position of the piperidine ring was synthesized and applied as a building block for the generation of combinatorial libraries, which were rendered pseudostatic; the thus generated pseudostatic hydrazone libraries were screened for their binding affinities towards mGAT1 in MS based binding experiments. This approach of combined library generation and screening by means of MS Binding Assays allowed to screen for a vast diversity of lipophilic residues as part of mGAT1 inhibitors utilizing DCC reactions for test compound formation. This represents a powerful tool for structure-activity relationship studies for ligands of mGAT1. With hydrazone *rac*-**16h** displaying a pK_i of 6.62 ± 0.04 one hit with submicromolar potency towards mGAT1 was identified and evaluated. This compound, *rac*-**16h**, is bearing a 5-(2-phenylethynyl)thiophen-2-yl residue attached to the 5-position of nipecotic acid (**6**) via a three atom spacer and accordingly represents a structure so far unprecedented for GAT1 inhibitors known so far. Although, *rac*-**16h** displayed only low to moderate functional activity and GAT subtype selectivity as determined in GABA uptake experiments, this compound is particularly interesting due to its noncompetitive inhibition mode. Hence, the herein introduced hydrazone *rac*-**16h** is displaying a mode of action distinctly different from that of bench mark GAT1 inhibitors such as tiagabine (**2**) and could thus represent a novel compound of a yet barely known class of GAT1 ligands. Though further investigations are still required to explore physiological and pharmacological effects of the noncompetitive inhibition of GAT1 mediated GABA transport, substituting the 5-position of nipecotic acid (**6**) with lipophilic residues has again been demonstrated as a possible means of obtaining new GABA uptake inhibitors with promising characteristics.

Experimental Section

Chemistry

General: Solvents for synthesis, extraction and flash chromatography were distilled before use. Other commercially available reagents (by ABCR, Acros, Alfa Aesar, Fisher Scientific, Maybridge, Merck, Sigma-Aldrich, TCI and VWR) were used without further purification. Thin-layer chromatography was carried out on precoated silica gel F_{254} glass plates (Merck) and detected by staining with a ninhydrin solution (0.3 g ninhydrin and 3 mL acetic acid dissolved in 100 mL 1-butanol[33]). Flash column chromatography was performed on silica gel 60 (grading 0.035–0.070 mm, purchased from Merck and Acros). NMR spectroscopy was performed on Avance III HD Bruker BioSpin (Bruker; ^{1}H NMR: 400 or 500 MHz, ^{13}C NMR: 101 or 126 MHz) or JNMR-GX (JEOL; ^{1}H NMR: 400 or 500 MHz, ^{13}C NMR: 101 or 126 MHz) spectrometers. The spectra were processed with the NMR software MestReNova, versions 8.1, 10.0 and 12.0 (Mestrelab Research S.L.). Chemical shifts were internally referenced to TMS (*rac*-**18**) or MeOH (*rac*-**15** x HCl), except for hydrazone *rac*-**16h**, which was referenced to DMSO solvent signals (^{1}H NMR: 2.53 ppm; ^{13}C NMR: 39.13 ppm). IR spectroscopy was performed on a FT-IR Paragon 1000 (Perkin-Elmer) spectrometer and analyzed with the software Spectrum v2.00 (Perkin-Elmer); samples were pressed in KBr pellets. High-resolution mass spectrometry (ESI) was performed with Thermo Finnigan LTQ FT Ultra mass spectrometer (ThermoFischer Scientific). Elemental analysis for hydrazine *rac*-**15** x HCl was performed with a Vario EL Cube (Elementar) and an 888 Titrando (Metrohm) in order to determine the corresponding amounts of hydrogen chloride. Melting points were determined in open capillaries on a BÜCHI 510 melting point apparatus and are uncorrected. For purity testing of hydrazine *rac*-**15** x HCl quantitative NMR spectroscopy (qNMR) was performed in accordance to the literature references[34,35] on an Avance III HD Bruker BioSpin spectrometer (Bruker; ^{1}H NMR: 400 MHz). As internal calibrant (IC) maleic acid (TraceCERT® certified reference compound, Lot-No.: BCBM8127V, purity: 99.94%) purchased from Sigma-Aldrich was used; the purity was calculated with the NMR software MestReNova, versions 10.0 and 12.0 (Mestrelab Research S.L.). The metastable hydrazone *rac*-**16h** was used without purity determination, but was synthesized from ≥ 95% pure building blocks and reaction progress was monitored by NMR.

Aldehydes (14a–14hp): Aldehyde libraries were compiled as previously described.[20]

***rac*-(3*R*,5*S*)-(5-Hydrazinylpiperidine-3-carboxylic acid)–hydrogen chloride (1/2) (*rac*-15 x HCl):** *rac*-**18** (339 mg, 0.907 mmol) was suspended in 1 M aqueous HCl (12 mL, 12 mmol) and the mixture was refluxed for 1.5 h. Then the reaction was cooled to rt and quenched with H_2O (15 mL). The aqueous phase was washed with DCM (3 x 20 mL) and after lyophilisation *rac*-**15** x HCl was obtained as white solid (202 mg, 96%): mp: 227 °C (decomposition); ^{1}H NMR (500 MHz, 1 M NaOD in D_2O, 25 °C): δ=1.18 (q, *J*=11.9 Hz, 1 H), 2.14 (dd, *J*=12.0/10.8 Hz, 1 H), 2.20 (dm, *J*=12.2 Hz, 1 H), 2.35 (tt, *J*=11.8/3.2 Hz, 1 H), 2.41 (t, *J*=11.6 Hz, 1 H), 2.67 (tt, *J*=11.3/4.0 Hz, 1 H), 3.10 (dm, *J*=11.1 Hz, 1 H), 3.17 ppm (dm, *J*=12.3 Hz, 1 H);[36] ^{13}C NMR (126 MHz, 1 M NaOD in D_2O, 25 °C): δ=32.6, 45.1, 48.3, 49.0, 58.4, 182.9 ppm; IR (KBr): $\tilde{\nu}$=3416, 3229, 2976, 2847, 2739, 2576, 2518, 1722, 1608, 1578, 1488 cm^{-1}; HRMS-ESI *m/z* [*M*+H]$^+$ calcd for $C_6H_{14}O_2N_3$: 160.1081, found 160.1080; Anal. calcd for $C_6H_{13}O_2N_3$ x 2 HCl: C 31.05, H 6.51, N 18.10, Cl 30.55, found: C 30.79, H 6.46, N 17.95, Cl 30.28. Purity (qNMR: 1 M NaOD in D_2O, 25 °C, maleic acid; m_S=4.738 mg; m_{IC}=7.451 mg): 95.2%.

***rac*-(3*R*,5*S*)-{5-[(*E*)-2-{[5-(2-Phenylethynyl)thiophen-2-yl]methylidene}hydrazin-1-yl]piperidine-3-carboxylic acid}–sodium chloride (1/2) (*rac*-16h):** The reaction was performed in a sealed 1.5 mL tube under Ar. To DMSO-d_6 (850 µL) a 200 mM stock solution of *rac*-**15** x HCl in D_2O (55 µL, 0.011 mmol), a 1 M solution of NaOD in D_2O (20 µL, 0.020 mmol) and D_2O (25 µL) were added to reach a total volume of 950 µL. The reaction was started by the addition of a 200 mM stock solution of

5-(2-phenylethynyl)thiophene-2-carbaldehyde (**14h**) in DMSO-d_6 (50 µL, 0.010 mmol). The mixture was sonicated for 5 min and stored at rt over night to obtain *rac*-**16h** in solution: ^{1}H NMR (500 MHz, DMSO-d_6/D_2O 9:1, 25 °C): δ=1.40 (q, *J*=12.2 Hz, 1 H), 2.22 (d, *J*=12.8 Hz, 1 H), 2.44–2.58 (m, 2 H), 2.66 (t, *J*=12.3 Hz, 1 H), 3.23–3.34 (m, 2 H), 3.41 (tt, *J*=11.4/4.1 Hz, 1 H), 7.06 (d, *J*=3.8 Hz, 1 H), 7.30 (d, *J*=3.8 Hz, 1 H), 7.42–7.45 (m, 3 H), 7.51–7.55 (m, 2 H), 7.86 ppm (s, 1 H);[36,37] ^{13}C NMR (126 MHz, DMSO-d_6/D_2O 9:1, 25 °C): δ=32.1, 40.1, 45.7, 47.0, 52.3, 83.1, 93.1, 119.9, 121.7, 126.0, 128.9, 129.1, 131.1, 131.8, 133.2, 143.3, 173.9 ppm;[37] HRMS-ESI *m/z* [*M*+H]$^+$ calcd for $C_{19}H_{20}N_3O_2S$: 354.1271, found 354.1270.
All NMR and HRMS measurements as well as the MS Binding Assays and GABA uptake assays were performed using this 10 mM solution of *rac*-**16h** without further purification.[28] Analysis of the ^{1}H NMR spectrum showed that besides the major *E*-isomer the *Z*-isomer was present in 5% and that the reaction equilibrium was to 90% on the hydrazone side (determined by integration of the remaining signal of the aldehyde proton).

***rac*-(3*R*,5*S*)-{1-(*tert*-Butyl) 3-methyl 5-[2-(*tert*-butoxycarbonyl)hydrazinyl]piperidine-1,3-dicarboxylate} (*rac*-18):** Ketone **17**[20] (126 mg, 0.490 mmol) and *tert*-butyl carbazate (79 mg, 0.58 mmol) were dissolved in MeOH (5 mL) and the solution was cooled to 0 °C. Acetic acid (0.06 mL, 1 mmol) and subsequently after 10 min $NaBH_3CN$ (78 mg, 1.2 mmol) were added to the mixture and it was stirred at 0 °C for further 30 min and at rt for 16 h. Then the reaction was quenched with a saturated $NaHCO_3$ solution in H_2O (35 mL) and extracted with DCM (4 x 30 mL). The combined organic phases were dried over Na_2SO_4 and concentrated under reduced pressure. After purification by flash chromatography (*iso*-hexanes/EtOAc 2:1) *rac*-**18** was obtained as white solid (144 mg, 79%): R_f=0.23 (*iso*-hexanes/EtOAc 2:1); mp: 80 °C; ^{1}H NMR (400 MHz, $C_2Cl_4D_2$, 80 °C): δ=1.40–1.48 (m, 19 H), 2.15 (d, *J*=12.6 Hz, 1 H), 2.40–2.61 (m, 2 H), 2.76–2.99 (m, 2 H), 3.67 (s, 3 H), 3.87 (s, 1 H), 4.01 (d, *J*=13.0 Hz, 1 H), 4.10 (d, *J*=14.2 Hz, 1 H), 6.00 ppm (s, 1 H); ^{13}C NMR (101 MHz, $C_2Cl_4D_2$, 80 °C): δ=28.4, 28.4, 31.7, 40.1, 45.4, 47.7, 51.8, 55.1, 79.9, 80.6, 154.5, 156.8, 173.0 ppm; IR (KBr): $\tilde{\nu}$=3329, 3261, 2978, 2935, 2871, 1741, 1697, 1545, 1477 cm^{-1}; HRMS-ESI *m/z* [*M*+Na]$^+$ calcd for $C_{17}H_{31}O_6N_3Na$: 396.2105, found: 396.2109.

UV-monitoring of hydrazone formation: UV-monitoring was performed in quartz glass cuvettes (3.5 mL; Hellma) with a SpectraMax M2e (Molecular Devices) plate reader at 37 °C and analyzed with SoftMax Pro 5.4 software. Incubation buffer (as described for the MS Binding Assays; see below) containing 1% DMSO was used and the total volume of the samples was 3.0 mL. For monitoring reaction progress incubation buffer (2940 µL) was supplemented with the desired aldehyde (**14s** or **14w**) dissolved in DMSO (800 µM, 30 µL). The reaction was started by adding the hydrazine (*rac*-**15** x HCl) dissolved in incubation buffer (20 mM, 30 µL) and the absorption values at a wavelength of 356 nm were measured immediately after placing the cuvette in the instrument and then at intervals of 2 min for 12 h.

MS Binding Assays

mGAT1 membrane preparation. Membrane preparations of HEK293 cells stably expressing mGAT1[31] were prepared, stored, and applied as previously described.[24,30,38]

Library screening. Library screening experiments were performed according to our established protocol[24,30] with modifications as reported recently:[20] Quadruplicate samples in a total volume of 250 µL with incubation buffer (12.5 mM Na_2HPO_4 x 2 H_2O, 12.5 mM NaH_2PO_4 x H_2O, 1 M NaCl and 200 µM sodium L-ascorbate; pH was adjusted to 7.1 with 2 M NaOH) containing 1% DMSO (final concentration) were prepared in 1.2 mL polysterene 96-deep-well plates (Sarstedt). Compounds were added in 10-fold concentrated stock solutions. Aldehydes were applied in a final concentration of 1.0 µM per sample (with each aldehyde library representing a mixture of eight different aldehydes) and hydrazine *rac*-**15** x HCl in 200 µM. The first incubation period (for library generation) of 4 h at 37 °C in a shaking water bath was started immediately after adding the mGAT1 membrane preparation to the mixture of hydrazine and aldehydes. Then the second incubation period (for equilibration) of 40 min at 37 °C was started by adding MS marker **4** in a concentration of 20 nM (final concentration in the sample). The incubation was terminated by vacuum filtration (96-well filter plate, Acroprep, glass fiber, 1.0 µm, 350 µL; Pall). After washing with ice-cold aqueous 1 M NaCl (5 x 150 µL per well), the filter plates were dried at 50 °C for 60 min and cooled to room temperature. The marker **4** was subsequently liberated by elution with MeOH (3 x 100 µL per well) and the eluate was collected in a 96-deep-well plate. To each sample 1 nM [$^2H_{10}$]NO711 in MeOH (200 µL) was added as internal standard. All samples were dried to completeness at 50 °C for 16 h and subsequently reconstituted in 10 mM NH_4HCO_2 buffer (pH 7.0) containing 5% MeOH (200 µL). Quantification was performed by LC-ESI-MS/MS.

Total binding was determined with analogously constituted samples lacking any inhibitor and nonspecific binding was determined in the presence of 100 mM GABA. All experiments additionally obtained matrix blanks, zero samples, and matrix standards. For calibration, blank matrix (after the liberation/elution step) was supplemented with methanolic calibration standards (200 µL) with 20 pM, 50 pM, 100 pM, 200 pM, 500 pM, 1.0 nM, 2.5 nM and 5.0 nM NO711 (**4**), respectively (these samples were employed for generating calibration curves for marker quantitation after processing as described above).

Deconvolution experiments. The deconvolution experiments were analogously performed[20,24,30] as the library screening experiments but employing single aldehydes (1.0 µM per sample) instead of a mixture of eight aldehydes.

Competition experiments for establishing binding affinities. Full-scale MS binding experiments with pure hydrazone *rac*-**16h**[28] were performed as reported[29,38] applying the incubation buffer as described under "Library screening".

Saturation experiments for investigation of test compound's mode of interaction. MS based saturation experiments with NO711 (**4**) as reporter ligand (concentration range: 2.5 nM–480 nM) addressing mGAT1 were performed as previously described.[29,38] Pure hydrazone *rac*-**16h**[27] was added in the desired concentrations to the binding samples before incubation was started by addition of the mGAT1 membrane preparation. All other conditions (e.g. incubation buffer, filtration and washing of binding samples, drying of eluates and reconstitution of samples) were exactly the same[20] as described under "Library screening".

LC-ESI-MS/MS. Quantification by LC-ESI-MS/MS was performed on a API 3200 or 3200 Q TRAP triple-quadrupole mass spectrometer (AB Sciex) with all other LC and MS parameters as previously described.[29]

Data Analysis in mGAT1 MS Binding Assays. Data analysis was performed as previously described.[20,24,29,30,38] Binding affinities for test compounds are expressed as pK_i values (with K_i values calculated according to Cheng and Prussoff;[39] taking into account that the investigated test compound and NO711 (**4**) may not address the same binding site, the K_i values could be considered as apparent K_i values). Affinities (K_d) for NO711 (**4**) and densities of binding sites (B_{max}) in the absence or presence of test compound were calculated from saturation isotherms. B_{max} values are given in [pmol/(mg protein)], K_d values in [nM]. All results represent means ± SEM, determined in at least three separate experiments. To distinguish between competitive and noncompetitive binding interactions between test compound and reporter ligand **4** a Schild-like coefficient { = [log ($K_{d\_NO711\_app}/K_{d\_NO711}$ -1)$_{higher\ concentrated\ test\ compound}$ - log ($K_{d\_NO711\_app}/K_{d\_NO711}$ -1)$_{lower\ concentrated\ test\ compound}$] / [log (higher concentration test compound) - log (lower concentration test compound)]} was calculated according to Hulme and Trevethick.[32]

GABA uptake assays

[^{3}H]GABA uptake assays were performed as reported[31] except that sodium L-ascorbate (200 µM) was added to all samples as antioxidant.

Supporting Information

Additional information regarding hit verification and NMR spectra of compounds (PDF) as well as molecular-formula strings (CSV) are provided within the Supporting Information on the journal's website.

Acknowledgements

We like to thank Dr. Lars Allmendinger and Dr. Jörg Pabel for technical assistance, and Silke Duensing-Kropp, Tanja Franz and Miriam Sandner for performing saturation experiments and GABA uptake assays.

Keywords: binding assays • combinatorial chemistry • GABA uptake • hydrazones • mass spectrometry

References:

[1] A. S. Kristensen, J. Andersen, T. N. Jørgensen, L. Sørensen, J. Eriksen, C. J. Loland, K. Strømgaard, U. Gether. *Pharmacol. Rev*. **2011**, *63*, 585–640.

[2] K. K. Madsen, R. P. Clausen, O. M. Larsson, P. Krogsgaard-Larsen, A. Schousboe, H. S. White. *J. Neurochem*. **2009**, *109*, 139–144.

[3] P. Wellendorph, J. Jacobsen, J. Skovgaard-Petersen, A. Jurik, S. B. Vogensen, G. Ecker, A. Schousboe, P. Krogsgaard-Larsen, R. P. Clausen in: *Transporters as Drug Targets, 1st ed* (Eds.: G. F. Ecker, R. P. Clausen, H. H. Sitte), Wiley-VCH, Weinheim, **2017**, pp. 69–106.

[4] C. K. Thoeringer, S. Ripke, P. G. Unschuld, S. Lucae, M. Ising, T. Bettecken, M. Uhr, M. E. Keck, B. Mueller-Myhsok, F. Holsboer, E. B. Binder, A. Erhardt. *J. Neural. Transm*. **2009**, *116*, 649–657.

[5] P. Genton, R. Guerrini, E. Perucca. *Epilepsia* **2001**, *42*, 42–45.

[6] S. M. LaRoche, S. L. Helmers. *JAMA* **2004**, *291*, 605–614.

[7] L. M. Yunger, P. J. Fowler, P. Zarevics, P. E. Setler. *J. Pharmacol. Exp. Ther.* **1984**, *228*, 109–115.

[8] F. E. Ali, W. E. Bondinell, P. A. Dandridge, J. S. Frazee, E. Garvey, G. R. Girard, C. Kaiser, T. W. Ku, J. J. Lafferty, G. I. Moonsammy, H.-J. Oh, J. A. Rush, P. E. Setler, O. D. Stringer, J. W. Venslavsky, B. W. Volpe, L. M. Yunger, C. L. Zirkle. *J. Med. Chem*. **1985**, *28*, 653–660.

[9] L. A. Borden, T. G. M. Dhar, K. E. Smith, R. L. Weinshank, T. A. Branchek, C. Gluchowski. *Eur. J. Pharmacol*. **1994**, *269*, 219–224.

[10] K. Salat, A. Podkowa, N. Malikowska, F. Kern, J. Pabel, E. Wojcieszak, K. Kulig, K. T. Wanner, B. Strach, E. Wyska. *Neuropharmacology* **2017**, *113*, 331–342.

[11] H.-H. Frey, C. Popp, W. Loescher. *Neuropharmacology* **1979**, *18*, 581–590.

[12] C. Müller-Uri, E. A. Singer, W. Fleischhacker. *J. Med. Chem.* **1986**, *29*, 125–132.

[13] G. Lapuyade, G. Schlewer, V. N'Goka, J.-C. Vernieres, J.-P. Chambon, J. Lagrange, P. Lagrange, C. G. Wermuth. *Eur. J. Med. Chem.* **1987**, *22*, 383–391.

[14] V. N'Goka, G. Schlewer, J.-M. Linget, J.-P. Chambon, C. G. Wermuth. *J. Med. Chem*. **1991**, *34*, 2547–2557.

[15] C. E. Hoesl, G. Höfner, K. T. Wanner. *Tetrahedron* **2004**, *60*, 307–318.

[16] V. N'Goka, C. Bissantz, P. Bisel, T. B. Stenbøl, P. Krogsgaard-Larsen, G. Schlewer. *Eur. J. Med. Chem*. **2004**, *39*, 633–638.

[17] V. N'Goka, T. B. Stenbøl, P. Krogsgaard-Larsen, G. Schlewer. *Eur. J. Med. Chem.* **2004**, *39*, 889–895.

[18] T. Wein, M. Petrera, L. Allmendinger, G. Höfner, J. Pabel, K. T. Wanner. *ChemMedChem* **2016**, *11*, 509–518.

[19] T. Hellenbrand, G. Höfner, T. Wein, K. T. Wanner. *Bioorg. Med. Chem*. **2016**, *24*, 2072–2096.

[20] T. J. Hauke, T. Wein, G. Höfner, K. T. Wanner. *J. Med. Chem.* **2018**, *61,* 10310–10332.

[21] A. Sarup, O. M. Larsson, T. Bolvig, B. Frølund, P. Krogsgaard-Larsen, A. Schousboe. *Neurochem. Int.* **2003**, *43*, 445–451.

[22] H. S. White, W. P. Watson, S. L. Hansen, S. Slough, J. Perregaard, A. Sarup, T. Bolvig, G. Petersen, O. M. Larsson, R. P. Clausen, B. Frølund, E. Falch, P. Krogsgaard-Larsen, A. Schousboe. *J. Pharm. Exp. Ther.* **2005**, *312*, 866–874.

[23] J. M. V. Timple, L. G. Magalhães, K. C. Souza Rezende, A. C. Pereira, W. R. Cunha, M. L. Andrade e Silva, O. V. Mortensen, A. C. K. Fontana. *J. Nat. Prod.* **2013**, *76*, 1889–1895.

[24] M. Sindelar, K. T. Wanner. *ChemMedChem* **2012**, *7*, 1678–1690.

[25] F. T. Kern, K. T. Wanner. *ChemMedChem* **2015**, *10*, 396–410.

[26] T. Fujimoto, Y. Imaeda, N. Konishi, K. Hiroe, M. Kawamura, G. P. Textor, K. Aertgeerts, K. Kubo. *J. Med. Chem*. **2010**, *53*, 3517–3531.

[27] General remark on hydrazine stability: The hydrazine *rac*-**15** was prone for degradation and was thus isolated and used in all further experiments as its more stable hydrochloride. As stated in reference,[20] neither the use as hydrochloride nor the low hydrazine stability itself affected the outcome of the screening experiments when the antioxidant sodium L-ascorbate (200 µM) was added to the incubation buffer. The hydrazine *rac*-**15** was obtained with 2 equivalents of HCl (verified by elemental analysis).

[28] Likewise the hydrazine[27] also the corresponding hydrazone showed a limited stability and thus manipulation was reduced to a minimum. The hydrazone was obtained in solution with 2 equivalents of NaCl and its structure was confirmed by NMR and HRMS measurements. Although the hydrazine was applied in slight excess (1.1 fold) for the synthesis, the reaction equilibrium was not completely on the hydrazone side. As shown in the Supporting Information, this had no remarkable effect on the determination of the binding affinity.

[29] C. Zepperitz, G. Höfner, K. T. Wanner. *ChemMedChem* **2006**, *1*, 208–217.

[30] M. Sindelar, T. A. Lutz, M. Petrera, K. T. Wanner. *J. Med. Chem*. **2013**, *56*, 1323–1340.

[31] A. Kragler, G. Höfner, K. T. Wanner. *Eur. J. Med. Chem*. **2008**, *43*, 2404–2411.

[32] E. C. Hulme, M. A. Trevethick. *Br. J. Pharmacol*. **2010**, *161*, 1219–1237.

[33] E. Merck. Anfärbereagenzien für Dünnschicht- und Papier-Chromatographie, MERCK, Darmstadt, 1970.

[34] M. Cushman, G. I. Georg, U. Holzgrabe, S. Wang. *J. Med. Chem*. **2014**, *57*, 9219.

[35] G. F. Pauli, S. N. Chen, C. Simmler, D. C. Lankin, T. Godecke, B. U. Jaki, J. B. Friesen, J. B. McAlpine, J. G. Napolitano. *J. Med. Chem*. **2014**, *57*, 9220–9231.

[36] Peaks for the protons of OH and NH groups disappeared due to deuterium exchange and corresponding signals were not detectable in ^{1}H NMR spectra of compounds *rac*-**15** x HCl and *rac*-**16h**.

[37] In addition to the signals listed ^{1}H NMR and ^{13}C NMR spectra showed signals of low intensity corresponding to the *Z*-isomer and starting materials.

[38] C. Zepperitz, G. Höfner, K. T. Wanner. *Anal. Bioanal. Chem*. **2008**, *391*, 309–316.

[39] Y. C. Cheng, W. H. Prussoff. *Biochem. Pharmacol*. **1973**, *22*, 3099–3108.

Entry for the Table of Contents

Searching for novel GABA uptake inhibitors: An MS based screening of pseudostatic dynamic combinatorial hydrazone libraries revealed a new ligand of the GABA transporter mGAT1 representing a 5-substituted nipecotic acid derivative. Hit verification by means of MS Binding Assays indicated a submicromolar potency and a noncompetitive interaction mode at mGAT1 for the compound synthesized in pure form.

Content:

1. Additional information regarding hit verification

When synthesizing hydrazone *rac*-**16h** in pure form for hit verification, analysis of the ^{1}H NMR spectrum showed that about 10% of building blocks, aldehyde **14h** and hydrazine *rac*-**15**, remained unreacted in solution (i.e. implying reaction equilibrium was only to about 90% on hydrazone side). In order to examine whether this affected the outcome of the biological evaluation, *rac*-**16h*** was synthesized by applying aldehyde **14h** in excess to force the equilibrium on the hydrazone's side. Hence, 2.0 equivalents of aldehyde **14h** were reacted with 1.0 equivalent hydrazine *rac*-**15** x HCl to obtain *rac*-**16h*** under the otherwise same conditions as for the synthesis of *rac*-**16h** and the mixture was directly used in solution for NMR measurements and biological evaluations. The ^{1}H NMR spectrum of *rac*-**16h*** (see Figure S1) revealed that hydrazine *rac*-**15** reacted quantitatively (i.e. corresponding signals disappeared nearly completely). Besides an additional set of minor signals indicating the presence of the *Z*-isomer of *rac*-**16h**, signals of excessive aldehyde **14h** and target compound *rac*-**16h** (as *E*-isomer) were detected dominating in the ^{1}H NMR spectrum of *rac*-**16h***.

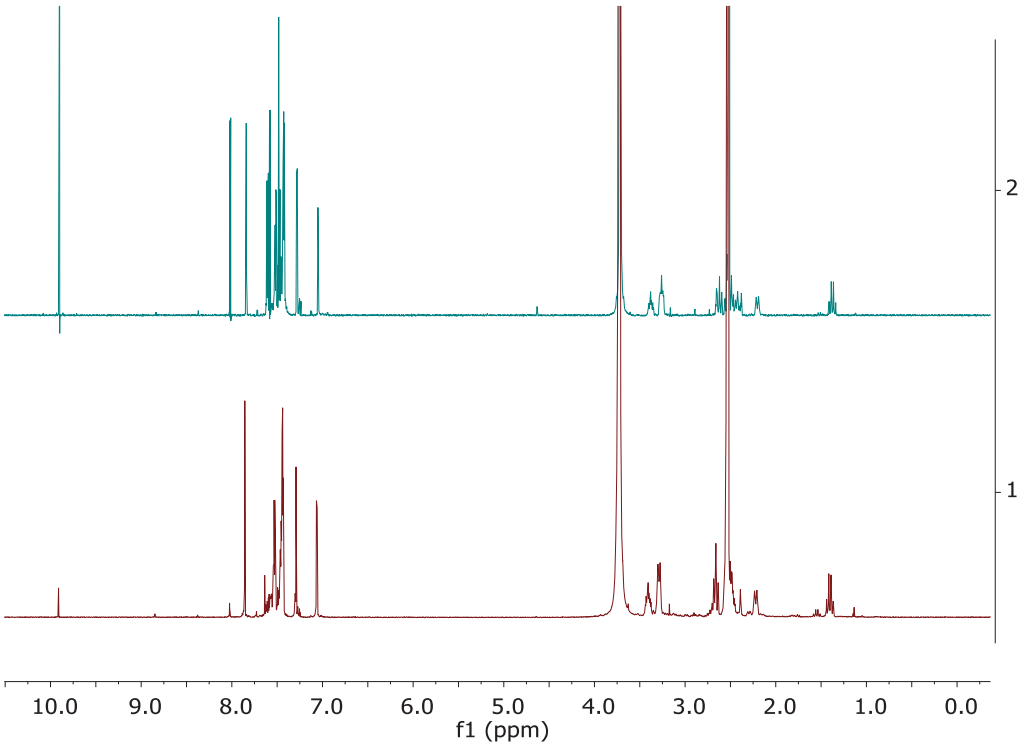

Figure S1. ^{1}H NMR spectra (500 MHz, DMSO-d_6/D_2O, 25 °C) of *rac*-**16h** (row 1) and *rac*-**16h*** (row 2).

* representing a 1:1 mixture of hydrazone *rac*-**16h** and excessive aldehyde **14h**.

Finally, *rac*-**16h*** was used for determination of its binding affinity towards mGAT1 (see Table S1). With a pK_i value of 6.72 ± 0.06 there is no statistically significant difference (P = 0.245; according to two-tailed Student's *t*-tests) in the binding affinity for *rac*-**16h*** compared to the results obtained when *rac*-**16h** was applied without excessive aldehyde **14h**. Besides, individually applied building blocks, hydrazine *rac*-**15** x HCl and aldehyde **14h**, did not show a binding affinity high enough for reliable determination of a pK_i value in concentrations up to 1 mM, demonstrating that neither excessive aldehyde **14h** (in case of *rac*-**16h***) nor unreacted building blocks (in case of *rac*-**16h**) altered the binding affinities determined for the hydrazones remarkably in the applied concentrations. Hence, it was concluded that neither unreacted aldehyde **14h** and hydrazine *rac*-**15**, respectively, nor the position of the equilibrium itself (causing a concentration of the hydrazone slightly lower as the nominal 10 mM) affected the biological evaluation of *rac*-**16h** to a remarkable extent.

Table S1. Binding affinities (pK_i) determined in MS Binding Assays at mGAT1 for hydrazone *rac*-**16h** synthesized in pure form, for *rac*-**16h*** synthesized by applying the two-fold amount of aldehyde **14h** and for building blocks hydrazine *rac*-**15** x HCl and aldehyde **14h**.

compd	pK_i[a] (mGAT1)
rac-**16h**	6.62 ± 0.04
rac-**16h***	6.72 ± 0.06
rac-**15** x HCl	60%
14h	70%

[a] pK_i values are given as means ± SEM of at least three different experiments. In case of low affinities percentages are given that represent remaining specific binding of NO711 (**4**) in presence of 1 mM test compound.

* representing a 1:1 mixture of hydrazone *rac*-**16h** and excessive aldehyde **14h**.

2. NMR spectra of compounds

1H NMR of rac-18 (400 MHz, tetrachlorethane-d2, 80 °C)

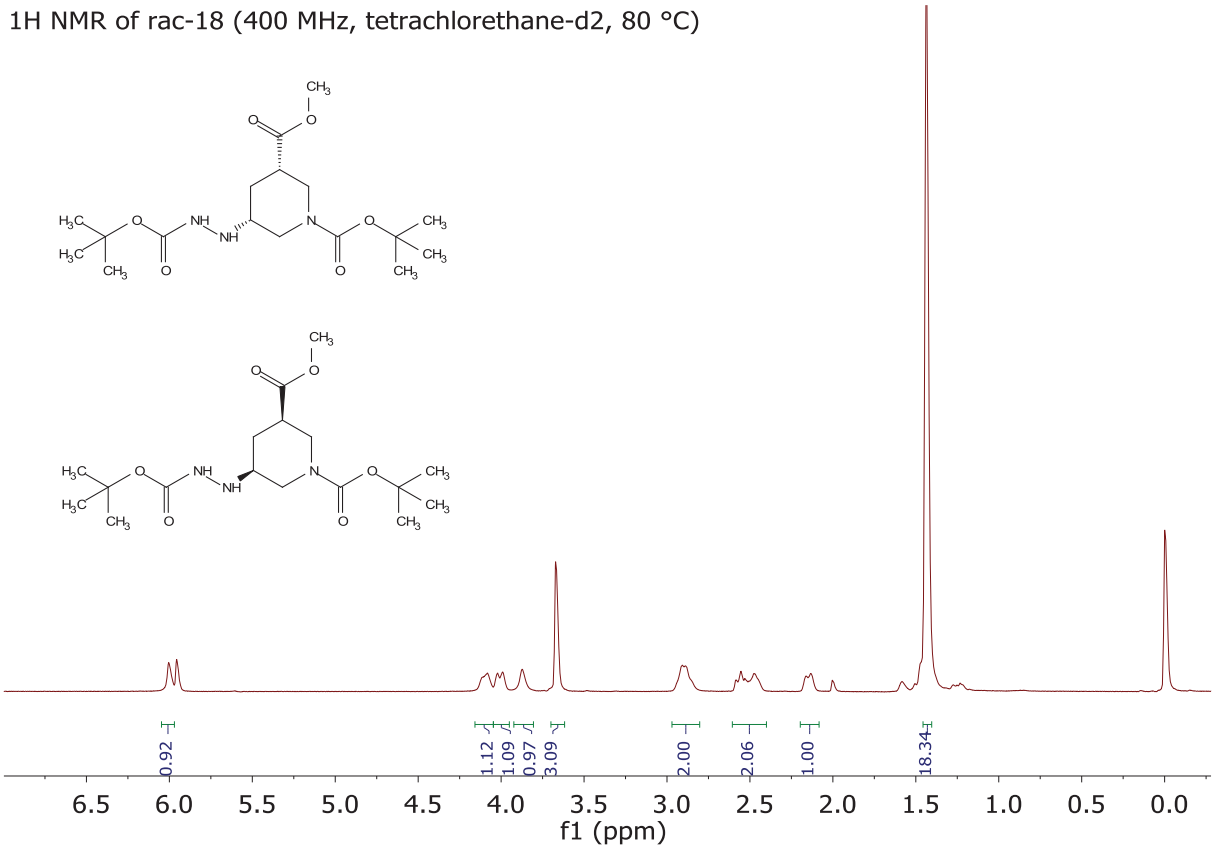

13C NMR of rac-18 (101 MHz, tetrachlorethane-d2, 80 °C)

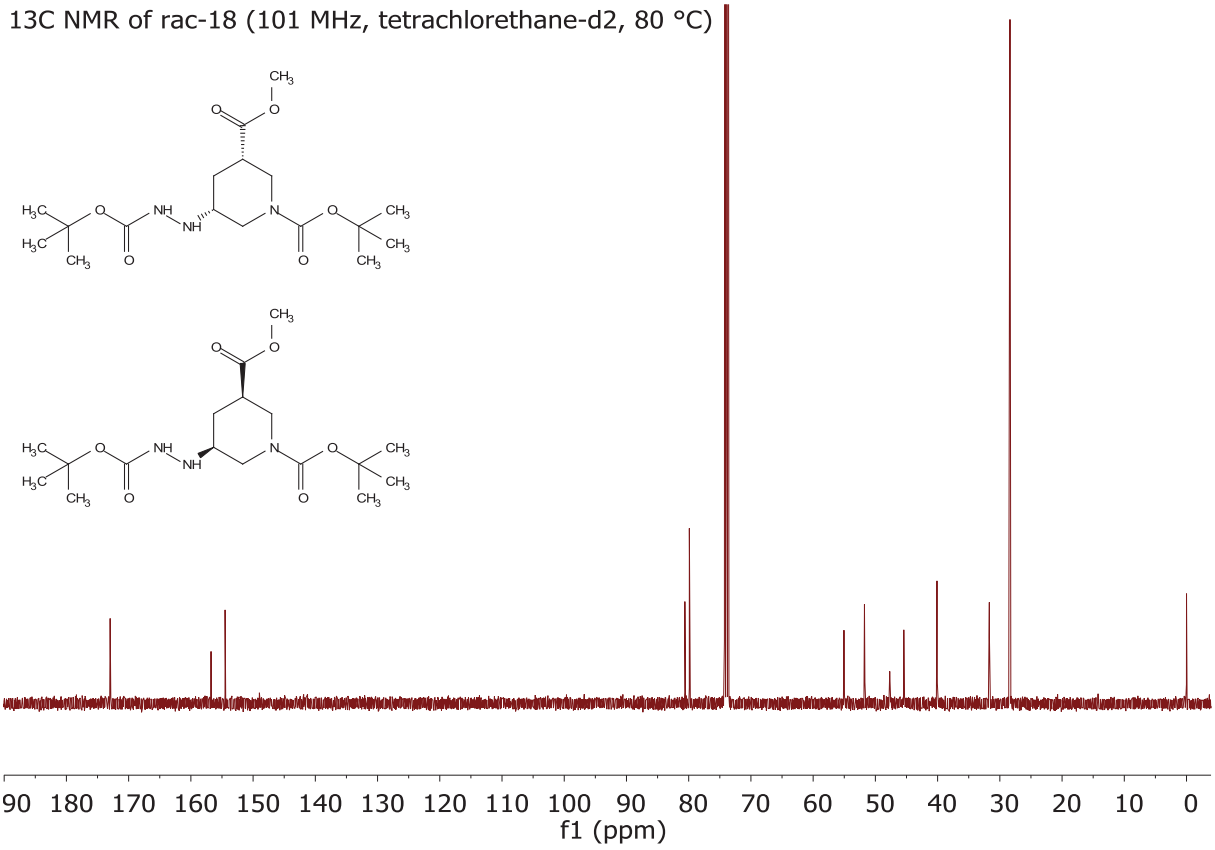

1H NMR of rac-15 x HCl (500 MHz, sodium deuteroxide in deuterium oxide, 25 °C)

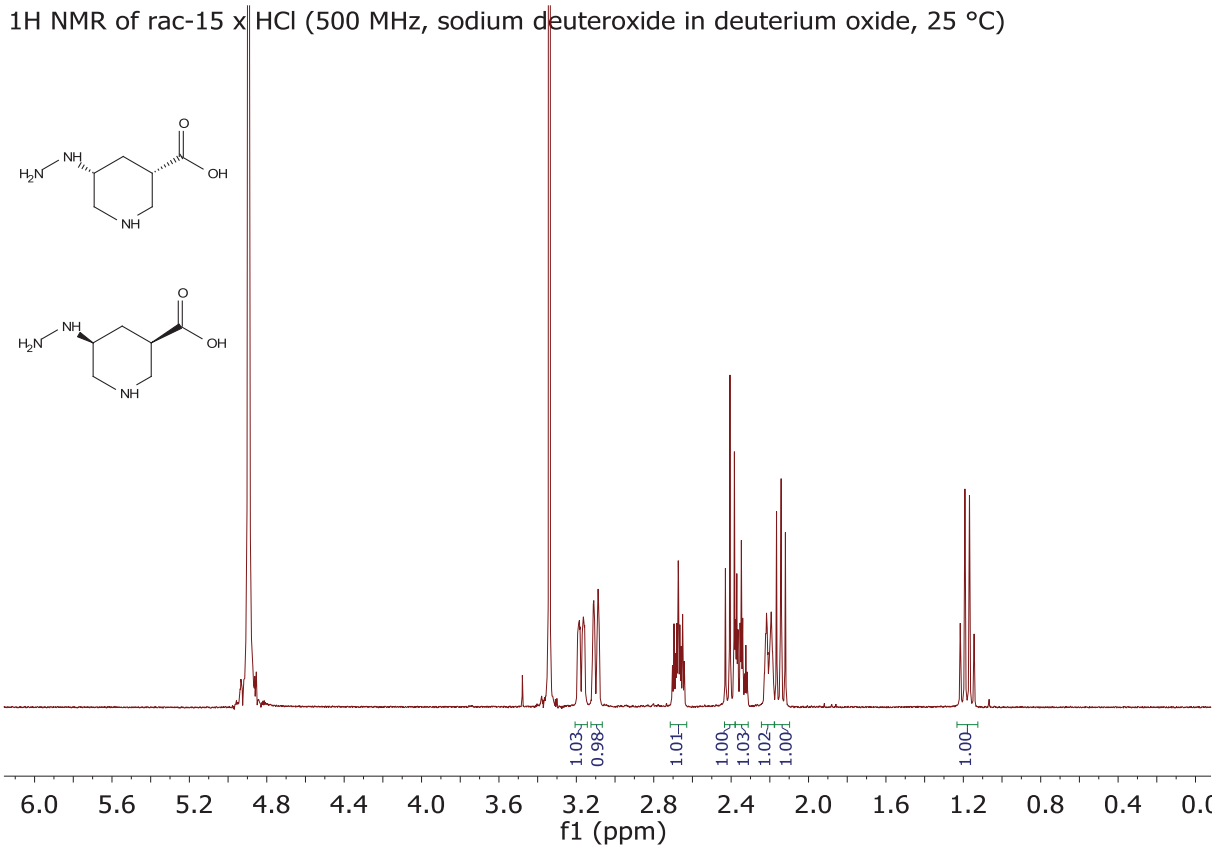

13C NMR of rac-15 x HCl (126 MHz, sodium deuteroxide in deuterium oxide, 25 °C)

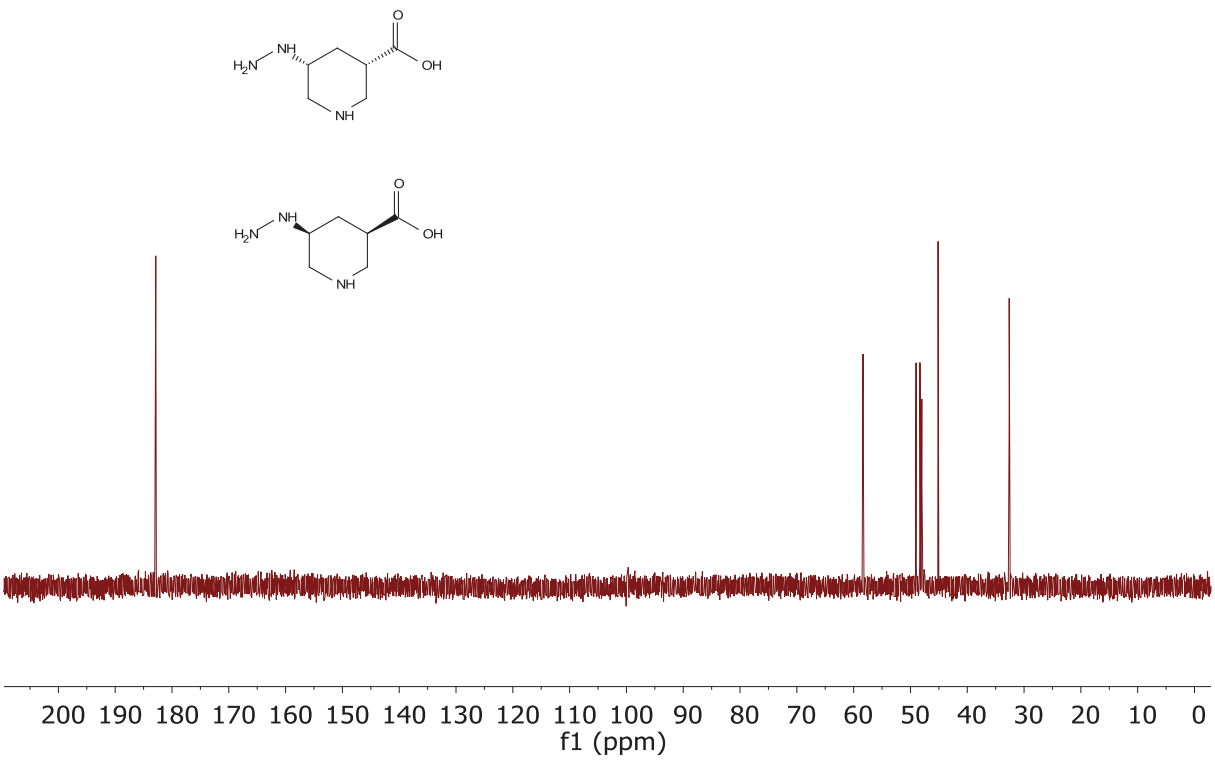

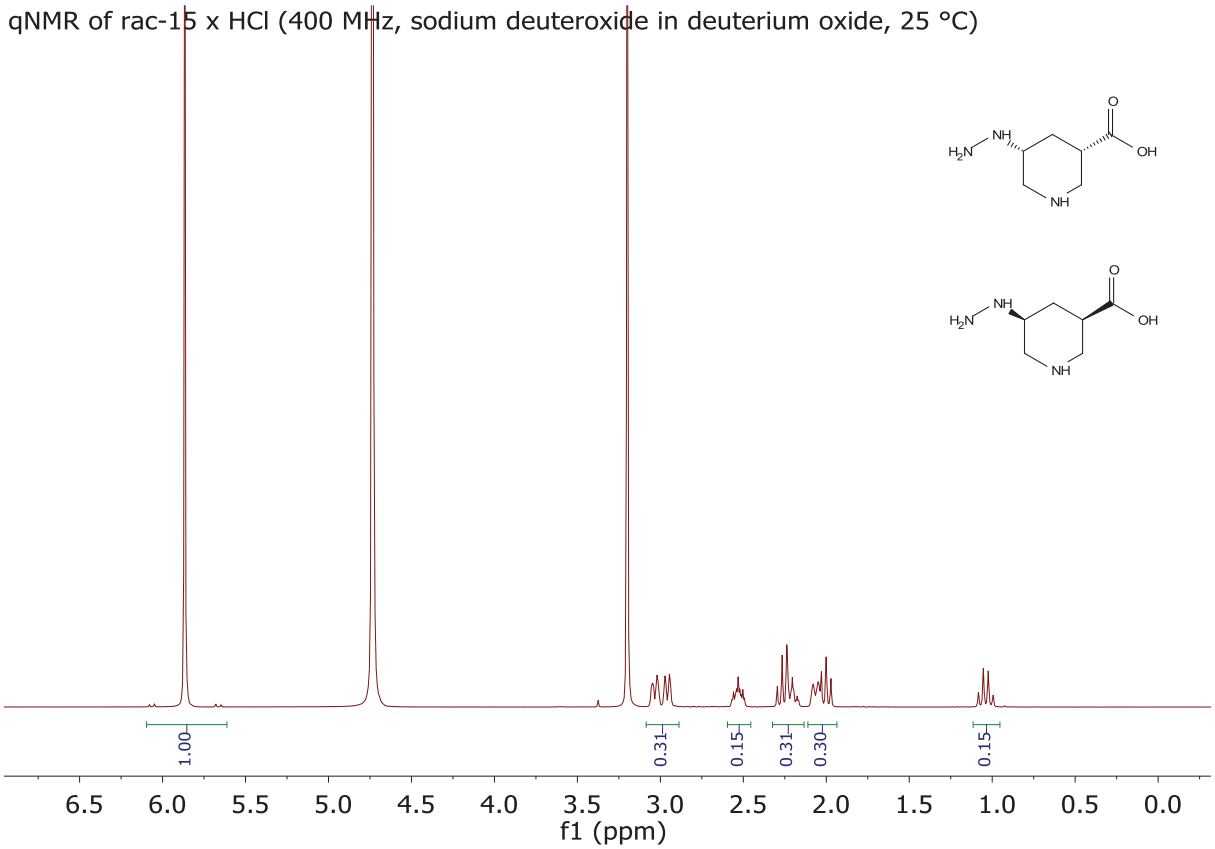

For the purity determination the sample weight was 4.738 mg and the assumed molecular weight 232.11 g/mol (calculated for the dihydrochloride of the hydrazine). Maleic acid was used as internal calibrant with a weight of 7.451 mg, a molecular weight of 116.07 g/mol and a purity of 99.94%. A purity of 95.2% was calculated for the sample using the MestReNova NMR software.

1H NMR of rac-16h (500 MHz, DMSO-d6/deuterium oxide, 25 °C)

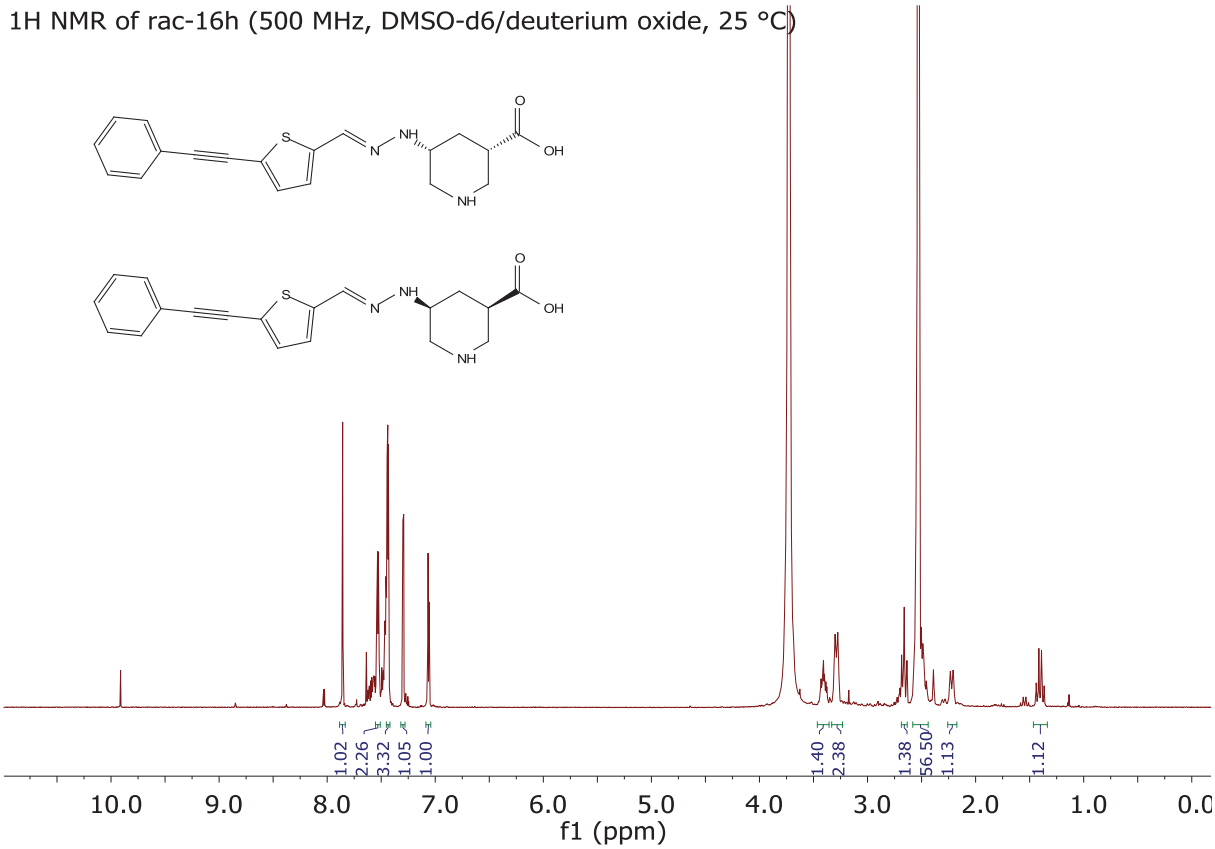

13C NMR of rac-16h (126 MHz, DMSO-d6/deuterium oxide, 25 °C)

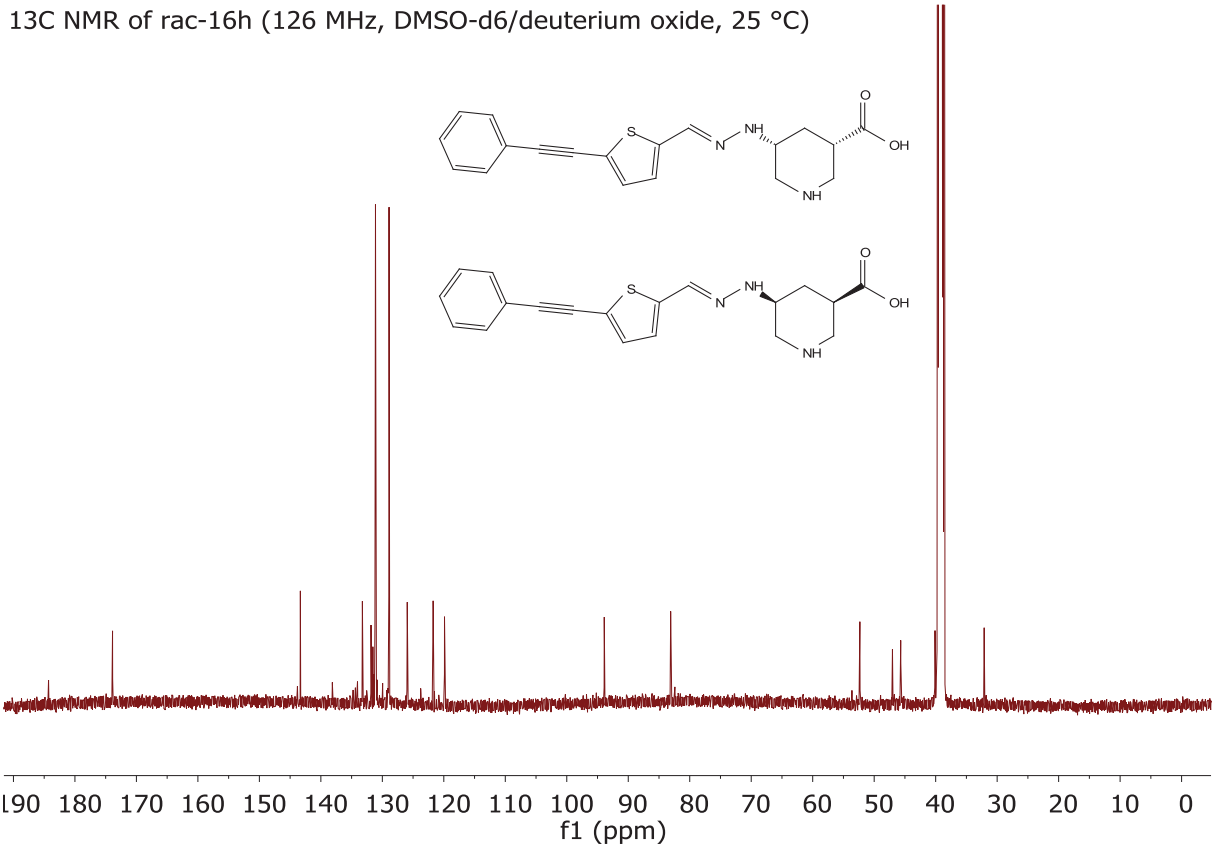

Bioorganic & Medicinal Chemistry 27 (2019) 144–152

Contents lists available at ScienceDirect

Bioorganic & Medicinal Chemistry

journal homepage: www.elsevier.com/locate/bmc

Generation and screening of pseudostatic hydrazone libraries derived from 5-substituted nipecotic acid derivatives at the GABA transporter mGAT4

Tobias J. Hauke, Georg Höfner, Klaus T. Wanner*

Department of Pharmacy – Center for Drug Research, Ludwig-Maximilians-Universität München, Butenandtstr 5–13, 81377 Munich, Germany

ARTICLE INFO

Keywords:
GABA uptake
mGAT4
Combinatorial chemistry
Hydrazones
Nipecotic acid

ABSTRACT

The γ-aminobutyric acid (GABA) transporter mGAT4 represents a promising drug target for the treatment of epilepsy and other neurological disorders; however, the lack of highly potent and selective inhibitors for mGAT4 still retards its pharmacological elucidation. Herein, the generation and screening of pseudostatic combinatorial hydrazone libraries at the murine GABA transporter mGAT4 for the search of novel GABA uptake inhibitors is described. The hydrazone libraries contained more than 1100 compounds derived from nipecotic acid derivatives substituted at the 5-position instead, as common, at the 1-position of the core structure. Two hits were found and evaluated, which display potencies in the lower micromolar range at mGAT4 and its human equivalent hGAT3. These compounds possess a lipophilic moiety derived from a biphenyl residue attached to the 5-position of the hydrophilic nipecotic acid moiety via a three-atom spacer. Thus, the novel structures with potencies close to that of the bench mark mGAT4 inhibitor (*S*)-SNAP-5114 add new insights into the structure–activity relationship of mGAT4 inhibitors and could provide a promising starting point for the development of new mGAT4 inhibitors with even higher potencies.

1. Introduction

Worldwide, about 50 million people suffer from epilepsy making this disease one of the most prevalent neurological disorders globally[1] associated with a high economic burden.[2,3] The principal inhibitory neurotransmitter in the CNS is γ-aminobutyric acid (GABA; **1**; Fig. 1) and an impaired GABAergic neurotransmission has been demonstrated to play a dominant role in the pathophysiology of epilepsy.[4–7] For treatment, reduced GABAergic neurotransmission can be adjusted by agonists of GABA receptors, by inhibition of catabolic enzymes or by targeting GABA transport proteins.[8] Four subtypes of membrane bound GABA transporters (GATs) from the solute carrier 6 (SLC6) gene family are known that are designated as mGAT1, mGAT2, mGAT3 and mGAT4 when expressed in mice; due to inconsistent nomenclature in dependence on the species from which the transporters are cloned, for all other species, and also adopted by the Human Genome Organization (HUGO), they are termed as GAT1 (≙ mGAT1), BGT1 (≙ mGAT2), GAT2 (≙ mGAT3) and GAT3 (≙ mGAT4).[9,10] Amongst the four different subtypes, mGAT1 and mGAT4 are predominately found in the mammalian brain closely to GABAergic synapses and remove GABA from the synaptic cleft by utilizing a sodium- and chloride-dependent transport.[11–13] mGAT1 is mainly located on presynaptic neurons mediating neuronal GABA uptake, whereas mGAT4 is mainly located on astrocytes mediating glial GABA uptake, while mGAT2 and mGAT3 are weakly expressed in most parts of the brain.[14–16] mGAT1 is a well-known target for achieving anticonvulsant effects and several potent and selective mGAT1 inhibitors such as tiagabine (**2**) and structurally related compounds have been developed.[17–20] Tiagabine (**2**) was approved as add-on treatment of partial-onset seizures and is the only GAT inhibitor in clinical use up to now[21,22]; main drawbacks, however, are its side effects including dizziness, asthenia, nervousness, tremor, diarrhea, and depression.[23,24] Conversely, for mGAT4 as well as for the other GABA transporter subtypes (mGAT2 and mGAT3) there is a lack of highly potent inhibitors that could be employed as pharmacological tools for elucidating the therapeutic potential of inhibitors of these GAT subtypes. Hence, the functional role of the other GABA transporter subtypes still has to be elucidated in more detail, although particularly mGAT2 and mGAT4 are already considered as promising drug targets for the treatment of epilepsy and other neurological disorders such as anxiety and pain.[9,12,13] In the more recent years several efforts have been undertaken to synthesize and evaluate potential ligands of different GAT subtypes[25–30]; thereby, compounds could be identified with selectivities for mGAT2–mGAT4, although their potencies are remarkably lower than those of potent mGAT1 inhibitors. The compound (*S*)-SNAP-5114 (**3**) represented the first prototypic inhibitor with moderate potency at and selectivity for mGAT4[31] and chemically more

* Corresponding author.
E-mail address: klaus.wanner@cup.uni-muenchen.de (K.T. Wanner).

https://doi.org/10.1016/j.bmc.2018.11.028
Received 6 September 2018; Received in revised form 29 October 2018; Accepted 20 November 2018
Available online 22 November 2018
0968-0896/

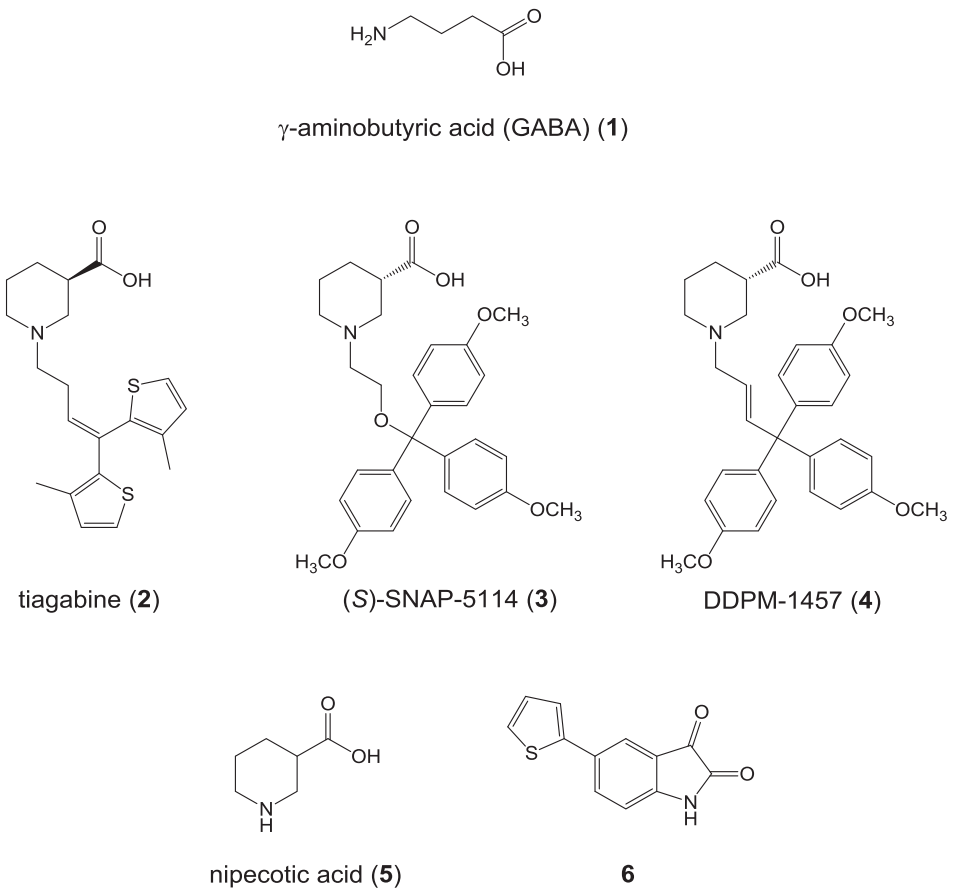

Fig. 1. Structures of GABA and selected GABA uptake inhibitors.

stable carba analogs of this trityloxy derivative **3** could be synthesized later, of which DDPM-1457 (**4**) displays similar potency.[32] Most of the potent and selective GAT inhibitors with selectivities for either mGAT1 or mGAT4 are typically derivatives of small cyclic amino acids such as nipecotic acid (**5**), of which the hydrophilic amino acid moiety is substituted with lipophilic aromatic residues attached to the amino group (i.e. the 1-position of the piperidine moiety) via a linker. Notably, nipecotic acid (**5**) itself displays already reasonable potency at different GAT subtypes; however, it is nearly inactive *in vivo* due to limited blood–brain barrier permeability as a direct consequence of its high polarity.[33] Besides, a series of isatin derivatives including compound **6** was more recently reported representing a new class of mGAT4 inhibitors structurally distinctly different from aforementioned nipecotic acid (**5**) derivatives.[34]

Herein, we describe the screening of hydrazone libraries, generated by dynamic combinatorial chemistry (DCC), at mGAT4 with the aim of exploring novel structures as potential GABA uptake inhibitors.

2. Results and discussion

2.1. Structures of hydrazone libraries

Most recently, we generated and screened hydrazone libraries at mGAT1 for exploring an uncommon substitution pattern of nipecotic acid (**5**) derivatives as means of obtaining novel bioactive compounds. Based on *in silico* studies the 5-position of the nipecotic acid (**5**) core structure instead of the common 1-position was substituted with aromatic residues attached to it via a spacer. In order to enable a vast and easy to perform structural variation of the lipophilic moiety library generation and screening was performed according to an established procedure.[35,36] This proven procedure combines the formation of combinatorial hydrazone libraries with the read-out of their binding affinities towards mGAT1 by means of mass spectrometry based binding assays (MS Binding Assays). This approach is described in detail elsewhere (as well as the syntheses of hydrazines *rac*-**7**–*rac*-**11** and the compilation of aldehyde libraries **12**, see below).[37,38] Despite being possibly prone to hydrolysis, the hydrazone function has proven to represent a well-suited linker with sufficient stability also in presence of the biological target material; it allowed the identification of new highly potent inhibitors for the GABA transporter mGAT1 bearing a hydrazone function in the spacer as already demonstrated, previously.[35,36]

Considering that the nipecotic acid (**5**) moiety is also present as parent structure in prototypic mGAT4 inhibitors such as (*S*)-SNAP-5114 (**3**), the aforementioned combinatorial hydrazone libraries containing the same nipecotic acid (**5**) derivatives, bearing an extraordinary substitution pattern and a vast diversity of lipophilic residues, were utilized for a new screening campaign for mGAT4 inhibitors as described herein. As in the mentioned previous approaches, hydrazone libraries were generated by reacting hydrophilic building blocks possessing a hydrazine function with lipophilic building blocks equipped with an aldehyde function. The hydrazine function was attached to the 5-position of nipecotic acid (**5**) directly (*rac*-**7**) or via a spacer containing one (*rac*-**8** and *rac*-**9**) or two C-atoms (*rac*-**10** and *rac*-**11**) and the linker residue was either *cis*- (*rac*-**7**, *rac*-**8** and *rac*-**10**) or *trans*-oriented (*rac*-**9** and *rac*-**11**) with respect to the carboxylic acid function in 3-position of the piperidine ring (note that commercially available, achiral methyl 5-hydroxynicotinate was used as starting material for the syntheses of all hydrazines, the latter of which were accordingly obtained as racemates[37]). By reaction with appropriate aldehydes **12** these nipecotic acid (**5**) derived hydrazines were converted into the corresponding hydrazones with a three (*rac*-**13**), four (*rac*-**14** and *rac*-**15**) and five

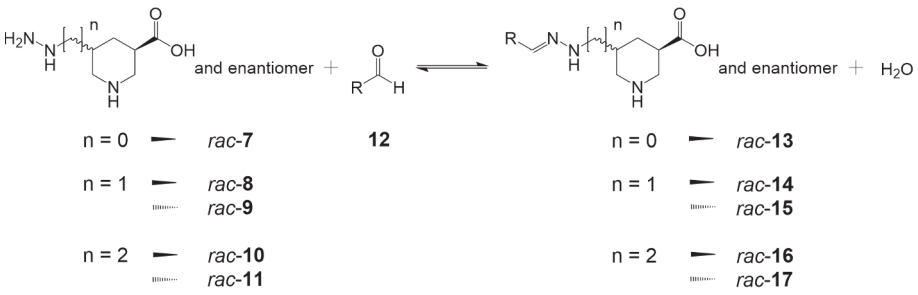

Scheme 1. Condensation of nipecotic acid derived hydrazines *rac*-**7**–*rac*-**11** with diverse aldehydes **12** to afford hydrazones with general structures *rac*-**13**–*rac*-**17** (each hydrazine and hydrazone, respectively, was obtained as racemate as indicated in this scheme; for the sake of simplicity, only one enantiomer is depicted in the following schemes and figures).

atom spacer (*rac*-**16** and *rac*-**17**; Scheme 1). As pattern for the lipophilic moiety a total of 224 mostly aromatic aldehydes grouped in 28 aldehyde libraries was employed (Fig. 2) and combined separately with all five hydrazines, *rac*-**7**–*rac*-**11**. As these 140 libraries comprise more than 1,100 compounds their screening at mGAT4 could be expected to reveal new insights into the structure–activity relationship and to yield potentially new scaffolds for mGAT4 inhibitors.

2.2. Generation and screening of hydrazone libraries

In contrast to the screening at mGAT1, which is based on MS Binding Assays using LC-MS/MS quantification of the non-labelled GAT1-selective inhibitor NO711 as reporter ligand, binding assays for screening at mGAT4 are, due to the lack of ligands with sufficient affinity, up to now not available. Accordingly, in this present approach we tried to combine combinatorial generation of pseudostatic hydrazone libraries with the [^{3}H]GABA uptake assay routinely used in our group (described in detail by Kragler et al. [39,40]). As this functional assay is based on intact HEK cells stably expressing mGAT4 (in contrast to the MS based screening at mGAT1, for which membrane fragments were utilized), library generation and screening had to be decoupled, due to the conditions required for *in situ* library generation that would severely impair viability of the cells. Therefore, combinatorial hydrazone libraries were generated by preincubating the concentrated mixture of a single hydrazine (from a 10 mM stock solution in phosphate buffer) with each aldehyde library containing eight individual aldehydes (each in a concentration of 100 µM in a stock solution in DMSO) for 30–40 min. The hydrazine was used in large excess compared to aldehydes (5 mM hydrazine versus 400 µM total aldehyde concentration during preincubation) in order to speed up hydrazone formation and most of all to achieve a constant library composition even if a thermodynamic equilibrium were operating; that way, the dynamic combinatorial libraries were rendered pseudostatic (i.e. forced to a fixed composition). To prove that these conditions appeared appropriate to guarantee quantitative hydrazone formation, control experiments were carried out: Therefore, hydrazone formation was exemplarily performed with all five hydrazines, *rac*-**7**–*rac*-**11**, which were individually reacted with aldehyde **12w**. This aldehyde, **12w**, had been demonstrated in previous approaches to be comparatively slower reacting than other evaluated aldehydes (in experiments performed under identical conditions, i.e. solvent composition and concentrations), when preparing the libraries for the screening experiments.[35,37] When the progress of the reactions was monitored by ^{1}H NMR, the signal of the aldehyde proton of **12w** was found to completely (for reactions with *rac*-**7**–*rac*-**9**) or nearly completely (*rac*-**10** and *rac*-**11**) disappear within 10 min after mixing the individual building blocks (note that the aldehyde was observed to be in equilibrium with the geminal diol of its hydrate form, the latter of which also disappeared during hydrazone formation). Within the same time, the ^{1}H NMR signal resulting from the formed hydrazone grew to full intensity indicating an almost quantitative to quantitative hydrazone formation within 10 min and even more in the set time period for library generation (30–40 min).

The libraries that were formed according to the abovementioned procedure are termed "*cis*-C0", "*cis*-C1", "*trans*-C1", "*cis*-C2" and "*trans*-C2" for hydrazones derived from *rac*-**13**, *rac*-**14**, *rac*-**15**, *rac*-**16** and *rac*-**17**, respectively, throughout this paper to indicate their relative configurations and different spacer lengths (Fig. 3).

As we aimed to screen for compounds with low micromolar or submicromolar potency, the original pseudostatic hydrazone libraries were diluted to a final concentration of 1 µM (1 µM for each hydrazone) and studied for their inhibitory potencies in [^{3}H]GABA uptake assays for mGAT4. Libraries were considered active, if they reduced remaining [^{3}H]GABA uptake below 50%. Given the large number of compounds included in the library screening, we decided to use this single, strict "activity criterion" (i.e. reduction of remaining GABA uptake below 50% at a concentration of 1 µM of each library component) in order to screen exclusively for the most active compounds. The results of the screening process, i.e. the percentage of remaining [^{3}H]GABA uptake in the presence of each of the 140 hydrazone libraries, are summarized in Table 1.

The hydrazone libraries showed a broad range of inhibitory potencies, but only two fulfilled the "activity criterion" by reducing remaining [^{3}H]GABA uptake below 50% (by mean values of three replicates), that were *cis*-C0 hydrazone library 9 and *cis*-C0 hydrazone library 24 with remaining [^{3}H]GABA uptake of 45% for each. Interestingly, both "active" libraries are derived from hydrazone *rac*-**13** and thus represent the compounds with the shortest spacer lengths (i.e. three atoms) of all analogs. Notably, the hydrazines *rac*-**7**–*rac*-**11**, when tested in pure form without prior preincubation with an aldehyde library, did not show any remarkable activity in concentrations of 100 µM.

After the initial screening step, the two libraries found to be "active" were subjected to deconvolution experiments in order to identify their most active components. The deconvolution experiments were performed in the same way as the screening experiments except that only a single hydrazone was generated and applied by employing only a single aldehyde instead of a library representing a mixture of eight compounds. The results from [^{3}H]GABA uptake assays obtained for individual components of *cis*-C0 hydrazone libraries 9 and 24 are summarized in Table 2. None of the 16 hydrazones from the two most "active" libraries reduced remaining [^{3}H]GABA uptake below 50%. Hence, the inhibitory potencies observed for both libraries in the initial screening appear to be the result of additive effects rather than due to a single component with submicromolar potency (and besides additive effects, inevitable variations associated with the application of a functional biological test system based on living cells, which on their own have only minor effects, could cumulatively cause a degree of scattering that may also be an explanation for these discrepancies). However, the two most active hydrazones from deconvolution, i.e. *rac*-**13bq** and *rac*-**13bt**, still reduced remaining [^{3}H]GABA uptake to a remarkable extent with mean values of 69% and 72%, respectively. These two "active" hydrazones were both contained in *cis*-C0 hydrazone library 9, while surprisingly none of the individual components of library 24 reduced uptake substantially. Being the most active compounds and hence representing the hits from these screening and deconvolution experiments, the two hydrazones *rac*-**13bq** and *rac*-**13bt** were subjected to further analysis in order to establish their inhibitory potencies (pIC_{50}) and subtype selectivities.

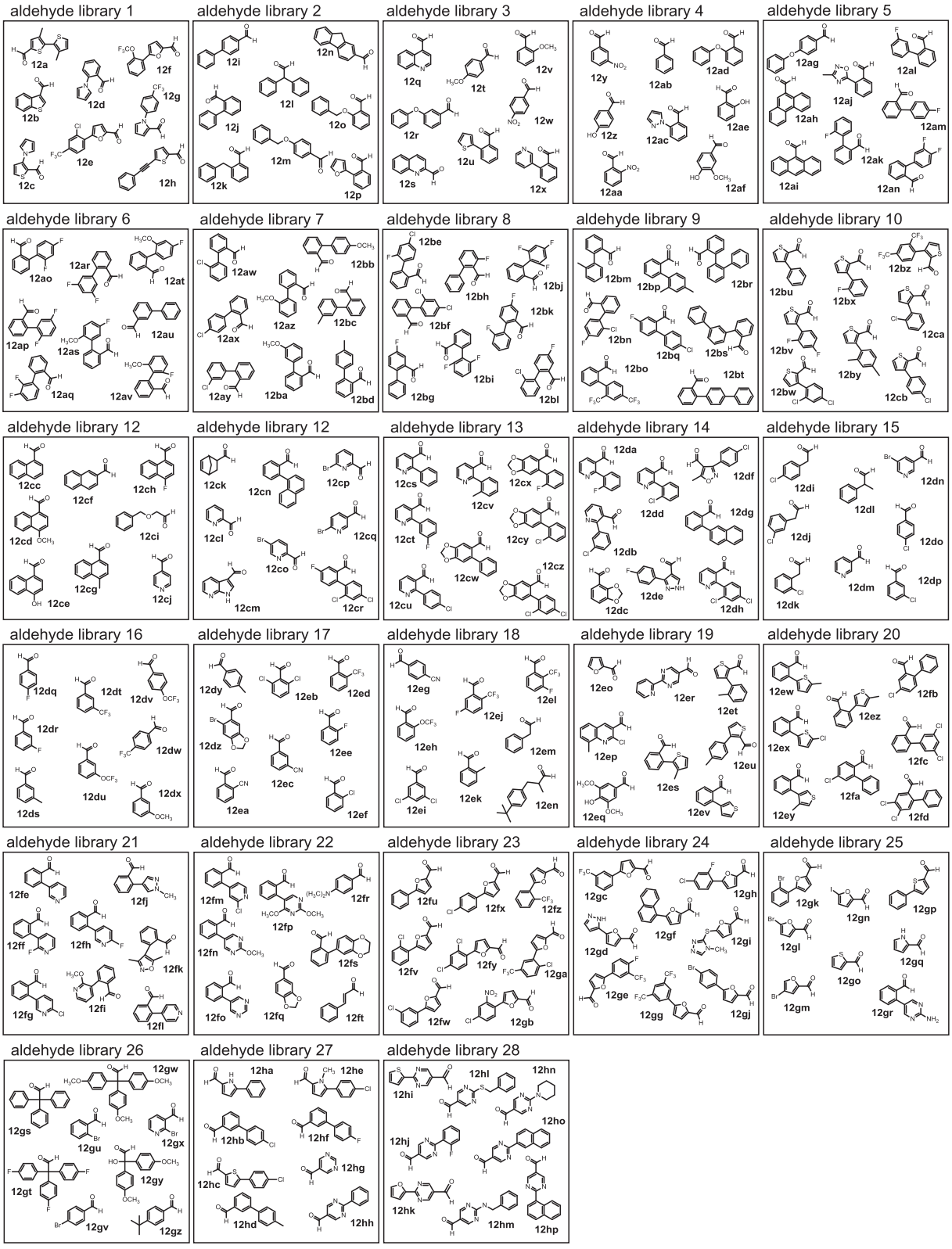

Fig. 2. Libraries consisting of aldehydes **12a–12hp**.

2.3. Hit verification

For hit verification, the two most active hydrazones, *rac*-**13bq** and *rac*-**13bt**, were each separately synthesized in pure form. To this end, hydrazine *rac*-**7** was reacted with aldehydes **12bq** and **12bt**, respectively, yielding corresponding hydrazones *rac*-**13bq** and *rac*-**13bt** as shown in Table 3.

In order to demonstrate that these hydrazones, *rac*-**13bq** and *rac*-**13bt** (synthesized in pure form and without excessive hydrazine as applied during the screening experiments), show sufficient hydrolytic stability for the subsequent full-scale GABA uptake assays, we performed control experiments. To this end, the hydrazones were diluted

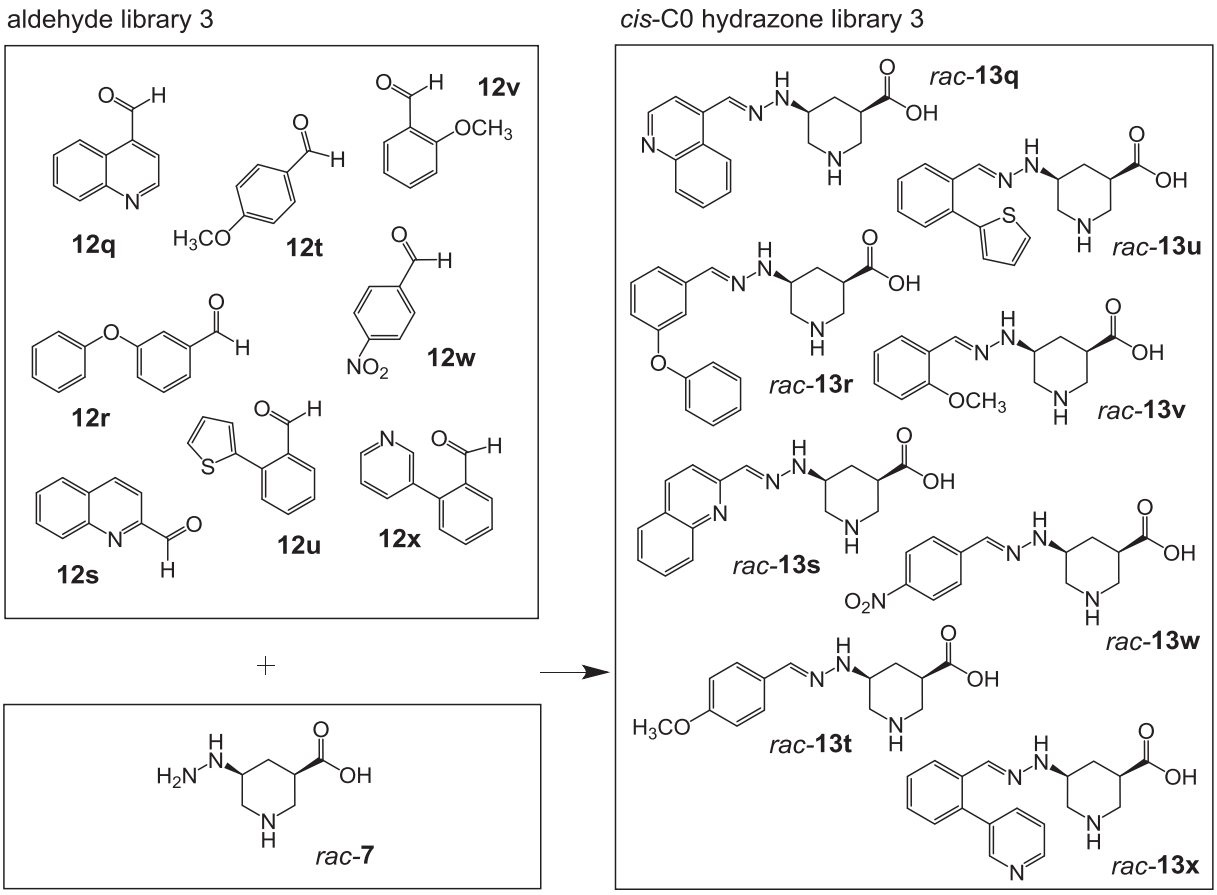

Fig. 3. Example for the conversion of aldehyde library 3 with hydrazine *rac*-**7** into *cis*-C0 hydrazone library 3.

in the incubation buffer (containing millimolar concentrations of salts, glucose and tris(hydroxymethyl)aminomethane; pH = 7.2),[40] to which GABA (**1**) was added, and the solution was monitored by ^{1}H NMR at 37 °C over 2.5 h (corresponding ^{1}H NMR spectra of hydrazone *rac*-**13bq** are exemplarily shown in Fig. 4). During the kinetic experiments no degradation of the hydrazones could be observed and both *rac*-**13bq** and *rac*-**13bt** appeared stabile at 37 °C over the observation period (2.5 h). Accordingly, it may be concluded that the incubation buffer as well as the presence of GABA (**1**), as to be utilized during the corresponding GABA uptake assays, does not affect the hydrazone stability, even when the hydrazones were applied in pure form and without excessive hydrazine (as it is the case during screening experiments to render hydrazone libraries pseudostatic).

Both hydrazones were then tested for their inhibitory potencies at mGAT4 as well as at the other three GABA transporter subtypes (mGAT1–mGAT3) in order to determine their subtype selectivities. Therefore, full-scale [^{3}H]GABA uptake assays were performed using HEK cells stably expressing mGAT1–mGAT4[39,40]; the data from which were used to generate the respective concentration-inhibition curves and calculation of IC_{50} values. In order to confirm potencies and to establish IC_{50} values also at the human equivalent of this GABA transporter subtype, both compounds were additionally characterized at hGAT3 in competitive MS based GABA transport experiments (MS Transport Assays)[41,42] utilizing COS cells stably expressing hGAT3. The results obtained in these experiments are summarized (as pIC_{50} values) in Table 4. For hydrazone *rac*-**13bq** pIC_{50} values of 5.27 at mGAT4 and 5.56 at hGAT3 and for *rac*-**13bt** of 4.99 at mGAT4 and 5.03 at hGAT3, respectively, were established. Notably, the pIC_{50} values of *rac*-**13bq** and *rac*-**13bt** at hGAT3 are close to that of bench mark mGAT4/hGAT3 inhibitor (*S*)-SNAP-5114 (**3**), while the pIC_{50} values at mGAT4 are somewhat lower for the hydrazones as compared to **3** (with the nominal difference amounting to 0.38–0.66 log units). In this context it is worth mentioning that the hydrazones are, in contrast to (*S*)-SNAP-5114 (**3**), racemic, providing the possibility that the corresponding eutomers could be even a bit more potent. Furthermore, the inhibitory potencies of the two hydrazones, *rac*-**13bq** and *rac*-**13bt**, at both mGAT4 and hGAT3 appear nominally slightly superior (or at least similarly, i.e. for *rac*-**13bt** at hGAT3) than those of isatin derivative **6** as a yet published example of a non-nipecotic acid (**5**) derived GAT inhibitor. Thus, the hydrazones *rac*-**13bq** and *rac*-**13bt** represent novel mGAT4 and hGAT3 inhibitors, respectively, with promising potencies in the lower micromolar range. Thereby, the inhibitory potency of *rac*-**13bq** at mGAT4 and hGAT3 appears to be slightly superior to that of *rac*-**13bt**.

The inhibitory potency of hydrazone *rac*-**13bt** at mGAT1 and mGAT2 appears to be too low to reduce [^{3}H]GABA uptake to 50% or below, even at a concentration of 100 µM. Hence, no pIC_{50} value could be determined using 100 µM as the highest test concentration, but it may be concluded that the pIC_{50} values of *rac*-**13bt** at these two transporters are likely to be lower than 4.0. Thus, both hydrazones, *rac*-**13bq** and *rac*-**13bt**, are at least one order of magnitude more potent towards mGAT4 than towards mGAT1 and mGAT2, respectively, indicating a reasonable subtype selectivity over the latter two GAT subtypes. Conversely, for both hydrazones *rac*-**13bq** and *rac*-**13bt** pIC_{50} values at mGAT3 are similar to those at mGAT4 indicating a poor subtype selectivity for mGAT4 over mGAT3. This is, however, a problem frequently observed for other mGAT4 inhibitors reported in literature.[27,32,40,42] For both hydrazones, *rac*-**13bq** and *rac*-**13bt**, the lipophilic domains are derived from a biphenyl moiety; while a biphenyl moiety is well known as a lipophilic domain of mGAT1 inhibitors,[36,43] it is to our knowledge unprecedented for mGAT4 inhibitors with high potencies ($pIC_{50} \geq 5$).

Table 1
Screening of *cis*-C0 (*rac*-**13**), *cis*-C1 (*rac*-**14**), *trans*-C1 (*rac*-**15**), *cis*-C2 (*rac*-**16**) and *trans*-C2 hydrazone libraries (*rac*-**17**) at mGAT4.

library	remaining [^{3}H]GABA uptake [%][a]				
	cis-C0	*cis*-C1	*trans*-C1	*cis*-C2	*trans*-C2
library 1	122 ± 4	113 ± 0.4	107 ± 10	113 ± 29	122 ± 18
library 2	118 ± 20	81 ± 8	113 ± 16	106 ± 20	125 ± 11
library 3	113 ± 4	80 ± 34	102 ± 10	90 ± 5	98 ± 8
library 4	118 ± 8	97 ± 12	112 ± 8	95 ± 18	106 ± 13
library 5	116 ± 4	75 ± 2	133 ± 27	95 ± 10	100 ± 8
library 6	100 ± 13	66 ± 12	110 ± 8	89 ± 8	97 ± 14
library 7	87 ± 15	61 ± 6	105 ± 5	92 ± 16	61 ± 19
library 8	88 ± 9	88 ± 12	114 ± 1	84 ± 8	89 ± 15
library 9	**45 ± 6**	76 ± 3	99 ± 28	102 ± 27	89 ± 14
library 10	72 ± 22	55 ± 3	106 ± 11	91 ± 10	112 ± 8
library 11	109 ± 2	71 ± 7	101 ± 11	82 ± 18	66 ± 5
library 12	112 ± 13	75 ± 10	126 ± 34	86 ± 13	106 ± 2
library 13	90 ± 8	78 ± 18	123 ± 14	97 ± 18	98 ± 9
library 14	83 ± 8	91 ± 0.4	123 ± 21	85 ± 6	85 ± 17
library 15	89 ± 15	80 ± 6	112 ± 6	82 ± 5	92 ± 6
library 16	129 ± 6	92 ± 5	108 ± 14	87 ± 19	87 ± 15
library 17	64 ± 8	82 ± 20	111 ± 19	71 ± 14	79 ± 8
library 18	80 ± 7	78 ± 19	107 ± 11	90 ± 5	74 ± 25
library 19	88 ± 6	81 ± 4	123 ± 12	85 ± 16	86 ± 14
library 20	91 ± 16	56 ± 4	107 ± 7	84 ± 13	63 ± 4
library 21	93 ± 10	67 ± 3	92 ± 4	93 ± 5	58 ± 15
library 22	98 ± 10	92 ± 9	99 ± 17	103 ± 7	67 ± 6
library 23	105 ± 12	65 ± 5	109 ± 29	77 ± 18	73 ± 15
library 24	**45 ± 6**	64 ± 3	109 ± 6	60 ± 11	61 ± 12
library 25	94 ± 7	82 ± 16	110 ± 20	105 ± 16	83 ± 9
library 26	82 ± 12	75 ± 12	118 ± 17	109 ± 19	72 ± 17
library 27	86 ± 4	71 ± 12	108 ± 42	85 ± 3	57 ± 2
library 28	78 ± 11	64 ± 3	101 ± 16	92 ± 13	67 ± 16
only hydrazine[b]	116 ± 8	92 ± 13	86 ± 6	102 ± 19	85 ± 10

[a] Percentage of remaining [^{3}H]GABA uptake in the presence of corresponding pseudostatic hydrazone libraries containing eight components each in a concentration of 1 μM; data represent means ± SD of three replicates. The limit for further analysis of a hydrazone library was defined as 50% remaining [^{3}H]GABA uptake (libraries considered "active" are highlighted in bold letters).
[b] Pure hydrazines *rac*-**7**, *rac*-**8**, *rac*-**9**, *rac*-**10** and *rac*-**11**, respectively, were applied in a concentration of 100 μM for control.

Table 2
Deconvolution of *cis*-C0 hydrazone libraries (*rac*-**13**) considered "active" at mGAT4.

library	*cis*-C0 hydrazone	remaining [^{3}H]GABA uptake [%][a]
library 9	*rac*-**13bm**	90 ± 4
	rac-**13bn**	96 ± 11
	rac-**13bo**	83 ± 18
	rac-**13 bp**	84 ± 5
	rac-**13bq**	**69 ± 1**
	rac-**13br**	92 ± 11
	rac-**13bs**	89 ± 5
	rac-**13bt**	**72 ± 7**
library 24	*rac*-**13gc**	95 ± 5
	rac-**13gd**	96 ± 4
	rac-**13ge**	88 ± 8
	rac-**13gf**	102 ± 7
	rac-**13gg**	86 ± 4
	rac-**13gh**	85 ± 6
	rac-**13gi**	92 ± 8
	rac-**13gj**	93 ± 6

[a] Percentage of remaining [^{3}H]GABA uptake in the presence of individual *cis*-C0 hydrazones in a concentration of 1 μM; data represent means ± SD of three replicates. Values of hydrazones chosen for further analysis are highlighted in bold letters.

3. Conclusion

In summary, the generation and screening of combinatorial hydrazone libraries derived from 5-substituted nipecotic acid (**5**) derivatives at mGAT4 is described herein. The hydrazone libraries were rendered pseudostatic and contained more than 1,100 individual compounds with varying spacer lengths and lipophilic moieties. The generated libraries were screened in a functional assay for their inhibitory potencies at mGAT4, i.e. in [^{3}H]GABA uptake experiments using HEK cells stably expressing this target. With hydrazones *rac*-**13bq** and *rac*-**13bt** two hits were obtained from the screening and deconvolution experiments. Hit verification revealed a promising potency at mGAT4 of these two compounds only slightly inferior to that of best prototypic mGAT4 inhibitors known so far. These compounds, *rac*-**13bq** and *rac*-**13bt**, possess a novel structural scaffold for this kind of bioactive compounds, comprising a 5-substitution instead of the common 1-substitution of the nipecotic acid (**5**) moiety, as well as biphenyl residues as lipophilic domaines. There is still a lack of highly potent and selective mGAT4 inhibitors that would allow to elucidate the pharmacological role of this GABA transporter subtype, which is thought to be a promising drug target. The two hydrazones described herein represent new structural motifs for mGAT4 inhibitors, which could serve as useful starting points for further exploring structure–activity relationship of mGAT4 inhibitors and facilitate the rational design of new ligands with higher potencies at this molecular target.

4. Experimental section

4.1. Chemistry

4.1.1. General methods

NMR spectroscopy was performed on an Avance III HD Bruker BioSpin spectrometer (Bruker; ^{1}H NMR: 500 MHz, ^{13}C NMR: 126 MHz, ^{19}F NMR: 376 MHz) equipped with a CryoProbe™ Prodigy broadband probe head; the spectra were processed with the NMR software MestReNova, version 12.0 (Mestrelab Research S.L.). Chemical shifts were referenced to DMSO solvent signals (^{1}H NMR: 2.53 ppm; ^{13}C NMR: 39.13 ppm). High-resolution mass spectrometry (ESI) was performed with Thermo Finnigan LTQ FT Ultra mass spectrometer (ThermoFischer Scientific). Syntheses of hydrazines *rac*-**7**–*rac*-**11**, which were applied as hydrochlorides, and compilation of libraries containing aldehydes **12a–12hp** are described elsewhere.[37,38] For hit verification individual hydrazones were synthesized in sealed 1.5 mL tubes under Ar. Reaction progress (determined by integration of the remaining signal of the aldehyde proton) was monitored by ^{1}H NMR. All NMR and HRMS measurements as well as the GABA uptake assays were performed using the 10 mM hydrazone solutions without further purification or drying.

4.1.2. Synthesized compounds

*4.1.2.1. rac-(3R,5S)-{5-[(E)-2-({4′-Chloro-4-fluoro-[1,1′-biphenyl]-2-yl} methylidene)hydrazin-1-yl]piperidine-3-carboxylic acid}–sodium chloride (1/2), (rac-**13bq**).* To DMSO-d_6 (850 μL) a 200 mM stock solution of *rac*-**7** in D_2O (50 μL, 0.010 mmol), a 1 M solution of NaOD in D_2O (20 μL, 0.020 mmol) and D_2O (30 μL) were added to reach a total volume of 950 μL. The reaction was started by the addition of a 200 mM stock solution of 4′chloro 4 fluoro [1,1′biphenyl] 2carbaldehyde (**12bq**) in DMSO-d_6 (50 μL, 0.010 mmol). The mixture was sonicated for 5 min and stored at rt over night to obtain *rac*-**13bq** in solution (remaining aldehyde ≤ 2%).

^{1}H NMR (500 MHz, DMSO-d_6/D_2O = 9:1, 25 °C): δ = 1.36 (q, J = 12.2 Hz, 1H), 2.18 (d, J = 12.7 Hz, 1H), 2.35–2.46 (m, 1H),

Table 3
Syntheses of *cis*-C0 hydrazones *rac*-**13bq** and *rac*-**13bt** in pure form.[a]

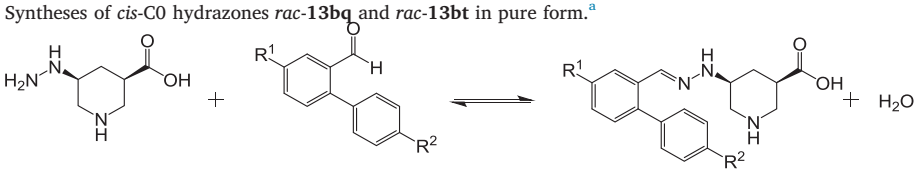

entry	aldehyde	R^1	R^2	hydrazone[b]	yield
1	**12bq**	-F	-Cl	*rac*-**13bq**	nearly quant.[c]
2	**12bt**	-H	-phenyl	*rac*-**13bt**	nearly quant.[c]

[a] Hydrazine *rac*-**7** was applied as hydrochloride and stoichiometric amounts of NaOD were used to neutralize the introduced HCl.
[b] Besides the major *E*-isomer minor amounts (≤10%) of the *Z*-isomer were formed.
[c] The reaction was performed in deuterated solvents in order to be able to monitor reaction progress by ^{1}H NMR. The hydrazones were used from this stock solution for all further experiments without additional drying and purification.

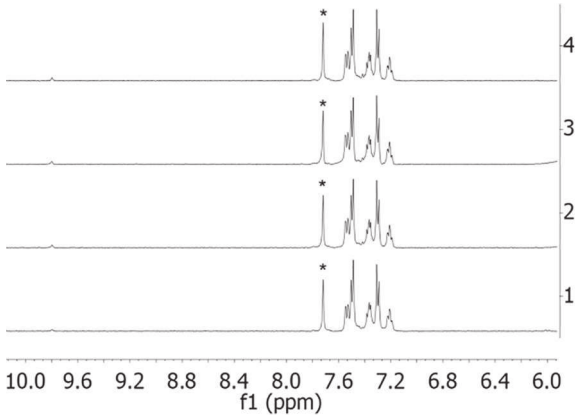

Fig. 4. Excerpts of ^{1}H NMR spectra (~6–10 ppm, displaying hydrazone proton* and aromatic region) of hydrazone *rac*-**13bq** diluted 1:10 to 1 mM in Krebs puffer (pH = 7.2), to which 2 mM sodium L-ascorbate and 40 μM GABA (**1**) were added. The spectra were recorded 5 min (1), 30 min (2), 60 min (3) and 150 min (4) after sample preparation at 37 °C.

2.47–2.59 (m, 1H), 2.63 (t, J = 12.3 Hz, 1H), 3.25 (dd, J = 12.5/4.1 Hz, 1H), 3.30 (dd, J = 11.7/4.2 Hz, 1H), 3.36 (tt, J = 11.0/4.0 Hz, 1H), 7.17 (td, J = 8.4/2.7 Hz, 1H), 7.25–7.35 (m, 3H), 7.50–7.53 (m, 3H), 7.58 (dd, J = 10.6/2.7 Hz, 1H) ppm. ^{13}C NMR (126 MHz, DMSO-d_6/D_2O = 9:1, 25 °C): δ = 32.45, 40.50, 45.92, 47.27, 52.71, 110.02 (d, J_{CF} = 23.0 Hz), 114.60 (d, J_{CF} = 25.4 Hz), 128.48, 131.41, 132.32 (d, J_{CF} = 9.0 Hz), 132.37, 133.81, 134.70 (d, J_{CF} = 2.7 Hz), 135.34 (d, J_{CF} = 8.0 Hz), 137.52, 161.77 (d, J_{CF} = 243.2 Hz), 174.07 ppm. ^{19}F {1H} NMR (376 MHz, DMSO-d_6/D_2O = 9:1, 25 °C): δ = -114.33 ppm. HRMS (ESI): $[M + H]^+$ calcd. for $C_{19}H_{20}N_3O_2ClF$, 376.1223; found: 376.1224.

Besides the major *E*-isomer the *Z*-isomer was present in 8% according to ^{1}H NMR; in addition to the signals listed for the *E*-isomer NMR spectra showed signals of low intensity corresponding to the *Z*-isomer. Peaks for the protons of OH and NH groups disappeared due to deuterium exchange and corresponding signals were not detectable in the ^{1}H NMR spectrum.

*4.1.2.2. rac-(3R,5S)-{5-[(E)-2-[(2-{[1,1′-Biphenyl]-4-yl}phenyl) methylidene]hydrazin-1-yl]piperidine-3-carboxylic acid}–sodium chloride (1/2), (rac-**13bt**).* To DMSO-d_6 (850 μL) a 200 mM stock solution of *rac*-**7** in D_2O (50 μL, 0.010 mmol), a 1 M solution of NaOD in D_2O (20 μL, 0.020 mmol) and D_2O (30 μL) were added to reach a total volume of 950 μL. The reaction was started by the addition of a 200 mM stock solution of 2-{[1,1′biphenyl] 4yl}benzaldehyde (**12bt**) in DMSO-d_6 (50 μL, 0.010 mmol). The mixture was sonicated for 5 min and stored at rt over night to obtain *rac*-**13bt** in solution (remaining aldehyde ≤ 7%).

^{1}H NMR (500 MHz, DMSO-d_6/D_2O = 9:1, 25 °C): δ = 1.39 (q, J = 12.3 Hz, 1H), 2.22 (d, J = 13.2 Hz, 1H), 2.44–2.61 (m, 2H), 2.68 (t, J = 12.4 Hz, 1H), 3.26–3.44 (m, 3H), 7.29–7.33 (m, 1H), 7.37–7.40 (m, 2H), 7.40–7.43 (m, 3H), 7.50–7.53 (m, 2H), 7.70 (s, 1H), 7.72–7.75 (m, 2H), 7.76–7.80 (m, 2H), 7.88–7.93 (m, 1H) ppm. ^{13}C NMR (126 MHz, DMSO-d_6/D_2O = 9:1, 25 °C): δ = 32.18, 39.81, 45.40, 47.02, 52.45, 124.71, 126.61, 126.68, 127.62, 127.68, 127.95, 129.13, 130.14, 130.15, 132.72, 136.36, 138.69, 139.03, 139.40, 139.54, 173.76 ppm. HRMS (ESI): $[M+H]^+$ calcd. for $C_{25}H_{26}N_3O_2$, 400.2020; found: 400.2020.

Besides the major *E*-isomer the *Z*-isomer was present in 10% according to ^{1}H NMR; in addition to the signals listed for the *E*-isomer NMR spectra showed signals of low intensity corresponding to the *Z*-isomer. Peaks for the protons of OH and NH groups disappeared due to deuterium exchange and corresponding signals were not detectable in the ^{1}H NMR spectrum.

4.1.3. Monitoring of hydrazone formation for library generation by ^{1}H NMR

NMR samples were prepared by mixing 300 μL of a 10 mM stock solution of the corresponding hydrazine in phosphate buffer (1 M NaCl, 12.5 mM Na_2HPO_4, 12.5 mM NaH_2PO_4, 200 μM sodium L-ascorbate in H_2O; pH = 7.1) with 300 μL of an 800 μM stock solution of aldehyde **12w** in DMSO-d_6 directly in the NMR tube (resulting in an initial concentration of 5 mM hydrazine and 400 μM aldehyde after mixing).

The NMR kinetic experiments were performed at 25 °C using a standard proton pulse sequence with water suppression by excitation sculpting provided by the Bruker TopSpin pulse program library; the spectra were recorded with 32 transients and a relaxation delay of 1 s. The first NMR spectrum was measured 5 min after sample preparation and a 5 min time increment was chosen for further measurements.[35]

4.1.4. Monitoring of hydrazone stability in incubation buffer by ^{1}H NMR

For NMR sample preparation, to 480 μL "Krebs" buffer (119 mM NaCl, 2.5 mM $CaCl_2$, 1.2 mM $MgSO_4$, 1.2 mM KH_2PO_4, 4.7 mM KCl, 11 mM glucose, 25 mM tris(hydroxymethyl)aminomethane; pH = 7.2)[40] 60 μL of a solution of 20 mM sodium L-ascorbate and 400 μM GABA (**1**) in H_2O and 60 μL of a 10 mM solution of the corresponding in DMSO-d_6/D_2O (= 9:1) were added. The monitoring was started after the addition of the hydrazone to the NMR tube.

The NMR kinetic experiments were performed at 37 °C using a standard proton pulse sequence with water suppression by excitation sculpting provided by the Bruker TopSpin pulse program library; the spectra were recorded with 64 transients and a relaxation delay of 1 s.

Table 4
Evaluation of *cis*-C0 hydrazones *rac*-**13bq** and *rac*-**13bt** as GABA uptake inhibitors and a comparison with reference compounds from literature.

Entry	Compd.	pIC_{50}[a]				
		mGAT1[b]	mGAT2[b]	mGAT3[b]	mGAT4[b]	hGAT3[c]
1	*rac*-**13bq**	4.26 ± 0.05	4.28 ± 0.07	5.11 ± 0.01	5.27 ± 0.06	5.56 ± 0.15
2	*rac*-**13bt**	75%/100 μM	72%/100 μM	5.18 ± 0.04	4.99 ± 0.08	5.03 ± 0.12
3	tiagabine (**2**)	6.88 ± 0.12[d]	52%/100 μM[d]	64%/100 μM[d]	73%/100 μM[d]	78%/250 μM[d]
4	(*S*)-SNAP-5114 (**3**)	4.07 ± 0.09[e]	63%/100 μM[e]	5.29 ± 0.04[e]	5.65 ± 0.02[e]	5.48 ± 0.10[e]
5	isatin derivative **6**	4.53	52%/100 μM	44%/100 μM	4.61	5.09

[a] pIC_{50} values are given as means ± SEM of at least three independent experiments (except for compound **6**, for which only two experiments were performed and accordingly no SEM is given). In case of low inhibitory potencies percentages are given that represent remaining GABA uptake in presence of 100 μM test compound (except for tiagabine (**2**) at hGAT3, which was applied in a concentration of 250 μM).

[b] Results of [^{3}H]GABA uptake assays performed with HEK cells stably expressing mGAT1–mGAT4 in our laboratory.

[c] Results of MS Transport Assays performed with COS cells stably expressing hGAT3 in our laboratory.

[d] Values from reference literature[40] (mGAT1–mGAT4) and reference literature[42] (hGAT3).

[e] Values based on repetitive testing over several years of (*S*)-SNAP-5114 as a reference mGAT4 inhibitor in our laboratory; as the mean values are continuously updated, they might differ from previously published values [e.g. 4.07 ± 0.09 at mGAT1, 56%/100 μM at mGAT2, 5.29 ± 0.04 at mGAT3, 5.81 ± 0.10 at mGAT4 (each from literature reference[40]) and 5.4 ± 0.1 at hGAT3 (from literature reference[42])].

The first NMR spectrum was measured 5 min after sample preparation and a 5 min time increment was chosen for further measurements.[37]

4.2. Biological evaluation

4.2.1. Cells expressing GABA transporters

HEK cells stably expressing mGAT1–mGAT4 were prepared and processed as described in reference[40] and COS cells stably expressing hGAT3 as in reference.[42]

4.2.2. Library generation and screening

For library generation a 10 mM stock solution of the corresponding hydrazine in phosphate buffer (1 M NaCl, 12.5 mM Na_2HPO_4, 12.5 mM NaH_2PO_4, 200 μM sodium L-ascorbate in H_2O; pH = 7.1) was mixed 1:1 with a library stock solution in DMSO containing eight individual aldehydes each in a concentration of 100 μM; after vortexing the mixture was kept at room temperature for 30–40 min to allow quantitative hydrazone library formation. To the thus preincubated mixture (20 μL) a 20 mM solution of sodium L-ascorbate in H_2O (10 μL) and Krebs buffer (2.5 mM $CaCl_2$, 1.2 mM $MgSO_4$, 1.2 mM KH_2PO_4, 4.7 mM KCl, 11 mM glucose, 25 mM Tris, 119 mM NaCl, pH 7.2; 70 μL) were then added to obtain solutions of hydrazones (10 μM) and sodium L-ascorbate (2 mM) 10-fold concentrated compared to the intended final assay concentrations.

The uptake assays for library screening were performed in triplicate samples in a total volume of 250 μL Krebs buffer containing 1% DMSO in the 96-well plate format basically as described for full-scale experiments[40] except that 200 μM sodium L-ascorbate was added to all samples and that the test compounds (i.e. hydrazone libraries) were added only in a single concentration (1 μM for each library component with remaining excessive hydrazine). In short, an aliquot of the suspension of HEK cells stably expressing mGAT4 was equilibrated with the hydrazone libraries (added from the aforementioned preincubated and diluted solution additionally containing sodium L-ascorbate; 25 μL) in a shaking water bath at 37 °C for 25 min. Then a solution of [^{3}H]GABA (8 nM final assay concentration) and unlabelled GABA (32 nM final assay concentration) in Krebs buffer was added (25 μL) and it was further incubated for 4 min. The incubation was terminated by filtration under reduced pressure. After rinsing with a cold 0.9% NaCl solution the filters were transferred to a 96-well plate. Rotiszint Eco Plus (Roth) was added (200 mL per well) and the radioactivity was determined in a MicroBeta liquid scintillation counter (Perkin Elmer LAS). Non-specific uptake was defined in the presence of 1 mM GABA accordingly and was subtracted from total uptake to obtain specific uptake.

4.2.3. Deconvolution experiments

The deconvolution experiments were analogously performed as the experiments with the libraries but employing single aldehydes (100 μM per sample) instead of a mixture of eight aldehydes during preincubation for library generation; the test compounds' resulting assay concentration was 1 μM.

4.2.4. [^{3}H]GABA uptake assays

[^{3}H]GABA uptake assays were performed as reported[40] except that sodium L-ascorbate (200 μM) was added to all samples as antioxidant.

4.2.5. MS Transport assays

Competitive MS Transport Assays were performed as reported[42] except that sodium L-ascorbate (200 μM) was added to all samples as antioxidant.

4.2.6. Data analysis

Data analysis was performed as reported.[40,42] The results of screening and deconvolution experiments are given as percentages of remaining specific [^{3}H]GABA uptake in the presence of corresponding test compounds (either hydrazone libraries or single hydrazones) compared to specific [^{3}H]GABA uptake in absence of test compounds; data represent means ± SD of three replicates. Inhibitory potencies of test compounds from full-scale experiments with mGAT1–mGAT4 ([^{3}H]GABA uptake assays) and hGAT3 (MS Transport Assays) are given as pIC_{50} values; IC_{50} values were determined by non-linear regression using Prism 6 (GraphPad Software). The results are expressed as means ± SEM of at least three separate experiments, each carried out with triplicate samples.

Acknowledgements

We like to thank Dr. Lars Allmendinger and Dr. Jörg Pabel for technical assistance, and Silke Duensing-Kropp, Tanja Franz and Miriam Sandner for performing GABA uptake assays and MS Transport Assays.

References

1. World Health Organization (WHO). Fact sheet "Epilepsy"; online at: http://www.who.int/news-room/fact-sheets/detail/epilepsy (accessed 23.07.18.).
2. Begley CE, Beghi E. The economic cost of epilepsy: a review of the literature. *Epilepsia.* 2002;43:3–9.
3. Allers K, Essue BM, Hackett ML, et al. The economic impact of epilepsy: a systematic review. *BMC Neurol.* 2015;15:245.
4. Scharfman HE. The neurobiology of epilepsy. *Curr Neurol Neurosci Rep.* 2007;7:348–354.
5. Bradford HF. Glutamate, GABA and epilepsy. *Prog Neurobiol.* 1995;47:477–511.

6. Treiman DM. GABAergic mechanisms in epilepsy. *Epilepsia.* 2001;42:8–12.
7. Kleppner SR, Tobin AJ. GABA signalling: therapeutic targets for epilepsy, Parkinson's disease and Huntington's disease. *Expert Opin Ther Targets.* 2001;5:219–239.
8. Kowalczyk P, Kulig K. GABA system as target for new drugs. *Curr Med Chem.* 2014;21:3294–3309.
9. Madsen KK, Clausen RP, Larsson OM, Krogsgaard-Larsen P, Schousboe A, White HS. Synaptic and extrasynaptic GABA transporters as targets for anti-epileptic drugs. *J Neurochem.* 2009;109:139–144.
10. Wellendorph P, Jacobsen J, Skovgaard-Petersen J, et al. γ-Aminobutyric acid and glycine neurotransmitter transporters. In: Ecker GF, Clausen RP, Sitte HH, eds. *Transporters as Drug Targets.* 1st ed. Wiley-VCH: Weinheim; 2017:69–106.
11. Borden LA. GABA transporter heterogeneity: pharmacology and cellular localization. *Neurochem Int.* 1996;29:335–356.
12. Madsen KK, White HS, Schousboe A. Neuronal and non-neuronal GABA transporters as targets for antiepileptic drugs. *Pharmacol Ther.* 2010;125:394–401.
13. Kristensen AS, Andersen J, Jørgensen TN, et al. SLC6 neurotransmitter transporters: structure, function, and regulation. *Pharmacol Rev.* 2011;63:585–640.
14. Minelli A, DeBiasi S, Brecha NC, Zuccarello LV, Conti F. GAT-3, a high-affinity GABA plasma membrane transporter, is localized to astrocytic processes, and it is not confined to the vicinity of GABAergic synapses in the cerebral cortex. *J Neurosci.* 1996;16:6255–6264.
15. Jin XT, Galvan A, Wichmann T, Smith Y. Localization and function of GABA transporters GAT-1 and GAT-3 in the basal ganglia. *Front Syst Neurosci.* 2011;5:63.
16. Zhou Y, Danbolt NC. GABA and glutamate transporters in brain. *Front Endocrinol.* 2013;4:165.
17. Yunger LM, Fowler PJ, Zarevics P, Setler PE. Novel inhibitors of gamma-aminobutyric acid (GABA) uptake: anticonvulsant actions in rats and mice. *J Pharmacol Exp Ther.* 1984;228:109–115.
18. Ali FE, Bondinell WE, Dandridge PA, et al. Orally active and potent inhibitors of γ-aminobutyric acid uptake. *J Med Chem.* 1985;28:653–660.
19. Dalby NO. GABA-level increasing and anticonvulsant effects of three different GABA uptake inhibitors. *Neuropharmacology.* 2000;39:2399–2407.
20. Borden LA, Dhar TGM, Smith KE, Weinshank RL, Branchek TA, Gluchowski C. Tiagabine, SK&F 89976-A, CI-966, and NNC-711 are selective for the cloned GABA transporter GAT-1. *Eur J Pharmacol.* 1994;269:219–224.
21. Genton P, Guerrini R, Perucca E. Tiagabine in clinical practice. *Epilepsia.* 2001;42:42–45.
22. LaRoche SM, Helmers SL. The new antiepileptic drugs: scientific review. *JAMA.* 2004;291:605–614.
23. Leppik IE. Tiagabine: the safety landscape. *Epilepsia.* 1995;36:S10–S13.
24. Leach JP, Brodie MJ. Tiagabine. *Lancet.* 1998;351:203–207.
25. Vogensen SB, Jørgensen L, Madsen KK, et al. Selective mGAT2 (BGT-1) GABA uptake inhibitors: design, synthesis, and pharmacological characterization. *J Med Chem.* 2013;56:2160–2164.
26. Vogensen SB, Jørgensen L, Madsen KK, et al. Structure activity relationship of selective GABA uptake inhibitors. *Bioorg Med Chem.* 2015;23:2480–2488.
27. Stefan T, Renukappa-Gutke T, Höfner G, Wanner KT. Design, synthesis and SAR studies of GABA uptake inhibitors derived from 2-substituted pyrrolidine-2-yl-acetic acids. *Bioorg Med Chem.* 2015;23:1284–1306.
28. Hellenbrand T, Höfner G, Wein T, Wanner KT. Synthesis of 4-substituted nipecotic acid derivatives and their evaluation as potential GABA uptake inhibitors. *Bioorg Med Chem.* 2016;24:2072–2096.
29. Kerscher-Hack S, Renukappa-Gutke T, Höfner G, Wanner KT. Synthesis and biological evaluation of a series of *N*-alkylated imidazole alkanoic acids as mGAT3 selective GABA uptake inhibitors. *Eur J Med Chem.* 2016;124:852–880.
30. Tóth K, Höfner G, Wanner KT. Synthesis and biological evaluation of novel *N*-substituted nipecotic acid derivatives with an alkyne spacer as GABA uptake inhibitors. *Bioorg Med Chem.* 2018;26:3668–3687.
31. Dhar TGM, Borden LA, Tyagarajan S, et al. Design, synthesis and evaluation of substituted triarylnipecotic acid derivatives as GABA uptake inhibitors: identification of a ligand with moderate affinity and selectivity for the cloned human GABA transporter GAT-3. *J Med Chem.* 1994;37:2334–2342.
32. Pabel J, Faust M, Prehn C, et al. Development of an (*S*)-1-{2-[tris(4-methoxyphenyl) methoxy]ethyl}piperidine-3-carboxylic acid [(*S*)-SNAP-5114] carba analogue inhibitor for murine gamma-aminobutyric acid transporter type 4. *ChemMedChem.* 2012;7:1245–1255.
33. Frey H-H, Popp C, Löscher W. Influence of the inhibitors of high affinity GABA uptake on seizure threshold in mice. *Neuropharmacology.* 1979;18:581–590.
34. Damgaard M, Al-Khawaja A, Vogensen SB, et al. Identification of the first highly subtype-selective inhibitor of human GABA transporter GAT3. *ACS Chem Neurosci.* 2015;6:1591–1599.
35. Sindelar M, Wanner KT. Library screening by means of MS Binding Assays – exemplarily demonstrated for a pseudo-static library addressing GAT1. *ChemMedChem.* 2012;7:1678–1690.
36. Sindelar M, Lutz TA, Petrera M, Wanner KT. Focused pseudostatic hydrazone libraries screened by mass spectrometry binding assay: optimizing affinities toward γ-aminobutyric acid transporter 1. *J Med Chem.* 2013;56:1323–1340.
37. Hauke TJ, Wein T, Höfner G, Wanner KT. Novel allosteric ligands of γ-aminobutyric acid transporter 1 (GAT1) by MS based screening of pseudostatic hydrazone libraries. *J Med Chem.* 2018;61(22):10310–10332.
38. Hauke TJ, Höfner G, Wanner KT. MS based screening of 5-substituted nipecotic acid derived hydrazone libraries as ligands of the GABA transporter 1. Manuscript submitted.
39. Kragler A, Höfner G, Wanner KT. Novel parent structures for inhibitors of the murine GABA transporters mGAT3 and mGAT4. *Eur J Pharmacol.* 2005;519:43–47.
40. Kragler A, Höfner G, Wanner KT. Synthesis and biological evaluation of aminomethylphenol derivatives as inhibitors of the murine GABA transporters mGAT1–GAT4. *Eur J Med Chem.* 2008;43:2404–2411.
41. Schmitt S, Höfner G, Wanner KT. MS Transport Assays for γ-aminobutyric acid transporters – an efficient alternative for radiometric assays. *Anal Chem.* 2014;86:7575–7583.
42. Schmitt S, Höfner G, Wanner KT. Application of MS Transport Assays to the four human γ-aminobutyric acid transporters. *ChemMedChem.* 2015;10:1498–1510.
43. Kern FT, Wanner KT. Generation and screening of oxime libraries addressing the neuronal GABA transporter GAT1. *ChemMedChem.* 2015;10:396–410.